UNIVERSITEIT VAN PRETORIA
UNIVERSITY OF PRETORIA
YUNIBESITHI YA PRETORIA

DESIGN AND PERFORMANCE EVALUATION OF A FULL RATE, FULL DIVERSITY SPACE-TIME-SPREADING CODE FOR AN ARBITRARY NUMBER OF Tx ANTENNAS

By

Francois De Villiers Maasdorp

Submitted in partial fulfilment of the requirements for the degree

Masters of Engineering (Electronic)

In the

Department of Electrical, Electronic and Computer Engineering

of the

Faculty of Engineering, Built Environment and Information Technology

at the

UNIVERSITY OF PRETORIA

Promoter: Professor L.P. Linde

Co-leader : Mr. L. Staphorst

July 2008

SUMMARY

DESIGN AND PERFORMANCE EVALUATION OF A FULL RATE, FULL DIVERSITY SPACE-TIME-SPREADING CODE FOR AN ARBITRARY NUMBER OF Tx ANTENNAS

by

Francois De Villiers Maasdorp

Promoter : Professor L.P. Linde

Department of Electrical, Electronic and Computer Engineering

Masters of Engineering (Electronic)

Since the mid 1990's, the wireless communications industry has witnessed explosive growth. The worldwide cellular and personal communication subscriber base surpassed 600 million users by late 2001, and the number of individual subscribers surpassed 2 billion at the end of 2006 [1, 2]. In order to attract and accommodate these subscribers, modern communication systems, like the Third Generation (3G) and Fourth Generation (4G) cellular networks, will have to provide attractive new features such as increased data throughput rates, greater system capacity, and better speech quality. These modern communication systems promise to have advantages such as wireless access in ways that have never been possible before, providing, amongst others services such as live television (TV) broadcasting to Mobile Stations (MS)s, multi-megabit Internet access, communication using Voice over Internet Protocol (VoIP), unparalleled network capacity, seamless accessibility and many more.

With specific, but not exclusive reference to the cellular environment, there are numerous ways to increase the data throughput rate and system capacity. From an economical perspective, it would be more efficient to add equipment to the Base Station (BS) rather than the MSs. To achieve these improvements the motivation to utilise transmit diversity's capabilities have been identified as a key research issue in this study. Alamouti [3] proposed a transmit diversity technique using two transmit antennas and one receive antenna, providing the same diversity order than using one transmit antenna and two receive antennas. Since Alamouti's publication in 1998, many papers in the field of Space-Time (ST) coding have been published. Current research in the field of ST coding consists of finding methods to extend the number of transmit antennas to more than four, while still achieving full rate, as well as full diversity which is the main motivation for this study.

This study proposes a novel idea of breaching the limitations with ST coding theory by combining ST coding with Spread Spectrum (SS) modulation techniques in order to extend the number of transmit antennas to more than four and still achieve full rate as well as full diversity. An advantage of the proposed scheme, called Direct Sequence Space-Time Spreading (DSSTS) has over current Space-Time Spreading (STS) techniques is that it uses 50% less spreading codes. A performance evaluation platform for the DSSTS scheme was developed to simulate the performance of the scheme in a realistic mobile communication environment. A mobile communication channel that has the ability to simulate time-varying multipath fading was developed and used to evaluate the performance of the DSSTS scheme. From the simulation results obtained, it is evident that Walsh sequences that exhibit particularly good cross-correlation characteristics, cannot overcome the effect of the antenna self-noise in order to exploit the diversity gain by adding extra antennas, i.e. diversity extension. The research also showed that an optimal trade-off exists between antenna diversity and antenna created self-noise. Performance results of the DSSTS scheme in slow and fast fading channels for a different number of transmit antennas are also presented in this study. With the capacity analysis of the DSSTS scheme, it was shown that the addition of extra transmit antennas to the system indeed increased the system capacity.

A further addition to this study is the investigation into the assumption that the channel should be quasi-static over the frame length of the ST code. A Space Sequence Transmit Diversity (SSTD) technique is consequently proposed that allows the transmission of the Alamouti symbols during one time interval instead of two. This relieves the ST code from the assumption that the channel should be quasi-static, allowing it to be used in a more realistic multi-user environment. A performance evaluation platform for the SSTD scheme was developed and used to obtain simulation results in a multipath fading channel. It was also shown that the proposed SSTD scheme is successful in combating the effects of multipath fading for small Code Division Multiple Access (CDMA) user loads. However, as a rule of thumb, the square root of the spreading sequence length divided by two depicts the user load at which the SSTD scheme was not capable of overcoming the combined effects of Multi-User Interference (MUI) and multipath fading.

Keywords: 3G, 4G, transmit diversity, capacity, ST Block coding, full rate, full diversity, Spread Spectrum, SSTD, DSSTS, time varying multipath fading, cross-correlation, antenna self-noise, quasi-static, CDMA, MUI.

SAMEVATTING

ONTWERP EN WERKVERRIGTING EVALUERING VAN N VOL TEMPO, VOL DIVERSITEIT RUIMTE-TYD-SPREIDING KODE VIR N ARBITRERE AANTAL UITSAAI ANTENNAS

deur

Francois De Villiers Maasdorp

Promoter : Professor L.P. Linde

Departement Elektriese, Elektroniese en Rekenaar-Ingenieurswese

Meester in Ingenieurswese (Elektronies)

Sedert die middel 1990's het die draadlose kommunikasie-industrie 'n reuse ontploffing in gebruikersgetalle beleef. Die wêreldwye getal sellulêre en persoonlike kommunikasie gebruikers het die 600 miljoen kerf bereik, en die getal het 2 biljoen bereik aan die einde van 2006 [1, 2]. Om al hierdie aantekenare te akkommodeer, sal moderne kommunikasiestelsels, soos die Derde-Generasie (3G) en Vierde-Generasie (4G) selfoonnetwerke, grootliks moet aanpas om hul datatempo te verhoog, groter stelsel kapasiteit hê, beter stemkwaliteit te verkry, ens. Hierdie moderne kommunikasiestelsels beloof om voordele soos draadlose toegang te verleen, wat nog nooit van tevore moontlik was nie, soos byvoorbeeld direkte televisie uitsendings na mobielestasies, multi-megagreep Internet-toegang, kommunikasie wat gebruik maak van stem-oor-internet-protokol (VoIP), altyd-aan Internet-toegang, en meer.

Met spesifieke, maar nie eksklusiewe verwysing na die sellulêre omgewing nie, is daar 'n verskeidenheid maniere om die datatempo, asook die stelselkapasiteit te verhoog. Uit 'n ekonomiese lewensvatbare oogpunt is dit meer effektief om toerusting by die basisstasie te plaas as by die mobielestasie. Om hierdie voordele te behaal, is uitsaai-diversiteit dus as 'n sleutel navorsingsveld in hierdie studie geïdentifiseer. Alamouti [3] het 'n uitsaai diversiteitskema voorgestel wat twee uitsaai-antennas en een ontvangs-antenna gebruik en dieselfde diversiteitsorde het as 'n stelsel wat een uitsaai-antenna en twee ontvangs-antennas het. Sedert Alamouti se publikasie in 1998 is talle publikasies oor Ruimte-Tyd (RT) kodering gepubliseer. Hedendaagse navorsing op die terrein van RT-kodering wat metodes behels wat fokus op die uitbreiding van die aantal uitsaai-antennas na meer as vier, terwyl volle datatempo en volle diversiteit steeds bereik word, het gelei tot die hooftema van hierdie studie. Hierdie studie stel 'n skema voor wat die beperkings in RT-kodering oorbrug deur Sprei-Spektrum (SS) modulasie te kombineer met RT-kodering om die aantal uitsaai-antennas

te vermeerder na meer as vier, terwyl volle datatempo, sowel as volle diversiteit, steeds gehaal word. ’n Voordeel wat die voorgestelde skema, naamlik Direkte Sekwensie Ruimte-Tyd Spreiding (DSRTS), oor konvensionele Ruimte-Tyd-Spreiding (RTS) het, is dan ook dat 50% minder spreisekwensies gebruik word. ’n Werkverrigting evaluasie-platform vir die DSRTS-skema is ontwikkel om die werkverrigting van die skema in ‘n werklike omgewing te simuleer. ’n Mobiele kommunikasiekanaal wat die vermoë het om tyd-variërende multipad-deinende kanaaltoestande te simuleer, is ontwikkel en gebruik om die DSRTS-skema se werkverrigting te evalueer. Uit die simulasieresultate was dit ooglopend dat die Walsh-sekwensies, wat besonder goeie infasige kruiskorrelasie-eienskappe besit, nie die effekte van die antenna-self-ruis kon oorkom ten einde die diversiteit wat deur die byvoeging van ekstra antennas verskaf word, te benut nie, d.i. diversiteits-uitbreiding. Uit die studie was dit ook duidelik dat daar ‘n optimale uitruiling bestaan tussen antenna-diversiteit en antenna-self-ruis. Werkverrigtings-resultate van die DSRTS-skema in stadig - sowel as vinnig - deinende kanale vir verskillende aantal uitsaai-antennas, word ook in hierdie studie voorgelê. Met die kapasiteitsanalise wat van die DSRTS skema gedoen is, is bewys dat die uitbreiding van uitsaai-antennas wel die stelselkapasiteit verhoog.

In ’n verdere uitbreiding op hierdie studie is ondersoek ingestel na die onrealistiese aanvaarding dat die kanaal quasi-stationêr oor die vensterperiode van die RT-kode is. ’n Ruimte-Sekwensie Uitsaai-Diversiteits (RSUD)-metode word voorgestel in hierdie studie wat die uitsaai van die Alamouti simbole oor een tydsinterval, in plaas van twee tydsintervalle laat geskied. Dus hoef die kanaal vir ‘n RT-kode nie meer quasi-stationer te wees nie en kan dit gebruik word in ’n meer realistiese multi-gebruiker omgewing. ’n Werkverrigtings-evaluasieplatform vir die RSUD is ontwikkel om simulasieresultate vir ’n deinende multipad kanaal te verkry. Die studie toon ook dat die voorgestelde RSUD-skema suksesvol is in die oorkoming van deinende multipad-kanaal effekte vir ’n klein Kode-Divisie-Veelvuldige-Toegang (KDVT) gebruikersbelading. As ‘n algemene reël kan die vierkantswortel van die sekwensielengte gedeel deur twee beskou word as die gebruikerslading waar die RSUD skema egter nie die gekombineerde effekte van die deinende kanaal en Multi-Gebruiker-Steuring (MGS) kan oorkom nie.

Sleutelwoorde: 3G, 4G, uitsaai diversity, kapasiteit, RT kodering, volle tempo, volle diversiteit, Sprei Spekrum, RSUD, DSRTS, tyd varieërende multipad deining, kruis-korrelasie, antenna self-ruis, quasi-staties, KDVT, MGS.

ACNOWLEDGEMENTS

I wish to thank my Heavenly Father for blessing me with many talents and giving me determination in pursuing the goals in my life. For this, I dedicate this study to my God Almighty.

Further, I wish to thank the following people and institutions, that I am deeply grateful for, for their support during this study:

First of all, I wish to thank my wonderful parents for being an example to me to strive for. Without their continuous support and guidance over the years, and especially the difficult times, I would never have attained the successes in life as it stands today.

I am especially grateful towards my study leader, Prof L.P. Linde and co-leader, Mr. L. Staphorst, who made this study possible, for their insight and guidance throughout the duration of this study.

Credit also goes to the University of Pretoria as well as the National Research Foundation for their financial support of this study. I also wish to thank the University of Pretoria for allowing me to make use of their Intel I-percube high performance cluster that enabled me to produce the simulation results presented in this study.

TABLE OF CONTENTS

LIST OF FIGURES

LIST OF TABLES

LIST OF ABBREVIATIONS

1G	First Generation
1xEV-DO	Single Carrier Evolution Data Only/Optimised
1xEV-DV	Single Carrier Evolution Data and Voice
2G	Second Generation
3G	Third Generation
3GPP	3G Partnership Project
3GPP2	3G Partnership Project Two
8PSK	Eight-Phase Shift Keying
ABC	Analytic Bandlimited Complex
AWGN	Additive White Gaussian Noise
BCH	Bose-Chaudhuri-Hocquenghen
BER	Bit Error Rate
BLAST	Bell-Labs Layered Space-Time
BPSK	Binary Phase Shift Keying
BS	Base Station
CCDFs	Complementary Cumulative Distribution Functions
CDMA	Code Division Multiple Access
CD-ROM	Compact Disk Read Only Memory
CE	Constant Envelope
CE-LI-RU	Constant Envelope Linearly Interpolated
CSI	Channel State Information
CSS	Complex Spreading Sequence
dB	Decibels
DC	Direct Current
DS/SSMA	Direct Sequence Spread Spectrum multiple Access
DSB CE LI RU GCL	Double Sideband Constant Envelope Linearly Interpolated Root-of-Unity Filtered General Chirp Like
DSB	Double Sideband
DSPs	Digital Signal Processors
DS-SS	Direct Sequence Spread Spectrum
DSSTS	Direct Sequence Space-Time Spreading
ECSD	EDGE Circuit Switched Data
EDGE	Enhanced Data Rates for GSM Evolution

EGPRS	Enhanced GPRS
FDMA	Frequency Division Multiple Access
FER	Frame Error Rate
FFCS	Flat Fading Channel Simulator
FH-SS	Frequency Hopped Spread Spectrum
GAST	Generalised Algebraic ST
Gbps	Giga bits per second
GCL	General Chirp-like
GMSK	Gaussian Minimum Shift Keying
GPRS	General Packet Radio Services
GSM	Global System Mobile
HSCSD	High Speed Circuit Switched Data
HSDPA	High Speed Downlink Packet Access
IMT-2000	International Mobile Telephone 2000
IS-136	Interim Standard 136
IS-95	Interim Standard 95
IS-95B	Interim Standard 95B
ISI	Inter Symbol Interference
ITU	International Telecommunication Union
Kbps	Kilo bits per second
LCR	Level Crossing Rate
LOS	Line of sight
MAC	Medium Access Control
MAI	Multiple Access Interference
MAP	Maximum a-Posteriori
Mbps	Mega bits per second
MIMO	Multiple Input Multiple Out
ML	Maximal Length
ML	Maximum Likelihood
MPSK	M-ary Phase Shift Keying
MRRC	Maximal Ratio Receiver Combining
MS	Mobile Station
MUI	Multi-User Interference
NLOS	non-line of sight
OFDMA	Orthogonal Frequency Division Multiple Access

OOP	Object Orientated Programming
OVSF	Orthogonal Variable Spreading Factor
PAM	Pulse Amplitude Modulation
PCS	Personal Communications Systems
PDC	Pacific Digital Cellular
PDF	Probability Density Function
PG	Processing Gain
PN	Pseudo-Noise
PSK	Phase Shift Keying
QAM	Quadrature Amplitude Modulation
QPH	Quadriphase
QPSK	Quadrature Phase Shift Keying
RF	Radio Frequency
RMS	Root Mean Square
RS	Reed-Solomon
SNR	Signal to Noise Ratio
SS	Spread Spectrum
SSB	Single Sideband
SSTD	Space-Sequence Transmit Diversity
ST	Space-Time
STS	Space-Time Spreading
STTC	Space-Time Trellis Coding
STTD-OTD	Space-Time Transmit Diversity- Orthogonal Transmit Diversity
TCM	Trellis Coded Modulation
TDMA	Time Division Multiple Access
TV	Television
UMTS	Universal Mobile Telecommunications Service
VA	Viterbi Algorithm
VoIP	Voice over Internet Protocol
WCDMA	Wideband CDMA
WLAN	Wireless Local Area Networks
WiMAX	Worldwide Interoperability for Microwave Access
ZC	Zadoff-Chu

LIST OF IMPORTANT SYMBOLS

a_n	n'th signal point in signal constellation ν
ν	Signal constellation
A	ST-transmission matrix
X	DSSTS design matrix
Γ	E_b/N_o
E_b	Energy per bit
E_s	Energy per symbol
N_o	Noise spectral density
μ	Cross-correlation between path h_1 and h_2
τ	Time shift
b_n	n'th bit in bitsteam *b(t)*
b(t)	Bitstream
g(t)	Spreading sequence
θ_c	Carrier phase
θ_i	i'th delay phase in the mulipath fading channel
f_c	Carrier frequency
T_s	Symbol period
T_c	Chip period
ς	Spreading sequence *g(t)* length
G	Spreading codes for STS in matrix form
S	Transmit symbols for STS in matrix form
B	Bits in matrix form for STS
υ	Noise variable in STS
β_i	i'th path amplitude in multipath fading
Ω	Data bits in a code word
p	Probability
L	Independent fading replicas/paths
χ	Total length of a block code word
n	Number of transmit antennas
m	Number of receive antennas
t	Time
r(t)	Received signal

$d(t)$	Channel output
$R_a(\tau)$	Periodic auto-correlation function
$R_c(\tau)$	Periodic cross-correlation function
$h(t)$	Complex channel path gain
η	AWGN
c	Transmitted ST symbols
l	ST code frame length
C	ST coding design matrix
x	Transmission matrix enties
A	Transmit signal constellation
q	Number of bits representing a symbol
M	Hadamard Matrix
N	Length of spreading sequence
R_c	Code rate
R_b	Bit rate
ϑ	Delay spread
BW_s	Signal bandwidth
BW_d	Doppler bandwidth
BW_c	Coherence bandwidth
B_{ss}	SS signal bandwidth
σ^2	Variance (power)
z	Amplitude
K	Rician factor
$u(t)$	Channel input signal
α	Channel Fading amplitude
ϕ	Channel phase
$d(t)$	Channel output
$\bar{\gamma}$	Matrix containing shifted symbols from DSSTS scheme
y	Number of ST-encoders in DSSTS scheme
ξ	Duration of a fade
ρ	RMS level (level crossings)
κ	Convolutional code constraint length
DM	ST decoder decision metric
PG	Processing gain

P_e Probability of error

$S_c(f)$ Doppler power spectrum

f_d Doppler frequency

$pdf(z)$ Probability density function of the amplitude z

f_{samp} Sampling frequency

$CLOS$ Line-of-Sight component added to the in-phase branch of the FFCS

C_{SCALE} FFCS output scaling factor

$\Phi_{MFC}(t)$ Multipath power delay profile

T_n DSSTS scheme's transmission matrix with n transmit antennas

Δ Despreaded DSSTS symbols

CHAPTER ONE

INTRODUCTION

Since the mid 1990's, the wireless communications industry has witnessed explosive growth. The worldwide cellular and personal communication subscriber base surpassed 600 million users in the late 2001, and the number of individual subscribers reached 2 billion at the end of 2006 [1, 2]. Most countries in the world also experience cellular subscription increases in excess of 40% per year. The rapid worldwide growth in cellular telephone subscribers has demonstrated conclusively that wireless communications is a popular voice and data transport mechanism. The widespread success of cellular communications has lead to the development of newer wireless systems and standards for many other types of communication traffic, besides mobile voice and data calls. For example, new standards and technologies such as Worldwide Interoperability for Microwave Access (WiMAX), are being implemented to allow wireless networks to replace fiber optic or copper lines between fixed points separated by several kilometres (fixed wireless access). Similarly, wireless networks have been increasingly used as a replacement for wires within homes, buildings, and offices through the deployment of Wireless Local Area Networks (WLANs). (See *Chapter 1, Section 1.6* for an in depth discussion on WLANs).

1.1 EVOLUTION OF CELLULAR NETWORKS, 2G – 2.5G

Most of today's cellular networks are currently in the phase of migrating from what is commonly known as Second Generation (2G) technologies to 3G technologies. The 2G mobile cellular systems uses digital radio transmission for traffic, as opposed to First Generation (1G) systems' analogue radio transmission. Thus, 2G networks have much higher capacity than the 1G systems. One frequency channel is simultaneously divided among several users (either by code or time division). Furthermore, hierarchical cell structures, in which the service area is covered by macrocells, microcells, and picocells, enhance the system capacity even further.

The four most popular 2G standards include three Time Division Multiple Access (TDMA) standards and one CDMA standard:

- Global System for Mobile (GSM) that is widely deployed in Europe, Asia, Australia, Africa, South America and some parts of the US,
- Interim Standard 136 (IS-136) in North America,
- Pacific Digital Cellular (PDC) that was deployed in Japan, and
- Interim Standard 95 (IS-95), a CDMA standard that was deployed in North and South America, Korea, China and Australia.

The 2G standards mentioned above represent the first set of wireless air interfaces to rely on digital modulation and sophisticated Digital Signal Processors (DSPs) in both the handset and BS.

Since 2G technologies use circuit-switched data modems that limit the data users to a single circuit-switched voice channel, data transmissions are generally limited to the data throughput rate of an individual user. This throughput rate is in the order of 10 kilo bits per second (kbps), which is too slow for rapid email and Internet browsing applications. In an effort to comply with increasing data throughput demands, new data-centric standards as well as packet switching techniques have been deployed that can be overlaid on existing 2G technologies. These new standards represent 2.5G technologies and allow 2G equipment to be upgraded to support the higher data rate transmissions for web-browsing, email traffic, mobile commerce etc.

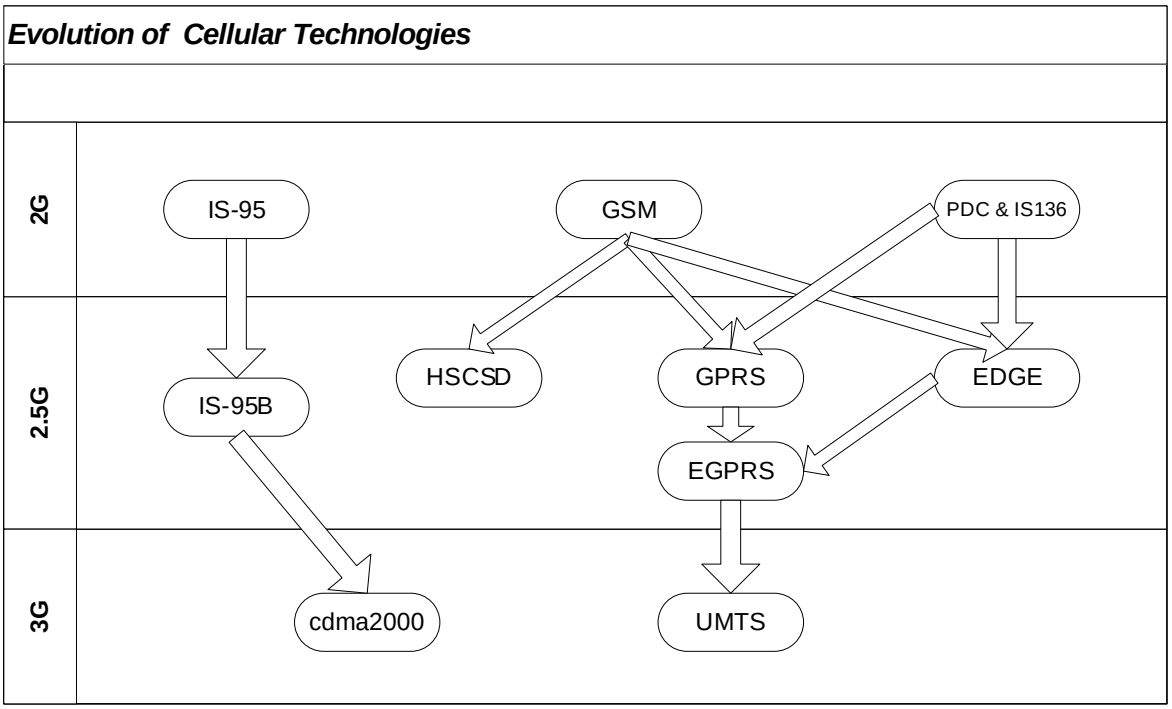

Figure 1.1. Various upgrade paths for 2G technologies [1].

The appropriate 2.5G upgrade path for a particular wireless carrier must match the original 2G technology choice. For example, the 2.5G upgrade solution for GSM must be based on the original 2G GSM technology since it would otherwise be incompatible and require complete equipment changes at the BS. *Figure 1.1* illustrates the various 2.5G and 3G upgrade paths for the major 2G technologies [1]. Also note that 3G technologies are discussed in *Section 1.2*.

The four most popular 2.5G standards include three TDMA standards, based on the GSM, IS-136 and PDC technologies, as well as one CDMA standard based on IS-95 technology, viz.

- 2.5G High Speed Circuit Switched Data (HSCSD) for GSM,
- 2.5G General Packet Radio Services (GPRS) for GSM and IS-136,
- 2.5G Enhanced Data Rates for GSM Evolution (EDGE) for GSM and IS-136, and
- The 2.5G IS-95B evolution of IS-95.

The main problem with GSM was its low air interface data rates that could originally provide only a 9.6 kbps user data rate, although a 14.4 kbps data rate specification was included later. HSCSD provided an easy way to speed things up by theoretically enabling the MS to use several time slots for a data connection, instead of only one time slot. Thus, the total rate is simply the number of time slots times the data rate of one slot. Although circuit switching is expensive in terms of resources, HSCSD was a relatively inexpensive way to upgrade the data capabilities, as it requires only software upgrades to the network (plus, of course, new HSCSD-capable phones). However, in current commercial implementations, the maximum number of time slots used is usually two, where one time slot may either use 9.6 kbps or 14.4 kbps data rates [4].

With GPRS technology, theoretical data rates of up to 171-kbps [4] with eight 21.5 kbps downlink timeslots can be obtained, or even higher if error correction is neglected. However, realistically, throughput rates of 40–60 kbps is currently being obtained [2]. Besides increased throughput rates, GPRS is packet switched, and thus does not occupy radio resources continuously. Bursty data is also well handled with GPRS, as it can adjust the assigned resources according to current needs. A drawback with GPRS is that it is not well suited for real-time applications, because the resource allocation in GPRS is contention based. Although the implementation of a GPRS system is much more expensive than that of an HSCSD system, it is seen as a necessary step toward improved data capabilities and an important step toward a 3G system, as 3G Partnership Project (3GPP) core networks are based on combined GSM and GPRS core networks.

With EDGE, Eight-Phase Shift Keying (8PSK) was adopted that increased the data rates of standard GSM up to three times [4]. EDGE is an attractive upgrade for GSM networks, as it only requires a software upgrade of BSs if the Radio Frequency (RF) amplifiers can handle the non-constant envelope modulation with EDGE's relatively high peak-to-average power ratio. It does not replace, but rather coexists with the old Gaussian Minimum Shift Keying (GMSK) modulation, so mobile users can continue using their old phones. Thus, it provides a trade-off for quality of service, i.e. data rate vs. Bit Error Rate (BER). Another reason for retaining the old GMSK is that 8PSK can only be used effectively over a short distance; thus GMSK is still needed for wide area coverage.

Combining EDGE with GPRS results in the combination known as Enhanced GPRS (EGPRS). The maximum data rate of EGPRS using eight time slots (and adequate error protection) is 384 kbps. Note that the much advertised 384 kbps is only achieved by using all radio resources per allocated frequency carrier, and even then only when the MS is close to the BS. EDGE Circuit Switched Data (ECSD) is the combination of EDGE and HSCSD and it also provides data rates three times that offered by standard HSCSD.

The evolutionary path from an IS-95 system into a full cdma2000 system can take many forms [4]. The first step would be IS-95B, which increases the data rate from 14.4 kbps to 64 kbps. The next step is the cdma2000 1xRTT system that consists of four levels: The first level is known as 1xRTT release 0, or simply 1xRTT. This release can provide a 144-kbps peak data rate. The next level is the 1xRTT release A, which can give 384 kbps rates. Level 3, i.e. Single Carrier Evolved Data Only (1xEV-DO) can be regarded as a 3G system according to the International Telecommunication Union (ITU). This level, which only comprises of a data channel, can provide data rates up to 2.4 Mega bits per second (Mbps). The final level supporting data and voice is known as Single Carrier Evolved Data and Voice (1xEV-DV) and provides data rates of up to 3 Mbps.

Note that only new coding schemes and small changes in how data are slotted into the time frames improved the effective throughput rate of the data in all of the above mentioned 2.5G technologies. However, this was not the case for further improvement to 3G. New research had to be done in order to further improve data throughput rates beyond 1.8 Mbps, for example, High Speed Downlink Packet Access (HSDPA) that can provide theoretical data rates of up to 14.4 Mbps. However, effective throughput rates of 800 kbps is currently being obtained.

1.2 3G WIRELESS NETWORKS

With the increased data throughput rates of current 3G systems, wireless access is provided in ways that have never been possible before, e.g. TV broadcasting to MSs, etc. Multi-megabit Internet access, communication using VoIP, unparalleled network capacity and “always on” access are just some of the advantages delivered by current 3G systems.

Furthermore, with the increased data throughput rates provided by 3G, users have the ability to receive live music, conduct interactive web sessions and have simultaneous voice and data access with multiple parties at the same time using a single mobile handset, whether driving, walking or standing still.

The ITU formulated a plan to implement a global frequency band in the 2000 MHz range that would support a single wireless communication standard for all countries throughout the world. This plan, called International Mobile Telephone 2000 (IMT-2000), has been successful in helping to cultivate active debate and technical analysis for new high-speed mobile telephone solutions, compared to 2G. However, as seen in *Figure 1.1*, the hope for a single worldwide standard has not materialized, as the worldwide user community remains split between two camps, namely: GSM, IS-136, PDC and the IS-95B SS technologies, respectively.

The eventual 3G evolution of the IS-95B system lead to cdma2000. Several variants of cdma2000 are currently being developed, but they are all based on the fundamentals of IS-95 and IS-95B technologies, i.e. SS technology. The eventual 3G evolution for GSM, IS-136, and PDC systems lead to the Universal Mobile Telecommunications Service (UMTS). UMTS is based on the network fundamentals of GSM, as well as the merged versions of GSM and IS-136 through EDGE. The ITU IMT-2000 standards organizations are currently separated into two major organizations reflecting the two 3G camps, namely: 3G Partnership Project (3GPP) for UMTS standards (Europe and Asia) and 3G Partnership Project Two (3GPP2) for cdma2000 standards (USA). It is fair to say that these two major 3G technology camps, i.e. cdma2000 and UMTS, will remain popular throughout the early part of the 21st century. It should also be stated here that Wideband CDMA (WCDMA) terminology is used for both UMTS and cdma2000. By definition, the bandwidth of a WCDMA system is 5 MHz or more. Thus, the nominal bandwidth was also chosen to be 5 MHz for all 3G WCDMA proposals. This particular bandwidth was chosen because it is sufficient to provide data rates of 144 and 384 kbps (i.e. 3G targets), and even 2 Mbps under favourable conditions, while providing sufficient temporal resolution to exploit the multipath structures of typical mobile channels, called multipath diversity by employing RAKE combining techniques [11]. This concept is briefly introduced in the next section.

1.3 DIVERSITY TECHNIQUES FOR MULTIPATH CHANNELS

Transmit and/or receive diversity are a powerful communication technique that provides wireless link improvement at relatively low cost. Diversity techniques are based on the notion that errors occur at reception when the channel attenuation is large, e.g., when the channel is in a deep fade. If the receiver can be supplied with several replicas of the same information signal, transmitted over independent fading channels, the probability that all the signal components will fade simultaneously is reduced considerably. That is, if p is the probability that any one signal will fade below some critical value, then p^L is the probability that all L independent fading replicas of the same signal will simultaneously fade below the critical value. Several ways exist in which the receiver can be provided with L independent fading replicas of the same information bearing signal. The most widely used are:

- **Frequency diversity [1, 5, 6, 7].** The same information bearing signal is transmitted on L carriers, where the separation between successive carriers equals or exceeds the coherence bandwidth of the channel (see Appendix C, *Sections C.4*).
- **Time diversity [1, 5, 6, 7].** A second method for achieving L independently fading versions of the same information bearing signal is to transmit the signal in L different time slots, where the separation between successive time slots equals or exceeds the coherence time of the channel (see Appendix C, *Sections C.4*). Note that the fading channel fits the model of a bursty error channel.
- **Antenna diversity [6, 8, 9, 10].** This method is also known as space diversity. It achieves diversity by employing multiple antennas, where the antenna correlation properties depend on angular spread. For example, a single transmit antenna may be employed with multiple receive antennas. The latter must be spaced sufficiently far apart so that the multipath components in the signal have significantly different propagation paths at the receive antennas. Usually a separation of a few wavelengths is required between two antennas in order to obtain signals that fade independently. For example, GSM uses an antenna separation distance of ten wavelengths at their BSs.

Furthermore, the transmission of the same information may either be viewed at different frequencies or in different time slots (or both) as a simple form of repetition coding. The separation of the diversity transmissions in time (the coherence time of the channel) or in frequency (the coherence bandwidth of the channel), is basically a form of block-interleaving of the bits in a repetition code in an attempt to break up the error bursts, thereby obtaining independent errors that facilitates the incorporation of powerful coding mechanisms traditionally designed for AWGN channels.

A more sophisticated method for obtaining diversity is based on the use of a signal having a bandwidth much greater than the coherence bandwidth of the channel. Such signals, typically known as wideband signals, will resolve the multipath components (see *Chapter 3*), providing the receiver with several independently fading signal paths. The optimum receiver for processing the wideband signal is a RAKE correlator capturing all multipath paths and was invented by Price and Green in 1958 [11].

Other notable diversity techniques are angle-of-arrival diversity and polarization diversity [1]. However, these techniques have not been used as widely as the techniques described above.

1.4 CLASSIC ERROR CORRECTION CODING

Channel coding protects digital data from errors by selectively introducing temporal redundancy in the transmitted data. Channel codes that are used to detect errors are called error detection codes, while codes that can detect and correct errors are called error correction codes.

A channel coder operates on the digital message (source) data by encoding the source information into a code sequence for transmission through the channel. The most widely used error detection and correction codes are:

- Block codes,
- Convolutional codes, and
- Coded Modulation.

Block codes encode blocks of data at a time and the encoding process only considers current data. Convolutional codes also encode blocks of data, but the encoding algorithm also considers previous data. Coded modulation is a type of coding that maximises the bandwidth efficiency of a modulation technique, for example Trellis Coded Modulation [6]. Other forms of coding also exist, for example concatenated codes are used to combine the best features of coding schemes that may be made up of block codes and convolution codes. The first concatenated code was proposed by Forney in 1966 [12] where the output of a RS code was then convolutionally encoded. Iteratively decoded codes is a type of code that are decoded in an iterative way, for example Turbo codes [13] and codes employing belief propagation (Bayesian Interference) [6]. The first two mentioned codes are briefly described below, merely for completeness. For a general overview of error correction codes, see Proakis [6]. The aim of this section is simply to provide an example to show the performance increase of a communication system when error correction coding is used (See *Figure 1.4*).

1.4.1 Block codes

A block code consists of a set of fixed-length vectors, called code words. The length of a code word is the number of elements in the vector, denoted by χ. Block codes, as shown in *Figure 1.2*, use an encoding scheme that takes Ω-data bits to produce χ encoded bits, where $\Omega < \chi$. The resulting block code is referred to as a (χ, k) code, and the ratio $\Omega/\chi = R_c$ is defined to be the rate of the code. Besides the code rate parameter R_c, an important parameter of block codes is the minimum Hamming distance of the code set. This is a measure of the error detection and correction capabilities of the code word. Some of the block coding algorithms used in practice include: Hamming codes, Hadamard codes, Golay codes, cyclic Golay codes and Bose-Chaudhuri-Hocquenghem (BCH) codes [6]. An example of a powerful non-binary BCH code is Reed-Solomon (RS) codes [6], which have good distance properties and allow protection against burst errors. Hard decision decoding algorithms, such as the Berlekamp-Massey algorithm [14], have also been developed for RS codes, making these codes applicable for real time implementation in many applications, such as Compact Disk Read Only Memories (CD-ROMs).

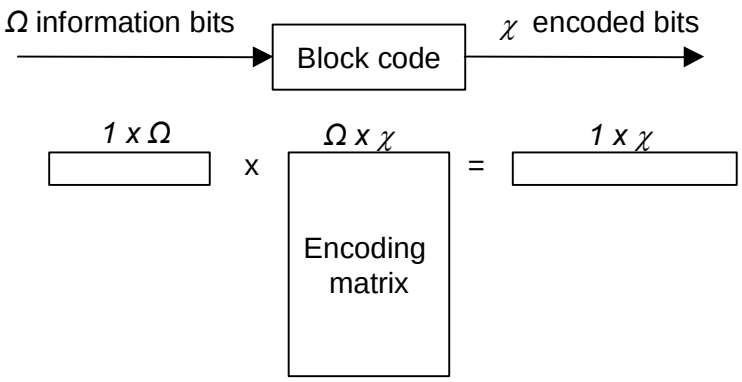

Figure 1.2. Block coding.

1.4.2 Convolutional codes

Convolutional codes are fundamentally different from block codes in that information sequences are not grouped into distinct blocks and then encoded. Instead, a continuous sequence of information bits is mapped into a continuous sequence of encoder output bits. Information bits are encoded by passing Ω-information bits at a time through a linear *Q*-stage shift register, as shown in *Figure 1.3*. A sequence of χ-encoded bits are obtained after Ω-information bits have been passed serially through an *Q*-stage shift register. The code rate $R_c = \Omega / \chi$. The parameter κ, called the constraint length, indicates the number of input data bits that the current output is dependent on and determines how powerful and

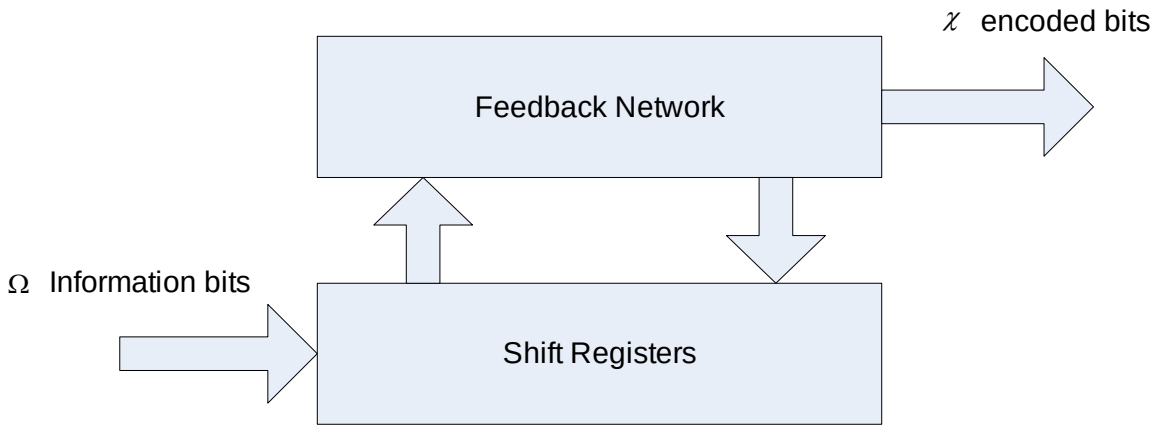

Figure 1.3. Convolutional coding consisting of a shift register and feedback network.

complex the code will be. The two popular algorithms used to decode convolutional codes are the Viterbi Algorithm (VA) [6] and the Maximum a-Posteriori (MAP) algorithm. The MAP algorithm is numerically more complex than the VA, but it offers a better BER performance [6], whereas the VA offers a better frame error rate (FER).

1.5 PERFORMANCE GAIN USING ERROR CORRECTION CODING

As an example of how error correction coding can improve the performance of a communication system, see *Figure 1.4* (taken from [15]). In *Figure 1.4* the performance of a Viterbi decoded (7,5,3) RS block code, is shown in flat fading channel conditions. Notice that the coded performance has a much lower bit error probability than the uncoded performance. Furthermore, it can also be noted that soft decision decoding has a 2dB asymptotic performance advantage over hard decision decoding.

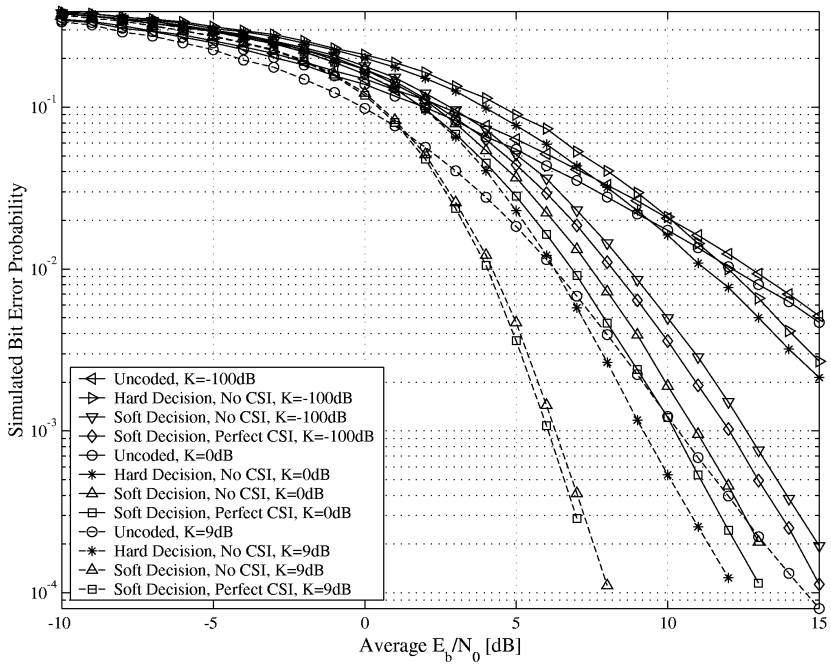

Figure 1.4. BER performance of a (7,5,3) RS block code in flat fading channel conditions, taken from [15]. K = -100dB denotes Rayleigh fading, whereas K = 0dB and K = 9dB denotes Rician fading.

1.6 RELEVANCE OF THIS DISSERTATION

As stated above, wireless communication systems, such as 3G communication systems, are constantly in demand of improving performance, such as improved voice quality, higher bit rate data services (greater than 2 Mbps), power efficiency, etc. At the same time, the remote units (mobile cellular phones) are required to be small, compact and lightweight. Further demands require that the mobile units operate reliably in various types of environments, for example, micro -, macro -, and picocellular, indoor, outdoor and urban, as well as suburban environments. In other words, the communication systems are required to have:

- increased throughput rates,
- increased capacity,
- better speech quality,
- better coverage,
- more power efficiency,
- better bandwidth efficiency, and
- to be deployed in various environments.

All of the above mentioned are constrained to services that must remain affordable for widespread market acceptance.

Time-varying multipath fading [1, 5, 6, 16] is a phenomenon which makes reliable wireless transmission very difficult. It is known to be extremely difficult to increase signal quality or reduce the BER in multipath fading channels compared to Additive White Gaussian Noise (AWGN) channels. In AWGN channels, the BER may be improved from 10^{-2} to 10^{-3} with a power sacrifice of only 1 or 2dB higher Signal to Noise Ratio (SNR) in the case of using Binary Phase Shift Keying (BPSK) (see Appendix C, *Figure C.19*). However, to achieve the same with fading channel conditions, it may require up to 10 dB more SNR (see Appendix C, *Figure C.19*). Thus, improvements in SNR may not be achievable by simply increasing transmit power or additional bandwidth, because of the increasing demand of power and bandwidth efficiency. A partial solution to this problem is to find

methods to effectively reduce the effect of multipath fading at both the mobile unit and the BS, without a sacrifice in bandwidth or the need for additional power availability.

Transmitter power control is theoretically an effective technique to mitigate multipath fading in a wireless channel [1,5]. In addition, if the channel multipath conditions, as experienced by the receiver, are known at the transmitter, the transmitter can predistort the signal in order to compensate for the effect of the distortion introduced by the channel [1].

Other effective techniques to mitigate multipath fading are time-, frequency- and antenna diversity [6]. When possible, wireless communication systems should be designed to encompass all forms of available diversity to ensure adequate performance. From a practical point of view, space diversity reception in the uplink (MS to BS) is one of the most effective and, hence, widely applied techniques for mitigating the effects of multipath fading. The classical approach is to use multiple antennas at the receiver and perform combining or selection and switching in order to improve the received signal quality. The major problems with the receive diversity approach at the MS are cost, size and power. As a result, antenna diversity techniques have almost exclusively been applied to the BS. A BS often serves hundreds to thousands of MSs. From an economical perspective it will thus be more efficient to add equipment to the BS rather than the MSs. For this reason a motivation arose for developing transmit diversity schemes. Alamouti [3] proposed a transmit diversity technique using two transmit antennas and one receive antenna, providing the same diversity order than using one transmit antenna and two receive antennas. This technique is capable of effectively mitigating the effects of multipath fading in the downlink (BS to MS) without adding any additional antennas at the MS. Thus, by using multiple antennas the effective throughput as well as system capacity of the system can be improved. Presently, communication systems like 3G and WLANs make use of two transmit antennas in order to improve the data throughput rate and system capacity. However, this dissertation strives to extend the number of transmit antennas at the BS to more than 2 antennas with full rate and full diversity in order to further increase data throughput rates and system capacity. Together with the multiple antennas diversity approach, techniques such as time interleaving used with error correction coding, can provide further performance increases.

1.7 CONTRIBUTIONS AND PUBLICATIONS

1.7.1 Contributions

This study's main focus is directed towards ST coding and modulation techniques within the field of digital communications. Minor contributions include a communication channel simulator, which had to be reproduced from Staphorst [17], in order to simulate the Direct Sequence Space-Time Spreading (DSSTS) in realistic environments. This baseband equivalent communication channel simulator was implemented and verified by comparing the simulation results with theoretical results. One advantage of using this channel is that Doppler and fading effects can be simulated without the need to simulate an RF carrier frequency.

1. Major contributions from this study on ST coding and modulation are as follows:
   a. Increasing the number of transmit and receive antennas in wireless communications has been researched over the past few years because of advantages such as increased data throughput rate as well as increased system capacity. However, inherent limitations with ST coding theory discussed in *Section 2.3*, only 2 and 4 transmit antennas can obtain both full rate and full diversity. As a result, this study was motivated by the quest for having more than 4 transmit antennas that can achieve both full rate and full diversity in order to exploit diversity gain as well as increase system capacity. Thus, a scheme called DSSTS was proposed in this study that achieves full rate and full diversity for any number of transmit antennas in multiples of two. It extends conventional ST coding theory by combining ST coding with SS modulation. An advantage of DSSTS over current Space-Time Spreading (STS) techniques is that it uses 50% less spreading codes.

   b. A novel idea to relax the Alamouti ST coding transmit diversity scheme's dependency on the channel being quasi-static. The condition of the channel being quasi-static over two consecutive time intervals in low throughput rate applications with a high Doppler component has been countered by replacing the concept of a

two interval approach with two conventional simple complex-spreaded RAKE receiver-based Direct Sequence Spread Spectrum Multiple Access (DS/SSMA) communication systems operating in parallel in one combined time interval. This new approach will henceforth be referred to as the Space-Sequence Transmit Diversity (SSTD) alternative to Alamouti's two-symbol ST coding transmit diversity technique.

2. Major contributions from this study in terms of modelling and simulation of communication systems are as follows:
   a. Flexible DSSTS transmitter and receiver structures are presented in *Chapter 5*. These structures are flexible in the sense that it allows for any type of spreading sequence to be used in conjunction with the ST coding.

   b. The novel performance evaluation platform used to create the DSSTS simulation results presented in *Chapter 6*, are presented in *Chapter 5*. This performance evaluation platform allows the user to simulate results for any number of transmit antennas at different Doppler frequencies under Rayleigh or Rician fading channel conditions.

   c. The novel SSTD transmitter and receiver structures are presented in *Chapter 5*.

3. Important contributions from this study's simulation results are as follows:
   a. It was shown that the use of Walsh spreading sequences in a Rayleigh fading channel was insufficient to exploit the diversity gain over self-noise, created by adding additional antennas to the DSSTS scheme. However, with a Rayleigh fading-channel the number of transmit antennas effects the performance of the DSSTS scheme differently in low and high mobility environments: At low velocities, i.e. at low Doppler frequencies, the DSSTS's 10 transmit antennas outperformed the DSSTS's 10 transmit antennas scenario for high mobile velocities.

b. It was also shown that the use of Walsh spreading sequences in a Rician fading channel did not produce any diversity gain due to self-noise created by adding additional antennas to the DSSTS scheme. The effect of Doppler spread in a Rician fading environment has no effect on the DSSTS scheme's BER performance at a Rician factor of 9dB and higher.

c. From the results presented in *Chapter 6*, it is evident that there exists an optimal trade-off between diversity and self-noise. Considering DSSTS in a Rician or Rayleigh fading channel, the 2 transmit antenna scenario yields the best diversity gains in both channels.

d. From the capacity simulation results presented in *Chapter 6*, it is evident that the DSSTS scheme achieves equal capacity performance gain than an open loop capacity system. It was also shown that the DSSTS 4 Tx antenna scenario outperformed other 4 Tx diversity schemes as presented in Papadias *et al.* [18].

e. The proposed SSTD scheme is successful in combating the effects of multipath fading for small Code Division Multiple Access (CDMA) user loads. However, as a rule of thumb, a user load equal to the square root of the spreading sequence length, *N*, divided by two constitutes the user load at which the SSTD scheme was not capable of overcoming the combined effects of Multi-User Interference (MUI) and multipath fading.

1.7.2 Publications

During this study, the author researched and co-authored two local conference papers and submitted one paper for possible publication in an accredited journal. These papers are listed below, as well as their relevance to this dissertation:

1. *Simulation Study of a Space-Sequence Transmit Diversity Scheme for DS/SSMA Systems (Part I)* [19], co-authored by L. Staphorts and L.P. Linde, presented at ICT 2005 in Cape Town South Africa, described the SSTD scheme proposed in this

dissertation. The 1st of the two papers elaborated on the Complex Spreading Sequence (CSS) families employed, as well as the complex DS/SSMA Quadrature Phase Shift Keying (QPSK) transmitter and RAKE receiver simulator structures.

2. The 2nd of the two paper series, *Simulation Study of a Space-Sequence Transmit Diversity Scheme for DS/SSMA Systems (Part II)* [20], presented the encoder and decoder structures of the proposed SSTD scheme, the complete multi-user multipath fading simulation platform, built around the proposed SSTD scheme and several simulation results, comparing the performances of simple uncoded and SSTD encoded wideband systems in multi-user multipath fading channel conditions for the different CSS families considered.

3. *A Full Rate, Full Diversity Space-Time Block Code for an Arbitrary number of Transmit Antennas* [21], presented the encoder and decoder structures of the proposed DSSTS scheme, several BER performance simulation results as well as the DSSTS capacity analysis.

1.8 OVERVIEW OF CHAPTERS

This dissertation is structured as follows: In *Chapter 2*, ST block coding is presented as a transmit diversity scheme. The chapter includes ST encoding, decoding, ST theory and ST capacity. Lastly, an overview of current ST literature is presented. In *Chapter 3* SS modulation techniques are presented. The chapter includes theory on Direct Sequence Spread Spectrum (DS-SS) and CSSs, as well as theory on the techniques of combining ST coding and SS modulation techniques. Lastly, an overview of current ST CDMA literature is presented. In *Chapter 4* the flat fading channel simulation platform used in this dissertation is presented, as well as a mathematical analysis of the channel. In *Chapter 5* the encoding, decoding and capacity of the new DSSTS scheme are presented, as well as how to use SSTD to relieve the Alamouti ST block-decoding scheme from the necessity for the channel to be quasi-static [3, 19, 20]. In *Chapter 6,* BER simulation results, as well

as capacity plots for the new DSSTS scheme are presented. The BER simulation results were obtained from the simulation platform described in *Chapter 4*. Lastly, conclusions on the performance of the new DSSTS scheme, as well as possible future work, are presented.

CHAPTER TWO

TRANSMIT DIVERSITY TECHNIQUES

As stated in the introduction, the fundamental phenomenon that makes reliable wireless communications difficult is time varying multipath fading. Improving the information quality or reducing the effective BER in a multipath fading channel is known to be a daunting task. Besides improving the BER through channel coding, an effective technique to combat multipath fading is through transmitter power control [1, 5]. By predistorting the signal at the transmitter, the effects of the channel can be overcome at the receiver if the transmitter knows the channel conditions experienced at the receiver. Problems encountered with this approach are as follows:

- Increased power levels. Increasing the transmitter power is costly due to the high cost involved in developing power amplifiers with large dynamic output power ranges, while at the same time having the ability to respond to fast power fluctuations.
- Lack of knowledge of the channel conditions. The transmitter normally does not have knowledge of the channel conditions. The received information at the receiver can be fed back to the transmitter in order to obtain the channel effects, but this causes a delay in the system. By using feedback, the effective throughput is also reduced and complexity is added to the circuitry at the transmitter, as well as the receiver.

Antenna diversity [6, 8, 22, 23] is a practical and effective method to combat time-varying multipath fading and improve the wireless link quality. In contrast to the classical approach to using multiple receive antennas at the receiver, a new approach of using multiple transmit antennas at the transmitter has recently been developed [3]. This scheme enables wireless cellular networks to use multiple antennas exclusively at the BS and obtain diversity in the uplink as well as downlink, i.e. receive diversity in the uplink, and transmit diversity in the downlink. The use of multiple receive antennas as a receive diversity technique and applying Maximal Ratio Receiver Combining (MRRC) principles are discussed in detail in Appendix A.

This chapter is structured as follows: In *Section 2.1* a general overview of transmit diversity is presented. In *Section 2.2* the transmission model, as well as encoder and decoder structures of ST block coding are presented, followed by ST coding theory in S*ection 2.3*. An analysis of ST coding probability of error is presented in *Section 2.4*, and ST capacity in *Section 2.5*. Lastly, the focus of *Section 2.6* and *Section 2.7* is on ST coding literature.

2.1 TRANSMIT DIVERSITY

Transmit diversity is a method of using multiple transmit antennas to achieve the same diversity as would be gained by using multiple receive antennas. The work done by Alamouti [3], followed by Tarokh *et al*. [22], laid the foundation for research in the field of ST coding, i.e. a method of obtaining transmit diversity. Results obtained from the transmit diversity scheme presented by Alamouti [3], showed that it performed within 3dB of the MRRC scheme employing multiple receive antennas. This was also theoretically derived and verified by Gao *et al*. [24]. It was also shown in [25] that by using four transmit antennas and m receive antennas, performances similar to an $4m$ level MRRC scheme can be achieved.

The following topics are discussed in detail in the Appendix A:

- A mathematical formulation of the encoding, transmission and decoding models.

- Performance comparison between MRRC and transmit diversity employing 2 transmit antennas.
- Implementation issues concerned with the differences observed between the transmit diversity scheme and the MRRC scheme.

2.1.1 Throughput increase of multiple antenna systems

Three mechanisms of multiple antenna systems that can improve the throughput of current communication systems are [25, 26, 27]:

- Beamforming
- Diversity combining
- Spatial multiplexing

Beamforming involves the weighing and summation of signals at each individual antenna to control the angular response of the array. Thus, angular isolation between wanted signals and interference signals is an important advantage of beamforming. This technique can be applied to both transmit as well as receive diversity if knowledge of the channel is available. Another advantage beamforming offers, is an increased SNR at the receiver, thus improving link reliability, and increasing the communications range.

Diversity combining is a well established technique for combating fading, thus improving the mean throughput rate. To obtain diversity by means of multiple antenna systems, the same information is transmitted from different antennas at the same time. Provided that the paths the individual information signals traverses on their way to the receiver antenna array are uncorrelated, reception is improved because if one channel experience a deep fade, the information may still be conveyed through the other channel. Thus, for each additional diversity branch added by adding a new antenna, the probability of the combined received signal being badly attenuated decreases. However, because of the inherent limitations with ST coding theory discussed in *Section 2.3*, only 2 and 4 transmit antennas can obtain both full rate and full diversity. Thus, this study was motivated by the quest for having more than 4 transmit antennas that can achieve both full rate and full diversity in order to exploit diversity gain.

Spatial multiplexing involves the use of *m*-receive antennas to separate the interfering substreams of data that were transmitted from *n*-antennas at the transmitter. In theory, separating the interfering substreams directly, translates to improved BER performance and a corresponding improvement of the data throughput rate.

2.1.2 Capacity and spectral efficiency

The effect of adding multiple antennas does not only increase the throughput rate of a communication system, but also has an effect on the capacity and spectral efficiency of the communications system. Shannon's research [29] on the channel capacity determined the upper bound on the rate of error-free communication in the case of a single band-limited AWGN channel. Extensions to Multiple Input Multiple Out (MIMO) systems that make use of multiple antennas, promise dramatic improvements in spectral efficiency [26, 27]. Recent research [26, 27, 30, 31] has shown that the capacity of a system, employing *n*-transmit and *m*-receive antennas, grows linearly with min(*n*,*m*), but only logarithmically with the SNR. Thus, multiple antennas are a realistic solution of improving the spectral efficiency for communications systems.

2.2 ST CODING AS A TRANSMIT DIVERSITY TECHNIQUE

Tarokh *et al*. [22] generalized Alamouti's transmit diversity scheme of two transmit antennas and proved that it is based on orthogonal designs. This laid the foundation for ST block code designs for both real and complex signal constellations. These ST block codes achieve the maximum possible transmission rate for any number of transmit antennas using real signal constellations, such as Pulse Amplitude Modulation (PAM). For complex signal constellations, such as Phase Shift Keying (PSK) and Quadrature Amplitude Modulation (QAM), ST block codes can theoretically only achieve full rate and full diversity for 2 transmit antenna, whereas ½ of the maximum possible transmission rate for any other number of transmit antennas [14] can be obtained. For specifically 3 and 4 transmit antennas, Tarokh *et al*. [25] showed that ¾ of the maximum transmission rate can be achieved using the orthogonal designs presented in [22].

2.2.1 Transmission model

Suppose the downlink in a cellular environment consists of a BS with *n* antennas and a mobile with *m* antennas. In each time slot *t*, signals c_t^i, i = 1, 2, 3, …, *n* are transmitted from *n* transmit antennas. Assuming a flat fading channel, described in *Chapter 4*, *Section 4.1*, with path gains defined as $h = \mathrm{Re}\{h\} + j \cdot \mathrm{Im}\{h\}$, constant over a frame length *l*, the received signal at antenna *j* at time *t* is

$$r_t^j = \sum_{i=1}^{n} h_{i,j}\, c_t^i + \eta_t^j \tag{2.1}$$

where $h_{i,j}$ is defined as the path gain from transmit antenna *i* to receive antenna *j*. Here η_t is the AWGN defined in Appendix C, *Section C.5*. The average energy of the symbol transmitted from each antenna is scaled by the factor 1/*n*, thus producing unit transmit power and unit receive power at each receive antenna if the channel power is also normalised to unity.

Assuming the availability of perfect Channel State Information (CSI), the receiver computes the decision metric [7]

$$DM = \sum_{t=1}^{l} \sum_{j=1}^{m} \left| r_t^j - \sum_{i=1}^{n} h_{i,j} c_t^i \right|^2 \tag{2.2}$$

over all signals

$$c_1^1, c_1^2, \ldots c_1^n, c_2^1, c_2^2, \ldots c_2^n, \ldots c_l^1, c_l^2, \ldots, c_l^n \tag{2.3}$$

and decides in favour of the signal that minimizes the sum of (2.2).

2.2.2 Encoding algorithm

To elaborate on the transmit diversity scheme, a ST block code is defined by an *l x n* transmission matrix *C*. The matrix *C* consists of linear combinations of *k* variables,

denoted as x_1, x_2, x_3,…,x_k, as well as their conjugates. These variables and conjugates are grouped in such a manner that the matrix is orthogonal [22]. The topic of orthogonality is discussed in *Section 2.3*. For example, C_2^{1rate} represents a code that utilizes two transmit antennas and obtains full rate. C_2^{1rate} can be defined by

$$C_2^{1rate} = \begin{bmatrix} x_1 & x_2 \\ -x_2^* & x_1^* \end{bmatrix} \tag{2.4}$$

i.e., the well known Alamouti matrix proposed in [3]. It is evident from C_2^{1rate} that n = 2, indicating that two transmission antennas are used (seen from the number of columns in C_2^{1rate}) and l = 2, which means that the frame length is equal to 2 symbol periods (seen as the number of rows in C_2^{1rate}).

Assume that transmission occurs in baseband and a signal constellation ν is employed with 2^q signal points, where q denotes the number of bits in a signal point. At time slot t = 1, kq bits from bitstream $b(t)$ arrive at the encoder and are mapped to constellation signals a_1, a_2, a_3,…,a_k of the signal constellation ν. An additional matrix A is then formed by setting x_i = a_i for i = 1, 2, 3, …, k from C. Thus, similar to C, A consists of linear combinations of constellation points and their conjugates, as shown in *Equation (2.5)*.

$$A_2^{1rate} = \begin{bmatrix} a_1 & a_2 \\ -a_2^* & a_1^* \end{bmatrix} \tag{2.5}$$

These constellation signals are transmitted from the n transmit antennas. So, the i'th column of A represents the symbols transmitted from the i'th antenna and the t'th row represents the transmitted symbols at time t. Because of C's orthogonality [22], A is also orthogonal and thus allows a simple decoding process at the receiver. Since l time slots are used to transmit k symbols, $R = k/l$ can be defined as the code rate. For example, in C_2^{1rate}, R = 1.

Other examples are the following ½ rate ST block codes [25]. These codes are orthogonal designs presented in [22].

$$C_3^{1/2\,rate} = \begin{bmatrix} x_1 & x_2 & x_3 \\ -x_2 & x_1 & -x_4 \\ -x_3 & x_4 & x_1 \\ -x_4 & -x_3 & x_2 \\ x_1^* & x_2^* & x_3^* \\ -x_2^* & x_1^* & -x_4^* \\ -x_3^* & x_4^* & x_1^* \\ -x_4^* & -x_3^* & x_2^* \end{bmatrix} \tag{2.6}$$

$$C_4^{1/2\,rate} = \begin{bmatrix} x_1 & x_2 & x_3 & x_4 \\ -x_2 & x_1 & -x_4 & x_3 \\ -x_3 & x_4 & x_1 & -x_2 \\ -x_4 & -x_3 & x_2 & x_1 \\ x_1^* & x_2^* & x_3^* & x_4^* \\ -x_2^* & x_1^* & -x_4^* & x_3^* \\ -x_3^* & x_4^* & x_1^* & -x_2^* \\ -x_4^* & -x_3^* & x_2^* & x_1^* \end{bmatrix} \tag{2.7}$$

Examples of ¾ rate ST block codes are given in *Equations (2.8)* and *(2.9)* [22].

$$C_3^{3/4\,rate} = \begin{bmatrix} x_1 & x_2 & \frac{x_3}{\sqrt{2}} \\ -x_2^* & x_1^* & \frac{x_3}{\sqrt{2}} \\ \frac{x_3^*}{\sqrt{2}} & \frac{x_3^*}{\sqrt{2}} & \frac{-x_1 - x_1^* + x_2 - x_2^*}{2} \\ \frac{x_3^*}{\sqrt{2}} & -\frac{x_3^*}{\sqrt{2}} & \frac{x_2 + x_2^* + x_1 - x_1^*}{2} \end{bmatrix} \tag{2.8}$$

$$C_4^{3/4\,rate} = \begin{bmatrix} x_1 & x_2 & \frac{x_3}{\sqrt{2}} & \frac{x_3}{\sqrt{2}} \\ -x_2^* & x_1^* & \frac{x_3}{\sqrt{2}} & -\frac{x_3}{\sqrt{2}} \\ \frac{x_3^*}{\sqrt{2}} & \frac{x_3^*}{\sqrt{2}} & \frac{\left(-x_1 - x_1^* + x_2 - x_2^*\right)}{2} & \frac{\left(-x_2 - x_2^* + x_1 - x_1^*\right)}{2} \\ \frac{x_3^*}{\sqrt{2}} & -\frac{x_3^*}{\sqrt{2}} & \frac{\left(x_2 + x_2^* + x_1 - x_1^*\right)}{2} & -\frac{\left(x_1 + x_1^* + x_2 - x_2^*\right)}{2} \end{bmatrix} \tag{2.9}$$

2.2.3 Decoding algorithm

Tarokh *et al.* [25] has shown that Maximum Likelihood (ML) decoding of any ST block code can be achieved by using only linear processing at the receiver. The decoding algorithm is explained by means of an example. Consider the ST block code C_2^{1rate} defined in *Equation (2.4)*. Assume that 2^q bits from bitstream *b(t)* arrive at the encoder and select two complex symbols a_1 and a_2, as described in the previous section. These two symbols are simultaneously transmitted from antennas 1 and 2, respectively. At the second time slot, signals $-a_2^*$ and a_1^* are simultaneously transmitted from antennas 1 and 2, respectively.

Then, from *Equation (2.2)*, the ML detection amounts to minimizing the decision metric

$$DM = \sum_{j=1}^{m}\left(\left|r_1^j - h_{1,j}a_1 - h_{2,j}a_2\right|^2 + \left|r_2^j - h_{1,j}a_2^* - h_{2,j}a_1^*\right|^2\right) \tag{2.10}$$

over all possible values of a_1 and a_2.

Expanding *Equation (2.10)* and deleting terms that are independent of the codewords, the following equation is obtained [25].

$$DM = -\sum_{j=1}^{m}\left[r_1^j h_{1,j}^* a_1^* + (r_1^j)^* h_{1,j}a_1 + r_1^j h_{2,j}^* a_2^* + (r_1^j)^* h_{2,j}a_2 - r_2^j h_{1,j}^* a_2 - (r_2^j)^* h_{1,j}a_2^*\right.$$

$$+ r_2^j h_{2,j}^* a_1 + (r_2^j)^* h_{2,j} a_1^* \Big] + \left(|a_1|^2 + |a_2|^2\right) \sum_{j=1}^{m} \sum_{i=1}^{2} \left|h_{i,j}\right|^2 \tag{2.11}$$

which decomposes into two parts, one that is only a function of a_1,

$$DM_{a_1} = -\sum_{j=1}^{m} \left[r_1^j h_{1,j}^* a_1^* + (r_1^j)^* h_{1,j} a_1 + r_2^j h_{2,j}^* a_1 + (r_2^j)^* h_{2,j} a_1^* \right] + |a_1|^2 \sum_{j=1}^{m} \sum_{i=1}^{2} \left|h_{i,j}\right|^2 \tag{2.12}$$

and the other part that is only a function of a_2:

$$DM_{a_2} = -\sum_{j=1}^{m} \left[r_1^j h_{2,j}^* a_2^* + (r_1^j)^* h_{2,j} a_2 - r_2^j h_{1,j}^* a_2 - (r_2^j)^* h_{1,j} a_2^* \right] + |a_2|^2 \sum_{j=1}^{m} \sum_{i=1}^{2} \left|h_{i,j}\right|^2 \tag{2.13}$$

which, for both cases a_1 and a_2, are equivalent to

$$DM_{a_1} = \left| \left[\sum_{j=1}^{m} \left(r_1^j h_{1,j}^* + (r_2^j)^* h_{2,j} \right) \right] - a_1 \right|^2 + \left(-1 + \sum_{j=1}^{m} \sum_{i=1}^{2} \left|h_{i,j}\right|^2 \right) |a_1|^2 \tag{2.14}$$

and

$$DM_{a_2} = \left| \left[\sum_{j=1}^{m} \left(r_1^j h_{2,j}^* - (r_2^j)^* h_{1,j} \right) \right] - a_2 \right|^2 + \left(-1 + \sum_{j=1}^{m} \sum_{i=1}^{2} \left|h_{i,j}\right|^2 \right) |a_2|^2 \tag{2.15}$$

respectively. Thus, minimization of *Equation (2.10)* is equivalent to minimizing *Equation (2.14)* for a_1 and *Equation (2.15)* for a_2.

Note that *Equations (2.14)* and *(2.15)* are similar to Alamouti's scheme shown in *Appendix B, Section B.3*, and thus proves the generalization of his scheme to an arbitrary number of transmit antennas. Also note that *Equation (2.14)* can be written as

$$DM_{a_1} = \left| \tilde{a}_1 - a_1 \right|^2 + \left(-1 + \sum_{j=1}^{m} \sum_{i=1}^{2} \left|h_{i,j}\right|^2 \right) |a_1|^2 \tag{2.16}$$

where $\tilde{a}_1 = \sum_{j=1}^{m} \left(r_1^j h_{1,j}^* + (r_2^j)^* h_{2,j} \right)$. *Equation (2.15)* can be written as

$$DM_{a_2} = \left| \tilde{a}_2 - a_2 \right|^2 + \left(-1 + \sum_{j=1}^{m} \sum_{i=1}^{2} \left| h_{i,j} \right|^2 \right) \left| a_2 \right|^2 \tag{2.17}$$

where $\tilde{a}_2 = \sum_{j=1}^{m} \left(r_1^j h_{2,j}^* - (r_2^j)^* h_{1,j} \right)$.

2.3 ST BLOCK CODING THEORY

In [22], code designs were presented in order to create orthogonal block codes. These design criteria states that a matrix *X* must obey

$$X^H X = \left(\left| x_1 \right|^2 + \cdots + \left| x_n \right|^2 \right) \cdot I \tag{2.18}$$

where *I* is the identity matrix, *X* is a square matrix with *n* columns, X^H is the conjugate transpose of matrix *X* and $x_1, x_2, \ldots, x_n$ is the entries of the first row of matrix *X*. Also note that *n* is the number of transmit antennas used.

The concept of using *Equation (2.18)* in designing a square ST code can best be described by means of an example: Suppose a ST code *X*, using 2 transmit antennas, is to be designed. This code's general form is given by

$$X = \begin{bmatrix} x_{11} & x_{12} \\ x_{21} & x_{22} \end{bmatrix} \tag{2.19}$$

where x_{ij} are complex symbols. Thus $X^H X$ is given by

$$\begin{aligned} X^H X &= \begin{bmatrix} x_{11}^* & x_{21}^* \\ x_{12}^* & x_{22}^* \end{bmatrix} \cdot \begin{bmatrix} x_{11} & x_{12} \\ x_{21} & x_{22} \end{bmatrix} \\ &= \begin{bmatrix} \left| x_{11} \right|^2 + \left| x_{21} \right|^2 & x_{11}^* x_{12} + x_{21}^* x_{22} \\ x_{12}^* x_{11} + x_{22}^* x_{21} & \left| x_{12} \right|^2 + \left| x_{22} \right|^2 \end{bmatrix} \end{aligned} \tag{2.20}$$

By using the design criteria presented in *Equation (2.18)*, the code is only orthogonal if $X^H X$ is diagonal, i.e. when

$$x_{11}^* x_{12} + x_{21}^* x_{22} = 0 \tag{2.21a}$$

and

$$x_{12}^* x_{11} + x_{22}^* x_{21} = 0 \tag{2.21b}$$

By using and rearranging *Equation (2.21a)*, $x_{22} = -x_{11}^* x_{12} / x_{21}^*$. Substituting x_{22} into *Equation (2.19)*, yields X as

$$X = \begin{bmatrix} x_{11} & x_{12} \\ x_{21} & -\dfrac{x_{11}^* x_{12}}{x_{21}^*} \end{bmatrix} \tag{2.22}$$

Also note that a similar result may be obtained by using *Equation (2.21b)*. By setting $x_{21} = -x_{12}^*$ we obtain

$$X = \begin{bmatrix} x_{11} & x_{12} \\ -x_{12}^* & x_{11}^* \end{bmatrix} \tag{2.23}$$

which is well known as the Alamouti matrix (see *Equation (2.4)*). This completes the proof that the Alamouti matrix is an orthogonal block code.

2.4 ST CODING ERROR PROBABILITY

In a flat fading Rayleigh channel, the probability of error for a ST block code based on Alamouti's scheme and utilising M-ary Phase Shift Keying (MPSK) modulation was derived by Gao *et al*. [24]. This probability of error was derived from the Probability Density Function (PDF) of the phase of the received signal. It should also be stated here that, although the procedure given in [24] applies to any M-ary modulation scheme, only

the BPSK and QPSK modulation schemes are given in *Equations (2.24)* and *(2.25)* respectively, as only these apply to this dissertation.

The probability of error for a BPSK ST block code, is defined as [24]

$$P_{e,BPSK\ ST} = \frac{1}{2}\left[1-\mu-\frac{1}{2}\mu\left(1-\mu^2\right)\right] \tag{2.24}$$

and in the case of a QPSK modulation, the probability of error is [24]

$$P_{e,QPSK\ ST} = \frac{1}{2}\left[1-\frac{\mu}{\sqrt{2-\mu^2}}-\frac{\mu\left(1-\mu^2\right)}{\left(2-\mu^2\right)\sqrt{2-\mu^2}}\right] \tag{2.25}$$

where μ is defined as the normalised cross-correlation between two random variables, one that is a function of channel 1, h_1, and the other a function of channel 2, h_2 [24]. The normalised cross-correlation is given by

$$\mu = \sqrt{\frac{\Gamma}{(\Gamma+2)}} \tag{2.26}$$

where $\Gamma = E_b/N_0$ is the SNR per bit.

Equations (2.24) and *(2.25)* were simulated and are plotted in Appendix C, *Section C.8, Figure C.18* in order to compare the two error probability graphs. The probability of error for a flat fading Rayleigh channel (see Appendix C, *Section C.6.2, Equation (C.11)*), is also included as a reference graph. Also note that a 3dB difference exists between the BPSK and QPSK modulation techniques.

2.5 ST CODING CAPACITY

Digital communications using MIMO has recently emerged as one of the most significant technical breakthroughs in modern day communications. In [26] it has been shown that ST codes can achieve phenomenal capacity compared to a traditional single transmit and receive antenna system [29]. In order to define the concept of channel capacity, *Equation (2.1)* is rewritten in matrix form

$$\bar{r} = A\bar{h} + \bar{\eta} \tag{2.27}$$

where A is defined as a ST encoding matrix of transmitted symbols, $\bar{h}$ is the complex channel conditions and $\bar{\eta}$ is the received noise. $\bar{h}$ and $\bar{\eta}$ are defined as

$$\bar{h} = \begin{bmatrix} h_1 \\ \vdots \\ h_n \end{bmatrix}, \qquad \bar{\eta} = \begin{bmatrix} \eta_1 \\ \vdots \\ \eta_n \end{bmatrix} \tag{2.28}$$

However, the standard model used in [26] to derive MIMO channel capacity is

$$\bar{r} = H\bar{a} + \bar{\eta} \tag{2.29}$$

where

- $\bar{a} = [a_1 \cdots a_n]^T$ is the n x 1 vector of the transmitted symbols over n transmit antennas, each assumed to be of equal variance;
- H is the m x n channel matrix;
- $\bar{r}$ is the m x 1 vector of the received signals;
- $\bar{\eta}$ is defined in *Equation (2.28)* and represents a m x 1 vector of AWGN variables.

Thus, in order to use the MIMO channel capacity, *Equation (2.27)*, for ST coding schemes, the following condition must be satisfied:

$$A\bar{h} = H\bar{a} \tag{2.30}$$

By using the MIMO signal model in *Equation (2.29)*, the channel capacity bound of a Single-Input Single-Output system, i.e. the Shannon bound [29], is given by

$$CAP_{SISO}^{n=1,m=1} = \log_2\left(1 + SNR\,|h|^2\right) \tag{2.31}$$

where h is the normalised complex gain of a fixed wireless channel, i.e. $H = h$ in *Equation (2.29)*. In Foschini [26], *Equation (2.31)* was extended to accommodate the use of multiple transmit and receive antennas and hence the MIMO open-loop Shannon capacity of *Equation (2.29)* was derived. This capacity, known as MIMO channel capacity bound, is defined as:

$$CAP_{MIMO}^{n,m} = \log_2 \det\left(I_m + \frac{SNR}{n}\left(HH^H\right)\right) \tag{2.32}$$

where H is a (m x n) fading channel matrix. Note that *Equation (2.31)* and *Equation (2.32)* represents channel capacity bounds. In order to obtain the capacity, one needs to average over all fading states h. In *Chapter 6*, *Figure 6.22*, a plot of the capacity Complementary Cumulative Distribution Functions (CCDFs) for various systems with $n = m$ receive antennas is shown. Notice, as the number of antennas is increased, the capacity increases significantly. In fact, both Foschini [26] and Teletar [27] demonstrated that the capacity in *Equation (2.32)* grows linearly with min(m, n).

With the capacity defined as a random variable by *Equation (2.32)*, the issue of how to best characterise it, arises. Two commonly used methods are the mean capacity [27], and capacity outage [18, 26]. The mean capacity simply takes the expectancy, i.e. the mean of the capacity equations defined in *Equations (2.31)* and *(2.32)*, whereas capacity outage measures (by means of simulation) the probability that the capacity is above a certain capacity threshold. These are often denoted as $CAP_{0.1}$ or $CAP_{0.01}$, meaning that those capacity values are respectively supported 90% or 99% of the time and obtained from the CCDFs. Thus, this method also has an indication of the system reliability. In this study, the method of CCDFs will be used, as most authors tend to make use of this method.

2.6 OVERVIEW OF CURRENT ST CODING LITERATURE

Delay diversity [6] and other related schemes were among the first techniques presented to exploit transmit diversity. Delay diversity is a special case of Space-Time Trellis Coding (STTC) that was later developed by Tarokh *et al*. [32]. The generalized approach combines Trellis Coded Modulation (TCM) with transmit diversity techniques that perform very well in slow fading environments. The only drawback of these codes is that the decoding complexity grows exponentially with the number of antennas. A major contribution that emerged from this work was the rank and determinant criteria that became a benchmark in ST code design. A more structured method of STTC construction, ensuring full diversity, was later presented in [33, 34]. Due to receiver complexity, as stated above, alternative methods to employ effective ST coding was researched. The Alamouti code, given in *Equation (2.4)*, is remarkable for having an elegant and simple linear receiver and became a paradigm in ST block coding. Alamouti's scheme with two transmit antennas was later generalized by Tarokh *et al*. [22, 25], proving that the Alamouti matrix is based on orthogonal designs, which have full diversity and linear ML detectors that decouple the transmitted symbols. Unfortunately, the Hurwitz-Radon theorem showed that square complex linear processing orthogonal designs cannot achieve full diversity and full rate simultaneously for constant symbol constellations, except for the two transmit antenna case [22]. Using this work, a formula for the maximum achievable data rate for square code matrices was derived by Tirkkonen and Hottinen [35]. Several orthogonal codes have been discovered with full diversity for 3 or 4 transmit antennas, but these codes [22, 25] are only ¾ rate codes. As shown in [36, 37], it is possible to design orthogonal, full rate and full diversity complex codes for more than two transmit antennas for specific symbol constellations. For example, 4 transmit antennas obtaining full rate and full diversity, are presented in [36, 37] using constellation phase rotation for specialized PSK and PAM symbol constellations.

Another class of ST codes is the unitary ST modulation [38] and differential unitary modulation [39] that is almost similar to orthogonal codes. These codes use a set of unitary code matrices to represent data. The only drawback of the unitary modulation code

compared to orthogonal codes is that the optimal receiver is more complex than the orthogonal code's receiver. This is due to the fact that the code matrix is not structured by symbols that can be decoupled for detection. These codes are typically non-square and designed for systems where CSI is unknown at the receiver.

The ABBA[1] code presented in [40] and similar codes [18, 41, 42] have full rate, but are quasi-orthogonal and offer a diversity order of only 2. The ST Transmit Diversity-Orthogonal Transmit Diversity (STTD-OTD) code [43] provides some diversity gain by grouping symbols into Alamouti blocks and transforming them using a Walsh-Hadamard matrix. For the 4 transmit antenna case, this orthogonal code has full rate and diversity order 2. Recently, an orthogonal full diversity, full rate ST block code for 4 transmit antennas was presented in [44]. However, perfect knowledge of the channel at the transmitter and receiver is required to cancel Inter-Symbol Interference (ISI) and ensure orthogonality.

It has been shown that full diversity and full rate can be achieved with Generalised Algebraic ST (GAST) codes, which use rotated constellations with a Hadamard transform [45]. In addition, these non-orthogonal codes offer a coding gain over comparable orthogonal codes, especially for large constellations and many transmit antennas. Another code in the literature utilizes ST diversity with unitary constellation rotating precoders [46, 47]. Constellation rotating codes essentially transmit a linear combination of the phase-rotated symbols through one antenna at a time, while leaving the other antennas silent. These codes are capable of achieving full rate and full diversity, but are not orthogonal.

In El Gamal *et al*. [48], an algebraic approach was used to construct new trellis and block codes for BPSK and QPSK modulated systems with an arbitrary number of transmit antennas, which guarantees that the ST code achieves full spatial diversity. These codes are actually convolutional codes, and for that reason do not achieve full rate.

[1] The ABBA code received it's name from the transmission matrix structure, i.e $Matrix = \begin{bmatrix} A & B \\ B & A \end{bmatrix}$

Other recently proposed schemes and research to achieve transmit diversity are:

- A ***Differential Detection Scheme***, proposed by Tarokh *et al*. [49]. This scheme exploits diversity by two transmit antennas when neither the transmitter nor the receiver has access to CSI. A further advantage is that encoding is simple and the receiver can be implemented with low decoding complexity.

- ***Iterative Maximum-likelihood Sequence Estimation for Space-Time Coded Systems***, proposed by Li *et al*. [50], is another scheme to decode ST codes without CSI. This scheme is based on ML sequence estimation and can be used for both quasi-static and non-static fading channels.

- ***Spherical Space-Time Codes***, proposed by Terry *et al*. [51], extends the trellis ST code concept to include signal mappings drawn from a N-dimensional sphere. These signal points are designed to increase the minimum squared distance between points in the constellation, without increasing the average transmit energy.

- ***ST Codes Based on Number Theory***, proposed by Damen *et al*. [52], is a scheme that achieves full data rate over two transmit antennas and 2 symbol periods. A further advantage is that the coding gain outperforms Alamouti's scheme [3] at low and high SNR when the number of transmit antennas is greater than one.

- ***ML Detection and Decoding for ST Codes.*** All the other schemes mentioned concentrate on the optimal code-design for ST coding systems. This method, proposed by Larsson *et al*. [53] takes a unified approach to interference-resistant detection of symbols transmitted over a MIMO channel and optimal (in a ML sense) information transfer from the ST detector to the channel decoder. That is, using soft decision decoding rather than hard decision decoding.

2.7 MIMO SYSTEMS EMPLOYING ST CODES

The advantages, such as mobility of WLAN and portable devices, promise to revolutionise the people's way of living, working and playing. In order to achieve throughputs similar to current Ethernet standards and long range operations, improvements need to be incorporated into WLAN. One such solution is to incorporate multiple antennas.

The use of multiple antennas is most recently introduced to the third generation cellular systems as well as the IEEE 802.16d/e, i.e. WiMAX standards, where the 802.16d standard is intended for static applications and the 802.16e standard for mobile applications. The mayor advantage of using multiple antennas at either side of the communication link is an improvement in link reliability and throughput. Until recently, antenna arrays were considered to be an obstacle, however in the microwave band (> 5GHz), the use of dual polar antennas solves the problem of compact ergonomic packaging of MSs. These improvements will enable WLAN to be able to compete with current wired Ethernet standards, with the added advantage of a cable free environment. However, besides the improvements in throughput and link reliability, security, affordability and energy efficiency are also areas that have to be addressed in order to compete with wired technologies.

Current WLANs, such as the IEEE 802.11a or IEEE 802.11g standards, offer a peak rate of 108 Mbps at the physical layer. However, at higher order layers, such as the Medium Access Control (MAC) layer, the average throughput is typically less than 20Mbps.

As stated in *Section 2.1.2*, extensions to MIMO systems that make use of multiple antenna systems, promise dramatic improvements in spectral efficiency. Thus, multiple antennas are a realistic solution for improving the spectral efficiency for future WLANs.

CHAPTER THREE

SPREAD SPECTRUM MODULATION TECHNIQUES

SS technologies have been incorporated in numerous fields over recent years. In the military environment, Frequency Hopped Spread Spectrum (FH-SS) has been used extensively for robustness against jamming, while in telecommunications, such as power line communications and wireless services (voice and data), DS-SS has also been used extensively. To elaborate on the field of wireless cellular networks, the ITU established a suite of standards, collectively called IMT-2000. This standard is the driving force of the developments for the enhanced 3G standards in order to supply the current and future needs of wireless services. Particularly the 3GPP and 3GPP2 are developing the UMTS technologies and cdma2000 respectively, which in fact are based upon SS systems. One of the main challenges in the 3G evolution is the improvement of the downlink capacity, and for this reason one of the development directions moved to SS systems.

Further advantages provided by SS systems are, amongst others:

- Increased user capacity
- Ability of interfering signal rejection
- Multiple Access Interference (MAI) rejection capability
- Resistance to multipath fading

Modulation and demodulation techniques strive to achieve greater power and/or bandwidth efficiency in wireless channels. Since bandwidth is a limited resource, one of the primary design objectives of most modulation schemes is to minimize the required transmission bandwidth. SS techniques, on the other hand, employ a transmission bandwidth that is several orders of magnitude greater than the minimum required signal bandwidth. While this system is very bandwidth inefficient for a single user, the advantage of SS is that many users can simultaneously use the same bandwidth without significantly interfering with one another. Besides the power control problems experienced with SS systems, and the substantial prize paid in receiver complexity and processing power, SS systems become bandwidth efficient in a multiple-user environment.

Apart from occupying a very large bandwidth, SS signals are pseudorandom and have noise-like properties when compared with the digital information data. The spreading waveform is controlled by a spreading sequence or spreading code, which is a sequence that appears to be random, but can be reproduced in a deterministic manner by intended receivers. SS signals are demodulated at the receiver through cross-correlation with a locally generated version of the pseudorandom carrier. Cross-correlation with the correct spreading sequence despreads the SS signal and restores the modulated message in the same narrow-band as the original data, whereas cross-correlating the signal from an undesired user results in MAI at the receiver output.

SS modulation has many properties that make it particularly well suited for use in the mobile radio environment. The most important advantage is its inherent interference rejection capability. In the case of DSSS each user is assigned a unique spreading code which is approximately orthogonal to the codes of other users. The receiver can separate each user, based on their codes, even though they occupy the same spectrum at all times (note that this is

not the case with FH-SS). This implies that, up to a certain number of users, interference between SS signals using the same frequency is negligible. A general rule of thumb is that approximately 10% of the available spreading sequence family may be used before excessive MAI will occur, resulting in rapid receiver performance degradation. Not only can a particular SS signal be recovered from a number of other SS signals, it is also possible to recover information from a SS signal even when a narrowband interferer jams it. Since narrowband interference affects only a small portion of the SS signal, it can easily be removed through notch filtering without much loss of information [6].

Resistance to multipath fading [1, 6, 7] is another fundamental reason for considering SS systems for wireless communications, and in particular, this dissertation. It is known that wideband signals are frequency selective. Since the transmitted SS signals have uniform energy over a very large bandwidth, theoretically, only a small portion of the spectrum will undergo fading at any given time. Viewed in the time domain, the multipath resistance properties are due to the fact that the delayed versions of the transmitted spreading code sequence will have poor correlation with the original spreading code sequence, and will thus appear as another uncorrelated user, which is suppressed by the receiver. That is, as long as the multipath channel induces at least one chip delay, the multipath signals will arrive at the receiver such that they are shifted in time by at least one chip from the intended signal. The correlation properties of spreading code sequences are such that this slight delay causes the multipath to appear uncorrelated with the intended signal, so that the multipath contributions appear invisible to the desired received signal. SS systems are not only resistant to multipath fading, but they can also exploit the delayed multipath components to improve the performance of the system. This can be done by using a RAKE receiver that anticipates multipath propagation delays of the transmitted SS signal and combines the information obtained from several resolvable multipath components to form a stronger version of the signal. A RAKE receiver consists of a bank of correlators, each of which correlates with a particular multipath component of the desired signal. The correlator outputs may be weighted according to their relative strengths and summed, using maximum ratio receive combining methods to obtain the final signal estimate. For in depth discussions on RAKE receivers, see [6, 11].

This chapter is structured as follows: In *Section 3.1* a general overview of PN sequences is presented, followed with CSSs in *Section 3.2 and* Walsh Sequences in *Section 3.3*. In *Section 3.4* DS-SS theory is presented, followed with DS-SS probability of error theory in S*ection 3.5*. Space-Time Spreading (STS) theory is presented in *Section 3.6*, and lastly, the focus of *Section 3.7* is a literature study of ST coding, combined with CDMA technology.

3.1 SPREADING SEQUENCES

With SS modulation techniques, spreading codes are used to expand the bandwidth of the transmitted signal. The following are some of the different types of spreading codes commonly used:

- PN sequences
- Gold- and Kasami sequences
- Walsh sequences
- Complex Spreading sequences (CSS)

A PN or pseudorandom sequence is a binary sequence with an autocorrelation that resembles, over a period, the autocorrelation of a random binary sequence. Its autocorrelation also roughly resembles the autocorrelation of bandlimited white noise. Although it is deterministic, a PN sequence has many characteristics that are similar to those of random binary sequences, such as having a nearly equal number of zeros and ones, very low correlation between shifted versions of the sequence, very low cross-correlation between any two sequences, etc. PN sequences of length $N = 2^m-1$, generated by a linear feedback register of length m, are generally known as maximal length or m-sequences. PN sequences with improved periodic cross-correlation properties over maximal length sequences have been defined by Gold [54]. These codes are the well known Gold-sequences.

Walsh spreading codes are designed such that they do not interfere with each other in an ideal real life environment and are generally designed using the Hadamard matrix (an in depth discussion on the Hadamard matrix is presented in *Section 3.3*). However, orthogonality between the codes requires the codes to be time synchronized, i.e. they are only perfectly

orthogonal at zero relative time shifts and requires perfect chip synchronisation. Therefore orthogonal spreading codes are only used in the downlink of cellular 2.5G and beyond cellular systems. An example of an orthogonal spreading code is the Walsh-derived Orthogonal Variable Spreading Factor (OVSF) codes [11] used in the 3GPP and 3GPP2 standards.

Since the introduction of SS, binary spreading sequences have exhaustively been researched with DS-SS applications. Interest recently started to shift towards using non-binary and CSSs because of potential larger sets of sequences and improved cross-correlation properties compared to binary spreading sequences. Two mayor advantages of using CSSs in future 4G cellular systems are the possibility to transmit Constant Envelope (CE) and even Single Sideband (SSB) [55, 56] transmitter output signals. See *Section 3.2* for details regarding the CSSs used in this dissertation.

3.2 COMPLEX SPREADING SEQUENCES

This section briefly describes the filtered and un-filtered CSS families considered in this study.

3.2.1 Unfiltered Sequences

Zadoff-Chu Sequences

Zadoff-Chu (ZC) CSSs is a subclass of General Chirp-like (GCL) CSSs [57], which is generated and characterised as follows: Let $\bar{S}_{ZC}^{q} = \left\{S_{ZC}^{q}[0], S_{ZC}^{q}[1], \cdots, S_{ZC}^{q}[M_{seq}-1]\right\}$ represent the vector of chips of the q^{th} length-M_{seq} unfiltered continuous-time ZC sequence $S_{ZC}^{q}(t)$. With $j=\sqrt{-1}$, the i^{th} chip in this sequence is determined as follows [59], [60]:

$$S_{ZC}^{q}[i] = \begin{cases} \exp\left(j\dfrac{\pi \cdot a \cdot i^{2}}{M_{seq}}\right) & \text{if } M_{seq} \text{ is even} \\ \exp\left(j\dfrac{\pi \cdot a \cdot i(i+1)}{M_{seq}}\right) & \text{if } M_{seq} \text{ is odd} \end{cases} \tag{3.1}$$

where the sequence number a can only take on integer values relatively prime to M_{seq}. As such, the family size for length-M_{seq} ZC CSSs is calculated as follows:

$$M_{fam} = 1 + \sum_{a=2}^{M_{seq}-1} \begin{cases} 1 & if\ M_{seq} \bmod(a) \neq 0 \\ 0 & if\ M_{seq} \bmod(a) = 0 \end{cases} \tag{3.2}$$

Hence, the largest ZC CSS families are obtained when M_{seq} is an odd prime number. In such a case the family size is $M_{fam} = M_{seq}$ -1 [60].

Quadriphase Sequences

Quadriphase (QPH) sequences are closely related to binary sequences. A length- M_{seq} QPH sequence's chip vector $\bar{S}^q_{QPH} = \left\{S^q_{QPH}[0], S^q_{QPH}[1], \cdots, S^q_{QPH}[M_{seq}-1]\right\}$ is constructed using two length-M_{seq} binary sequences' chip vectors, denoted as $\bar{S}^q_A = \left\{S^q_A[0], S^q_A[1], \cdots, S^q_A[M_{seq}-1]\right\}$ and $\bar{S}^q_B = \left\{S^q_B[0], S^q_B[1], \cdots, S^q_B[M_{seq}-1]\right\}$, respectively. Calculation of the i^{th} chip of the QPH sequence is accomplished as follows [60]:

$$S^q_{QPH}[i] = \frac{1}{2\sqrt{2}}(1+j)S^q_A[i] + \frac{1}{2\sqrt{2}}(1-j)S^q_B[i] \tag{3.3}$$

It follows that each chip in the QPH sequence will have a value from the complex 4-symbol alphabet $\left\{\frac{1}{\sqrt{2}}+\frac{j}{\sqrt{2}}, \frac{1}{\sqrt{2}}-\frac{j}{\sqrt{2}}, -\frac{1}{\sqrt{2}}+\frac{j}{\sqrt{2}}, -\frac{1}{\sqrt{2}}-\frac{j}{\sqrt{2}}\right\}$, if the binary sequences' chip vectors $\bar{S}^q_A$ and $\bar{S}^q_B$ have chips from the antipodal alphabet $\{-1;1\}$. For *Alltop*-type QPH sequences [60], the family size is given as $M_{fam} = M_{seq}$ - 1, with the sequence length M_{seq} limited to prime values. Furthermore, using Gold binary sequences for $\bar{S}^q_A$ and $\bar{S}^q_B$ is a popular approach [61]. Since QPH sequences are binary in nature, it follows that their complex envelopes will not be constant.

3.2.2 Filtered Sequences

DSB CE-LI-RU Filtered GCL Sequences

It has been shown that ZC sequences contain all the frequencies in the range [0;M_{fam} / T_{chip}) [Hz], with T_{chip} the duration of a chip [61]. Thus, the bandwidth of such sequences are a function of the family size. In order to bandlimit $S_{ZC}^{q}(t)$ and remove its dependency on the sequence index a, a mod(2π) phase constraint can be incorporated, resulting in a *Chu* sequence's chip vector denoted as $\bar{S}_{Chu}^{q} = \left\{S_{Chu}^{q}[0], S_{Chu}^{q}[1], \cdots, S_{Chu}^{q}[M_{seq}-1]\right\}$ [59], [60]. The i^{th} chip of a *Chu* sequence is determined as follows:

$$S_{Chu}^{q}[i] = \begin{cases} \exp\left(j\dfrac{\pi \cdot a \cdot i^{2}}{M_{seq}}\right)\bmod(2\pi) & \text{if } M_{seq} \text{ is even} \\ \exp\left(j\dfrac{\pi \cdot a \cdot i(i+1)}{M_{seq}}\right)\bmod(2\pi) & \text{if } M_{seq} \text{ is odd} \end{cases} \tag{3.4}$$

It has been shown [60] that the bandwidth of *Chu* sequences are 1/T_{chip} [Hz]. Double Side Band Constant Envelope Linearly Interpolated Root-of-Unity (DSB CE-LI-RU) filtered GCL sequences are obtained by filtering $S_{Chu}^{q}[i]$ with a *linearly interpolating root-of-unity filter* [62] in order to achieve the minimum Nyquist bandwidth of 1/(2.T_{chip}) [Hz]. The family size of such sequences is also given by *Equation (3.2)*. Furthermore, these sequences exhibit constant complex envelopes.

ABC Sequences

Analytic Bandlimited Complex (ABC) sequences are generated by appropriately modifying the previously defined DSB CE-LIRU filtered GCL sequences in order to produce an injective function, as described in [56]. When used in balanced QPSK structures, ABC sequences [56] exhibit analytical properties, i.e. a SSB DS/SSMA signal is obtained after modulation onto the in-phase and quadrature carriers [60]. As with ZC and DSB CE-LI-RU filtered GCL sequences, the family size of ABC CSSs is determined using *Equation (3.2)*.

3.3 WALSH SEQUENCES

Walsh spreading codes are obtained from Hadamard matrices. A Hadamard matrix M_j is a j x j matrix (j is an even integer) of 1s and 0s with the property that any row differs from any other row in exactly $\frac{1}{2}j$ positions. One row of the matrix contains al zeros and the other rows contain $\frac{1}{2}j$ ones and $\frac{1}{2}j$ zeros. For j = 2, the Hadamard matrix is

$$M_2 = \begin{bmatrix} 0 & 0 \\ 0 & 1 \end{bmatrix} \tag{3.5}$$

Furthermore, from M_j, a Hadamard matrix of M_{2j} can be generated according to the relation

$$M_{2j} = \begin{bmatrix} M_j & M_j \\ M_j & \overline{M}_j \end{bmatrix} \tag{3.6}$$

where $\overline{M}_j$ denotes the complement (0s replaced by 1s and vice versa) of M_j. Thus, by substituting *Equation (3.5)* into *Equation (3.6)*, *Equation (3.7)* is obtained.

$$M_4 = \begin{bmatrix} 0 & 0 & 0 & 0 \\ 0 & 1 & 0 & 1 \\ 0 & 0 & 1 & 1 \\ 0 & 1 & 1 & 0 \end{bmatrix} \tag{3.7}$$

By the repeated application of *Equation (3.6)*, Hadamard matrix's with block length of $\varsigma = 2^i$ can be generated, where i is a positive integer. Once a Hadamard matrix is constructed, a Walsh code is obtained by selecting, as code words, the rows of a Hadamard matrix and the number of columns in the Hadamard matrix determines the length of the Walsh spreading code. For example, 2 Walsh spreading codes of length, ς = 4 from *Equation (3.7)* is

$$Code1 = 0\,1\,0\,1 \tag{3.8}$$

$$Code2 = 0\,0\,1\,1 \tag{3.9}$$

3.3.1 Correlation properties

The major tasks of any spreading code used in wireless communications systems are the following:

- Spreading the bandwidth of the modulated signal to a larger bandwidth, and
- to distinguish between the spreading sequences of different users' signals that utilise the same transmission bandwidth in a multiple-access scheme.

To meet these requirements, the sequences need special correlation properties, i.e. periodic auto-correlation, and periodic cross-correlation. Periodic autocorrelation, $R_a(\tau)$, in general, is defined by the integral

$$R_a(\tau) = \int_{-\infty}^{\infty} f(t) \cdot f(t-\tau) dt \qquad (3.10)$$

It is a measure of the similarity between a signal $f(t)$ and a τ-second time shifted replica of itself. In other words, the auto-correlation function is a plot of all time shifts τ, of $f(t-\tau)$ correlated with itself and is mostly used for synchronization purposes (see *Figure 3.1*).

From *Figure 3.1* it is evident that the periodic auto-correlation properties of Walsh sequences are not satisfactory. The multiple auto-correlation peaks over one sequence length, *N*, observed in *Figure 3.1* will lead to synchronisation ambiguities in the receiver. A satisfactory result would have been one single spike in time and the rest of the periodic autocorrelation function zero. In the case of the DSSTS scheme presented in *Chapter 5*, perfect synchronization is assumed and the simulations are not performed in a multipath environment, making the periodic auto-correlation unimportant. Thus, no echoes are received at the receiver and the auto-correlation is for this reason not a critical design factor. However, in the case of the SSTD scheme presented in *Chapter 5*, a multipath flat fading channel was considered and for this reason, Walsh spreading codes were not used in the SSTD scheme.

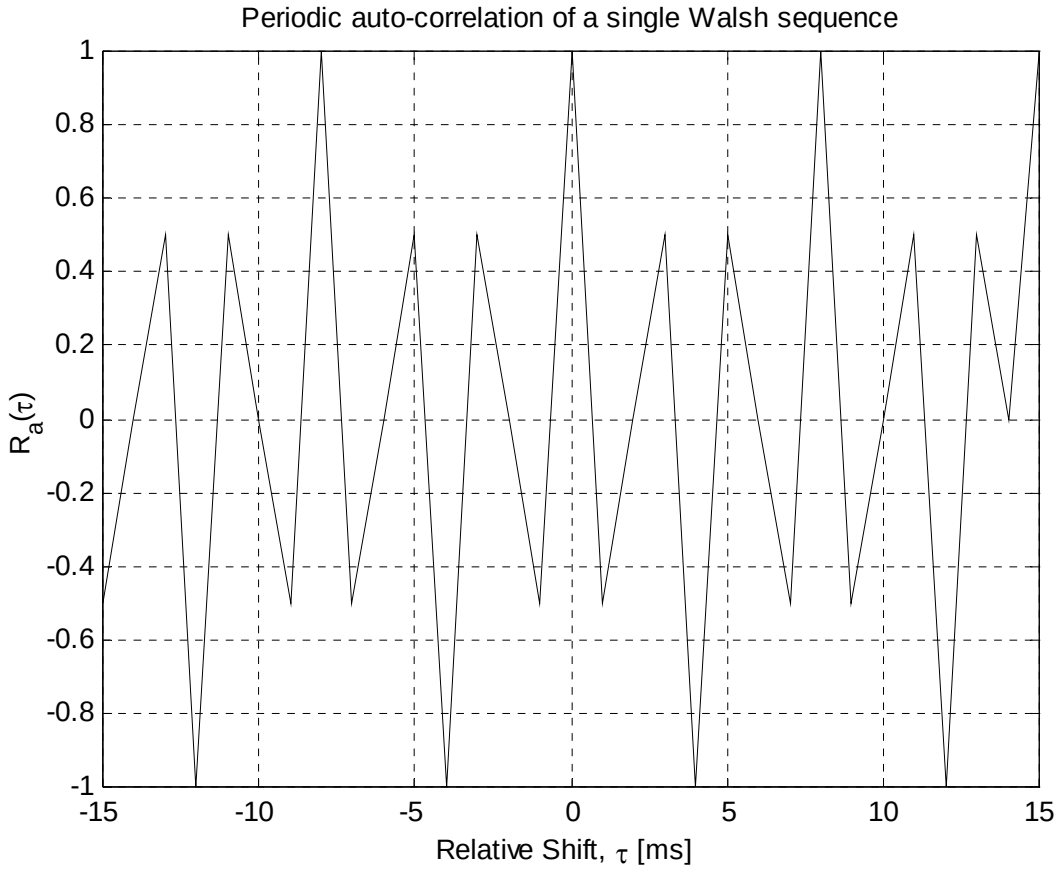

Figure 3.1. Periodic auto-correlation of a length *N* = 16 Walsh sequence taking one sample per chip.

The periodic cross-correlation between different antennas is rather an important design factor in both the DSSTS scheme as well as the SSTD scheme, because of the multi-antenna scenario. Periodic cross-correlation $R_c(\tau)$, is defined as the correlation of two different signals $f(t)$ and $g(t)$, and is defined as

$$R_c(\tau) = \int_{-\infty}^{\infty} f(t) \cdot g(t-\tau) dt \qquad (3.11)$$

The periodic cross-correlation function is a measure of the Walsh codes to reject other Walsh codes in a multi-user environment (see *Figure 3.2*). From *Figure 3.2* it is evident that the Walsh sequences have excellent periodic cross-correlation properties, meaning that two codes do not interfere with each other for all time shifts τ, since they are perfectly orthogonal, i.e. super-orhogonal in the cross-correlation function if only one sample per chip are taken. However, this result drastically deteriorates when multiple samples per chip is taken [63].

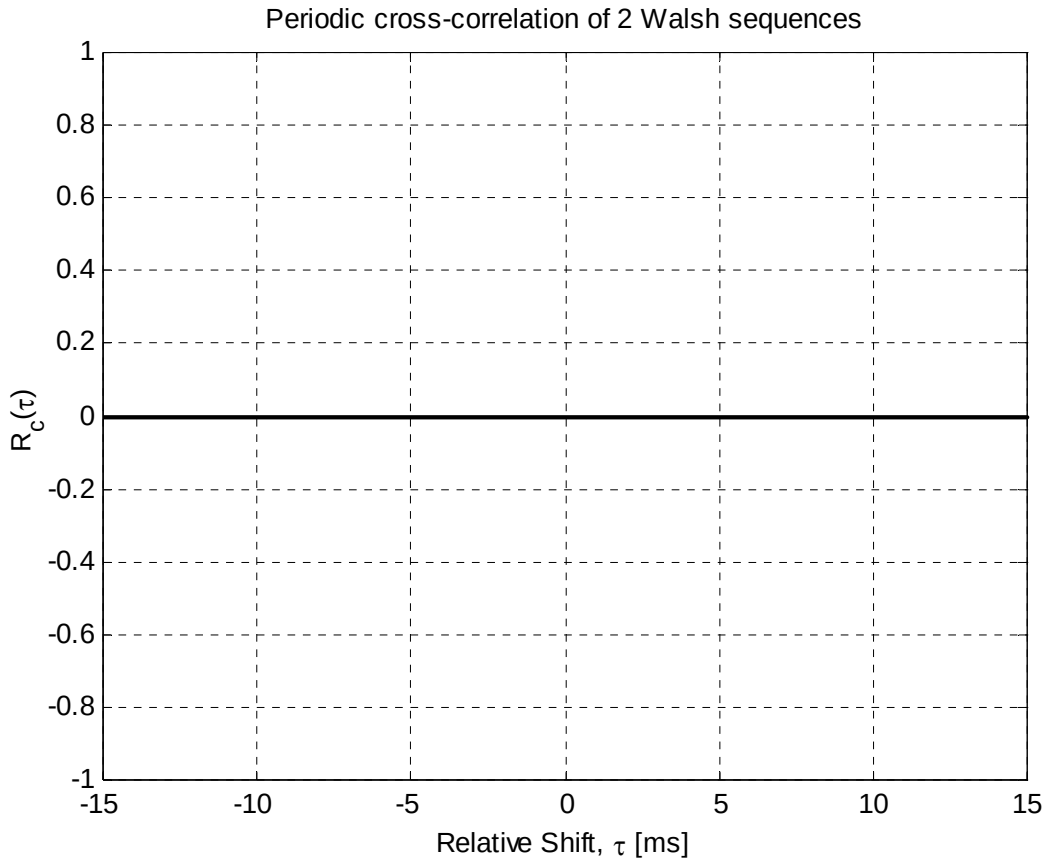

Figure 3.2 Periodic cross-correlation of two different length *N* = 16 Walsh sequences taking one sample per chip.

3.4 DIRECT SEQUENCE SPREAD SPECTRUM

A DS-SS system spreads the baseband data by directly multiplying the baseband data pulses with a pseudo-noise sequence that is produced by a pseudo-noise code generator as described in *Sections 3.1* and *3.3*. A single pulse or symbol of the spreading waveform is called a chip. The received SS signal for a single user in a DS-SS system can be represented as

$$s_{ss}(t) = \sqrt{\frac{2E_s}{T_s}}\,\mathrm{Re}\{b(t)g(t)\exp(-j2\pi f_c t + \theta)\} \qquad (3.12)$$

where E_s is the energy in the transmitted waveform, $b(t)$ is the information bit stream, $g(t)$ is the spreading sequence, f_c is the carrier frequency, and θ is the carrier phase angle at t = 0. The data waveform is a time sequence of non-overlapping rectangular pulses, each of which

has an amplitude equal to +1 or -1. Each symbol in *b(t)* represents a data symbol and has duration T_s. Each pulse in *g(t)* represents a chip, which is usually rectangular with an amplitude equal to +1 or -1, and has a duration of T_c. The transitions of the data symbols and chips occur in such a way that the ratio T_s to T_c is an integer. If B_{ss} is the bandwidth of $s_{ss}(t)$ and *BW* is the bandwidth of a conventionally modulated signal $\mathrm{Re}\{b(t)\exp(-j2\pi f_c t+\theta)\}$, the spreading due to *g(t)* results in $B_{ss} \gg BW$.

Assuming that code synchronisation has been achieved at the receiver, the received signal passes through a wideband filter and is multiplied by a local replica of the spreading sequence *g(t)*. If *g(t)* = +/- 1, then $g^2(t) = 1$, and this multiplication yields the despreaded signal $s_1(t)$ given by

$$s_1(t) = \sqrt{\frac{2E_s}{T_s}}\,\mathrm{Re}\{b(t)\exp(-j2\pi f_c t+\theta)\} \qquad (3.13)$$

at the input of the demodulator. Because $s_1(t)$ has the form of a BPSK signal, a coherent PSK demodulator can be used to extract *b(t)*. See *Figure 3.3* for a graphical representation of the waveforms and spectrums before and after spreading.

Figure 3.4 shows the received spectra of the desired SS signal and the interference at the output of the receiver wideband filter. Multiplication by the spreading waveform produces the spectra of *Figure 3.4* at the demodulator input. The signal bandwidth is reduced to *BW*, while the interference energy is spread over a RF bandwidth exceeding B_{ss}. The filtering action of the demodulator removes most of the interference spectrum that does not overlap with the signal spectrum. Thus, most of the original interference energy is eliminated by spreading and minimally affects the desired receiver signal. An approximate measure of the interference rejection capability is given by the ratio B_{ss} / *BW*, which is equal to the Processing Gain (PG) defined as

$$PG = \frac{T_s}{T_c} = \frac{R_c}{R_s} = \frac{B_{ss}}{2R_s} \qquad (3.14)$$

Thus, the greater the PG of the system, the greater will be its ability to suppress in-band interference.

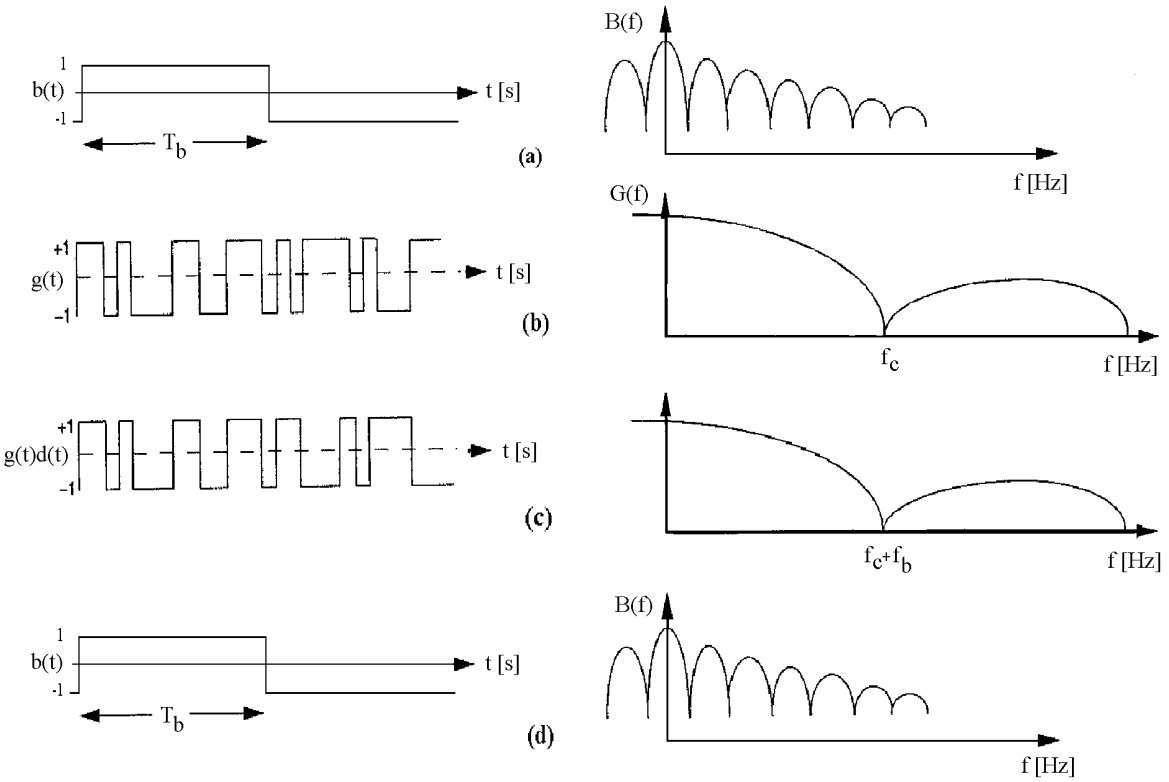

Figure 3.3. Representation of the time multiplication of a BPSK modulated signal with a spreading sequence and the resulting spectrums.

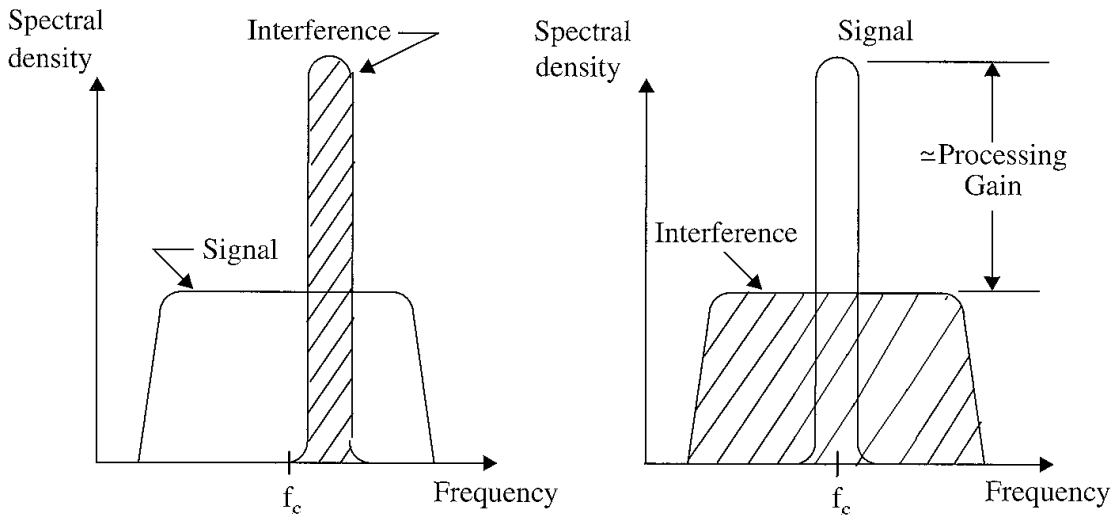

Figure 3.4. Spectra of desired received signal with interference at the wideband filter output and correlator output after despreading. Taken from [1].

3.5 PROBABILITY OF ERROR IN DS SPREAD SPECTRUM SYSTEMS

3.5.1 AWGN channel conditions

Assuming coherent demodulation in AWGN channel conditions , the probability of error for a DS-SS system employing binary PSK, is identical to the probability of error for conventional narrowband (unspreaded) binary PSK [64], that is

$$P_{e,DS-SS}^{AWGN} = Q\left(\sqrt{\frac{2E_b}{N_0}}\right) \tag{3.15}$$

where E_b denotes the energy per bit. See *Figure 3.5* for theoretical SS BER performance in AWGN channel conditions vs. flat fading channel conditions.

3.5.2 Slow Rayleigh flat fading channel conditions

Assuming coherent demodulation in slow Rayleigh flat fading channel conditions, the probability of error for a DS-SS system employing binary PSK is [17]:

$$P_{e,DS-SS}^{Rayleigh} = \frac{1}{2}\left(1-\sqrt{\frac{\frac{\bar{E}_b}{N_0}}{1+\frac{\bar{E}_b}{N_0}}}\right) \tag{3.16}$$

where $\bar{E}_b$ denotes the average energy per bit. However, this assumption is based on the fact that the fading is so slow that the Rayleigh distributed fading amplitude may be regarded as a constant over at least one symbol interval T_s. For purposes of comparison, SS's BER performance in slow Rayleigh fading channel conditions is also included in *Figure 3.5*. At this stage, the reader may wonder why DS-SS will experience flat fading? The answer lies in the fact that the DS-SS is not used for multiple users in this dissertation, but to create

orthogonality between the transmit antennas for a single user, therefore short spreading codes justifies the assumption of the signal bandwidth being smaller than the coherence bandwidth of the channel (see Appendix C, *section C.4.1*).

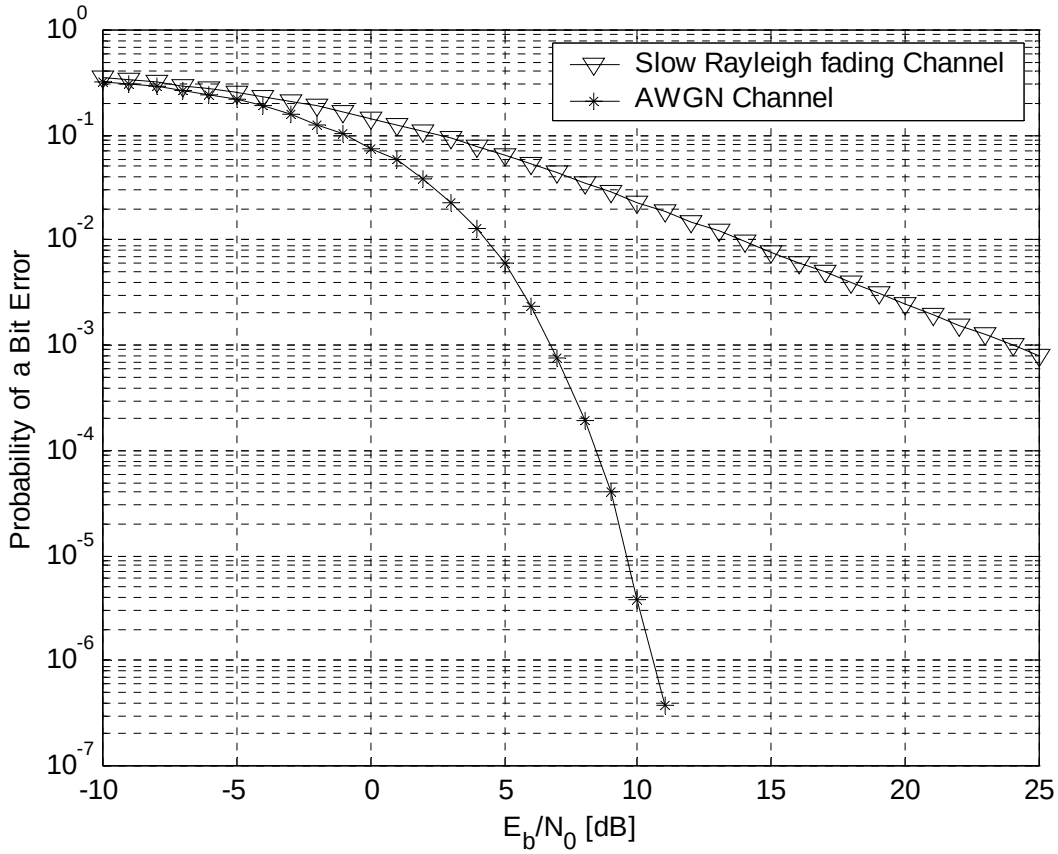

Figure 3.5. Theoretical Probability of Error vs. E_b/N_0 of a DS-SS system in flat fading channel conditions, compared to AWGN performance.

3.5.3 Multipath fading channel conditions

In [8] an approximate bit error probability is derived for RAKE receiver based DS/SSMA systems operating in a multipath environment assuming L different paths, or independent fading replicas, each having a path gain β_i. Note that the condition [4], $\sum_{i=1}^{L}(\beta_i)^2 = 1$ must be satisfied in order for the channel's output power to be equal to the input power. The probability of error is then given as

$$P_{e,DS-SS}^{multipat} = \frac{1}{2}\sum_{i=1}^{L}\left[\left(\prod_{a=1,a\neq i}^{L}\frac{\delta^i}{\delta^i-\delta^a}\right)\left(1-\sqrt{\frac{\delta^i}{1+\delta^i}}\right)\right] \tag{3.17}$$

where $\delta^i = E\left[\left(\beta_i\right)^2\right]\frac{E_b}{N_0}$.

3.6 SPACE- TIME SPREADING

STS, proposed by Hochwald *et al*. [65], is a transmit diversity technique that improves the downlink performance by using two transmit antennas at the BS and one or more antennas at the MS. However, it differs from other transmit diversity techniques in the sense that symbols are spread over multiple antennas in a way similar to ST coding. Thus, STS is a transmit diversity scheme that is based on orthogonal ST coding and combined with DS-SS. It should also be stated here that STS for the two transmit and single receive antennas was included in release A of the IS-2000 WCDMA standard.

3.6.1 General theory, real data symbols

For simplicity, assume that the normalisation factor $\sqrt{\frac{2E_s}{T_s}}$ is dropped from *Equation (3.12)* as well as the $\mathrm{Re}\{\exp(-j2\pi f_c t+\theta)\}$ term, as these two factors does not have an influence on the mathematical analysis here. *Equation (3.12)* can then be rewritten as

$$S = G \cdot B \tag{3.18}$$

where $S = s_{ss}(t)$, $G = g(t)$ and $B = b(t)$ defined in *Equation (3.19)*. Assuming n = 2, (i.e. 2 transmitter antennas are used) *Equation (3.18)* can be used in the following manner. G is a 2ς x 2 matrix consisting of two distinct spreading codes of length 2ς each. B is a 2x2 matrix consisting of the two baseband symbols to be spreaded and transmitted and S is the transmitted signals over the two transmit antennas, also represented by a 2ς x 2 matrix. Thus,

$$G = [\bar{g}_1 \quad \bar{g}_2], \qquad B = \begin{bmatrix} b_1 & b_2 \\ b_2 & -b_1 \end{bmatrix} \tag{3.19}$$

By using the channel model defined in *Chapter 2, Section 2.5, Equation (2.27)*, the received signal $\bar{r}$ at the single receive antenna is

$$\bar{r} = S\bar{h} + \bar{\eta} = GB\bar{h} + \bar{\eta} \tag{3.20}$$

where $\bar{h}$ is the complex channel conditions and $\bar{\eta}$ is the received noise. $\bar{h}$ and $\bar{\eta}$ are defined as

$$\bar{h} = \begin{bmatrix} h_1 \\ \vdots \\ h_n \end{bmatrix}, \qquad \bar{\eta} = \begin{bmatrix} \eta_1 \\ \vdots \\ \eta_n \end{bmatrix} \tag{3.21}$$

respectively. See *Chapter 4* for an in depth discussion on complex channel conditions, as well as the received noise. To recover the original transmitted signals, *Equation (3.20)* has to be despreaded by multiplying *Equation (3.20)* with G^H, which is the complex transpose of G. Note here that G^H is used in the case of a matched filter demodulator, where G^T can be used instead if detection is done by an integrate and dump demodulator. Because G^H can be used for both demodulator methods, this notation is used. Thus, multiplying *Equation (3.20)* with G^H, it can be written as

$$\begin{bmatrix} \bar{g}_1^H & \bar{g}_2^H \end{bmatrix} \bar{r} = \begin{bmatrix} \bar{g}_1^H & \bar{g}_2^H \end{bmatrix} \left(S\bar{h} + \bar{\eta} \right) = B\bar{h} + \begin{bmatrix} \bar{g}_1^H \eta_1 \\ \bar{g}_2^H \eta_2 \end{bmatrix} \tag{3.22}$$

$$= \begin{bmatrix} b_1 & b_2 \\ b_2 & -b_1 \end{bmatrix} \begin{bmatrix} h_1 \\ h_2 \end{bmatrix} + \bar{\upsilon}$$

$$\begin{bmatrix} \bar{g}_1^H & \bar{g}_2^H \end{bmatrix} \bar{r} = \begin{bmatrix} h_1 & h_2 \\ -h_2 & h_1 \end{bmatrix} \begin{bmatrix} b_1 \\ b_2 \end{bmatrix} + \bar{\upsilon}$$

$$= H\bar{b} + \bar{\upsilon} \tag{3.23}$$

where

$$H = \begin{bmatrix} h_1 & h_2 \\ -h_2 & h_1 \end{bmatrix}, \quad \bar{b} = \begin{bmatrix} b_1 \\ b_2 \end{bmatrix}, \quad \bar{\upsilon} = \begin{bmatrix} \bar{g}_1^H \eta_1 \\ \bar{g}_2^H \eta_2 \end{bmatrix} \tag{3.24}$$

Note that H can be used for the calculation of channel capacity to satisfy the condition stated in *Chapter 2, Section 2.5, Equation (2.30)*. The substreams are obtained by left-multiplying *Equation (3.23)* by H^H. In general, for n-fold diversity with n transmit antennas, the key identity that allows each user to decode each substream independently of others is

$$\mathrm{Re}\{H^H H\} = \bar{h}^H \bar{h} \cdot I \tag{3.25}$$

as described in *Section 2.3*, *Equation (2.18)*. Note that the $\mathrm{Re}\{\bullet\}$ term is included because only real data symbols are used. Thus, after multiplying *Equation (3.23)* with H^H the decoded substreams are

$$\begin{aligned} \begin{bmatrix} \bar{g}_1^H & \bar{g}_2^H \end{bmatrix} \bar{r} &= H^H H \bar{b} + H^H \bar{\upsilon} \\ &= \begin{bmatrix} |h_1|^2 + |h_2|^2 & h_1 h_2 - h_2 h_1 \\ h_2 h_1 - h_1 h_2 & |h_1|^2 + |h_2|^2 \end{bmatrix} \bar{b} + H^H \bar{\upsilon} \end{aligned} \tag{3.26}$$

Thus, taking only the real part of *Equation (3.26)*, results in

$$\begin{bmatrix} \bar{g}_1^H & \bar{g}_2^H \end{bmatrix} \bar{r} = \begin{bmatrix} |h_1|^2 + |h_2|^2 & 0 \\ 0 & |h_1|^2 + |h_2|^2 \end{bmatrix} \bar{b} + H^H \bar{\upsilon} \tag{3.27}$$

which in fact proves *Equation (3.25)*, and shows that the transmitted symbols $\bar{b} = \begin{bmatrix} b_1 \\ b_2 \end{bmatrix}$ are successfully decoded.

3.6.2 General theory, complex data symbols

By using complex data symbols at the transmitter instead of real symbols, as described above, the matrix H must obey

$$H^H H = \left(|h_1|^2 + \cdots + |h_n|^2\right) I = \bar{h}^H \bar{h} \cdot I \tag{3.28}$$

in order to decode each substream individually and provide n-fold diversity. Once again refer to *Chapter 2, Section 2.3, Equation (2.18)*. Note that *Equation (3.28)* differs from *Equation (3.25)* in the sense that the $\mathrm{Re}\{\bullet\}$ and $\mathrm{Im}\{\bullet\}$ parts are utilised. For n = 2, that can attain full diversity, the matrix H

$$H = \begin{bmatrix} h_1 & h_2 \\ -h_2^* & h_1^* \end{bmatrix} \tag{3.29}$$

which satisfies *Equation (3.28)*. By observing the product

$$\begin{aligned} H\bar{b} &= \begin{bmatrix} h_1 & h_2 \\ -h_2^* & h_1^* \end{bmatrix} \begin{bmatrix} b_1 \\ b_2 \end{bmatrix} \\ &= \begin{bmatrix} h_1 b_1 + h_2 b_2 \\ -h_2^* b_1 + h_1^* b_2 \end{bmatrix} \end{aligned} \tag{3.30}$$

it can be seen that we cannot find a B such that $H\bar{b} = B\bar{h}$, as is the case in *Equation (3.23)*, and for this reason it is unclear what we should transmit. However, if the second entry of *Equation (3.30)* is conjugated, then

$$\begin{aligned} \begin{bmatrix} h_1 b_1 + h_2 b_2 \\ -h_2^* b_1 + h_1^* b_2 \end{bmatrix} &= \begin{bmatrix} b_1 & b_2 \\ b_2^* & -b_1^* \end{bmatrix} \begin{bmatrix} h_1 \\ h_2 \end{bmatrix} \\ &= B\bar{h} \end{aligned} \tag{3.31}$$

where

$$B = \begin{bmatrix} b_1 & b_2 \\ b_2^* & -b_1^* \end{bmatrix} \tag{3.32}$$

Hence, the transmitted signal should be

$$S = G \cdot B \tag{3.33}$$

where G is defined in *Equation (3.19)* and B in *Equation (3.32)*. As in the real symbol case described in *Section 3.6.1*, the received signal $\bar{r}$ is despreaded by G^H to give

$$\begin{bmatrix} \bar{g}_1^H & \bar{g}_2^H \end{bmatrix} \bar{r} = G^H \left(S\bar{h} + \bar{\eta} \right) = B\bar{h} + \begin{bmatrix} \bar{g}_1^H \bar{\eta} \\ \bar{g}_2^H \bar{\eta} \end{bmatrix} \tag{3.34}$$

but, contrary to the real-symbol case, the second entry has to be conjugated as described by *Equation (3.31)*, to yield

$$\begin{aligned} \begin{bmatrix} \bar{g}_1^H & \bar{g}_2^H \end{bmatrix} \bar{r} &= H\bar{b} + \begin{bmatrix} \bar{g}_1^H \bar{\eta} \\ \left(\bar{g}_2^H \bar{\eta} \right)^* \end{bmatrix} \\ &= \begin{bmatrix} |h_1|^2 + |h_2|^2 & h_1^* h_2 - h_1^* h_2 \\ h_2^* h_1 - h_2^* h_1 & |h_1|^2 + |h_2|^2 \end{bmatrix} \bar{b} + H^H \bar{\upsilon} \\ &= \begin{bmatrix} |h_1|^2 + |h_2|^2 & 0 \\ 0 & |h_1|^2 + |h_2|^2 \end{bmatrix} \bar{b} + H^H \bar{\upsilon} \end{aligned} \tag{3.35}$$

where $\bar{\upsilon} = \begin{bmatrix} \bar{g}_1^H \bar{\eta} \\ \left(\bar{g}_2^H \bar{\eta} \right)^* \end{bmatrix}$. Hence, the transmitted symbols $\bar{b} = \begin{bmatrix} b_1 \\ b_2 \end{bmatrix}$ are successfully decoded.

Tarok *et al.* [13] showed that square matrices H obeying *Equation (3.28)* do not exist presently for $n > 2$, i.e. for more than 2 transmit antennas. The proposed scheme in this dissertation provides a method for obtaining full rate, full diversity for more than 2 transmit antennas.

3.7 OVERVIEW OF CURRENT ST CODING - CDMA LITERATURE

Research in the field of combining ST codes and CDMA technology have started to attract more researchers over the past few years, because of the advantages that multiple antenna systems provide in a wireless environment. Most existing transmission diversity strategies are based on Bell-Labs Layered Space-Time (BLAST) [66] or orthogonal ST block coding [65, 67]. There are three proposals in [66], i.e.

- Spreading all the symbols of one user with the same code to maximize the spectral efficiency.
- Assigning each user *n*-orthogonal spreading sequences, and then spreading each antenna's signal with its own spreading code.
- Transmitting each symbol simultaneously over *n* antennas with *n* different spreading codes, to improve the diversity gain.

For an in-depth discussion on orthogonal ST block coding [65], see *Section 3.6*.

All of the work presented in [65, 66, 67, 68, 69], apply the DS-SS technique over the codewords of conventional ST block coding, whereas CSSs are used in [70]. However, a resent publication by Doostnejad [28], proposed a two-dimensional STS code, that provides full transmit diversity and high spectral efficiency, and is based upon the principal that orthogonal user blocks are transmitted over *n* transmit antennas.

3.8 CONCLUDING REMARKS

Chapter 3 presented theoretical concepts with respect to spreading sequences. In particular, Walsh spreading sequences, known for their excellent cross-correlation properties and accordingly, the main reason for using them in this study, was discussed in detail. A brief overview of CSSs was also presented. Further, the applications of spreading sequences in DS-SS was discussed, and extended to the case where these spreading sequences are used in conjunction with ST coding techniques, generally known as STS. Lastly, recent development the research field of incorporating ST coding in CDMA platforms were discussed. Next, the mobile fading channel simulation platform is presented that was used to generate the simulation results presented in *Chapter 6*.

CHAPTER FOUR

MOBILE FADING CHANNELS

This chapter contains a concise summary of the fading channels used in the simulation platforms to generate the proposed DSSTS as well as SSTD scheme's simulation results. A typical model of a land mobile radio scenario, including Personal Communication Systems (PCS) and other digital cellular transmission links, is shown in Appendix C, *Figure C.1*. It consists of an elevated BS antenna (or multiple antennas) with a relatively short distance Line-of-Sight (LOS) propagation path, and many Non-Line-of-Sight (NLOS) reflected propagation paths towards the mobile antenna or antennas mounted on the vehicle or mobile unit. In most applications, no complete or direct LOS propagation exists between the BS antenna (also known as the access point) and the mobile antennas, because of natural and constructed obstacles (see Appendix C, *Figure C.1*). Thus, the transmitted radio waves reach the mobile unit from different directions and with different time delays, caused by the multiple paths. This scenario causes small-scale fading.

Small-scale fading, or simply fading, is used to describe the rapid fluctuations of the amplitudes, phases, or multipath delays of the radio signal over a short period of time or distance of travel. Thus, basically the time dependency of the fading is removed from the large-scale path losses in order to separate small-scale fading from large-scale fading.

Large-scale fading or path loss is the decrease in the signal's amplitude that travelled over a large distance. One popular method to calculate path losses over large distance is to use the free space propagation loss model [1].

This chapter is structured as follows: In *Section 4.1* a general overview of the Flat Fading Channel Simulator (FFCS) used in this dissertation is presented, followed by a multipath fading channel model in *Section 4.2*. Lastly, a Multipath Fading Channel Simulator (MFCS) are presented in *Sections 4.3*. Also see Appendix C and D for an in depth discussion on all multipath fading signal propagation effects.

4.1 FLAT FADING CHANNEL SIMULATOR MODEL

4.1.1 Description of the slow/fast fading channel simulator

A popular method of simulating a channel is by means of the classic *Clarke* FFCS, which is presented in Appendix D. However, the use of the Hilbert transform in a classic *Clarke* FFCS can be negated, as shown by Staphorst [17], by assuming that the signal components entering the fading channel has already been decomposed into real and imaginary baseband parts.

$$u(t) = \mathrm{Re}\{u(t)\} + j \cdot \mathrm{Im}\{u(t)\} \tag{4.1}$$

Thus, keeping the $\mathrm{Re}\{\ \}$ and $\mathrm{Im}\{\ \}$ branches apart, a complex flat fading process is given in *Equation (4.2)*:

$$h(t) = \alpha(t) \cdot \cos(\phi(t)) + j \cdot \alpha(t) \cdot \sin(\phi(t)) \tag{4.2}$$

where $\alpha(t)$ and $\phi(t)$ are the instantaneous fading amplitude and phase of the fading channel, respectively. In order to switch the channel's fading amplitude between a Rayleigh and Rician amplitude fading distributions, a constant $\sqrt{2K}$ is added to the $\mathrm{Re}\{\ \}$ branch of the fading channel simulator . Adding the $\sqrt{2K}$ component, to *Equation (4.2)* yields,

$$h(t) = \alpha(t) \cdot \cos(\phi(t)) + \sqrt{2K} + j \cdot \alpha(t) \cdot \sin(\phi(t)) \tag{4.3}$$

Defining *d(t)* as the output from the complex channel simulator, the complex input signal *u(t)* has to be multiplied by the fading channel *h(t)* in order to produce a fading output *d(t)*, thus

$$d(t) = u(t) \cdot h(t) \tag{4.4}$$

Substituting *Equations (4.1)* and *(4.3)* into *(4.4)*, results in:

$$\mathrm{Re}\{d(t)\} = \mathrm{Re}\{u(t)\} \cdot \mathrm{Re}\{h(t)\} - \mathrm{Im}\{u(t)\} \cdot \mathrm{Im}\{h(t)\} \tag{4.5}$$

and:

$$\mathrm{Im}\{d(t)\} = \mathrm{Re}\{h(t)\} \cdot \mathrm{Im}\{u(t)\} + \mathrm{Re}\{u(t)\} \cdot \mathrm{Im}\{h(t)\} \tag{4.6}$$

respectively, that represents the $\mathrm{Re}\{\bullet\}$ and $\mathrm{Im}\{\bullet\}$ outputs of the flat fading channel, operating on a complex input signal. The complex FFCS's realisation of the *Clarke*'s flat fading channel from *Equations (4.5)* and *(4.6)* are shown in *Figure 4.1*. From this figure it is clear that:

$$\mathrm{Re}\{d(t)\} = C_{SCALE}\left[\left(n_I(t) + \sqrt{2K}\right) \cdot \mathrm{Re}\{u(t)\} - n_I(t) \cdot \mathrm{Im}\{u(t)\}\right] \tag{4.7}$$

and:

$$\mathrm{Im}\{d(t)\} = C_{SCALE}\left[\left(n_I(t) + \sqrt{2K}\right) \cdot \mathrm{Im}\{u(t)\} + n_I(t) \cdot \mathrm{Re}\{u(t)\}\right] \tag{4.8}$$

where $n_I(t)$ and $n_Q(t)$ are the respective outputs of Doppler filters $DF_I(f)$ and $DF_Q(f)$ for Gaussian input signals. It is also assumed that the Gaussian input signals have zero mean and unit variance. The constant C_{SCALE} is chosen such that the channel simulator's input signal power and output signal power are equal in magnitude. It is given by the following expression:

$$C_{SCALE} = \frac{1}{\sqrt{2(1+K)}} \tag{4.9}$$

The Rician constant K defines the ratio between the *LOS* signal strength σ_{LOS}^2 and scatter signal strength σ_{NLOS}^2 (*NLOS*). Thus,

$$K = \left[\frac{\sigma_{LOS}^2}{\sigma_{NLOS}^2} \right] \tag{4.10}$$

By using *Equation (4.10)*, it can be shown that the component added to the $\mathrm{Re}\{\ \}$ branch is given by

$$CLOS = \sqrt{2K} \tag{4.11}$$

See Appendix D for the derivation of *Equations (4.9)* and *(4.11)*.

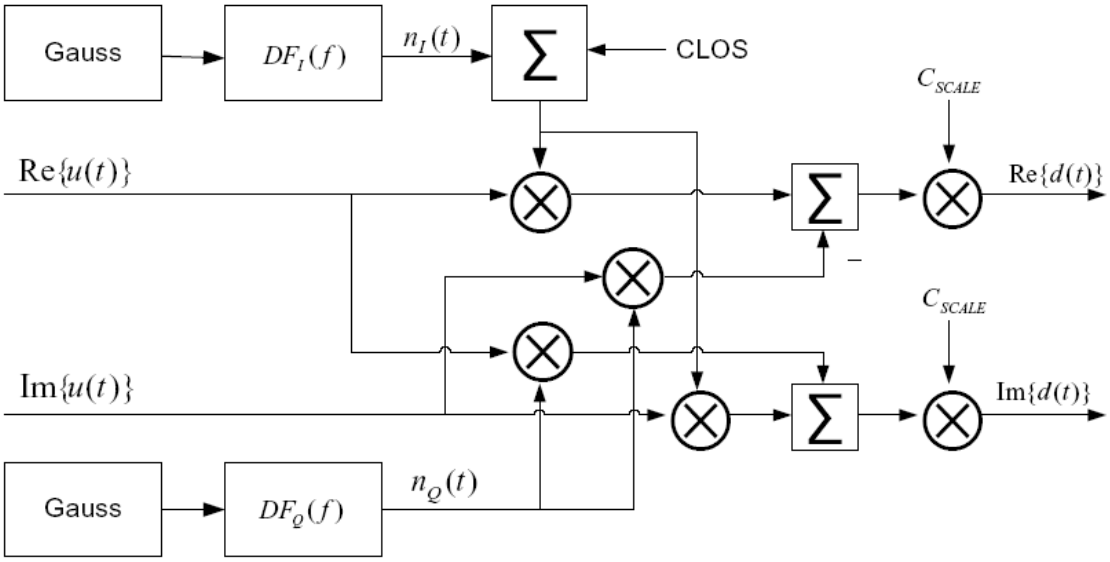

Figure 4.1. Clarke's model for a Complex FFCS employing both Rayleigh and Rice fading.

4.2 MULTIPATH FADING CHANNEL MODEL

The multipath fading phenomenon is primarily a result of the time variations in the phases of received signals at the receiver through *L*-paths. The received signal in the case of a discrete multipath channel is given by *Equation (4.12),*

$$d(t) = \sum_{i=1}^{L} \beta_i(t) \exp\left(-\, j\vartheta_i(t)\right) \qquad (4.12)$$

where $\theta_i(t) = 2\pi f_c \tau_i(t)$, $\tau_i(t)$ is the time delay associated with the *i*'th path of the multipath channel and $\beta_i(t)$ is the amplitude of the *i*'th path of the multipath channel (see Appendix D.3 for the derivation of *Equation 4.12*). Thus at time *t*, the received signal consists of the sum of a number of time-variant vectors (phasors) having amplitudes $\beta_i(t)$ and phases $\theta_i(t)$. That is, at times the randomly time-variant phases $\theta_i(t)$ associated with the vectors $\{\beta_i \exp(-j\theta_i)\}$ result in the vectors adding destructively (see Appendix C, *Figure C.2*). When this occurs, the resultant received signal $d(t)$ is very small or practically zero. At other times, the vectors $\{\beta_i \exp(-j\theta_i)\}$ add constructively, so that the received signal is large (see Appendix C, *Figure C.2*). Thus, the amplitude variations in the received signal, termed signal fading, are due to the time-variant multipath characteristics of the channel. Also note that the delays $\tau_i(t)$, associated with the different signal paths, will also change at different rates and in an unpredictable manner.

Two characteristics of a time-varying multipath channel are the introduction of delay spread, and the nature of all multipaths vary with time in accordance with the environmental changes. The time variations in the channel appear to be unpredictable to the user of the channel and for this reason, a time variant multipath channel is characterised statistically. For a more in depth discussion on the statistical analysis of a multipath fading channel, see Appendix D. A common term usually associated with multipath fading channels is the multipath power delay profile shown in *Figure 4.2.*

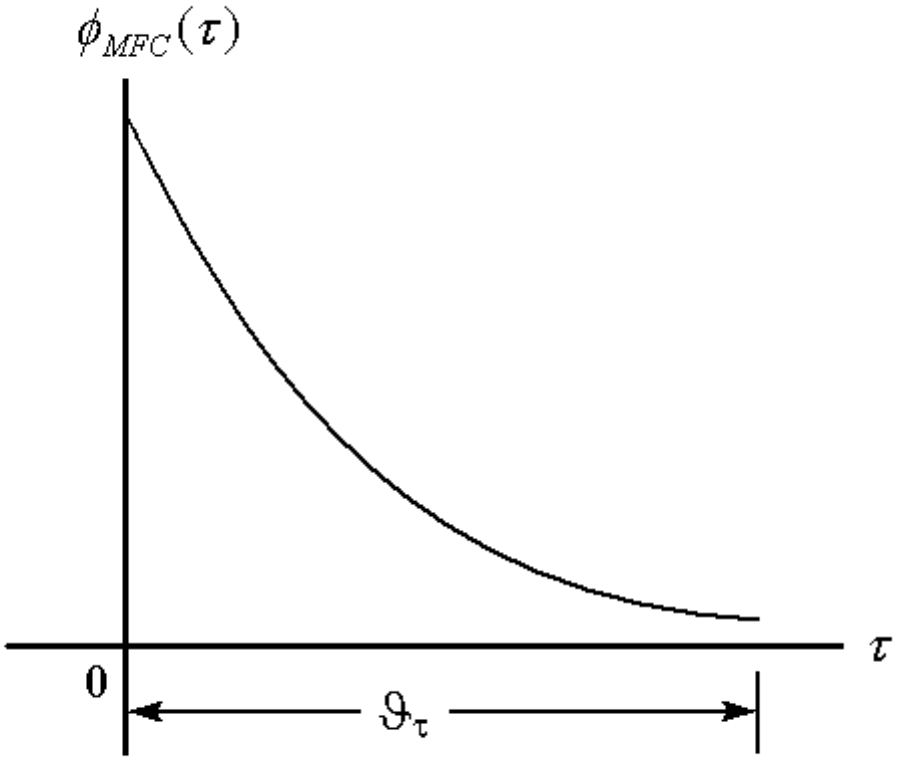

Figure 4.2 Multipath power delay profile with a delay spread of ϑ_τ.

In practice, the multipath power delay profile is measured by transmitting very narrow pulses or, equivalently, a wideband signal and cross-correlating the received signal with a delayed version of itself. The measured cross-correlation function of the multipath fading channel $\Phi_{MFC}(\tau)$ may appear as shown in *Figure 4.2* (see Appendix D). The range of values of τ over which $\Phi_{MFC}(\tau)$ is nonzero, or above a certain threshold, is called the delay spread ϑ_τ of the channel. As described in Appendix C, *Section C.4*, the delay spread ϑ_τ vs. the transmitted signal period determines whether the channel's fading is flat or frequency selective.

4.3. MULTIPATH FADING CHANNEL SIMULATOR MODEL

A flat or frequency selective fading channel, as described in *Section 4.2*, can be simulated using the general MFCS structure as shown in *Figure 4.3*. This simulator is capable of simulating a time-invariant multipath fading channel, consisting of *L* discrete and independently faded multipath components.

To simulate an appropriate power delay profile with the MFCS, *L*-paths are selected with their respective delays, denoted by τ_i. Next, each delayed version of the input signal is scaled by β_i to represent the average amplitude on the *i*'th path of the multipath channel. These delayed and scaled signals are then processed by *L*-FFCS, denoted as *FFCS 1* to *FFCS L* in *Figure 4.3*. Note that this approach allows the power delay profile to be configured such that each *i*'th path can be processed with its own unique Doppler frequency and Rician constant. The resultant outputs from the *L*-FFCS are then added to produce the output from the MFCS, denoted as *d(t)*. Recall from *Section 3.4.3*, that it is important that the condition, $\sum_{i=1}^{L}(\beta_i)^2 = 1$ must be satisfied in order for the channel's output power to be equal to the input power [4].

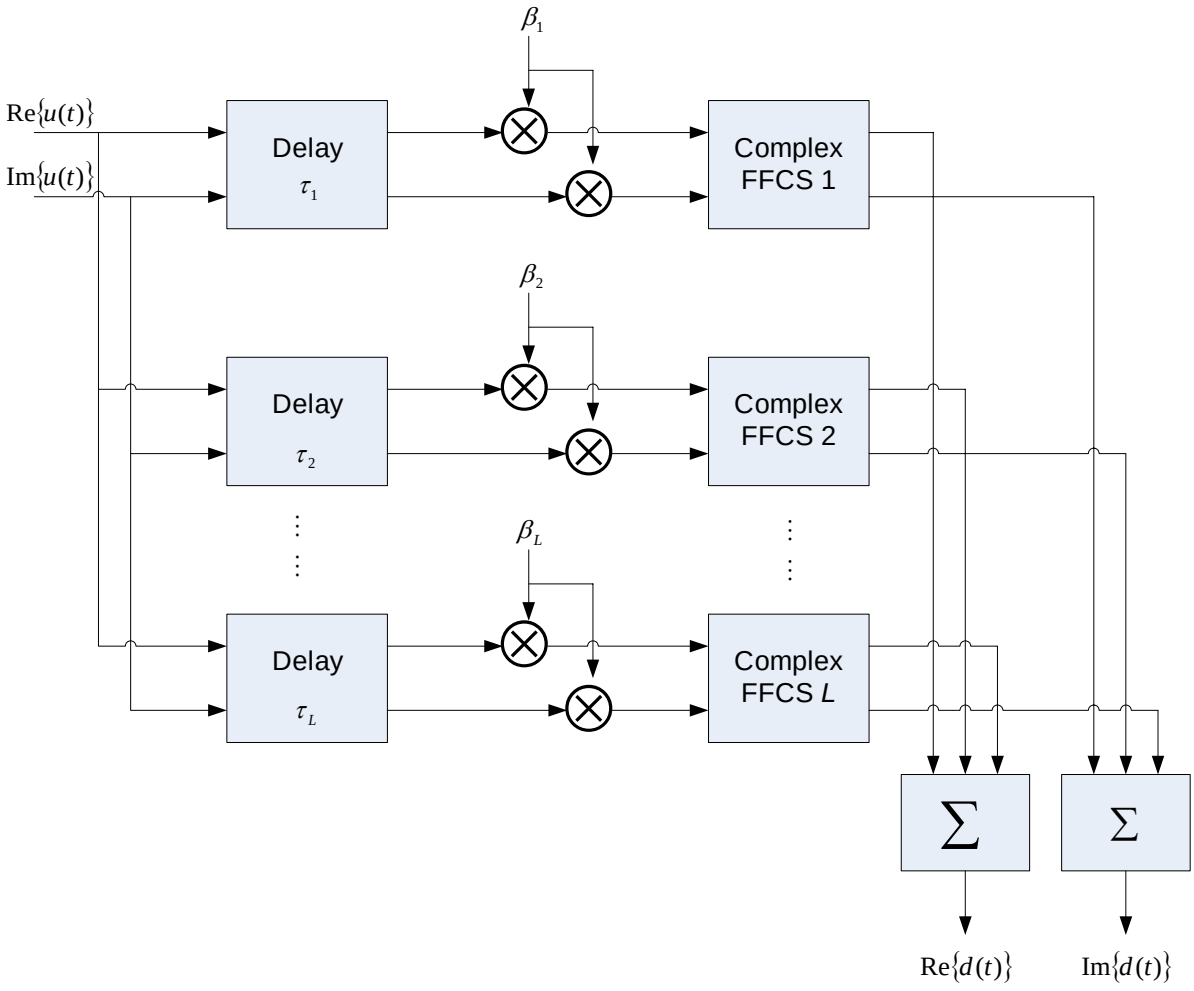

Figure 4.3 MFCS with *L* discrete and independently faded paths employing *L*-FFCS and *L*-time delays.

CHAPTER FIVE

PROPOSED SPACE-TIME SPREADING SCHEMES

In *Chapter 2* a communication system was presented that consisted of a BS with n transmit antennas (were $n = 2$) and a MS with only one receive antenna. In Chapter 5, a scheme to increase the number of transmit antennas at the BS to more than two transmit antennas is proposed. Although other schemes have been proposed that accomplished this (see *Chapters 2* and *3*), these schemes cannot achieve full rate and full diversity for more than 4 transmit antennas. As stated in the introduction, an objective of this study is to find a method of increasing the number of transmit antennas at the BS from two transmit antennas to an arbitrary number of transmit antennas that achieve both full rate and full diversity. This objective is met by the proposed scheme and referred to as DSSTS. Although only one receive antenna is assumed in this particular study, it can easily be extended to multiple receive antennas.

This chapter is structured as follows: In *Sections 5.1,* a general overview of the DSSTS scheme's transmission model, encoding and decoding algorithms are presented. Further,

the effect of non-perfect cross-correlation of spreading sequences at the receiver is analysed, the capacity for the DSSTS scheme is derived and the simulation platform used in this dissertation is presented. Lastly, the focus of *Section 5.2* is on a SSTD scheme presented in Maasdorp *et al*. [19, 20] to relieve Alamouti's ST decoding scheme from the assumption that the channel has to be quasi-static.

5.1 DIRECT SEQUENCE SPACE-TIME SPREADING SCHEME

5.1.1 DSSTS transmission model

The proposed DSSTS scheme that achieves full rate and full diversity is presented in *Figure 5.1*. It consists of the following building blocks:

- A symbol mapping function, for example QPSK, QAM etc,
- a cyclic shift register that shift symbols two symbols positions at even time periods, i.e. t = 2, 4, 6, …,
- y (2 x 2) Alamouti matrices from *Equation 5.1* and
- y orthogonal spreading codes.

Note that the number of ST block codes and spreading codes utilized in the DSSTS scheme will always be equal to $n/2$. Thus, $y = n/2$. It should also be stated here that any spreading code family could be used in the DSSTS scheme. Since perfect synchronization is assumed in this study, only the cross-correlation properties of the spreading sequences are important. Cross-correlation, as well as auto-correlation properties, were discussed in detail in *Chapter 3, Section 3.3*. As Walsh sequences have excellent periodic cross-correlation properties, it was the choice for this study. However, for real-life implementation, other spreading sequences that have excellent cross- as well as auto-correlation properties, for example CSSs, may be considered (See *Chapter 3, Section 3.2* for more information on CSSs).

For simplicity, only a QPSK symbol constellation is assumed, but any other possible symbol constellation can also be used. By using a QPSK symbol constellation, two incoming bits, b_1 and b_2 from bitstream $\bar{b}$, are mapped to a single symbol, presented as $[b_1 b_2] \rightarrow a_1$ from the

symbol constellation ν. Thus, if n transmit antennas are used, a block of $2n$ bits are mapped to n symbols, presented as a_1 to a_n. These mapped symbols, presented in matrix form as $[b_1 b_2 \quad b_3 b_4 \quad \cdots \quad b_{2n-1} b_{2n}]^T \rightarrow [a_1 \quad a_2 \quad \cdots \quad a_n]^T$, are shown in *Figure 5.1*. These n symbols are then shifted into the cyclic symbol shift register and shifted by 2 symbol positions after 2 time slots over a total of l time slots. The reason for the 2 symbol position shifts after every 2 time slots are as follows:

- Each of the y ST encoder blocks in *Figure 5.1* has an Alamouti matrix, see *Chapter 2, Section 2.2.2, Equation (2.4).* Note that $y = n/2$.
- At the first time slot t_1, the symbols in row one of *Equation (2.4)* are the output of the y'th ST-encoder.

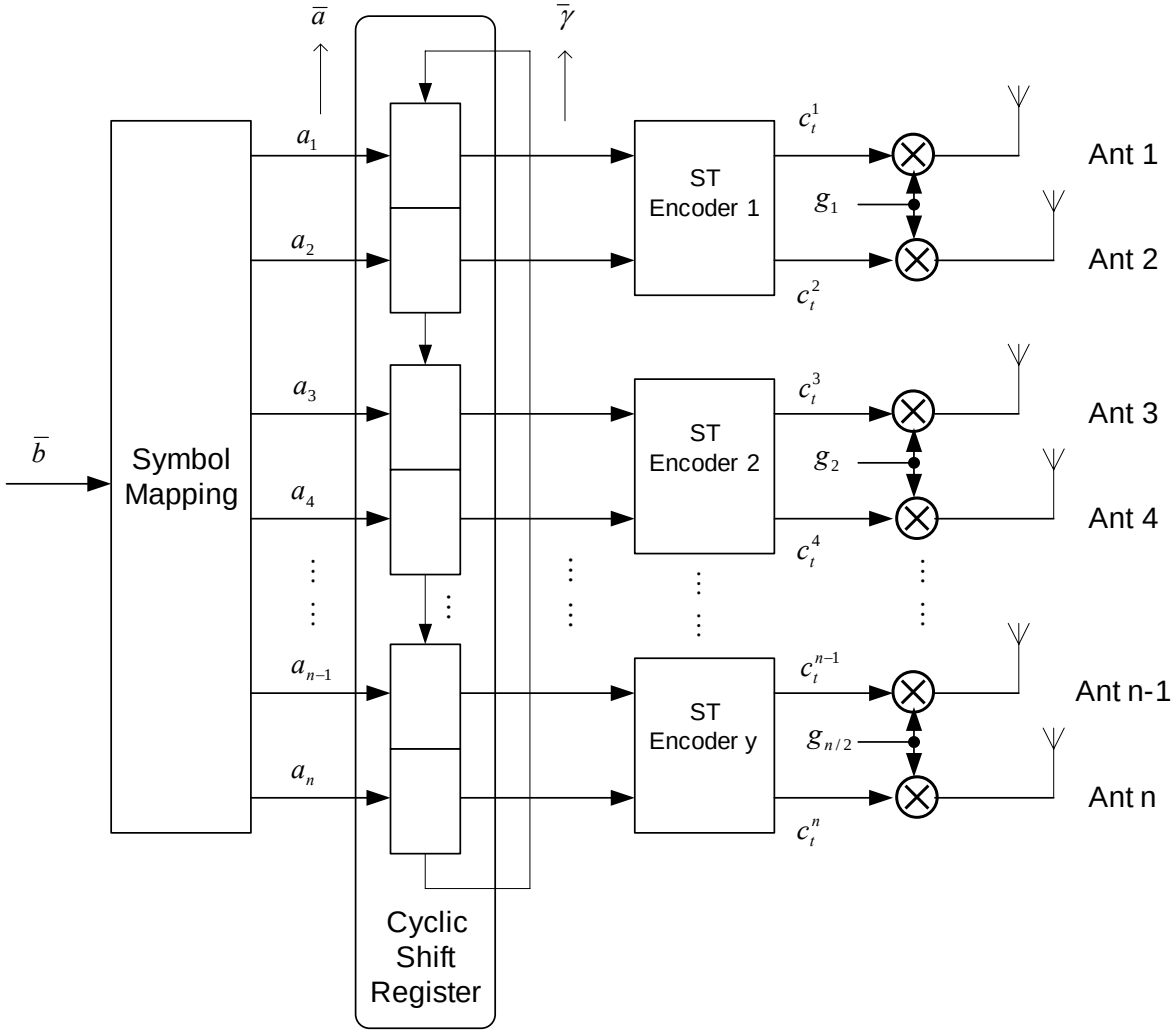

Figure 5.1. Proposed DSSTS transmitter structure, achieving full rate and full diversity.

- At the second time slot t_1+T_s, where T_S is the symbol period, the symbols in row two of *Equation (2.4)* are the output of the *y*'th ST-encoder.
- Thus, for every 2 input symbols at the *y*'th ST-encoder, 2 sets of 2 encoded symbols are present at the output after 2 time slots. For this reason the 2 input symbols at every *y*'th ST-encoder has to be shifted 2 symbols positions at every second time slot.

The output of the shift register, γ, for n symbols and $t = 1$ to l, can be shown in matrix form as:

$$\bar{\gamma} = \begin{bmatrix} \bar{\gamma}_1 & \bar{\gamma}_2 & \cdots & \bar{\gamma}_{l-1} & \bar{\gamma}_l \end{bmatrix} = \begin{bmatrix} a_1 & a_2 & \cdots & \cdots & a_{n-1} & a_n \\ a_1 & a_2 & \cdots & \cdots & a_{n-1} & a_n \\ a_{n-1} & a_n & a_1 & a_2 & \cdots & \cdots \\ a_{n-1} & a_n & a_1 & a_2 & \cdots & \cdots \\ \vdots & \vdots & \vdots & \vdots & \ddots & \vdots \\ \cdots & \cdots & a_{n-1} & a_n & a_1 & a_2 \end{bmatrix}^T \tag{5.1}$$

Note that the number of columns in *Equation (5.1)* represent the number of transmit antennas used, and that the number of rows represent the number of time periods, i.e. *l*-time slots. Also note that two consecutive time periods are the same, because the symbols are only shifted every second time slot.

For each time slot $t = 1, 2, 3, \ldots, l$, the shifted symbols $\bar{\gamma}_t$, are ST encoded (see *Section 5.2*). These ST encoded symbols c_t^i, $i = 1, 2, 3, \ldots..,n$, are then spreaded with a spreading code g_y, $y = 1, 2, 3\ldots\ldots, n/2$ and transmitted from n transmit antennas. Note that only one spreading code is used per ST block code. This is an advantage over STS schemes, presented in [27] because 50% less spreading codes are used in this scheme.

Using the same channel assumptions as in *Chapter 2*, i.e. a flat fading channel, the path gains are complex Gaussian random variables and the channel is constant over a frame length *l*, the received signal in *Figure 5.2* is

$$r_t = \sum_{i=1}^{n/2} \left(h_{2i-1}\, c_t^{2i-1} g_i + h_{2i}\, c_t^{2i} g_i \right) + \eta_t \tag{5.2}$$

where h_{2i-1} and h_{2i} are respectively defined as the path gains from transmit antennas ($2i$-1) and ($2i$) to the receive antenna and η_t is a zero mean complex Gaussian random variable. For a more detailed discussion on how h_i is defined, see *Chapter 4, Section 4.1*.

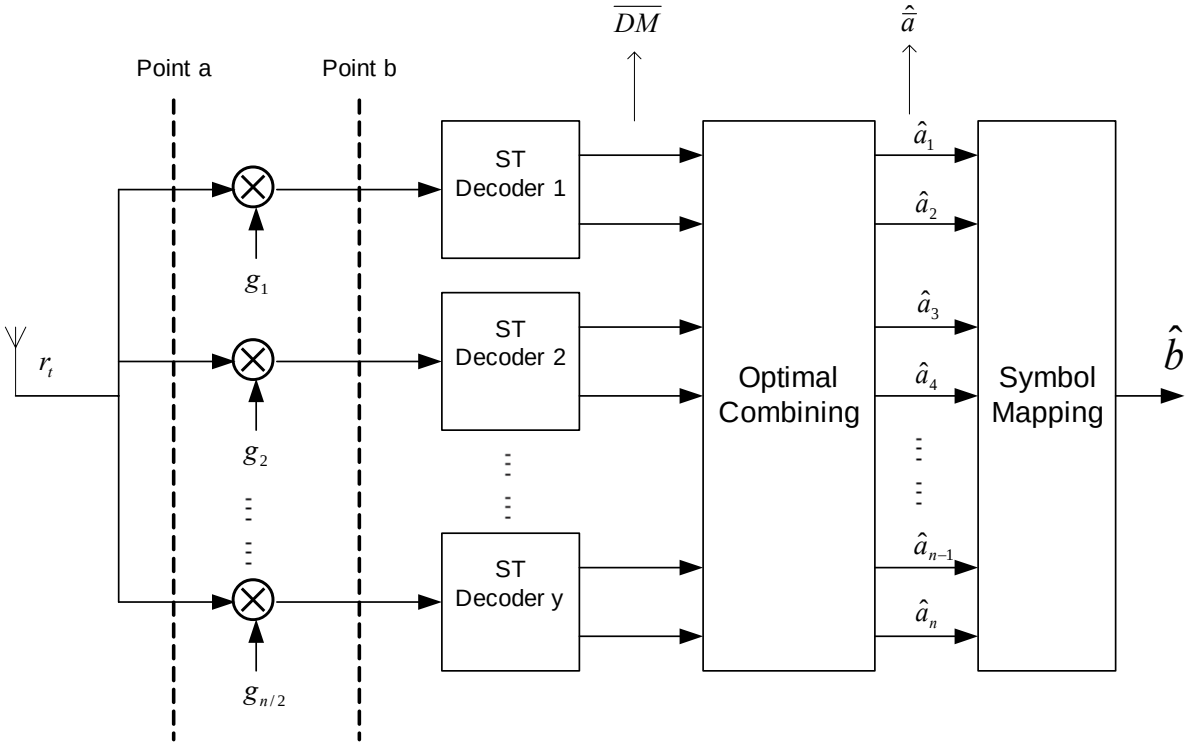

Figure 5.2. DSSTS receiver model.

Each received symbol stream r_t is despreaded with *Equation (5.3)*, i.e. point b in *Figure 5.2*.

$$\Delta_t^y = r_t g_y \qquad \text{where } y=1, 2, 3, \ldots..n/2, \quad \text{and } t = 1, 2, \ldots\ldots l \qquad (5.3)$$

Assuming perfect CSI is available after despreading, (point b in *Figure 5.2*) the receiver has to compute the decisions metrics

$$DM_j^y\Big|_{a_n} = \sum_{t=j-1}^{t+1} \left| \Delta_t^y - \sum_{i=y} \left(h_{2i-1}\, c_t^{2i-1} + h_{2i}\, c_t^{2i} \right) \right|^2 \qquad \text{for j = 2, 4, 6, ..,} l \qquad (5.4)$$

where *y* represents the ST decoder index and a_n represents one of *n* transmitted symbols. The decisions metrics are computed over all code words

$$c = \begin{bmatrix} c_1^1 & c_2^1 & \cdots & c_l^1 \\ c_1^2 & c_2^2 & \cdots & c_l^2 \\ \vdots & \vdots & \ddots & \vdots \\ c_1^n & c_2^n & \cdots & c_l^n \end{bmatrix} \tag{5.5}$$

Note that zero periodic cross-correlation between different Walsh spreading codes in *Equation (5.5)* is assumed. This topic is discussed in more detail in *Section 5.1.4* for the case when the periodic cross-correlation between different spreading sequences is not equal to zero.

The ST-decoders compute the decision metrics from *Equation (5.4)* and the output of all *y* ST decoders from *Figure 5.2* can be written in matrix form as

$$\overline{DM} = \left[DM_j^1\big|_{a_n} \quad DM_j^2\big|_{a_n} \quad \cdots \quad DM_j^{y-1}\big|_{a_n} \quad DM_j^y\big|_{a_n} \right]^T \tag{5.6}$$

for j = 2, 4, 6, ……..*l.* Note that the ST-decoders only has an output at every second time slot, because each ML detector needs two consecutive received signals in order to decouple the symbols (see *Chapter 2, Section 2.2.3*). In *Equation (5.7)*, the optimal combiner adds the decision metrics from *Equation (5.6)* to reconstruct estimates for symbols a_1 to a_n. Note that only decision metrics that are a function of the same symbol value (denoted by subscript $DM\big|_{a_i}$ in *Equation 5.7*) are added.

$$\hat{a}_i = \sum_{j=1}^{l/2} DM_{2j}^{t_{i,j}}\Big|_{a_i} \qquad \text{for } i = 1,2,3,\ldots\ldots,n \tag{5.7a}$$

$$\text{where } \iota = \begin{bmatrix} \iota_{1,1} & \iota_{1,2} & \cdots & \iota_{1,l/2} \\ \iota_{2,1} & \iota_{2,2} & \cdots & \iota_{2,l/2} \\ \iota_{3,1} & \iota_{3,2} & \cdots & \iota_{3,l/2} \\ \iota_{4,1} & \iota_{4,2} & \cdots & \iota_{4,l/2} \\ \vdots & \vdots & \ddots & \vdots \\ \iota_{n-1,1} & \cdots & \cdots & \iota_{n-1,l/2} \\ \iota_{n,1} & \cdots & \cdots & \iota_{n,l/2} \end{bmatrix} = \begin{bmatrix} 1, & 2, & \cdots & l/2 \\ 1, & 2, & \cdots & l/2 \\ l/2, & 1, & \cdots & (l-1)/2 \\ l/2, & 1, & \cdots & (l-1)/2 \\ \vdots & \vdots & \ddots & \vdots \\ 2, & \cdots & l/2, & 1 \\ 2, & \cdots & l/2, & 1 \end{bmatrix} \quad (5.7b)$$

Note the ι is a matrix with $\iota_{i,j}$ the *j*'th element in the *i*'th row. These soft symbol estimates, denoted as $\hat{a}_1$ to $\hat{a}_n$, are then mapped back to a bitstream $\hat{\hat{b}} = \left[\hat{b}_1 \hat{b}_2 \cdots \hat{b}_{2n-1} \hat{b}_{2n}\right]$ to form an estimate of the original transmitted bitstream.

5.1.2 DSSTS encoding algorithm

The new DSSTS scheme uses the Alamouti C_2 matrix, defined in *Chapter 2, Section 2.2.2, Equation (2.4)*, as building blocks. Note that henceforth in this dissertation, the Alamouti matrix will be defined as X_a. The reason for the change in notation is to show that the subscript *a* does not indicate the number of transmit antennas anymore, but is rather used as a substitution variable. In the new DSSTS scheme the Alamouti ST block codes X_a that are being spread with Walsh spreading codes g_y are used to define a l x n transmission matrix T_n,

$$T_n = \begin{bmatrix} g_1 X_1 & g_2 X_3 & \cdots & g_{n/2} X_{n-1} \\ g_1 X_{n-1} & g_2 X_1 & & \vdots \\ \vdots & & \ddots & \\ g_1 X_3 & \cdots & & g_{n/2} X_1 \end{bmatrix} \quad (5.8)$$

where each of the X_1, X_3, ... X_{n-1} Alamouti matrix's is defined as follows

$$X_a = \begin{bmatrix} x_a & x_{a+1} \\ -x_{a+1}^* & x_a^* \end{bmatrix} \quad (5.9)$$

Note that *Equation (5.9)* and *(2.4)* are exactly the same, except for the change in notation.

For example, transmission matrix T_4 in *Equation (5.8)* represents a code that utilizes four transmit antennas, as seen by the number of columns in T_4, and occurs over 4 frame lengths, i.e. $l = 4$, as seen by the number of rows in T_4. Thus, by substituting $n = 4$ into *Equation (5.8)*, *Equation (5.10)* is obtained.

$$T_4 = \begin{bmatrix} g_1 X_1 & g_2 X_3 \\ g_1 X_3 & g_2 X_1 \end{bmatrix} \tag{5.10}$$

By using *Equation (5.9)* to define X_1 and X_3 in *Equation (5.10)*, X_1 and X_3 is given by:

$$X_1 = \begin{bmatrix} x_1 & x_2 \\ -x_2^* & x_1^* \end{bmatrix} \text{ and } X_3 = \begin{bmatrix} x_3 & x_4 \\ -x_4^* & x_3^* \end{bmatrix} \tag{5.11}$$

Note that g_1X_1, g_1X_3 are transmitted from transmit antennas 1 and 2, respectively and g_2X_3, g_2X_1 are transmitted from transmit antennas 3 and 4, respectively. Orthogonality between the different Alamouti ST block codes are achieved by the spreading codes g_y,for y = 1,2,3,……n/2.

The selection of the transmitted symbols are the same as for the Alamouti ST block code presented in *Chapter 2, Section 2.2.2*. Transmission occurs in baseband and a QPSK signal constellation is employed with 2^q elements, $q = 2$. At time slot t = 1, nq bits arrive at the symbol mapping function and select signal constellation points a_1, a_2, a_3,…,a_n. The transmission matrix T_n is then formed by setting $x_i = a_i$ for i = 1, 2, 3, …,n in *Equation (5.11)* and substituting it into *Equation (5.10)*. These signal constellation points are thus spreaded with $g_{n/2}$ spreading codes and transmitted from the n transmit antennas. Since l time slots are used to transmit n symbols, the code rate can be defined as

$$R_c = n/l \tag{5.12}$$

Note that the code rate will always be equal to one, because the transmission matrix T_n is set up such that $l = n$ for all possible scenarios in the new DSSTS scheme.

An example of using six transmit antennas are given in order to explain the full rate, full diversity principle. Using the DSSTS scheme as given in *Figure 5.1* with n = 6, the transmitted symbols from the six antennas over six periods of time are given in *Figure 5.3*. The encoding procedure is as follow:

1. Symbols 1 to 6 are transformed by the Alamouti matrixes, spreaded by the Walsh codes and transmitted over two time periods.
2. Symbols 1 to 6 are then rotated over two symbol positions, such that each symbol pair is processed by a different Alamouti matrix (see *Figure 5.1*) and transmitted.
3. Step 1and 2 are repeated 3 times in the case of the six transmit antennas, so that every Alamouti matrix transforms each symbol pair.

Time	**1**	**2**	**3**	**4**	**5**	**6**
Ant1	$a_1 g_1$	$-a_2^* g_1$	$a_5 g_1$	$-a_6^* g_1$	$a_3 g_1$	$-a_4^* g_1$
Ant2	$a_2 g_1$	$a_1^* g_1$	$a_6 g_1$	$a_5^* g_1$	$a_4 g_1$	$a_3^* g_1$
Ant3	$a_3 g_2$	$-a_4^* g_2$	$a_1 g_2$	$-a_2^* g_2$	$a_5 g_2$	$-a_6^* g_2$
Ant4	$a_4 g_2$	$a_3^* g_2$	$a_2 g_2$	$a_1^* g_2$	$a_6 g_2$	$a_5^* g_2$
Ant5	$a_5 g_3$	$-a_6^* g_3$	$a_3 g_3$	$-a_4^* g_3$	$a_1 g_3$	$-a_2^* g_3$
Ant6	$a_6 g_3$	$a_5^* g_3$	$a_4 g_3$	$a_3^* g_3$	$a_2 g_3$	$a_1^* g_3$

Figure 5.3. Transmitted symbols from the six transmit antennas from figure 5.1 over six time periods.

From *Figure 5.3* it is evident that 6 symbols are transmitted from each one of the 6 transmit antennas (n = 6), hence giving the scheme full diversity. Six symbols are also transmitted over 6 time periods (l = 6), hence resulting in full rate by using *Equation (5.12)*.

5.1.3 DSSTS decoding : Disregarding spreading sequences

By using the same ML decoding scheme described in *Chapter 2, Section 2.2.3*, combined with despreading, only linear processing at the receiver is required in order to decode the received code words.

The decoding algorithm is explained by means of an example: Consider the ST block code T_4, defined in *Equation (5.10)*. Assuming that a QPSK symbol constellation with 2^q elements is used, $nq = 8$ bits from $\bar{b}$ arrive at the encoder, and select 4 complex symbols a_1, a_2, a_3 and a_4, as described in the *Section 5.2*. These four symbols are spreaded using spreading codes g_1 and g_2. The spreaded symbols, a_1g_1, a_2g_1, a_3g_2 and a_4g_2 are then transmitted simultaneously from antennas 1 to 4, respectively, as shown in the transmit matrix T_4 in *Equation (5.13)*. At the second, third and fourth time slots, the symbols form *Equation (5.13)*'s 2nd, 3rd, and 4th row are respectively transmitted.

$$T_4 = \begin{bmatrix} a_1g_1 & a_2g_1 & a_3g_2 & a_4g_2 \\ -a_2^*g_1 & a_1^*g_1 & -a_4^*g_2 & a_3^*g_2 \\ a_3g_1 & a_4g_1 & a_1g_2 & a_2g_2 \\ -a_4^*g_1 & a_3^*g_1 & -a_2^*g_2 & a_1^*g_2 \end{bmatrix} \tag{5.13}$$

The received symbol streams r_t are then despreaded by means of *Equation (5.3)* to obtain Δ_1 to Δ_4 given in *Equation (5.14)*

$$\Delta_1^1 = r_1g_1 \quad \text{and} \quad \Delta_1^2 = r_1g_2 \tag{5.14a}$$

$$\Delta_2^1 = r_2g_1 \quad \text{and} \quad \Delta_2^2 = r_2g_2 \tag{5.14b}$$

$$\Delta_3^1 = r_3g_1 \quad \text{and} \quad \Delta_3^2 = r_3g_2 \tag{5.14c}$$

$$\Delta_4^1 = r_4g_1 \quad \text{and} \quad \Delta_4^2 = r_4g_2 \tag{5.14d}$$

where r_1 to r_4 is defined in *Section 5.4*, *Equation (5.34)* to *Equation (5.37)*. After despreading, the receiver uses *Equation (5.4)* to compute the decision metrics

$$DM_2^1\Big|_{a_n} = \sum_{t=1}^{2}\left|\Delta_t^1 - \left(h_1\, c_t^1 + h_2\, c_t^2\right)\right|^2 \tag{5.15a}$$

$$DM_2^2\Big|_{a_n} = \sum_{t=1}^{2}\left|\Delta_t^1 - \left(h_3\, c_t^3 + h_4\, c_t^4\right)\right|^2 \tag{5.15b}$$

$$DM_4^1\Big|_{a_n} = \sum_{t=3}^{4}\left|\Delta_t^1 - \left(h_1\, c_t^1 + h_2\, c_t^2\right)\right|^2 \tag{5.15c}$$

$$DM_4^2\Big|_{a_n} = \sum_{t=3}^{4}\left|\Delta_t^1 - \left(h_3\, c_t^3 + h_4\, c_t^4\right)\right|^2 \tag{5.15d}$$

over all possible codewords c_t^i. Expanding *Equation (5.15)* the following is obtained:

$$DM_2^1\Big|_{a_n} = \left|\Delta_1^1 - h_1c_1^1 - h_2c_1^2\right|^2 + \left|\Delta_2^1 - h_1c_2^1 - h_2c_2^2\right|^2 \tag{5.16a}$$

$$DM_2^2\Big|_{a_n} = \left|\Delta_1^2 - h_3c_1^3 - h_4c_1^4\right|^2 + \left|\Delta_2^2 - h_3c_2^3 - h_4c_2^4\right|^2 \tag{5.16b}$$

$$DM_4^1\Big|_{a_n} = \left|\Delta_3^1 - h_1c_3^1 - h_2c_3^2\right|^2 + \left|\Delta_4^1 - h_1c_4^1 - h_2c_4^2\right|^2 \tag{5.16c}$$

$$DM_4^2\Big|_{a_n} = \left|\Delta_3^1 - h_3c_3^3 - h_4c_3^4\right|^2 + \left|\Delta_4^1 - h_3c_4^3 - h_4c_4^4\right|^2 \tag{5.16d}$$

By using *Equation (5.13)* to see which codeword c_t^i was transmitted (note that *t* represents the row entry and *i* the column entry of *Equation (5.13)*), *Equation (5.16)*, can be rewritten as

$$DM_2^1\Big|_{a_1,a_2} = \left|\Delta_1^1 - h_1a_1 - h_2a_2\right|^2 + \left|\Delta_2^1 + h_1a_2^* - h_2a_1^*\right|^2 \tag{5.17}$$

$$DM_2^2\Big|_{a_3,a_4} = \left|\Delta_1^2 - h_3a_3 - h_4a_4\right|^2 + \left|\Delta_2^2 + h_3a_4^* - h_4a_3^*\right|^2 \tag{5.18}$$

$$DM_4^1\Big|_{a_3,a_4} = \left|\Delta_3^1 - h_1a_3 - h_2a_4\right|^2 + \left|\Delta_4^1 + h_1a_3^* - h_2a_4^*\right|^2 \tag{5.19}$$

$$DM_4^2\Big|_{a_1,a_2} = \left|\Delta_4^1 - h_3a_1 - h_4a_2\right|^2 + \left|\Delta_4^2 + h_3a_2^* - h_4a_1^*\right|^2 \tag{5.20}$$

By noting that $\overline{DM}$ is of the same form as *Equation (2.10)* in *Chapter 2*, the decoupling method described in *Chapter 2, Section 2.2.3*, can be used to decouple *Equations (5.17)* to *(5.20)* into two parts. For example, $DM_2^1\big|_{a_1,a_2}$

$$DM_2^1\big|_{a_1} = \left| \left[\left(\Delta_1^1 h_1^* + (\Delta_2^1)^* h_2\right)\right] - a_1 \right|^2 + \left(-1 + \sum_{i=1}^{2} |h_i|^2\right)|a_1|^2 \tag{5.21}$$

which is only a function of a_1, and

$$DM_2^1\big|_{a_2} = \left| \left[\left(\Delta_1^1 h_2^* - (\Delta_2^1)^* h_1\right)\right] - a_2 \right|^2 + \left(-1 + \sum_{i=1}^{2} |h_i|^2\right)|a_2|^2 \tag{5.22}$$

which is only a function of a_2. For $DM_2^2\big|_{a_3,a_4}$

$$DM_2^2\big|_{a_3} = \left| \left[\left(\Delta_1^2 h_3^* + (\Delta_1^2)^* h_4\right)\right] - a_3 \right|^2 + \left(-1 + \sum_{i=3}^{4} |h_i|^2\right)|a_3|^2 \tag{5.23}$$

which is only a function of a_3, and

$$DM_2^2\big|_{a_4} = \left| \left[\left(\Delta_1^2 h_4^* - (\Delta_1^2)^* h_3\right)\right] - a_4 \right|^2 + \left(-1 + \sum_{i=3}^{4} |h_i|^2\right)|a_4|^2 \tag{5.24}$$

which is only a function of a_4. For $DM_4^1\big|_{a_3,a_4}$

$$DM_4^1\big|_{a_3} = \left| \left[\left(\Delta_3^1 h_1^* + (\Delta_4^1)^* h_2\right)\right] - a_3 \right|^2 + \left(-1 + \sum_{i=1}^{2} |h_i|^2\right)|a_3|^2 \tag{5.25}$$

which is only a function of a_3, and

$$DM_4^1\Big|_{a_4} = \Big| \left[\left(\Delta_3^1 h_2^* - (\Delta_4^1)^* h_1\right)\right] - a_4\Big|^2 + \left(-1 + \sum_{i=1}^{2} |h_i|^2\right)|a_4|^2 \tag{5.26}$$

which is only a function of a_4. For $DM_4^2\Big|_{a_1,a_2}$

$$DM_4^2\Big|_{a_1} = \Big| \left[\left(\Delta_3^2 h_3^* + (\Delta_4^2)^* h_4\right)\right] - a_1\Big|^2 + \left(-1 + \sum_{i=3}^{4} |h_i|^2\right)|a_1|^2 \tag{5.27}$$

which is only a function of a_1, and

$$DM_4^2\Big|_{a_2} = \Big| \left[\left(\Delta_3^2 h_4^* - (\Delta_4^2)^* h_3\right)\right] - a_2\Big|^2 + \left(-1 + \sum_{i=3}^{4} |h_i|^2\right)|a_2|^2 \tag{5.28}$$

which is only a function of a_2.

By using *Equation (5.7)*, i.e. the optimal combiner in *Figure 5.2*, the receiver combines the decision metrics by adding the soft estimates of similar symbol values. Thus, for symbol a_1 to a_4, *Equation (5.7a)* can be written as

$$\hat{a}_1 = \sum_{j=1}^{2} DM_{2j}^{t_{1,j}}\Big|_{a_1} \tag{5.29}$$

that combines the soft estimate outputs from the decision metrics of *Equations (5.21)* and *(5.27)*

$$\hat{a}_2 = \sum_{j=1}^{2} DM_{2j}^{t_{2,j}}\Big|_{a_2} \tag{5.30}$$

similarly, the soft estimate outputs from the decision metrics of *Equations (5.22)* and *(5.28)* are combined to yield:

$$\hat{a}_3 = \sum_{j=1}^{2} DM_{2j}^{t_{3,j}}\Big|_{a_3} \tag{5.31}$$

The soft estimate outputs from the decision metrics of *Equations (5.23)* and *(5.25)* are combined to form:

$$\hat{a}_4 = \sum_{j=1}^{2} DM_{2j}^{\iota_{4,j}}\Big|_{a_4} \tag{5.32}$$

Lastly, the soft estimate outputs from the decision metrics of *Equations (5.24)* and *(5.26)*, are combined, where *Equation (5.7b)* can be written as:

$$\iota = \begin{bmatrix} \iota_{1,1} & \iota_{1,2} \\ \iota_{2,1} & \iota_{2,2} \\ \iota_{3,1} & \iota_{3,2} \\ \iota_{4,1} & \iota_{4,2} \end{bmatrix} = \begin{bmatrix} 1, & 2 \\ 1, & 2 \\ 2, & 1 \\ 2, & 1 \end{bmatrix} \tag{5.33}$$

Using $\hat{a}_1\ \hat{a}_2\ \hat{a}_3\ \hat{a}_4$, the symbols are mapped back to the original bitstream $\hat{\hat{b}} = \left[\hat{b}_1\hat{b}_2\cdots\hat{b}_7\hat{b}_8\right]$.

5.1.4 DSSTS decoding : Taking spreading sequences into account

As discussed in *Sections 5.1.1* and *5.1.3*, it was assumed that the spreading codes at the receiver has zero cross-correlation after despreading each stream with its corresponding spreading sequence. However, this will not always be the case with the DSSTS, since no phase corrections are done before despreading. Therefore it is necessary to look into the case when the cross-correlation between different spreading codes are non-zero, to establish what effect it will have on the performance of the DSSTS scheme. This section can be best described by means of an example. Assume the same scenario described in *Section 5.1.3*, where a 4 transmit antenna DSSTS scheme is used. Thus, the transmission matrix is given by *Equation (5.13)*.

By using the T_4 transmission matrix from *Equation (5.13)*, the received signals at the receiver are given by *Equation (5.2)* in *Section 5.1.1*, i.e. point a in *Figure 5.2*. By expanding *Equation (5.2)* and substituting the correct code word into c_t^i, the following is obtained: For t = 1,

$$r_1 = a_1 g_1 h_1 + a_2 g_1 h_2 + a_3 g_2 h_3 + a_4 g_2 h_4 + \eta_1 \quad (5.34)$$

where $a_1 = c_1^1;\ a_2 = c_1^2;\ a_3 = c_1^3$ and $a_4 = c_1^4$.

For t = 2,

$$r_2 = -a_2^* g_1 h_1 + a_1^* g_1 h_2 - a_4^* g_2 h_3 + a_3^* g_2 h_4 + \eta_2 \quad (5.35)$$

where $-a_2^* = c_2^1;\ a_1^* = c_2^2;\ -a_4^* = c_2^3$ and $a_3^* = c_2^4$

For t = 3,

$$r_3 = a_3 g_1 h_1 + a_4 g_1 h_2 + a_1 g_2 h_3 + a_2 g_2 h_4 + \eta_3 \quad (5.36)$$

where $a_3 = c_3^1;\ a_4 = c_3^2;\ a_1 = c_3^3$ and $a_2 = c_3^4$

For t = 4,

$$r_4 = -a_4^* g_1 h_1 + a_3^* g_1 h_2 - a_1^* g_2 h_3 + a_2^* g_2 h_4 + \eta_4 \quad (5.37)$$

where $-a_4^* = c_4^1;\ a_3^* = c_4^2;\ -a_1^* = c_4^3$ and $a_2^* = c_4^4$

By using *Equation (5.3)*, the received symbol streams are then depreaded by multiplying each respective stream with its corresponding spreading sequence, i.e. at point b in *Figure 5.2*. Note that *Equation (5.14)* will be examined in detail in order to show the effect of perfect and non-perfect cross correlation.

Thus, by using r_1 to r_4 from *Equations (5.34)* to *(5.37)*, the despreaded streams are,

$$\Delta_1^1 = a_1 (g_1)^2 h_1 + a_2 (g_1)^2 h_2 + a_3 g_1 g_2 h_3 + a_4 g_1 g_2 h_4 + g_1 \eta_1 \quad (5.38a)$$

$$\Delta_2^1 = -a_2^* (g_1)^2 h_1 + a_1^* (g_1)^2 h_2 - a_4^* g_1 g_2 h_3 + a_3^* g_1 g_2 h_4 + g_1 \eta_2 \quad (5.38b)$$

$$\Delta_3^2 = a_3 g_1 g_2 h_1 + a_4 g_1 g_2 h_2 + a_1 (g_2)^2 h_3 + a_2 (g_2)^2 h_4 + g_2 \eta_3 \quad (5.38c)$$

$$\Delta_4^2 = -a_4^* g_1 g_2 h_1 + a_3^* g_1 g_2 h_2 - a_2^* (g_2)^2 h_3 + a_1^* (g_2)^2 h_4 + g_2 \eta_4 \quad (5.38d)$$

$$\Delta_1^2 = a_1 g_1 g_2 h_1 + a_2 g_1 g_2 h_2 + a_3 (g_2)^2 h_3 + a_4 (g_2)^2 h_4 + g_2 \eta_1 \quad (5.38e)$$

$$\Delta_2^2 = -a_2^* g_1 g_2 h_1 + a_1^* g_1 g_2 h_2 - a_4^* (g_2)^2 h_3 + a_3^* (g_2)^2 h_4 + g_2 \eta_2 \quad (5.38f)$$

$$\Delta_3^1 = a_3 (g_1)^2 h_1 + a_4 (g_1)^2 h_2 + a_1 g_1 g_2 h_3 + a_2 g_1 g_2 h_4 + g_1 \eta_3 \quad (5.38g)$$

$$\Delta_4^1 = -b_4^* (g_1)^2 h_1 + b_3^* (g_1)^2 h_2 - b_2^* g_1 g_2 h_3 + b_1^* g_1 g_2 h_4 + g_1 \eta_4 \quad (5.38h)$$

Perfect cross correlation

In the case of perfect cross correlation $g_1 g_2 = 0$ and $(g_1)^2 = 1$, $(g_2)^2 = 1$. Thus, *Equation (5.38)* reduces to *Equation (5.39)*

$$\Delta_1^1 = a_1 h_1 + a_2 h_2 + g_1 \eta_1 \quad (5.39a)$$

$$\Delta_2^1 = -a_2^* h_1 + a_1^* h_2 + g_1 \eta_2 \quad (5.39b)$$

$$\Delta_3^2 = a_1 h_3 + a_2 h_4 + g_2 \eta_3 \quad (5.39c)$$

$$\Delta_4^2 = -a_2^* h_3 + a_1^* h_4 + g_2 \eta_4 \quad (5.39d)$$

$$\Delta_1^2 = a_3 h_3 + a_4 h_4 + g_2 \eta_1 \quad (5.39e)$$

$$\Delta_2^2 = -a_4^* h_3 + a_3^* h_4 + g_2 \eta_2 \quad (5.39f)$$

$$\Delta_3^1 = a_3 h_1 + a_4 h_2 + g_1 \eta_3 \quad (5.39g)$$

$$\Delta_4^1 = -a_4^* h_1 + a_3^* h_2 + g_1 \eta_4 \quad (5.39h)$$

As described in *Section 5.1.3,* the ML detector attempts to minimise the decision metrics given in *Equation (5.15)*. However, these metrics can be written into a form that consist of single symbols, as given in *Equations (5.21)* to *(5.28)*. By noting that the second term in *Equations (5.21)* to *(5.28)* only consists of constants, the actual performance of the detection is based on the first term, i.e. minimizing the metric. Thus, only the first term will be taken into account from here on in this particular analysis. Substituting *Equation (5.39a)* into *Equation (5.21)*, the following is obtained

$$\Delta_1^1 h_1^* + (\Delta_2^1)^* h_2$$

$$
\begin{aligned}
&= (a_1 h_1 + a_2 h_2 + g_1 \eta_1) h_1^* + \left(-a_2 h_1^* + a_1 h_2^* + g_1^* \eta_2^*\right) h_2 \\
&= a_1 |h_1|^2 + a_2 h_1^* h_2 + g_1 \eta_1 h_1^* - a_2 h_1^* h_2 + a_1 |h_2|^2 + g_1^* \eta_2^* h_2 \\
&= a_1 |h_1|^2 + a_1 |h_2|^2 + a_2 h_1^* h_2 - a_2 h_1^* h_2 + g_1 \eta_1 h_1^* + g_1^* \eta_2^* h_2 \\
&= \underbrace{\left(|h_1|^2 + |h_2|^2\right) a_1}_{S} + \underbrace{g_1 \eta_1 h_1^* + g_1^* \eta_2^* h_2}_{N} \qquad (5.40)
\end{aligned}
$$

where S denotes the signal part and N the noise part. Substituting *Equation (5.39b)* into *Equation (5.22)* the following is obtained

$$
\begin{aligned}
&\Delta_1^1 h_2^* - (\Delta_2^1)^* h_1 \\
&= (a_1 h_1 + a_2 h_2 + g_1 \eta_1) h_2^* - \left(-a_2 h_1^* + a_1 h_2^* + g_1^* \eta_2^*\right) h_1 \\
&= a_1 h_1 h_2^* + a_2 |h_2|^2 + g_1 \eta_1 h_2^* + a_2 |h_1|^2 - a_1 h_1 h_2^* - g_1^* \eta_2^* h_1 \\
&= a_2 |h_1|^2 + a_2 |h_2|^2 + a_1 h_1 h_2^* - a_1 h_1 h_2^* + g_1 \eta_1 h_2^* - g_1^* \eta_2^* h_1 \\
&= \underbrace{\left(|h_1|^2 + |h_2|^2\right) a_2}_{S} + \underbrace{g_1 \eta_1 h_2^* - g_1^* \eta_2^* h_1}_{N} \qquad (5.41)
\end{aligned}
$$

By using the same method in obtaining *Equations (5.40)* and *(5.41)*, *Equations (5.39c)* to *(5.39h)* are substituted into *Equations (5.23)* to *(5.28)*, respectively, to yield:

$$
\Delta_1^2 h_3^* + (\Delta_2^2)^* h_4 = \underbrace{\left(|h_3|^2 + |h_4|^2\right) a_3}_{S} + \underbrace{g_2 \eta_3 h_3^* + g_2^* \eta_4^* h_4}_{N} \qquad (5.42)
$$

and

$$
\Delta_1^2 h_4^* - (\Delta_2^2)^* h_3 = \underbrace{\left(|h_3|^2 + |h_4|^2\right) a_4}_{S} + \underbrace{g_2 \eta_3 h_4^* - g_2^* \eta_4^* h_3}_{N} \qquad (5.43)
$$

is obtained by substituting *Equations (5.39e)* and *(5.39f)* into *Equations (5.23)* and *(5.24)*. Also note that *Equations (5.40)* to *(5.43)* are symbols detected over $t = 1$ and $t = 2$.

At t = 3 and t = 4, *Equations (5.44)* and *(5.45)* are obtained by substituting *Equation (5.39g)* and *(5.39h)* into *Equation (5.25)* and *(5.26)*.

$$\Delta_3^1 h_1^* + (\Delta_4^1)^* h_2 = \underbrace{\left(|h_1|^2 + |h_2|^2\right)a_3}_{S} + \underbrace{g_1\eta_3 h_1^* + g_1^*\eta_4^* h_2}_{N} \tag{5.44}$$

$$\Delta_3^1 h_2^* - (\Delta_4^1)^* h_1 = \underbrace{\left(|h_1|^2 + |h_2|^2\right)a_4}_{S} + \underbrace{g_1\eta_3 h_2^* - g_1^*\eta_4^* h_1}_{N} \tag{5.45}$$

and *Equations (5.46)* and *(5.47)* are obtained by substituting *Equations (5.39e)* and *(5.39f)* into *Equations (5.27)* and *(5.28)*

$$\Delta_3^2 h_3^* + (\Delta_4^2)^* h_4 = \underbrace{\left(|h_3|^2 + |h_4|^2\right)a_1}_{S} + \underbrace{g_2\eta_1 h_3^* + g_2^*\eta_2^* h_4}_{N} \tag{5.46}$$

$$\Delta_3^2 h_4^* - (\Delta_4^2)^* h_3 = \underbrace{\left(|h_3|^2 + |h_4|^2\right)a_2}_{S} + \underbrace{g_2\eta_1 h_4^* - g_2^*\eta_2^* h_3}_{N} \tag{5.47}$$

Using *Equation (5.7)* all of the equations of similar symbols are added, i.e. *Equations (5.40)* and *(5.46)* for symbol a_1, *Equations (5.41)* and *(5.47)* for symbol a_2, *Equations (5.42)* and *(5.44)* for symbol a_3, and *Equations (5.43)* and *(5.45)* for symbol a_4.

$$\hat{a}_1 = \underbrace{\left(|h_1|^2 + |h_2|^2 + |h_3|^2 + |h_4|^2\right)a_1}_{S} + \underbrace{g_1\eta_1 h_1^* + g_1^*\eta_2^* h_2 + g_2\eta_1 h_3^* + g_2^*\eta_2^* h_4}_{N} \tag{5.48}$$

$$\hat{a}_2 = \underbrace{\left(|h_1|^2 + |h_2|^2 + |h_3|^2 + |h_4|^2\right)a_2}_{S} + \underbrace{g_1\eta_1 h_2^* - g_1^*\eta_2^* h_1 + g_2\eta_1 h_4^* - g_2^*\eta_2^* h_3}_{N} \tag{5.49}$$

$$\hat{a}_3 = \underbrace{\left(|h_1|^2 + |h_2|^2 + |h_3|^2 + |h_4|^2\right)a_3}_{S} + \underbrace{g_2\eta_3 h_3^* + g_2^*\eta_4^* h_4 + g_1\eta_3 h_1^* + g_1^*\eta_4^* h_2}_{N} \tag{5.50}$$

$$\hat{a}_4 = \underbrace{\left(|h_1|^2 + |h_2|^2 + |h_3|^2 + |h_4|^2\right)a_4}_{S} + \underbrace{g_2\eta_3 h_4^* - g_2^*\eta_4^* h_3 + g_1\eta_3 h_2^* - g_1^*\eta_4^* h_1}_{N} \qquad (5.51)$$

Note that full diversity is obtained as described in *Chapter 3, Section 3.6*. Also note that full rate is obtained since 4 symbols are decoded over 4 time periods.

Non-Perfect cross correlation

In the case of non-perfect cross correlation $g_1 g_2 \neq 0$ and $(g_1)^2 = 1$, $(g_2)^2 = 1$. Thus, *Equations (5.38)* cannot be reduced, and are substituted directly into *Equation (5.21)* to *(5.28)*. Thus, following the same reasoning as the section on perfect correlation, *Equation (5.38a)* is substituted into *Equation (5.21)*,

$$\Delta_1^1 h_1^* + (\Delta_2^1)^* h_2$$

$$= \left(a_1(g_1)^2 h_1 + a_2(g_1)^2 h_2 + a_3 g_1 g_2 h_3 + a_4 g_1 g_2 h_4 + g_1\eta_1\right)h_1^* +$$
$$\left(-a_2^*(g_1)^2 h_1 + a_1^*(g_1)^2 h_2 - a_4^* g_1 g_2 h_3 + a_3^* g_1 g_2 h_4 + g_1\eta_2\right)^* h_2$$

$$= \left(a_1|h_1|^2 + a_2 h_1^* h_2 + a_3(g_1 g_2)h_1^* h_3 + a_4(g_1 g_2)h_1^* h_4 + g_1\eta_1 h_1^*\right) +$$

$$\left(-a_2 h_1^* h_2 + a_1|h_2|^2 - a_4(g_1 g_2)^* h_2 h_3^* + a_3(g_1 g_2)^* h_2 h_4^* + g_1^*\eta_2^* h_2\right)$$

$$= \left(a_1|h_1|^2 + a_1|h_2|^2 + a_3(g_1 g_2)h_1^* h_3 + a_3(g_1 g_2)^* h_2 h_4^* + g_1\eta_1 h_1^*\right) +$$
$$\left(a_4(g_1 g_2)h_1^* h_4 - a_4(g_1 g_2)^* h_2 h_3^* + g_1^*\eta_2^* h_2\right)$$

$$= \underbrace{\left(|h_1|^2 + |h_2|^2\right)a_1}_{S} + \underbrace{a_3(g_1 g_2)h_1^* h_3 + a_3(g_1 g_2)^* h_2 h_4^* + g_1\eta_1 h_1^* +}_{N_1}$$
$$\underbrace{\left(a_4(g_1 g_2)h_1^* h_4 - a_4(g_1 g_2)^* h_2 h_3^* + g_1^*\eta_2^* h_2\right)}_{N_2} \qquad (5.52)$$

where S once again denotes the signal part, and N_1 and N_2 the first and second noise parts respectively. Substituting *Equation (5.38b)* into *Equation (5.22)* the following is obtained

$$\Delta_1^1 h_2^* - (\Delta_2^1)^* h_1$$

$$= \left(a_1 (g_1)^2 h_1 + a_2 (g_1)^2 h_2 + a_3 g_1 g_2 h_3 + a_4 g_1 g_2 h_4 + g_1 \eta_1\right) h_2^* -$$
$$\left(-a_2^* (g_1)^2 h_1 + a_1^* (g_1)^2 h_2 - a_4^* g_1 g_2 h_3 + a_3^* g_1 g_2 h_4 + g_1 \eta_2\right)^* h_1$$

$$= \left(a_1 h_1 h_2^* + a_2 |h_2|^2 + a_3 (g_1 g_2) h_2^* h_3 + a_4 (g_1 g_2) h_2^* h_4 + g_1 \eta_1 h_2^*\right) -$$
$$\left(-a_2 |h_1|^2 + a_1 h_1 h_2^* - a_4 (g_1 g_2)^* h_1 h_3^* + a_3 (g_1 g_2)^* h_1 h_4^* + g_1^* \eta_2^* h_1\right)$$

$$= \left(a_2 |h_1|^2 + a_2 |h_2|^2 + a_3 (g_1 g_2) h_2^* h_3 + a_4 (g_1 g_2) h_2^* h_4 + g_1 \eta_1 h_2^*\right) +$$
$$\left(a_4 (g_1 g_2)^* h_1 h_3^* - a_3 (g_1 g_2)^* h_1 h_4^* - g_1^* \eta_2^* h_1\right)$$

$$= \underbrace{\left(|h_1|^2 + |h_2|^2\right) a_2}_{S} + \underbrace{a_3 (g_1 g_2) h_2^* h_3 - a_3 (g_1 g_2)^* h_1 h_4^* + g_1 \eta_1 h_2^*}_{N_1} +$$
$$\underbrace{\left(+ a_4 (g_1 g_2) h_2^* h_4 + a_4 (g_1 g_2)^* h_1 h_3^* - g_1^* \eta_2^* h_1\right)}_{N_2} \qquad (5.53)$$

By using the same method in obtaining *Equations (5.52)* and *(5.53)*, Equations *(5.38c)* to *(5.38h)* are substituted into *Equations (5.23)* to *(5.28)*, to yield:

$$\Delta_1^2 h_3^* + (\Delta_2^2)^* h_4 = \underbrace{\left(|h_3|^2 + |h_4|^2\right) a_3}_{S} + \underbrace{a_1 (g_1 g_2) h_1 h_3^* + a_1 (g_1 g_2)^* h_2^* h_4 + g_2 \eta_1 h_3^* +}_{N_1}$$
$$\underbrace{\left(a_2 (g_1 g_2) h_2 h_3^* - a_2 (g_1 g_2)^* h_1^* h_4 + g_2^* \eta_2^* h_4\right)}_{N_2} \qquad (5.54)$$

and

$$\Delta_1^2 h_4^* - (\Delta_2^2)^* h_3 = \underbrace{\left(|h_3|^2 + |h_4|^2\right) a_4}_{S} + \underbrace{a_1 (g_1 g_2) h_1 h_4^* - a_1 (g_1 g_2)^* h_2^* h_3 + g_2 \eta_1 h_4^*}_{N_1} +$$

$$\underbrace{\left(+a_2(g_1g_2)h_2h_4^* + a_2(g_1g_2)^* h_1^* h_3 - g_2^*\eta_2^* h_3\right)}_{N_2} \tag{5.55}$$

is obtained from substituting *Equations (5.38e)* and *(5.38f)* into *Equations (5.23)* and *(5.24)*. Also note that *Equations (5.52)* to *(5.55)* are symbols detected over $t = 1$ and $t = 2$.

At $t = 3$ and $t = 4$, *Equations (5.56)* and *(5.57)* are obtained by substituting *Equation (5.38g)* and *(5.38h)* into *Equation (5.25)* and *(5.26)*

$$\Delta_3^1 h_1^* + (\Delta_4^1)^* h_2 = \underbrace{\left(|h_1|^2 + |h_2|^2\right)a_3}_{S} + \underbrace{a_1(g_1g_2)h_1^* h_3 + a_1(g_1g_2)^* h_2 h_4^* + g_1\eta_3 h_1^* +}_{N_1}$$
$$\underbrace{\left(a_2(g_1g_2)h_1^* h_4 - a_2(g_1g_2)^* h_2 h_3^* + g_1^*\eta_4^* h_2\right)}_{N_2} \tag{5.56}$$

and

$$\Delta_3^1 h_2^* - (\Delta_4^1)^* h_1 = \underbrace{\left(|h_1|^2 + |h_2|^2\right)a_4}_{S} + \underbrace{a_1(g_1g_2)h_2^* h_3 - a_1(g_1g_2)^* h_1 h_4^* + g_1\eta_3 h_2^* +}_{N_1}$$
$$\underbrace{\left(+a_2(g_1g_2)h_2^* h_4 + a_2(g_1g_2)^* h_1 h_3^* - g_1^*\eta_4^* h_1\right)}_{N_2} \tag{5.57}$$

and *Equations (5.58)* and *(5.59)* are obtained by substituting *Equations (5.38e)* and *(5.38f)* into *Equations (5.27)* and *(5.28)*

$$\Delta_3^2 h_3^* + (\Delta_4^2)^* h_4 = \underbrace{\left(|h_3|^2 + |h_4|^2\right)a_1}_{S} + \underbrace{a_3(g_1g_2)h_1 h_3^* + a_3(g_1g_2)^* h_2^* h_4 + g_2\eta_3 h_3^* +}_{N_1}$$
$$\underbrace{\left(a_4(g_1g_2)h_2 h_3^* - a_4(g_1g_2)^* h_1^* h_4 + g_2^*\eta_4^* h_4\right)}_{N_2} \tag{5.58}$$

and

$$\Delta_3^2 h_4^* - (\Delta_4^2)^* h_3 = \underbrace{\left(|h_3|^2 + |h_4|^2\right)a_2}_{S} + \underbrace{a_3(g_1g_2)h_1 h_4^* - a_3(g_1g_2)^* h_2^* h_3 + g_2\eta_3 h_4^* +}_{N_1}$$
$$\underbrace{\left(+a_4(g_1g_2)h_2 h_4^* + a_4(g_1g_2)^* h_1^* h_3 - g_2^*\eta_4^* h_3\right)}_{N_2} \tag{5.59}$$

Using *Equation (5.7)* all of the Equations of similar symbols are added, i.e. *Equations (5.52)* and *(5.58)* for symbol b_1, *Equations (5.53)* and *(5.59)* for symbol b_2, *Equations (5.54)* and *(5.56)* for symbol b_3, and *Equations (5.55)* and *(5.57)* for symbol b_4.

$$\hat{a}_1 = \underbrace{\left(|h_1|^2 + |h_2|^2 + |h_3|^2 + |h_4|^2\right)a_1}_{S} + \underbrace{a_3(g_1g_2)h_1^*h_3 + a_3(g_1g_2)^*h_2h_4^* + g_1\eta_1h_1^* + g_1^*\eta_2^*h_2 +}_{N_1}$$

$$\underbrace{a_3(g_1g_2)h_1h_3^* + a_3(g_1g_2)^*h_2^*h_4 + g_2\eta_3h_3^* + g_2^*\eta_4^*h_4}_{N_2} \quad (5.60)$$

$$\hat{a}_2 = \underbrace{\left(|h_1|^2 + |h_2|^2 + |h_3|^2 + |h_4|^2\right)a_2}_{S} + \underbrace{a_4(g_1g_2)h_2^*h_4 + a_4(g_1g_2)^*h_1h_3^* - g_1^*\eta_2^*h_1 + g_1\eta_1h_2^* +}_{N_1}$$

$$\underbrace{a_4(g_1g_2)h_2h_4^* + a_4(g_1g_2)^*h_1^*h_3 - g_2^*\eta_4^*h_3 + g_2\eta_3h_4^*}_{N_2} \quad (5.61)$$

$$\hat{a}_3 = \underbrace{\left(|h_1|^2 + |h_2|^2 + |h_3|^2 + |h_4|^2\right)a_3}_{S} + \underbrace{a_1(g_1g_2)h_1h_3^* + a_1(g_1g_2)^*h_2^*h_4 + g_2\eta_1h_3^* + g_2^*\eta_2^*h_4}_{N_1}$$

$$\underbrace{a_1(g_1g_2)h_1^*h_3 + a_1(g_1g_2)^*h_2h_4^* + g_1\eta_3h_1^* + g_1^*\eta_4^*h_2}_{N_2} \quad (5.62)$$

$$\hat{a}_4 = \underbrace{\left(|h_1|^2 + |h_2|^2 + |h_3|^2 + |h_4|^2\right)a_4}_{S} + \underbrace{a_2(g_1g_2)h_2h_4^* + a_2(g_1g_2)^*h_1^*h_3 - g_2^*\eta_2^*h_3 + g_2\eta_1h_4^* +}_{N_1}$$

$$\underbrace{a_2(g_1g_2)h_2^*h_4 + a_2(g_1g_2)^*h_1h_3^* - g_1^*\eta_4^*h_1 + g_1\eta_3h_2^*}_{N_2} \quad (5.63)$$

Comparing *Equations (5.60)* to *(5.63)* with *Equations (5.48)* to *(5.51)*, it can be seen that up to 4 times as much self noise is created in the DSSTS scheme when non-perfect cross-correlation occurs.

5.2 DSSTS CAPACITY

As mentioned earlier in this dissertation, the DSSTS is a transmit diversity scheme. In most cases with transmit diversity, the transmitter does not have knowledge of the channel. Hence,

the open-loop capacity for a Multiple-Input Single-Output (MISO) system with n transmit antennas applies [27]

$$CAP_{n,1}^{MISO,\max} = \log_2\left(1+\frac{SNR}{n}\sum_{i=1}^{n}|h_i|^2\right) \tag{5.64}$$

where h_i is the gain for receive antenna i and the normalisation by n ensures a fixed total transmitter power. Note that *Equation (5.64)* is obtained by substituting in *Chapter 2, Section 2.5, Equation (2.32)*, $m = 1$ and $H = \begin{bmatrix} h_1 & h_2 \cdots h_n \end{bmatrix}$.

The channel capacity of the DSSTS scheme can best be described by means of an example. By using the example of *Section 5.1.2*, *Equation (5.10)*, the transmission matrix of the DSSTS scheme, employing four transmit antennas, can be written as

$$T_4 = \begin{bmatrix} g_1x_1 & g_1x_2 & g_2x_3 & g_2x_4 \\ -g_1x_2^* & g_1x_1^* & -g_2x_4^* & g_2x_3^* \\ g_1x_3 & g_1x_4 & g_2x_1 & g_2x_2 \\ -g_1x_4^* & g_1x_3^* & -g_2x_2^* & g_2x_1^* \end{bmatrix} \tag{5.65}$$

Thus, form *Chapter 2, Section 2.5, Equation (2.27)*, received signal can written as

$$\bar{r} = T_4\bar{h} + \bar{\eta} \tag{5.66}$$

where $\bar{h} = \begin{bmatrix} h_1 & h_2 & h_3 & h_4 \end{bmatrix}^T$ and $\bar{\eta} = \begin{bmatrix} \eta_1 & \eta_2 & \eta_3 & \eta_4 \end{bmatrix}^T$

Thus, the four baseband signals arriving at the receive antenna can be expressed as

$$\begin{bmatrix} r_1 \\ r_2 \\ r_3 \\ r_4 \end{bmatrix} = \begin{bmatrix} g_1x_1h_1 + g_1x_2h_2 + g_2x_3h_3 + g_2x_4h_4 \\ -g_1x_2^*h_1 + g_1x_1^*h_2 - g_2x_4^*h_3 + g_2x_3^*h_4 \\ g_1x_3h_1 + g_1x_4h_2 + g_2x_1h_3 + g_2x_2h_4 \\ -g_1x_4^*h_1 + g_1x_3^*h_2 - g_2x_2^*h_3 + g_2x_1^*h_4 \end{bmatrix} + \begin{bmatrix} \eta_1 \\ \eta_2 \\ \eta_3 \\ \eta_4 \end{bmatrix} \tag{5.67}$$

By conjugating the second and fourth received signals, *Equation (5.67)* can equivalently be rewritten as

$$\begin{bmatrix} r_1 \\ r_2^* \\ r_3 \\ r_4^* \end{bmatrix} = \begin{bmatrix} g_1h_1 & g_1h_2 & g_2h_3 & g_2h_4 \\ g_1^*h_2^* & -g_1^*h_1^* & g_2h_4^* & -g_2^*h_3^* \\ g_2h_3 & g_2h_4 & g_1h_1 & g_1h_2 \\ g_2h_4^* & -g_2h_3^* & g_1h_2^* & -g_1h_1^* \end{bmatrix} \begin{bmatrix} x_1 \\ x_2 \\ x_3 \\ x_4 \end{bmatrix} + \begin{bmatrix} \eta_1 \\ \eta_2^* \\ \eta_3 \\ \eta_4^* \end{bmatrix} \tag{5.68}$$

Note that the condition stated in *Chapter 2, Section 2.5, Equation (2.30)* is satisfied by *Equation (5.68)*. After matched-filtering with H, we obtain

$$\begin{aligned} \hat{\bar{r}} &= H^H \bar{r} \\ &= \begin{bmatrix} |h_1|^2+|h_2|^2+|h_3|^2+|h_4|^2 & 0 & \cdots \\ 0 & |h_1|^2+|h_2|^2+|h_3|^2+|h_4|^2 & \\ 0 & 0 & \cdots \\ 0 & 0 & \end{bmatrix} \\ &\quad \begin{bmatrix} 0 & 0 \\ 0 & 0 \\ |h_1|^2+|h_2|^2+|h_3|^2+|h_4|^2 & 0 \\ 0 & |h_1|^2+|h_2|^2+|h_3|^2+|h_4|^2 \end{bmatrix} \begin{bmatrix} x_1 \\ x_2 \\ x_3 \\ x_4 \end{bmatrix} + \begin{bmatrix} \eta_1 \\ \eta_2^* \\ \eta_3 \\ \eta_4^* \end{bmatrix} \end{aligned} \tag{5.69}$$

where the noise vector $\bar{\eta}$ remains white. Note that the DSSTS scheme is fully decomposable in four (1,1) systems, where each has ¼ of the transmitted power. Thus, the total capacity of the DSSTS scheme with four transmit antennas is

$$CAP_{4,1}^{DSSTS} = \log_2\left(1+\frac{SNR}{4}\left(|h_1|^2+|h_2|^2+|h_3|^2+|h_4|^2\right)\right) \tag{5.70}$$

Comparing *Equation (5.70)* to *Equation (5.64)*, we see that

$$CAP_{4,1}^{DSSTS} = CAP_{4,1}^{MISO,\max} \tag{5.71}$$

Following the same reasoning for obtaining *Equation (5.71)*, similar results may be derived for the DSSTS 6, 8 and 10 transmit antenna scenarios. In general, the capacity performance of the DSSTS is similar to the open-loop capacity given in *Equation (5.72)*

$$CAP_{n,1}^{DSSTS} = CAP_{n,1}^{MISO,\max} \tag{5.72}$$

Capacity plots for the DSSTS with 2, 4, 6 transmit antennas, that is equal to $CAP_{n,1}^{MISO,\max}$, are plotted in *Chapter 6, Figure 6.23*. Note that the capacity increases as the number of transmit antennas increases. Also note that Capacity plots of other transmit diversity schemes, i.e. the Zero Forcing (ZF) [18] and a proposed (4x1) transmit diversity scheme in [18] are presented in *Chapter 6, Figure 6.23*. These are included to show the relative performance of the DSSTS schemes considered.

5.3 DSSTS PERFORMANCE EVALUTION PLATFORM

The complete FFCS platform used in this dissertation is shown in *Figure 5.4,* and the configuration parameters are presented in *Table 5.1*. This platform is built around the DSSTS scheme's encoder and decoder structures, discussed in *Sections 5.1.2* and 5*.1.3*.

At any given time, the bitstream $\bar{b}$ arrives at the DSSTS encoder (see *Section 5.1.1*). This bitstream is encoded and transmitted from antennas 1 to *n*. By using a complex FFCS from *Chapter 4, Section 4.1*, each symbol transmitted from an antenna is separated into it's real, $\mathrm{Re}\{\bullet\}$ and Imaginary, $\mathrm{Im}\{\bullet\}$ parts. At the receiver side, all the real and imaginary parts are added respectively. AWGN, denoted as η, and described in Appendix C*, Section C.5*, is added to the real and imaginary parts respectively and decoded by the DSSTS scheme's decoder. The decoder uses perfect CSI, denoted by *h*, from all the different channels used in the simulation, in order to decode the received bitstream. The output bitstream $\hat{\bar{b}}$ from the decoder is compared to the input bitstream $\bar{b}$ and the BER is calculated. These BER graphs are presented and discussed in *Chapter 6*.

Configuration Parameter	Setting
Unspread Symbol Rate	1000 [symbols/s]
Spreading Sequence Length, *N*	32 [chips]
Spreading Sequence Rate	32000 [chips/s]
Effective RF Carrier Frequency	900 [MHz]
Receiver Configuration	ML detection
Symbol Synchronization	Perfect
Carrier Synchronization	Perfect
Code Lock	Perfect
Spreading Sequences Supported	Walsh

Table 5.1. DSSTS Simulation Configurations.

Up to 10 transmit antennas are used in this simulation study, depicted in *Figure 5.4*. For each of the 10 transmit antennas, a complex FFCS, based on independent *Clarke*-based complex FFCS, were used to realise the 10 distinct transmission paths transversed by the outputs of the DSSTS scheme. The channels are also assumed to be quasi-static over two consecutive time periods in order to decode the received symbols by means of the ST decoder (see *Section 5.1.3*) In other words, every second time interval the channels experience statistical independent fading. Although this seems very unrealistic in a real world scenario, this method had to be used in order to compare it to the original Alamouti scheme's performance presented in [2].

Perfect power control was assumed, i.e. the average powers of all the users' corrupted signals received at the receive antenna are equal. As described in *Chapter 4*, the complex FFCS can be set to Doppler frequencies of 33, 66, and 100Hz to simulate spectral broadening due to mobility (i.e. fast fading), and the Rician factor determines the ratio of the LOS to NLOS components in the channel simulator. If *K*, in a dB scale, is large, the LOS is more prominent and Rician fading occurs. On the other hand if $K \to -\infty$ dB, the NLOS factor is more prominent and Rayleigh fading occurs. Perfect carrier, chip and symbol synchronisation were assumed at the receiver over the entire frame length *l* and perfect CSI was used by the decoder to decode the received symbols.

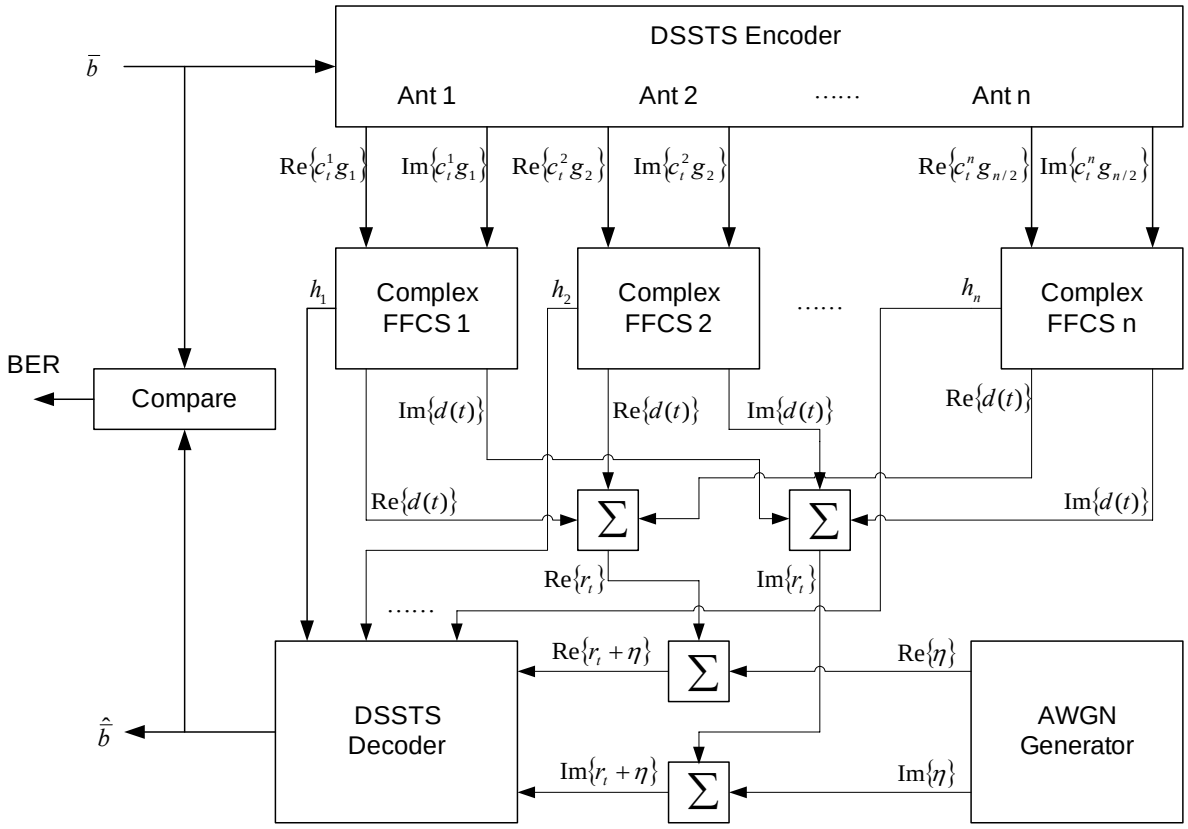

Figure 5.4. Performance evaluation platform of the new DSSTS scheme.

5.4 A SPACE - SEQUENCE TRANSMIT DIVERSITY SCHEME: SSTD

In *Chapter 3*, it was stated that Alamouti's classic ST coding scheme has an unrealistic assumption in the decoupling stage for environments with a low throughput rate and high Doppler component, i.e. that the channel is quasi-static over two consecutive symbol intervals. To address this deficiency, a new scheme called, Space-Sequence Transmit Diversity (SSTD), has been proposed by Maasdorp *et al*. [19, 20]. The proposed SSTD scheme is in essence a combination between the Alamouti matrix and a DS/SSMA scheme using CSSs, facilitating the transmission of all the ST symbols in one time interval. Also note that only a general overview of the SSTD is presented here in order to show that the quasi-static channel assumption can be addressed. Background information on CSSs, as well as detailed descriptions of the complex DS/SSMA QPSK transmitter and RAKE receiver simulator structures, can be obtained from Maasdorp *et al*. [19, 20].

5.4.1 SSTD encoder structure

Figure 5.5 shows the proposed SSTD encoder structure, constructed using four complex DS/SSMA QPSK transmitters. This diversity encoder is based on *Alamouti*'s original STC scheme, described in *Chapter 2*, *Section 2.2.2*. It functions as follows:

At the *m'th* encoding instance, four consecutive antipodal input data bits are inserted into the vector $b_m^q = \left[b_{m,0}^q \quad b_{m,1}^q \quad b_{m,2}^q \quad b_{m,3}^q \right]$. Using the following mapping, this vector is encoded into a 2-bit complex input (represented by the respective I-channel and Q-channel bits, $c_m^{I,(q,z)}$ and $c_m^{Q,(q,z)}$, with z = 0; 1; 2; 3) for each of the four complex DS/SSMA QPSK transmitters in user-q's SSTD encoder:

$$\begin{bmatrix} c_m^{I,(q,0)} = c_m^{I,(q,3)} \\ c_m^{I,(q,0)} = -c_m^{I,(q,3)} \\ c_m^{I,(q,1)} = -c_m^{I,(q,3)} \\ c_m^{I,(q,1)} = c_m^{I,(q,3)} \end{bmatrix} = \begin{bmatrix} 1 & 0 & 0 & 0 \\ 0 & 1 & 0 & 0 \\ 0 & 0 & -1 & 0 \\ 0 & 0 & 0 & 1 \end{bmatrix} \begin{bmatrix} b_{m,0}^q \\ b_{m,1}^q \\ b_{m,2}^q \\ b_{m,3}^q \end{bmatrix} \tag{5.73}$$

Thus, the wideband transmitters in the SSTD encoder (described in Maasdorp *et al*. [19]) each transmit W = 1 complex symbols during the m'th encoding instance. Let $\Omega_m^{(q,z)}(t)$, with z = 0; 1; 2; 3, denote the output waveforms generated by the 4 transmitters in user-q's SSTD encoder. These output waveforms, representing complex transmitter output symbols from the alphabet $\nu = \{\nu_0 \quad \nu_1 \quad \nu_2 \quad \nu_3\}$ (see *Equation (5.78)*), are now transmitted on the antenna pair, y=1 and y=2, using the following transmission matrix:

$$T = \begin{bmatrix} \Omega_m^{(q,0)}(t) & \Omega_m^{(q,2)}(t) \\ \Omega_m^{(q,1)}(t) & \Omega_m^{(q,3)}(t) \end{bmatrix} \begin{matrix} \} \\ \} \end{matrix} \begin{matrix} Transmits\ during \\ I_0 \end{matrix}$$
$$\begin{matrix} \uparrow & \uparrow \\ y=1 & y=2 \end{matrix} \tag{5.74}$$

where $I_0 : m \cdot T_s < t \le (m+1) \cdot T_s$ Thus, the outputs emanating from antenna y=1 and y=2 are given by:

$$s_m^{y=1,q}(t) = \mathrm{Re}\left\{\Omega_m^{(q,0)}(t)\right\} + \mathrm{Re}\left\{\Omega_m^{(q,1)}(t)\right\} + j\left(\mathrm{Im}\left\{\Omega_m^{(q,0)}(t)\right\} + \mathrm{Im}\left\{\Omega_m^{(q,1)}(t)\right\}\right) \qquad (5.75)$$

$$s_m^{y=2,q}(t) = \mathrm{Re}\left\{\Omega_m^{(q,2)}(t)\right\} + \mathrm{Re}\left\{\Omega_m^{(q,3)}(t)\right\} + j\left(\mathrm{Im}\left\{\Omega_m^{(q,2)}(t)\right\} + \mathrm{Im}\left\{\Omega_m^{(q,3)}(t)\right\}\right) \qquad (5.76)$$

respectively. Note that the assignment of CSSs to the 4 wideband complex DS/SSMA QPSK transmitters, to form a single user's SSTD encoder, constitutes a major design challenge.

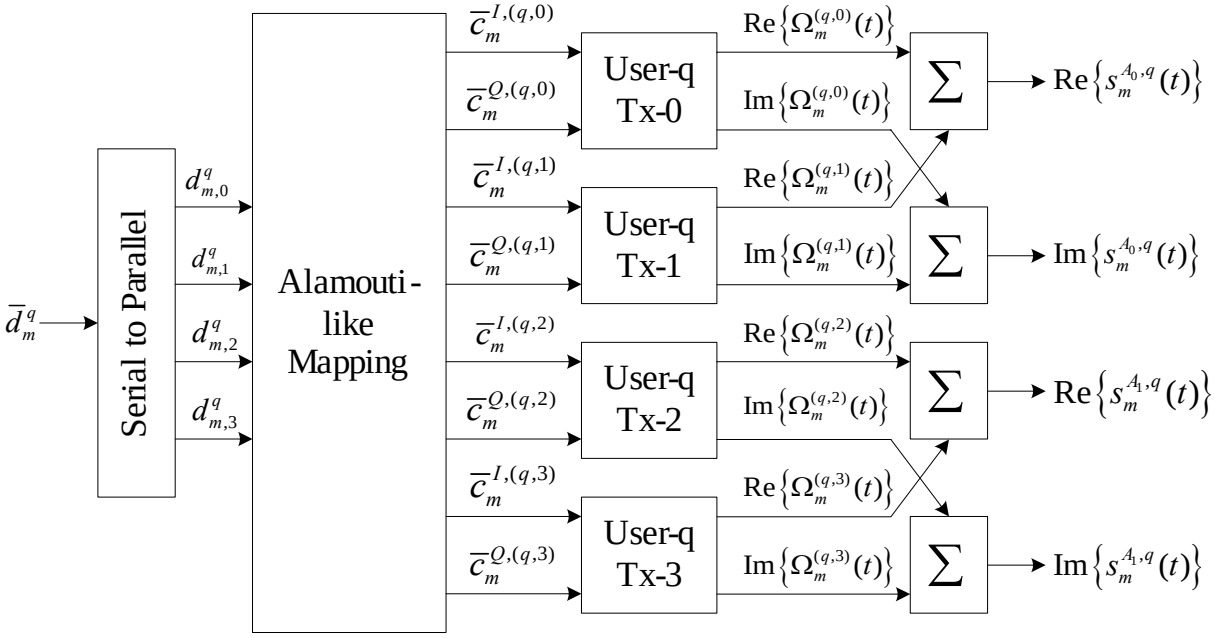

Figure 5.5. Proposed SSTD Encoder for user-q.

Presently, only two possible CSS assignment options were evaluated in this particular study, as described in *Chapter 6, section 6.4*. Also note that the transmit matrix *T* in *Equation (5.74)* is transmitted in one symbol time interval, as described by *Equations (5.75)* and *(5.76)*. Thus forcing the two consecutive symbols transmitted from antennas y=1 and y=2 respectively to have the same fading as they propagate through a channel path as a combined symbol. This effectively means that the assumption of the channel having to be quasi-static can be neglected, but the same decoding algorithm can be used.

5.4.2 SSTD decoder structure

Figure 5.6 shows the proposed SSTD decoder structure, constructed using four complex DS/SSMA QPSK RAKE receivers. The decoding process firstly involves demodulation of the received signals $r_m^{(q,k)}(t) = r_m^q(t)$ using the four separate RAKE receivers to obtain $y_m^{(q,k)}$, for k = 0, 1, 2, 3. These soft outputs are then appropriately combined to give $\overline{u}_m^{0,q}$ and $\overline{u}_m^{1,q}$.

Next, the following set of Euclidian distance metrics must be calculated for all combinations of the index parameters i = 0, 1, 2, 3 and j = 0, 1, 2, 3:

$$DM_{i,j}^{q} = \left|u_m^{0,q} - \hat{\alpha}_m^{n=1,q} \cdot v_i - \hat{\alpha}_m^{n=2,q} \cdot v_j\right|^2 + \left|u_m^{1,q} + \hat{\alpha}_m^{n=1,q} \cdot v_j^* - \hat{\alpha}_m^{n=2,q} \cdot v_i^*\right|^2 \qquad (5.77)$$

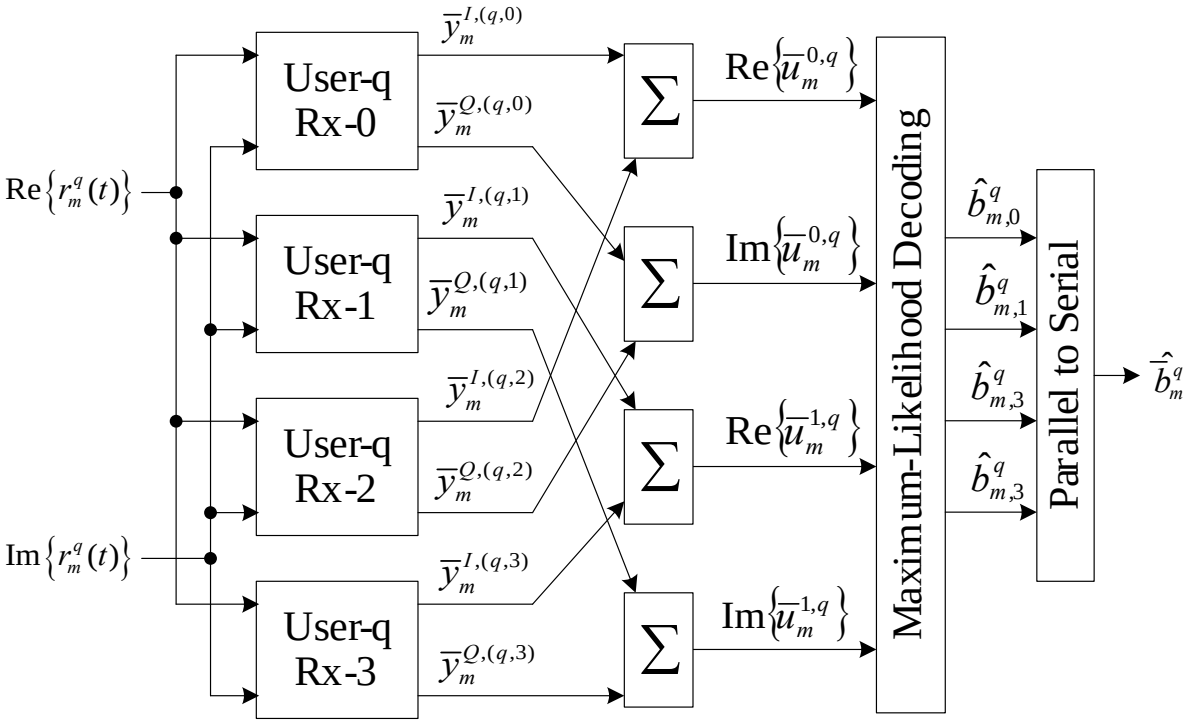

Figure 5.6. Proposed SSTD Decoder for user-q.

where $\nu_i \in \nu$ and $\nu_j \in \nu$, with ν the set of possible complex DS/SSMA QPSK output symbols, defined as follows:

$$\begin{aligned}\nu &= \{\nu_0 \quad \nu_1 \quad \nu_2 \quad \nu_3\} \\ &= \{(1, i) \quad (1,-i) \quad (-1,-i) \quad (-1, i)\}\end{aligned} \tag{5.78}$$

The average fading amplitude estimates associated with the signals transmitted by antenna y=1 and y=2 are given by $\hat{\alpha}_m^{n=1,q} = \hat{\alpha}_m^{(q,0)} = \hat{\alpha}_m^{(q,1)}$ and $\hat{\alpha}_m^{n=2,q} = \hat{\alpha}_m^{(q,2)} = \hat{\alpha}_m^{(q,3)}$ respectively. Maximum-Likelihood (ML) decoding involves finding $\min\{DM_{i,j}^q\} = DM_{i\,ML,j\,ML}^q$ over all combinations of i and j. The SSTD decoder's four output bit estimates are then determined as follows: $\hat{b}_{m,0}^q = \mathrm{Re}\{\nu_{i\,ML}\}, \hat{b}_{m,1}^q = \mathrm{Im}\{\nu_{i\,ML}\}, \hat{b}_{m,2}^q = \mathrm{Re}\{\nu_{jML}\}$ and $\hat{b}_{m,3}^q = \mathrm{Im}\{\nu_{j\,ML}\}$.

CHAPTER SIX

RESULTS

In this chapter, all theoretical as well as simulation results described in *Chapters 2* to *5* are presented. In more detail, this chapter is structured as follows: In *Section 6.1* performance results of the DSSTS scheme in Rayleigh as well as Rician fading conditions are presented. Further, performance results of a Rayleigh vs. Rician fading environment are also presented here. The results of the SSTD scheme is not presented in this study, but can be obtained in [19, 20]. Lastly, in *Section 6.2*, the capacity CCDFs for the DSSTS scheme are presented.

Following a similar approach as in [17], the performance evaluation platform was implemented in C++ using an Object Orientated Programming (OOP) approach. The C++ code was compiled using *Intel*'s *ICC* and *GNU*'s *G++* compilers for *Linux* platforms. The BER performance results presented in *Section 6.1* were obtained by distributing the processor load of the simulation software over multiple workstations in the *University of Pretoria*'s *I-percube*, donated by *Intel*. The *I-percube* consists of 16 2.4GHz *Pentium 4* stations, each station running a *Mandrake Linux* operating system. The 16 stations are

interconnected via *Fast Ethernet* connections, where process migration and message handling between the stations are managed transparently by *Open Mosix* for *Linux*. By using the I-percube, BER performance results that are usually time consuming, are obtained in a much faster fashion.

6.1 DSSTS RESULTS

The BER performance results of the DSSTS scheme's 2 to 10 antenna scenarios are presented in the following subsections for different channel parameters and environmental conditions. The simulation results were obtained by using the performance evaluation platform shown in *Chapter 5, Figure 5.4*. In all the BER performance graphs, the theoretical BER of a flat fading Rayleigh channel, as well as the theoretical BER of an AWGN channel is included as baseline reference to the performance of the proposed new DSSTS schemes. The theoretical derived BER of Alamouti's 2 antenna scenario is also included as reference against which subsequent DSSTS results will be benchmarked. The following assumptions were made during the evaluation of the DSSTS scheme:

- The total transmit power emanating from all of the DSSTS's different antenna scenarios equals the transmit power from a single transmit antenna scenario, i.e., perfect power conservation is assumed and unity power is transmitted in all cases.
- The fading amplitudes from each transmit antenna to the single receive antenna are mutually uncorrelated and Rayleigh or Rician distributed. In the case of the Rician distributed fading amplitudes, a LOS component of 6dB was added. See *Chapter 4, Section 4.1*.

Further assumptions include:

- The average powers received from each transmit antenna are the same at the receive antenna.
- The receiver has perfect knowledge of the channel, i.e. perfect CSI is assumed.

6.1.1 Performance results in a Rayleigh fading environment

Increasing the DSSTS scheme's number of antennas for a single user, directly effects it's BER performance. In order to show the effect of increasing the number of antennas for a single user on the BER performance of the DSSTS scheme in a Rayleigh fading environment (K = -100dB), the graphs are plotted at similar Doppler frequencies, i.e. 33Hz, 66Hz, and 100Hz, respectively. The simulation platform presented in *Chapter 5, Section 5.1.6* were used to simulate these effects and presented in *Figure 6.1*, *Figure 6.2*, and *Figure 6.3*, respectively.

From these figures the following general observations can be made:

- Improved BER performances of 7.5dB to 9dB are obtained by incorporating temporal (DS-SS) spreading into Alamouti's orthogonal ST coding scheme.
- A further improvement in BER performance of up to 2dB is obtained by increasing the number of transmit antennas. This improvement can be mainly attributed to transmit antenna diversity gain, i.e. the exploitation of additional space diversity.
- The 10 DSSTS antenna scheme performed the best and within 4dB of the AWGN channel scenario.

From *Figure 6.1*, i.e. with a Doppler frequency of 33Hz, the following important observations can be made:

- The DSSTS's 2 transmit antenna scenario obtained a 7.5dB gain over Alamouti's original 2 transmit antenna scheme.
- The DSSTS's 10 transmit antenna scenario performed the best; a 9.5dB gain is obtained at a BER of 10^{-4} over Alamouti's original 2 transmit antenna scheme. Note that it performed within 4dB of the AWGN channel scenario.

  The best performance gain between the different DSSTS schemes was obtained between the DSSTS's 2 transmit and 4 transmit antenna scenarios. A performance gain of 1dB is obtained at a BER of 10^{-4}. Smaller performance gains are obtained as the number of transmit antennas increase. This can be attributed to multi antenna interference as a result of the receiver's cross correlation between different

spreading sequences not being perfect, as described in *Chapter 5, Section 5.1.4*. As the number of transmit antennas increase, the level of non-perfect cross-correlation interference increases and less gain is obtained.

- The DSSTS's 10 transmit antenna scenario only obtained a 2dB gain over the DSSTS's 2 transmit antennas scenario.

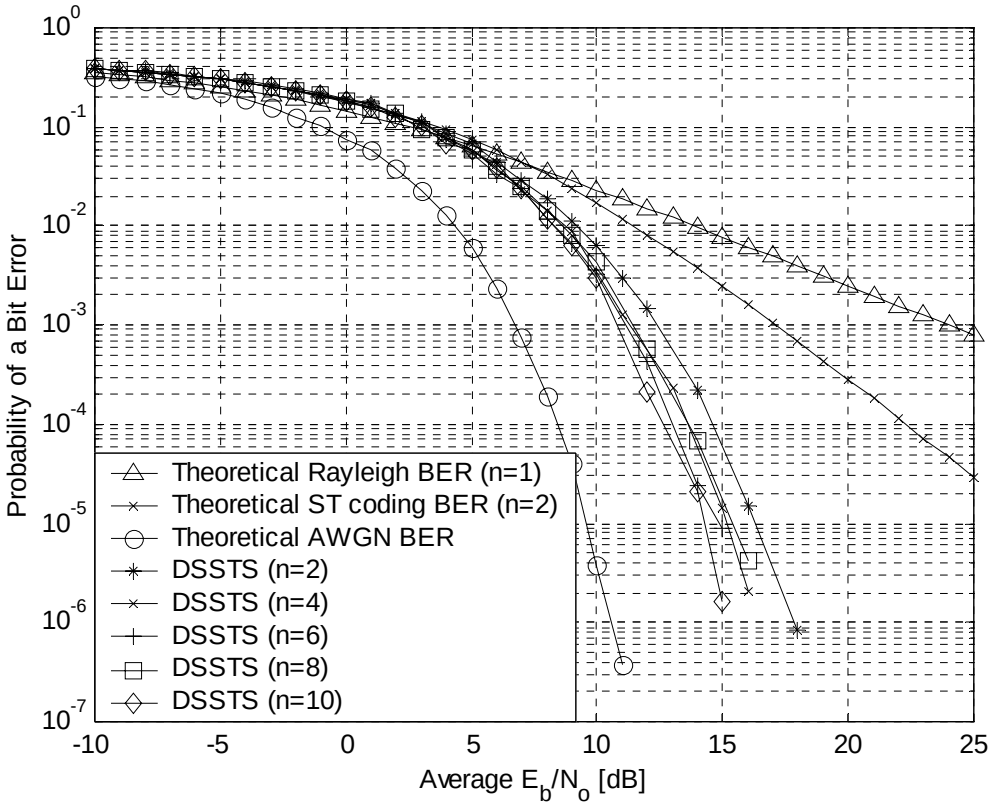

Figure 6.1. Single user performance evaluation for the DSSTS's 2 to 10 antennas scenario in a Rayleigh fading environment for f_d = 33Hz.

From *Figures 6.2* and *6.3* (i.e. with Doppler frequencies of 66Hz and 100Hz respectively), the following important observations can be made:

- The DSSTS's 2 transmit antenna scenario obtained a 8.5dB gain over Alamouti's original 2 transmit antennas scheme.
- The DSSTS's 10 transmit antenna scenario performed the best; a 9.5dB gain is obtained at a BER of 10^{-4} over Alamouti's original 2 transmit antennas scheme.

- As was the case with a Doppler frequency of 33 Hz, increasing the number of transmit antennas in the DSSTS scheme from 2 to 4 produced the best performance gain. A performance gain of 1dB is obtained at a BER of 10^{-4}. Also note that smaller performance gains are obtained as the number of transmit antennas increases. This is merely due to non-perfect cross-correlation interference caused by the increasing number of codes allocated to individual transmit antennas.
- The DSSTS's 10 transmit antennas scenario only obtained a 1dB gain over the DSSTS's 2 transmit antennas scenario.
- Less than 0.1dB gain is obtained between the DSSTS's 4, 6, 8 and 10 antennas scenarios.

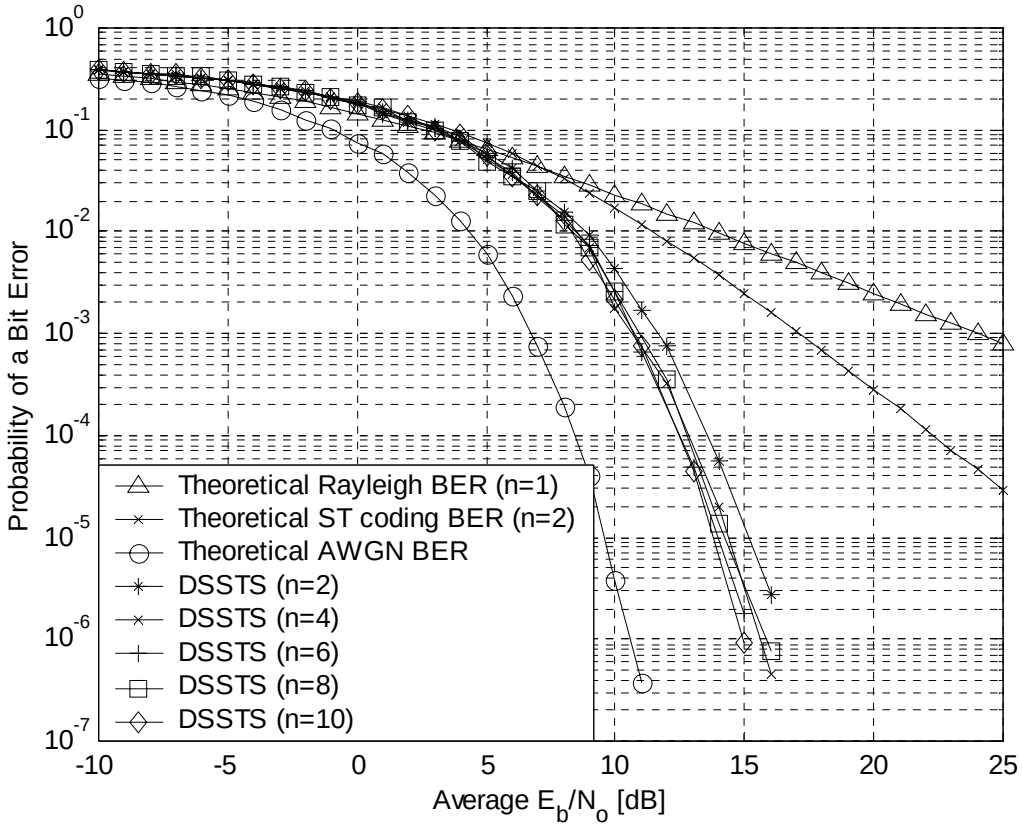

Figure 6.2. Single user performance evaluation for the DSSTS's 2 to 10 antennas scenario in a Rayleigh fading environment for f_d = 66Hz.

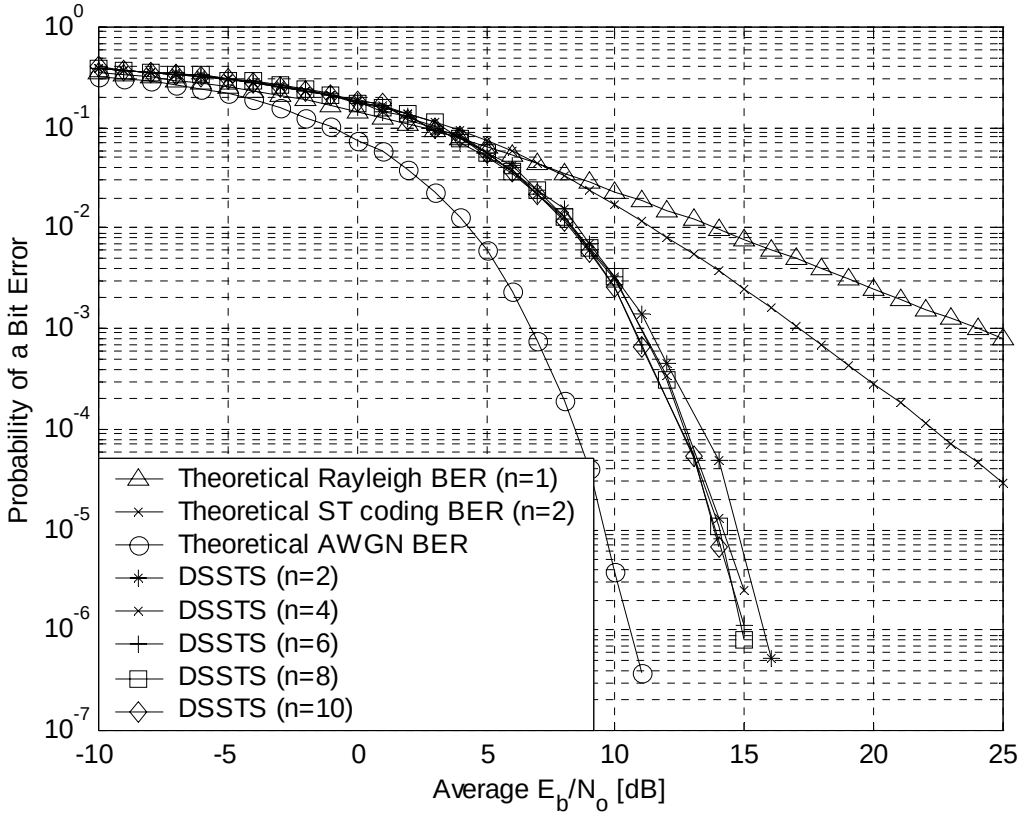

Figure 6.3. Single user performance evaluation for the DSSTS's 2 to 10 antennas scenarios in a Rayleigh fading environment with f_d = 100Hz.

In order to show the effect of the Doppler frequency on the BER performance of the DSSTS scheme in a Rayleigh fading environment (K = -100dB), the graphs are plotted for different Doppler frequencies with the number of transmit antennas held constant for each graph. These graphs are presented in *Figures 6.4, 6.5, 6.6, 6.7* and *6.8*. The following observations can be made:

- An improved BER performance is obtained for higher Doppler frequencies. This is mainly due to the fact that shorter error bursts occur, resulting in an improved BER performance. This performance gain is only at higher E_b/N_0, i.e. from 11dB upwards.
- With a Doppler frequency of 66Hz, a 1dB performance gain at a BER of 10^{-4} was obtained over the case where a Doppler frequency of 33Hz was used for the 2 transmit antennas scenario. However, a Doppler frequency of 100Hz only obtained a performance gain of 0.1dB over the 66Hz Doppler frequency case.

- Similar results are obtained for the 4, 6 and 8 antenna scenarios. In this case, a performance gain of 1dB is obtained at a BER of 10^{-4} with Doppler frequencies of 33Hz and 66Hz, where as no performance gain is obtained at Doppler frequencies of 66Hz and 100Hz.
- In the case of the DSSTS's 10 antennas scenario, no performance gains are obtained between different Doppler frequencies.

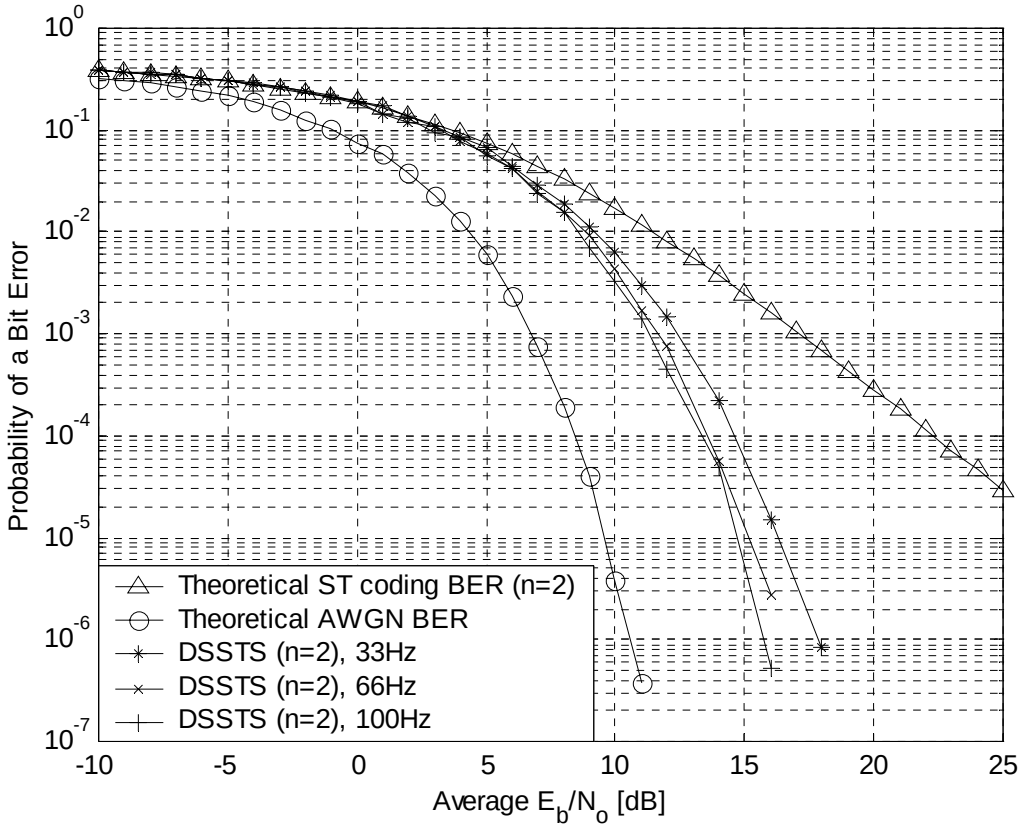

Figure 6.4. Single user performance evaluation for the DSSTS 2 antenna scheme in a Rayleigh fading environment for different Doppler frequencies.

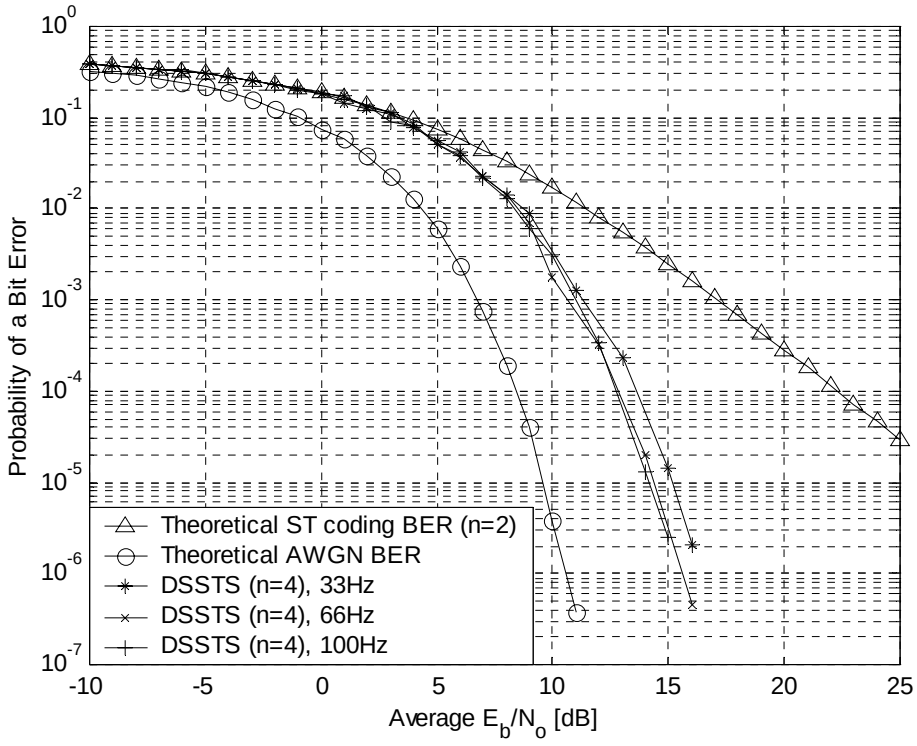

Figure 6.5. Single user performance evaluation for the DSSTS 4 antenna scheme in a Rayleigh fading environment for different Doppler frequencies.

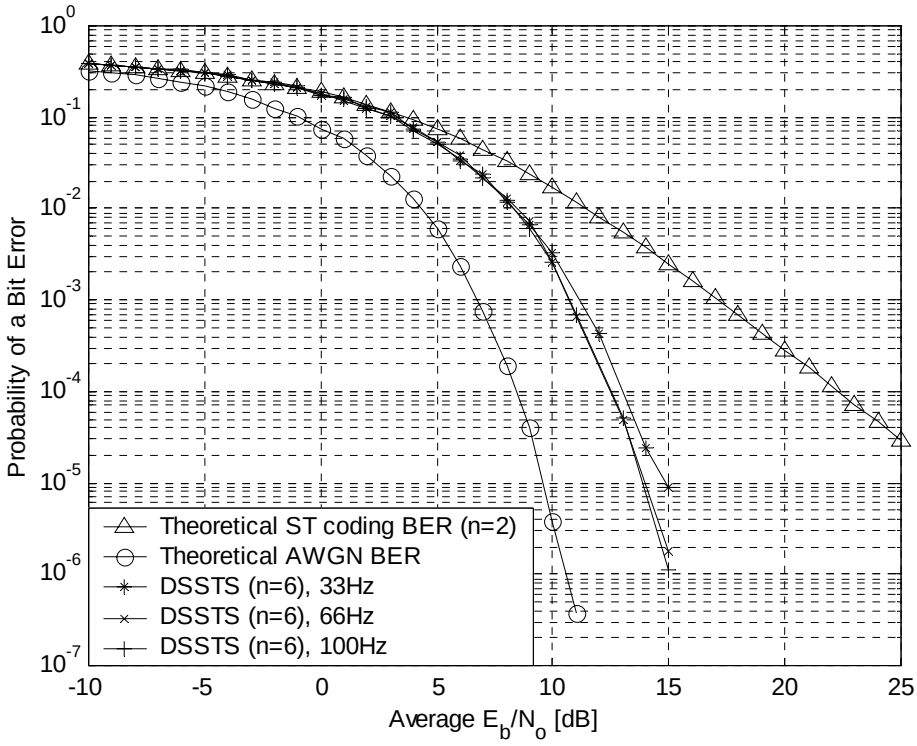

Figure 6.6. Single user performance evaluation for the DSSTS 6 antenna scheme in a Rayleigh fading environment for different Doppler frequencies.

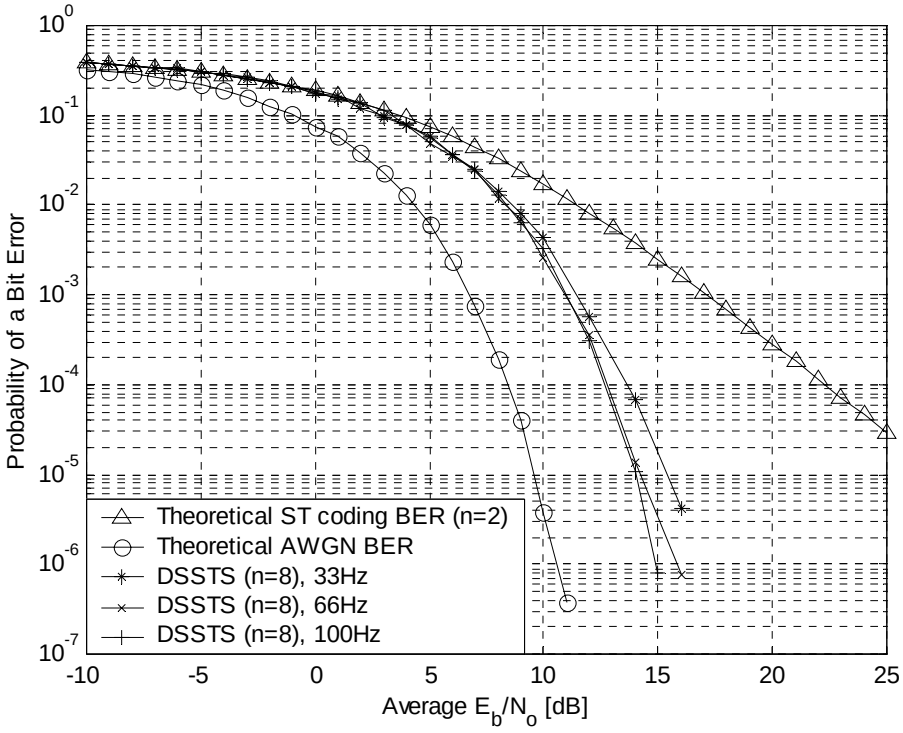

Figure 6.7. Single user performance evaluation for the DSSTS 8 antenna scheme in a Rayleigh fading environment for different Doppler frequencies.

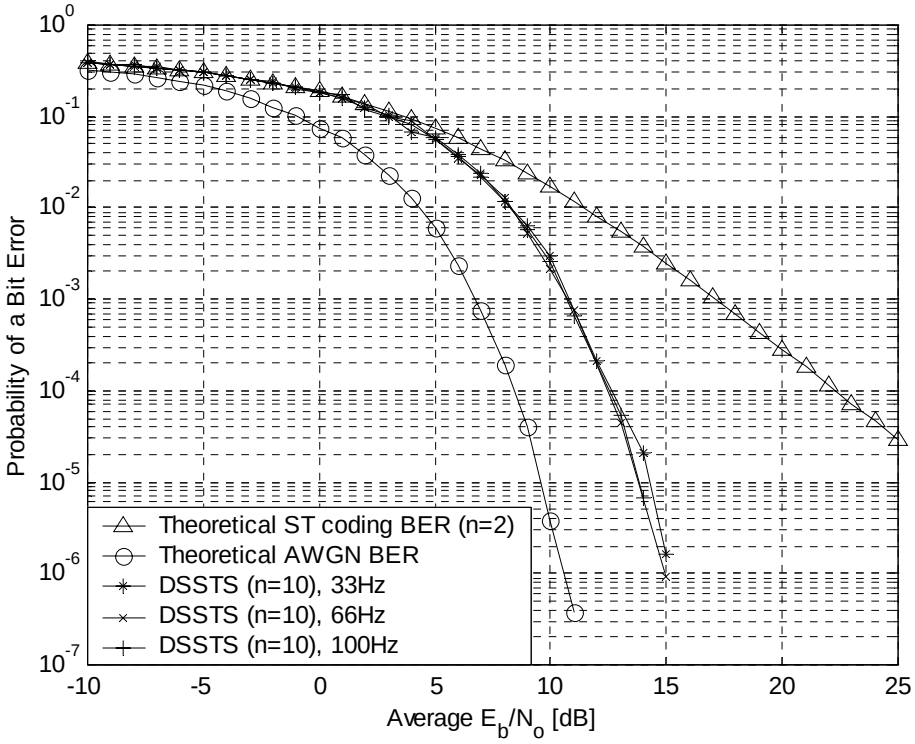

Figure 6.8. Single user performance evaluation for the DSSTS 10 antenna scheme in a Rayleigh fading environment for different Doppler frequencies.

6.1.2 Performance results in a Rician fading environment

In order to show the effect of increasing the DSSTS scheme's number of antennas on the BER performance of a single user in a Rician fading environment (K = 6dB), BER performance graphs were generated for similar Doppler frequencies, i.e. 33Hz, 66Hz, and 100Hz, respectively. The simulation platform presented in *Chapter 5, Section 5.1.6* were used to simulate these scenarios, presented in *Figure 6.9*, *Figure 6.10*, and *Figure 6.11*, respectively. From all of these figures the following general observations can be made:

- For a single user the DSSTS scheme's 2,4,6,8 and 10 transmit antenna scenarios all performed the same, viz. a 12.5dB gain is obtained over Alamouti's original 2 transmit antennas scheme at a BER of 10^{-4}.
- For a single user the DSSTS scheme's 2,4,6,8 and 10 transmit antenna scenarios performed 1dB worse than in a AWGN channel scenario at a BER of 10^{-4}.

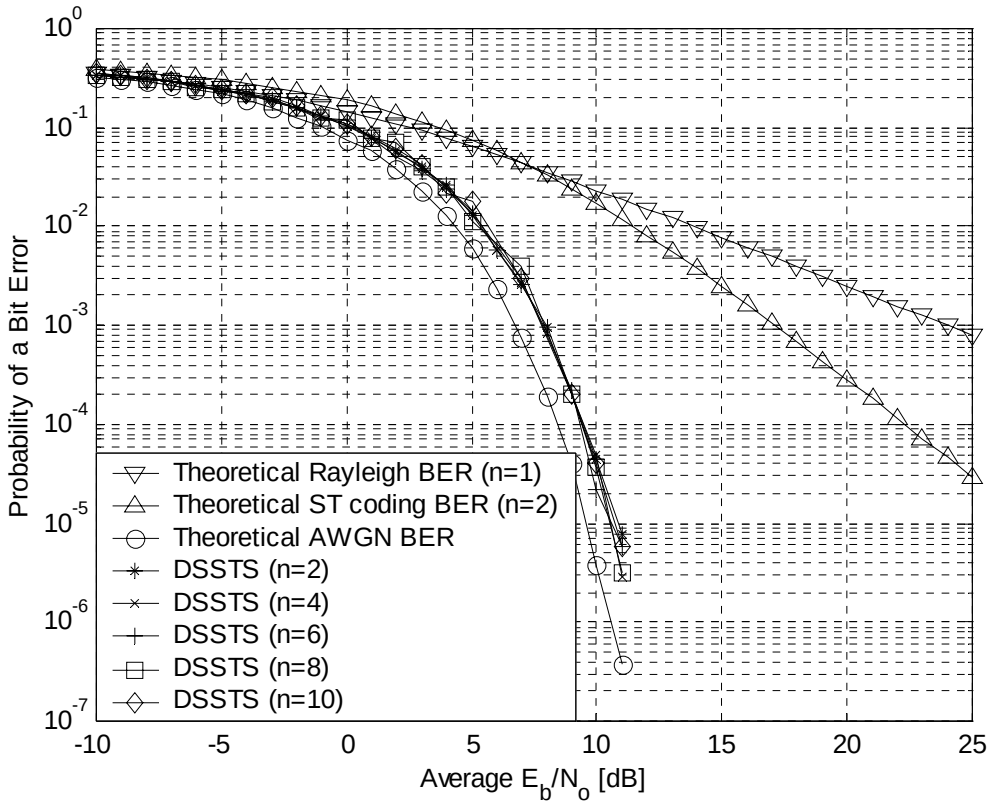

Figure 6.9. Single user performance evaluation for the DSSTS's 2 to 10 antennas in a Rician fading environment with K = 6dB and f_d = 100Hz.

In order to show the effect of the Doppler spread on the BER performance of the DSSTS scheme in a Rician fading environment (K = 6dB), BER performance graphs were generated for different Doppler frequencies. The number of transmit antennas was kept constant for each graph. These graphs are presented in *Figures 6.12, 6.13, 6.14, 6.15* and *6.16* and the following observations can be made:

- As opposed to some of the Rayleigh fading environment scenarios, no improved BER performance for a single user was obtained for higher Doppler frequencies in a Rician fading environment with a LOS to NLOS ratio of 6dB.
- This can mainly be attributed to the fact that the signal envelope is more constant with a Rician factor of 6dB, and no deep fades occurred for long periods, irrespective of the Doppler frequency.
- Note that the reference curve is the theoretical ST coding BER curve in Rayleigh fading

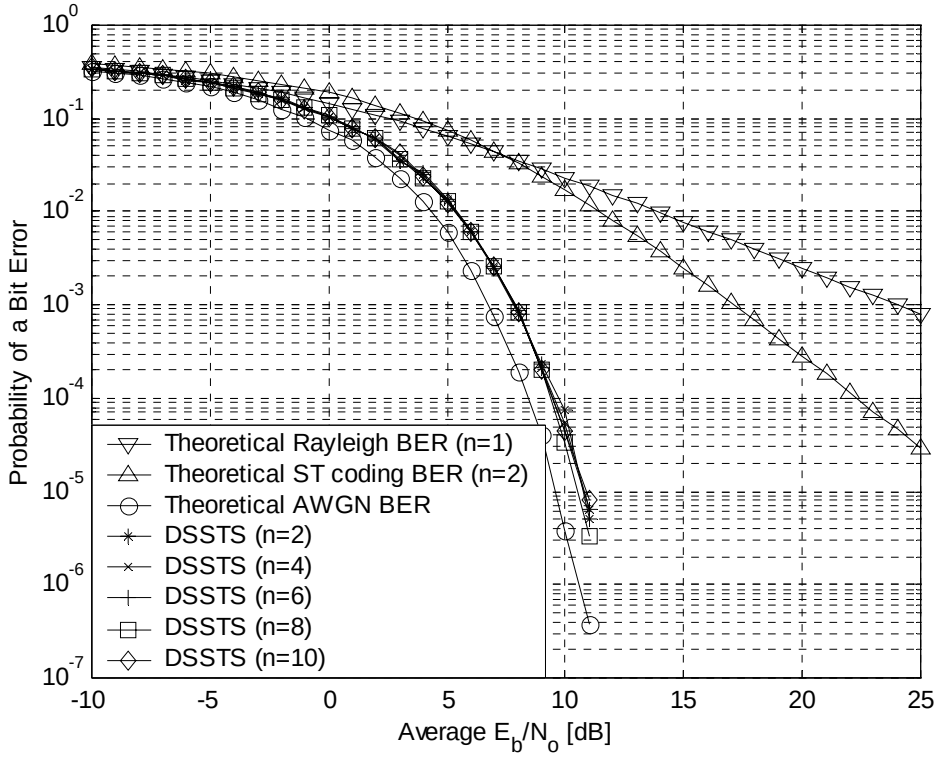

Figure 6.10. Single user performance evaluation for the DSSTS's 2 to 10 antennas in a Rician fading environment with K = 6dB and f_d = 66Hz.

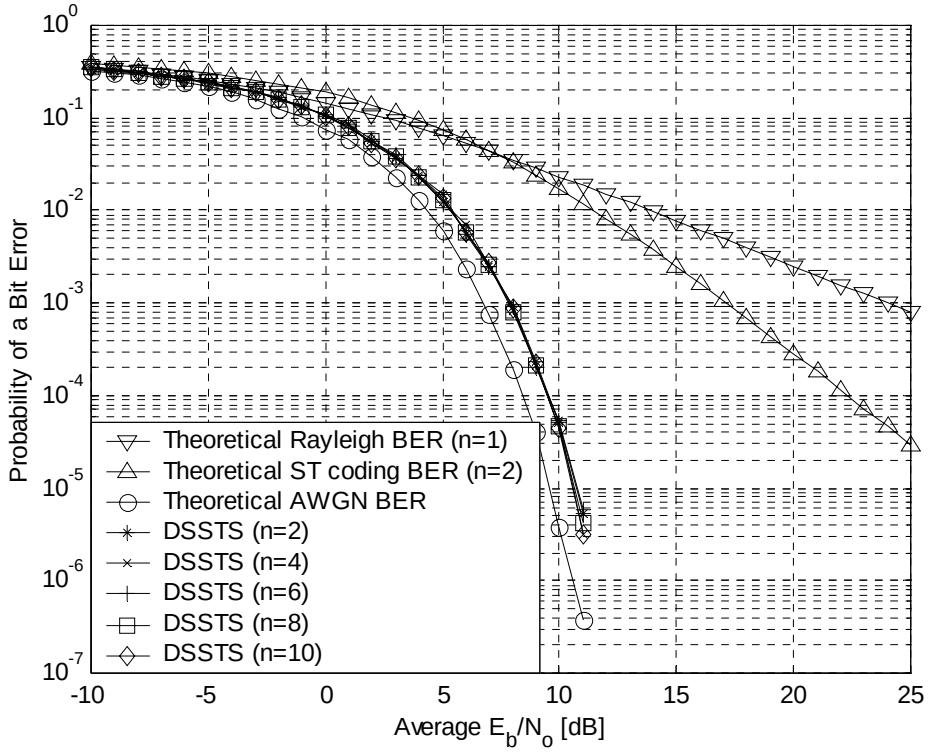

Figure 6.11. Single user performance evaluation for the DSSTS's 2 to 10 antennas in a Rician fading environment with K = 6dB and f_d = 33Hz.

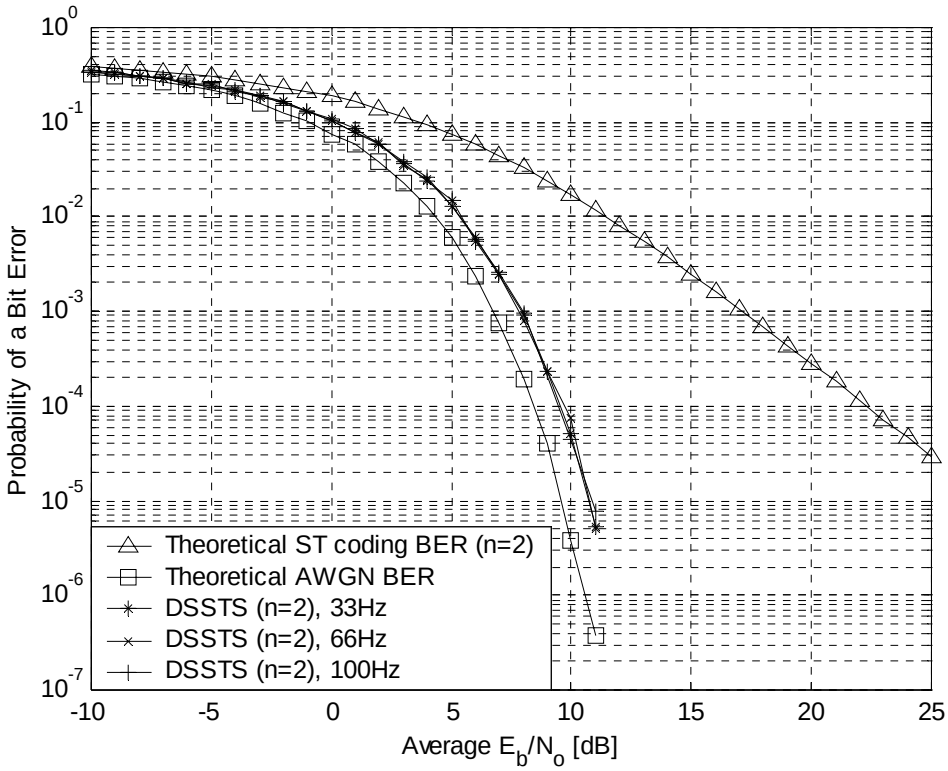

Figure 6.12. Single user performance evaluation for the DSSTS's 2 antenna scenario in a Rician fading environment with K = 6dB at different values of f_d.

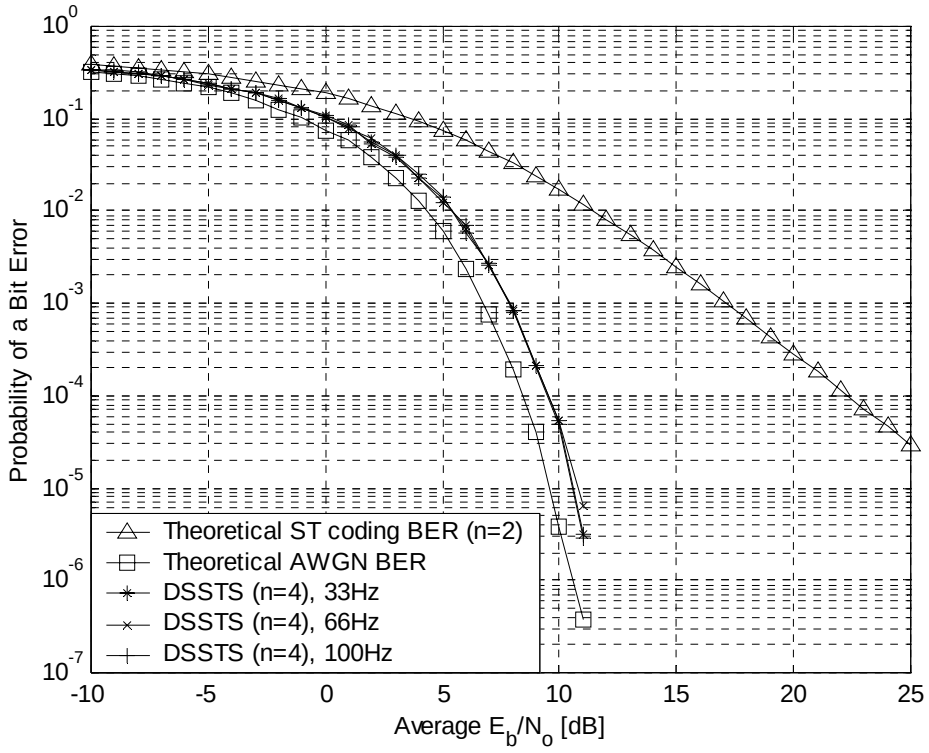

Figure 6.13. Single user performance evaluation for the DSSTS's 4 antenna scenario in a Rician fading environment with K = 6dB and different values of f_d.

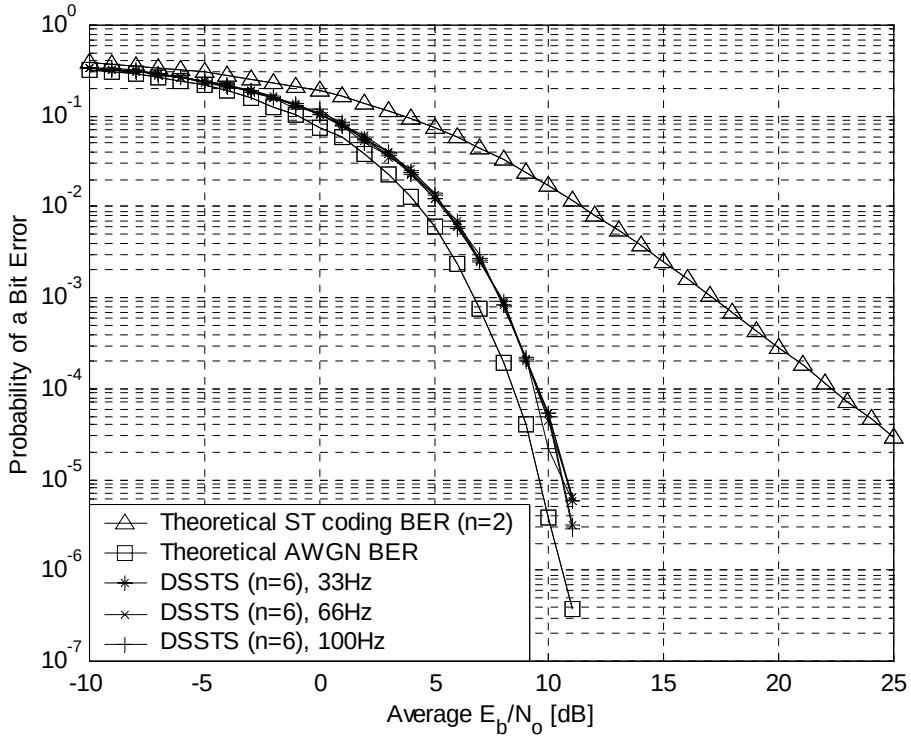

Figure 6.14. Single user performance evaluation for the DSSTS's 6 antenna scenario in a Rician fading environment with K = 6dB and different values of f_d.

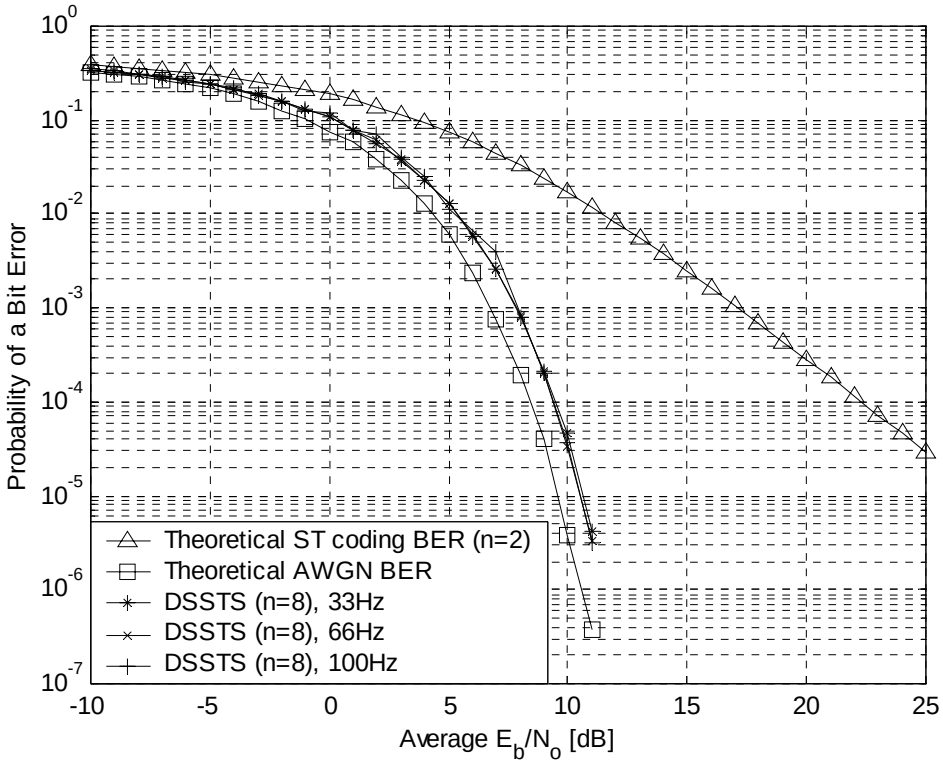

Figure 6.15. Single user performance evaluation for the DSSTS's 8 antenna scenario in a Rician fading environment with K = 6dB and different values of f_d.

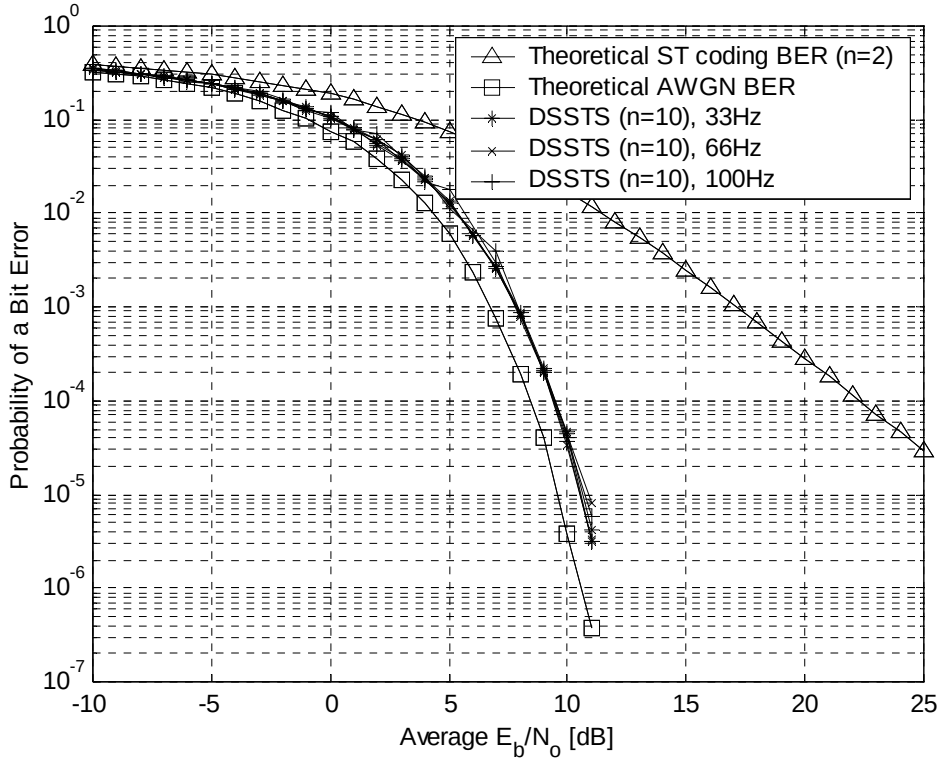

Figure 6.16. Single user performance evaluation for the DSSTS's 10 antenna scenario in a Rician fading environment with K = 6dB and different values of f_d.

6.1.3 Performance results of a Rayleigh versus Rician fading environment

In *Figures 6.17, 6.18, 6.19, 6.20* and *6.21* simulated BER performance curves are presented for 2, 4, 6, 8 and 10 transmit antennas, in a Rayleigh as well as Rician fading environment. Once again, the simulation platform presented in *Chapter 5, section 5.1.6* were used to simulate these effects. Also note that Alamouti's original 2 transmit antenna scheme is included as a reference benchmark. From *Figures 6.17* to *6.18*, it can be seen that an improved BER performance is obtained for a Rician fading environment over a Rayleigh fading environment. This is expected, as a Rician fading environment has an LOS visibility between the MS and BS whereas in a Rayleigh fading environment no direct LOS exists between the MS and BS (see *Chapter 4* and Appendix C).

For the DSSTS's scheme's 2 transmit antenna scenario presented in *Figure 6.17*, the following important observations can be made:

- In a Rician fading environment with f_d = 33Hz, the 2 transmit antenna scenario obtained a 5dB gain over a Rayleigh fading environment at a BER of 10^{-4}.
- However, this gain decreased to 4dB for Doppler frequencies of 66Hz and 100Hz. The decreased gain is due to the fact that a Rician fading environment has a constant BER performance for all Doppler frequencies opposed to Rayleigh fading environment where BER performance gains is obtained by increasing the Doppler frequency.

For the DSSTS scheme's 4 transmit antenna scenario, presented in *Figure 6.18*, the following important observations can be made:

- In a Rician fading environment with f_d = 33Hz, the 4 transmit antenna scenario obtained a 4dB gain over a Rayleigh fading environment at a BER of 10^{-4}.
- However, this gain decreased to 3.3dB for Doppler frequencies of 66Hz and 100Hz for the same reasons described in the 2 transmit antennas scenario.

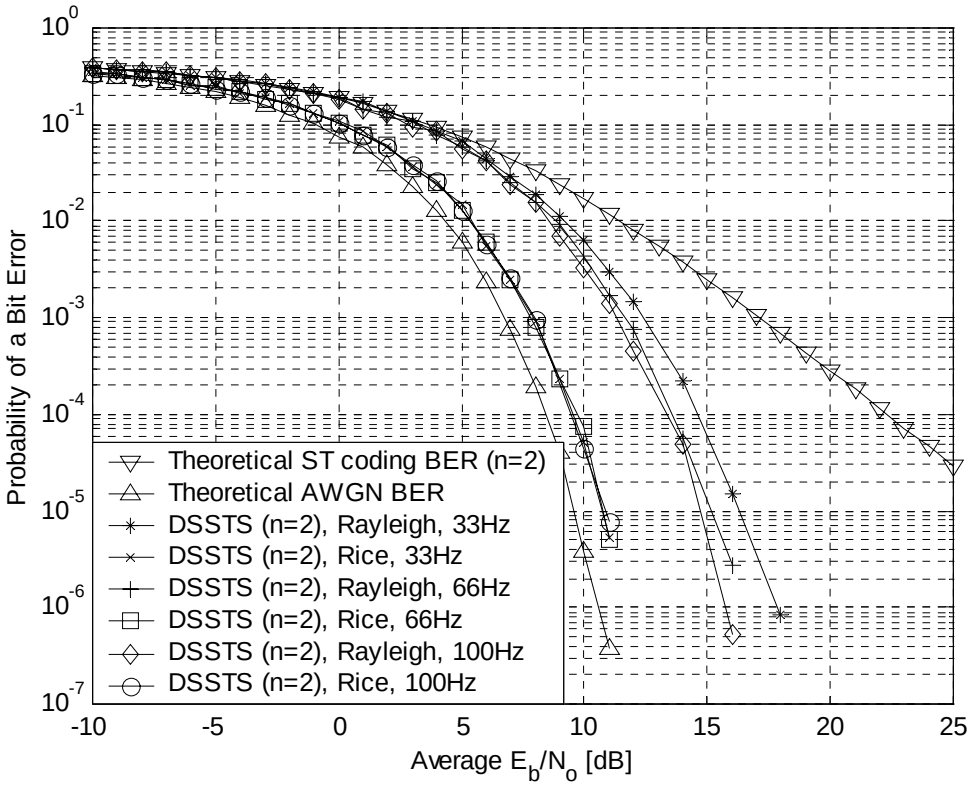

Figure 6.17. 1-user performance evaluation for the DSSTS's 2 antenna scenario in a Rayleigh vs. Rician (K=6dB) fading environment for different values of f_d.

For the DSSTS scheme's 6 and 8 transmit antenna scenario, presented in *Figures 6.19* and *6.20*, the following important observations can be made:

- Simulating the DSSTS scheme's 6 and 8 transmit antennas scenarios in a Rician fading environment with f_d = 33Hz, a gain of 3.5dB is obtained over a Rayleigh fading environment at a BER of 10^{-4}.
- However, this gain decreased to 3dB for Doppler frequencies of 66Hz and 100Hz for the same reasons described in the 2 transmit antennas scenario.

For the DSSTS scheme's 10 transmit antenna scenario, presented in *Figure 6.21*, the following important observations can be made:

- With a Rician fading environment the 10 transmit antenna scenario obtained a 3dB gain over a Rayleigh fading environment at a BER of 10^{-4}.
- However, this gain is similar for all three different Doppler frequencies. Once again, the same reasoning as described for the 2 transmit antennas scenario can be followed for this case as well.

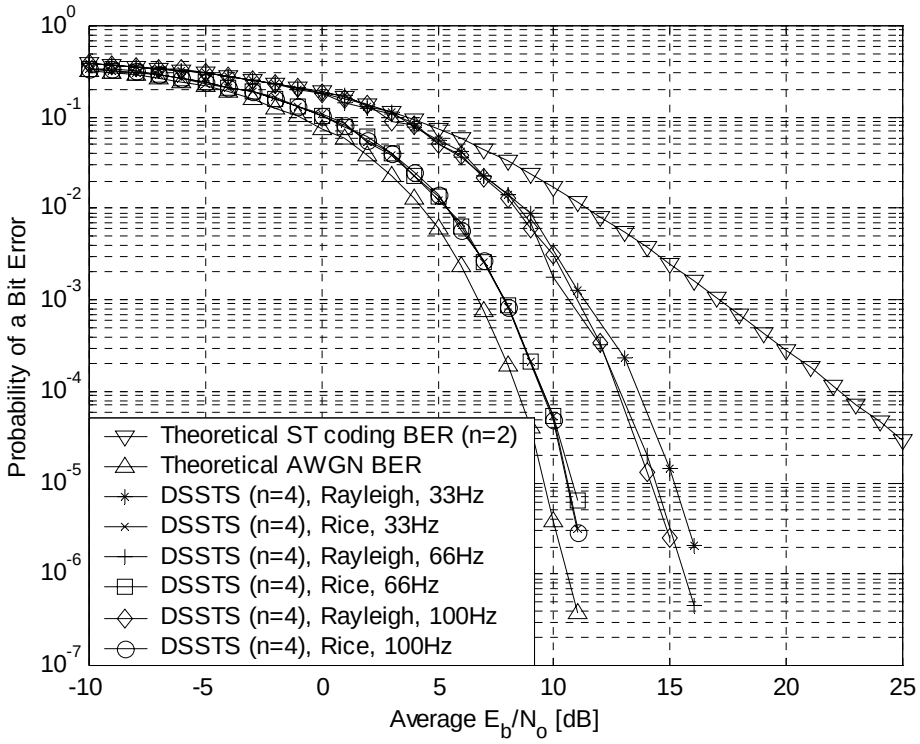

Figure 6.18. 1-user performance evaluation for the DSSTS's 4 antenna scenario in a Rayleigh vs. Rician (K=6dB) fading environment for different values of f_d.

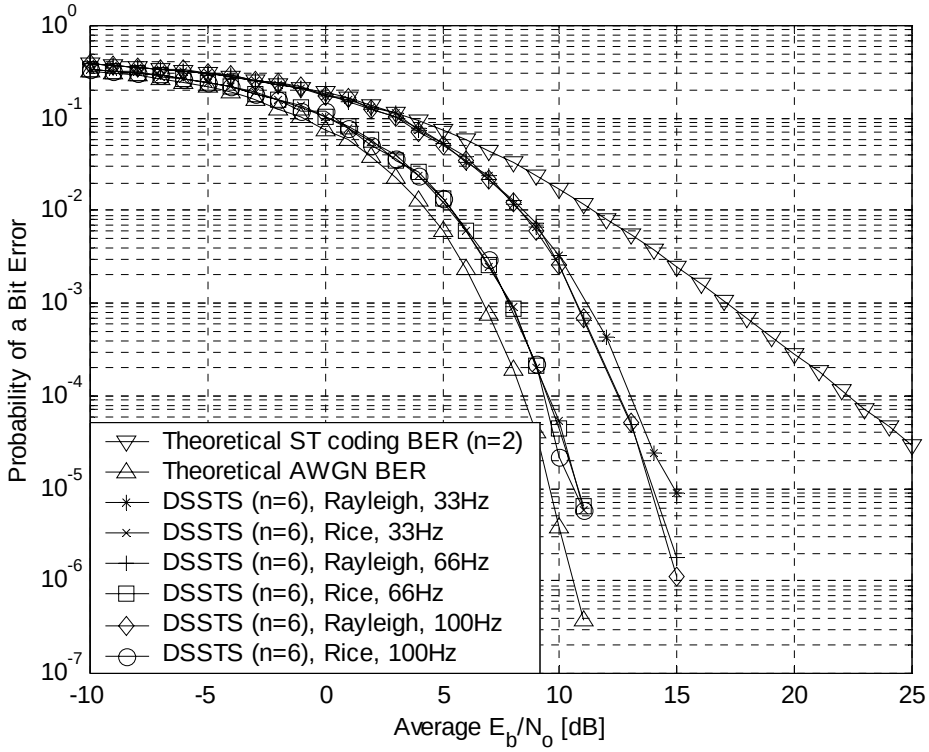

Figure 6.19. 1-user performance evaluation for the DSSTS's 6 antenna scenario in a Rayleigh vs. Rician (K=6dB) fading environment for different values of f_d.

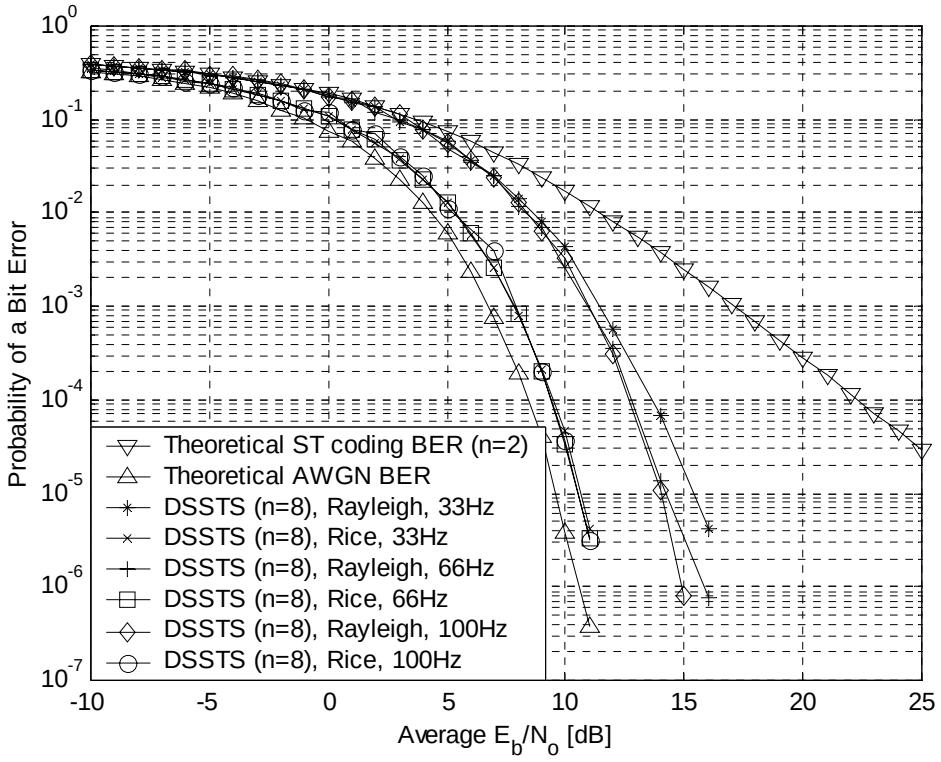

Figure 6.20. 1-user performance evaluation for the DSSTS's 8 antenna scenario in a Rayleigh vs. Rician (K=6dB) fading environment for different values of f_d.

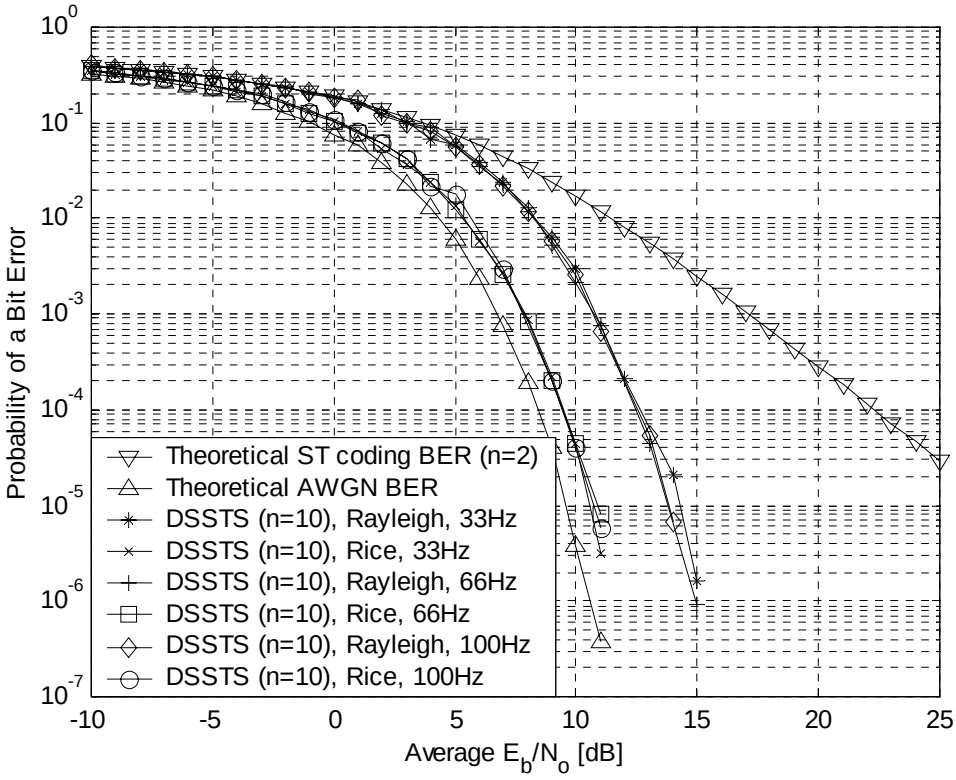

Figure 6.21. 1-user performance evaluation for the DSSTS's 10 antenna scenario in a Rayleigh vs. Rician (K=6dB) fading environment for different values of f_d.

6.2 DSSTS CAPACITY

A plot of the capacity CCDFs of (1x1) and (2x2) communication systems is presented in *Figure 6.22*. Important observations that can be made from *Figure 6.22* are as follows:

- At 10% channel capacity outage, the capacity of a (2x2) MIMO system has 3.3 times the capacity of a traditional (1x1) SISO system. In fact, at small SNR (i.e. 0dB to 3dB), the (2x2) MIMO system has a capacity of 6 times larger than a traditional (1x1) system.
- With a 3dB increase in SNR for a SISO system, i.e. doubling in power, the 10% capacity outage increased by 1.7 times the current channel capacity.
- With a 3dB increase in SNR for a MIMO system, the 10% capacity outage increased by 1.5 times the current channel capacity.

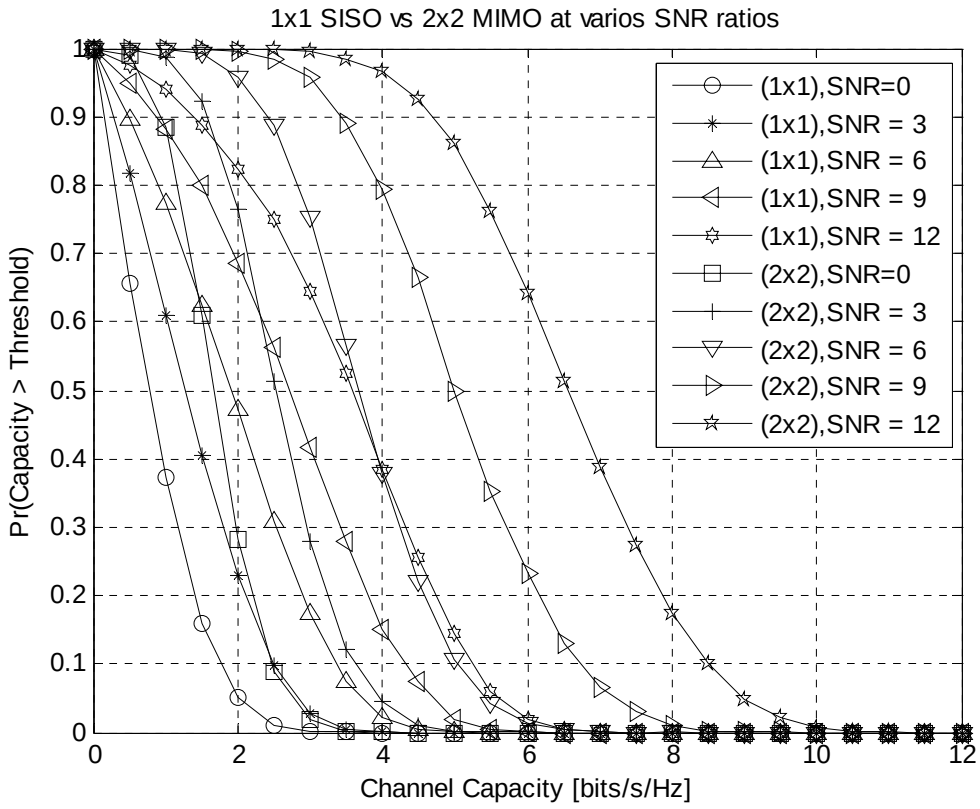

Figure 6.22. Capacity CCDFs of a (*n* = 1, *m* = 1) and (*n* = 2, *m* = 2) system.

Capacity plots for the DSSTS schemes at a SNR = 21dB, with 2, 4, 6 and 8 transmit antennas are plotted in *Figure 6.23* (see *Chapter 5, Section 5.1.5, Equation (5.64)*). From *Figure 6.23*, the following important observations can be made:

- The capacity increases as the number of transmit antennas increases.
- The (2x1) DSSTS scheme obtains a capacity increase of 1.3 bits/s/Hz over the (1x1) SISO system at a capacity outage of 10%.
- The (4x1) DSSTS obtains a further capacity increase of 0.6 bits/s/Hz over the (2x1) DSSTS system at a capacity outage of 10%.
- The (6x1) DSSTS only obtains a 0.25 bits/s/Hz capacity increase over the (4x1) DSSTS system at a capacity outage of 10%.
- The (8x1) DSSTS only obtains a 0.1 bits/s/Hz capacity increase over the (6x1) DSSTS system at a capacity outage of 10%.
- As the DSSTS number of transmit antennas tends to infinity, the capacity increase tend to zero.

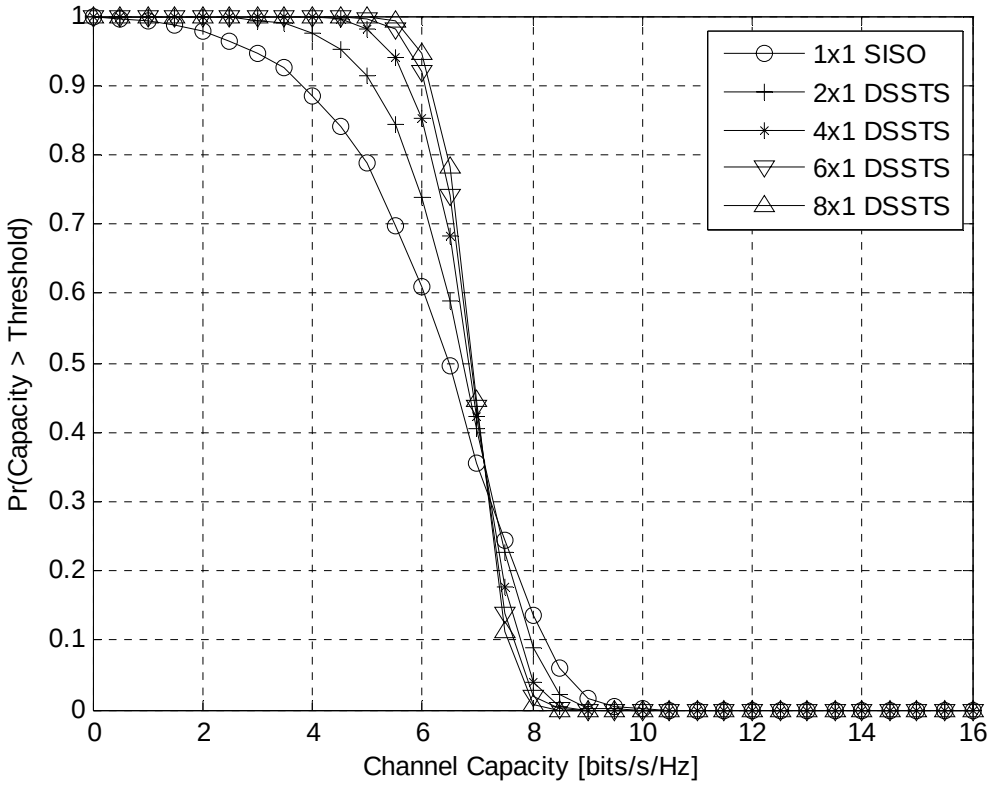

Figure 6.23. Theoretical capacity CCDFs of the DSSTS scheme with 2, 4, and 8 transmit antennas at a SNR = 21dB.

Capacity plots of other transmit diversity schemes, i.e. the Zero Forcing (ZF) [18] and a (4x1) transmit diversity scheme proposed by [18], are presented in *Figure 6.24*. These are included to show the relative performance of the DSSTS schemes. From *Figure 6.24*, the following important observations can be made:

- The (4x1) DSSTS outperforms the other transmit diversity schemes.
- The (4x1) DSSTS obtains a capacity advantage of 0.25 bits/s/Hz over the (4x1) scheme presented in [18] at a capacity outage of 10%.
- The (4x1) DSSTS obtains a capacity advantage of 0.6 bits/s/Hz over the (4x1) ZF system at a capacity outage of 10%.
- Note that much greater capacity is obtained with the (2x2) MIMO system.

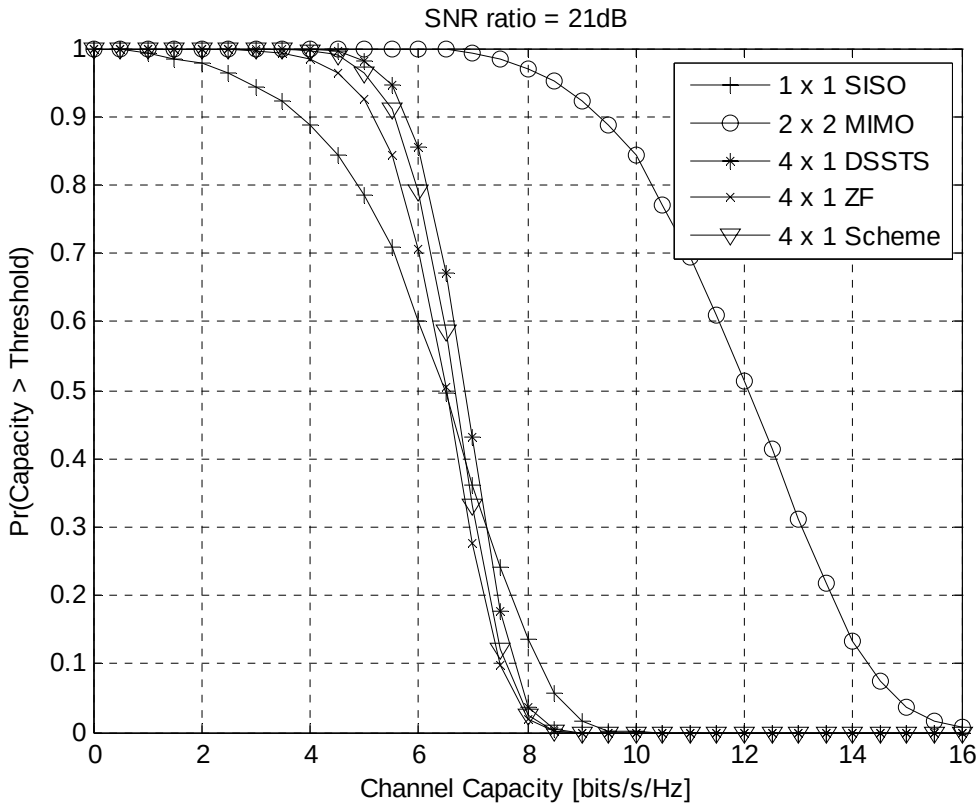

Figure 6.24. Theoretical capacity CCDFs of a (4x1) scheme and a ZF method [18] compared to the DSSTS scheme.

CHAPTER SEVEN

CONCLUSIONS AND SUGGESTIONS FOR FUTURE RESEARCH

This dissertation was structured as follows. Firstly, background information on ST coding and spread spectrum modulation techniques were presented. Secondly, a flat fading performance evaluation platform for the DSSTS scheme was presented. This baseband simulation model is capable of replicating the operation of a realistic flat fading channel, without the requirement of carriers and high sampling frequencies. This flat fading channel was also used as a platform for the multipath fading channel described and presented in *Chapter 4*. Thirdly, the DSSTS scheme's encoding and decoding structures were presented, which are capable of improving on communication system's throughput and channel capacity. A theoretical capacity equation was also derived for the DSSTS. Fourthly, the unrealistic ST coding assumption of the channel being quasi-static for low throughput rates with high Doppler frequencies were addressed with the SSTD scheme and a versatile complex multi-user multipath fading performance evaluation platform for the proposed SSTD scheme was described. Lastly, simulation results were presented and conclusive remarks will be made on these during the remainder of this chapter.

From the discussions on the results presented in *Chapter 6*, a number of conclusions can be made. The conclusions discussed during the remainder of this chapter include:

- The performance of the DSSTS scheme in a Rayleigh fading environment,

- the performance of the DSSTS scheme in a Rician fading environment,
- a comparison of the DSSTS scheme's performance in a Rayleigh versus Rician fading channel,
- the capacity increase obtained by using DSSTS, and lastly
- general conclusions and proposals for future work on the DSSTS scheme.

7.1 RAYLEIGH FADING

It is known that in digital communication systems the Doppler frequency does not have an effect on the BER of uncoded modulation systems. However, if the digital communication system employs coding, the BER is effected by the Doppler frequency. DSSTS, although not conventional coding, can be viewed as a scheme with "coding through diversity" because a symbol is send through different channels to the receiver. These multiple copies of a symbol are received at the receiver and combined into one symbol again. Hence, if the DSSTS is a "channel code", it can be classified under communication systems employing coding and will depend on the Doppler frequency as seen from the simulation results. However, this discussion of Doppler frequency vs. the DSSTS scheme's BER needs to be verified by further simulations and will be a topic for future research.

By keeping the above discussion in mind, the number of transmit antennas in a Rayleigh fading environment has an effect on the performance of the DSSTS scheme at low and high mobile velocities: At low velocities, i.e. a low Doppler frequency, the DSSTS's 10 transmit antenna scenario had a 9.5dB gain over Alamouti's original 2 transmit antenna scheme, and a 2dB gain over the DSSTS scheme's 2 transmit antenna scenario at a BER of 10^{-4}. At high velocities, i.e. a high Doppler frequency, the DSSTS's 10 transmit antenna scenario had an 8.5dB gain over Alamouti's original 2 transmit antenna scheme and a 1dB gain over the DSSTS scheme's 2 transmit antenna scenario at a BER of 10^{-4}. Thus, for high Doppler frequencies, the gains realized by increasing the number of transmit antennas from 2 to 10 may not be cost effective. Although better performance is obtained by increasing the number of transmit antennas at low Doppler frequencies, it is also not cost effective, since only a 2dB gain is realized. It should also be noted that the highest gain, i.e. a gain of 7.5dB at a BER of 10^{-4}, was obtained over the traditional 2 transmit antenna

scenario presented by Alamouti and spreading the 2 transmit antennas with a Walsh sequence. The reason for the DSSTS scheme's poor performance is that despreading is done following the RF stage and leaves no room for phase correction, equalisation or RAKE reception (see *Chapter 5, Figure 5.1*). Note that phase correction is only done during the ST decoding fase. As a result of no phase error corrections made at the receiver during the despreading fase, non-perfect cross-correlation is experienced and results in antenna self-noise created from the spreading sequences used on different transmit antennas. The problem with the antenna self-noise was addressed in *Chapter 5, Section 5.1.4*. Another way of viewing the lack of performance of the DSSTS scheme is that the diversity gain obtained by adding another antenna, is not sufficient to overcome the antenna self-noise caused by adding another code associated with that antenna. From *Figure 7.1* it can be seen that the BER performance increases as the number of transmit

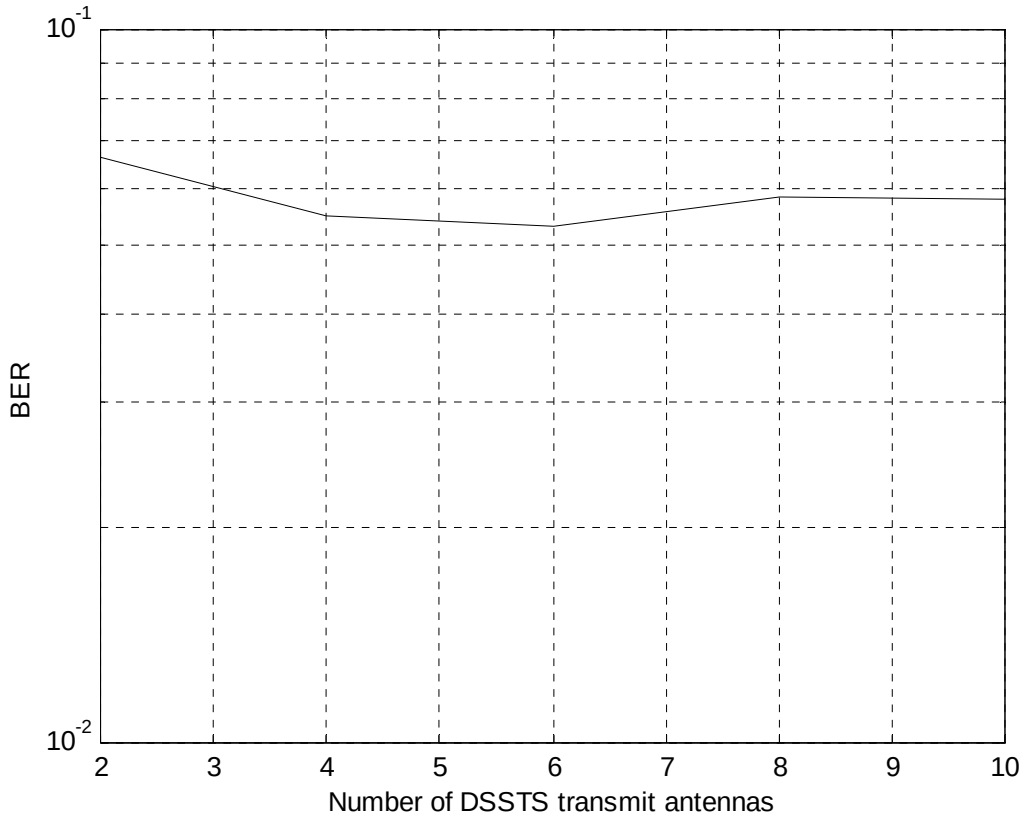

Figure 7.1. A single user DSSTS scheme's BER performance in a Rayleigh fading channel for 2 to 10 transmit antennas at E_b/N_0 = 5dB, f_d = 33Hz.

antennas increase up to 6 transmit antennas. Thereafter, the BER decrease as antenna self-noise exceeds the diversity gains obtained. Note that this statement is only true for this particular dissertation's DSSTS scheme and can possibly be corrected by further research, as discussed in more detail in *Section 7.4.*

7.2 RICIAN FADING

In a Rician fading environment the number of transmit antennas does not have a marked effect on the performance of the DSSTS scheme at low and high mobile velocities. Thus, the effect of Doppler spread, i.e. the speed at which the mobile moves, in contrast to the Rayleigh fading scenario, has no effect on the DSSTS schemes BER at a Rician Factor of 6dB. Similar to the Rayleigh fading channel, the case of spreading the 2 transmit antennas by a Walsh sequence had the highest gain. A gain of 12.5dB at a BER of 10^{-4} was *Chapter 6*, it is evident that there exists an optimal trade-off between diversity and antenna

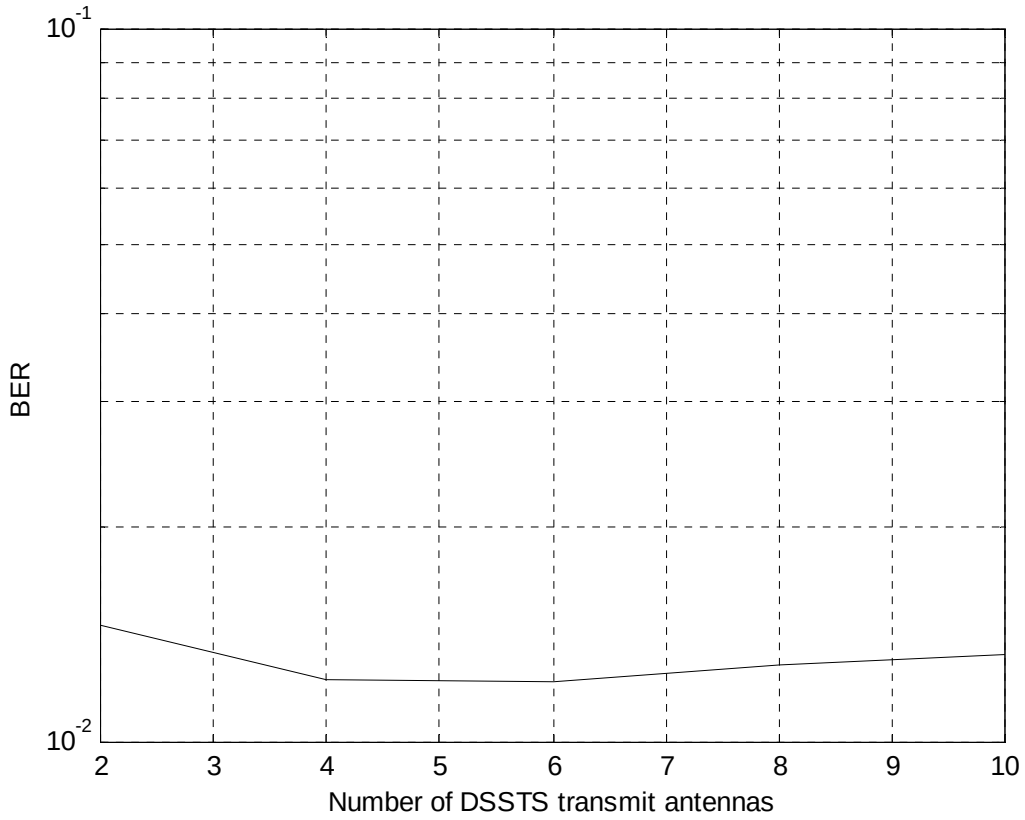

Figure 7.2. A single user DSSTS scheme's BER performance in a Rician fading channel for 2 to 10 transmit antennas at E_b/N_0 = 5dB, f_d = 33Hz.

obtained over the traditional 2 transmit antenna scenario presented by Alamouti. The performance of the DSSTS scheme's 2 transmit antenna scenario performed within 1dB of the performance of an uncoded system in an AWGN channel. From the results obtained inself-noise. In the case of the DSSTS scheme performing in a Rician fading channel, the 2 transmit antenna scenario obtains most of the diversity gain. By adding further transmit antennas, no significant transmit diversity gains is obtained. As was the case in the Rayleigh fading channel, the diversity gain obtained by adding another antenna, is not enough to overcome the antenna self-noise caused by adding the additional antenna. From *Figure 7.2* it can be seen that the BER performance increases as the number of transmit antennas increases up to 4 transmit antennas and once again decreases as antenna self-noise becomes greater than diversity gains.

7.3 DSSTS CAPACITY

From the capacity plots presented in *Chapter 6, Section 6.2*, it is evident that the capacity of a traditional one transmit, one receive antenna system can be increased by adding multiple transmit and receive antennas. In fact, a (2x2) MIMO system has a capacity three times greater than a traditional (1x1) SISO system at a capacity outage of 10%. However, with reference to *Figure 6.22*, every doubling in transmit power, the traditional SISO system capacity increase is slightly more than the capacity increase experienced in a MIMO system.

In this dissertation, only increasing the number of transmit antennas to more than four has been investigated. By increasing the number of transmit antennas, the capacity of the DSSTS system increases. However, as the number of transmit antennas increases, less capacity gain is obtained. Thus, as the number of transmit antennas tend to infinity, the capacity increase tends to zero. From an economical point of view, it seems that the amount of capacity gain obtained by adding an extra transmit antenna beyond six transmit antennas does not warrant the effort nor complexity nor cost. Note that this only applies to transmit diversity, as a (4x4) MIMO system has a huge capacity advantage over a (2x2) MIMO system.

It was furthermore shown that the DSSTS scheme obtained the same open-loop capacity gain as the theoretical open-loop capacity gain for a transmit diversity scheme. Note that this only applies to the Rayleigh fading case, as it is known that the channel capacity decreases [71] with a LOS component present in the channel, i.e. with a Rician fading channel.

7.4 RAYLEIGH VERSUS RICIAN FADING

From the discussions and results presented in *Chapter 6*, the following conclusion can be made on the effect different flat fading channel conditions has on the DSSTS scheme's performance.

Under Rician fading conditions the DSSTS scheme outperforms the DSSTS scheme in Rayleigh fading conditions, as would be expected. However, as the number of transmit antennas increases, the performance advantage of the Rician fading channel over the Rayleigh fading channel decreases. The reason for the performance advantage of the Rician fading channel over a Rayleigh fading channel is mainly due to the presence of a LOS component between the BS and MS, implying that the received signal's envelope is more constant without deep fades.

With less transmit antennas at the BS, i.e. 2, 4 and 6 transmit antennas, poor BER performances are obtained at low mobile speeds, i.e. low Doppler frequencies. Relative to the low mobile speeds, an improved BER performance is obtained when the mobile's speed increases, i.e. with high Doppler frequencies. The poor BER performance with low mobile speeds is mainly due to the received complex faded signals' tendency to be in deep fades for longer periods of time than at the high mobile speed scenarios, thus causing burst errors. However, as stated above, mobile velocity doesn't have a significant effect on the performance of the DSSTS scheme in a Rician fading environment.

With a high number of transmit antennas at the BS, e.g. 10 transmit antennas, the BER performance in Rayleigh as well as Rician fading channel conditions remains practically identical, with a large spreading derived diversity gain compared to the Alamouiti 2 transmit antenna case, regardless of the speed of the mobile. The lack of significant BER performance gain can be attributed to a neutralisation of additional diversity gain by a corresponding increase in antenna self-noise caused with increasing number of transmit antennas, as stated in the sections above.

7.5 GENERAL CONCLUSIONS AND FUTURE WORK

By using the DSSTS scheme presented in this dissertation, the theoretical diversity gains obtainable are not satisfactorily achieved. As outlined above, this was mainly due to antenna self-noise caused amongst the spreading codes allocated to different transmit antennas. Future research can be done to utilize antenna self-noise cancellation techniques on the DSSTS scheme in order to obtain more diversity gains. Another possibility is to use different carrier frequencies for each transmit antenna, thus eliminating the antenna self-noise problem by employing a Frequency Division Multiple Access (FDMA) scheme. This would however lead to a spectral deficiency problem characteristic of FDMA methods.

One possible scenario is to remove the Alamouti code and use a spreading code at each antenna, with the spreaded transmitted symbols rotated in a fashion similar to the DSSTS scheme over all of the transmit antennas. This scheme has the advantage that each substream can be phase corrected at the receiver side, but has the disadvantage that 50% more spreading codes are required compared to the DSSTS scheme. One main objective that was achieved employing the DSSTS scheme presented in this dissertation, was to save on the number of spreading codes, when compared to STS [65]. Besides a possible FDMA system, a TDMA scheme can also be considered as an alternative to combat antenna self-noise induced by the use of multiple spreading codes in the DSSTS scheme.

Another possibility would be to swap the spreading and the Alamouti code. Thus, place the Alamouti code at the channel side in order to resolve the phase rotation introduced by

the complex fading channel and then do the despreading. A problem with this scenario is that the number of transmit antennas can not be extended to more than 4 transmit antennas to obtain both full rate and full diversity, because of the lack of orthogonal transmit matrices for more than 4 transmit antennas, as presented in *Chapter 2*, *Sections 2.3* and *2.6*.

Instead of using the Alamouti ST block code, a differential detection scheme that is not dependant on CSI, can be used. Thus, CSI can now be used in the despreading of the received signal in order to improve cross-correlation between spreading sequences. However, it is known that a penalty of 2dB [49] is paid for using a differential detection scheme.

In this particular dissertation only a QPSK symbol constellation was used. Further research can also be done by using different symbol constellations in the DSSTS scheme, as this has a direct impact on the channel capacity of the system.

In this dissertation only cross-correlation amongst spreading codes was considered crucial, because the DSSTS scheme was only simulated in flat fading channel conditions. However, in more realistic channel conditions, a multipath channel should be considered. If this were the case, auto-correlation, as well as cross-correlation would affect the performance of the DSSTS scheme. In the mathematical formulation of the DSSTS scheme, it was assumed that the cross-correlation between different Walsh spreading sequences is zero. However, when it is non-zero, the symbols transmitted on the other antennas act as antenna self-noise. Thus, in the case of 8 transmit antennas, 4 times as much antenna self-noise will be generated compared to the 2 transmit antenna scenario, thereby degrading the diversity gain that was achieved (see *Chapter 5*, *Section 5.1.4*). In this dissertation it was assumed that the channel is quasi-static over the frame length of the code words. When this assumption is relaxed so that the channel is quasi-static over 2 time-periods in a frame-length codeword, a 3dB penalty is paid, because half of the noise doesn't cancel out, as seen in *Chapter 5, Section 5.1.4*. Thus, future research can also be directed to finding spreading sequences that exhibit perfect cross – and auto-correlation that can be used with the DSSTS scheme in order to minimise the antenna self-noise of the scheme.

REFERENCES

[1] T. S. Rappaport, “Wireless Communications - Principles and Practice”, Second Edition, Prentice-Hall, 2002

[2] http://www.gsmworld.com

[3] S. M. Alamouti, "A simple transmitter diversity scheme for wireless communications," *IEEE J. Select. Area Commun.*, vol. 16, pp. 1451-1458, Oct. 1998.

[4] J. Korhonen, “Introduction to 3G Mobile Communications, Second Edition”, Artech House, 2003

[5] K. Feher, “Wireless Digital Communications -Modulation and Spread Spectrum Applications”, 1st Edition, Prentice-Hall, 1995.

[6] J. G. Proakis, “Digital Communications, 4th Edition”, McGraw-Hill, 2001.

[7] S. Haykin, “*Communication systems*”, John Wiley and Sons, New York, 1994

[8] D. Rajan and S.D. Gray, “Transmit Diversity Schemes for CDMA-2000,” *IEEE Conf. On Wireless Commun. And Networking* (*WCNC1999)*, vol.2, pp. 669 – 673, New Orleans, Los Angles, September 1999.

[9] R. Katulski and M. Mikolajski, “Transmit Diversity in Mobile Communications,” *Int. Conf. On Microwaves, Radar and Wireless Commun.* (*MIKON2002)*, vol.3, pp. 878 – 881.

[10] D. Gerlach and P. Paulraj, "Adaptive Transmitting Antenna Arrays with Feedback," *IEEE Sig. Proc. Lett.*, vol. 1, no.10, pp. 150-152, October 1994.

[11] R. Price and P. E. Green, “A Communication Technique for Multipath Channels,” *Proc. IRE*, vol.46, pp. 555–570, March 1958.

[12] G.D. Forney, (1966), “Concatenated Codes”, Cambridge MA: MIT Press.

[13] C. Berrou, A. Glavieux and P. Thitimajshima, “Near Shannon Limit Error Correction Coding and Decoding: Turbo codes,” *IEEE Int. Conf. Commun.*, Geneva, Switzerland, pp. 1064 - 1070, May 1993.

[14] J. L. Massey, “Step-by-Step Decoding of BCH codes,” *IEEE Trans. Inform. Theory*, vol. IT-11, pp. 580 – 585, October 1965.

[15] L. Staphorst and L. P. Linde, “Performance evaluation of Viterbi Decoded Reed-Solomon Block Codes in Additive White Gaussian Noise and Flat Fading Channel Conditions”, *IEEE Conf. On Wireless Commun. And Networking (WCNC2002)*, Orlando, Florida, March 2002.

[16] J.C. Guey, M.P. Fitz, M.R. Bell and W.Y. Kuo, "Signal design for transmitter diversity wireless communication systems over Rayleigh fading channels," in *VTC’96: Vehicular Technology Conference*, pp. 136-140, 1996.

[17] L. Staphorst, “Viterbi Decoded Linear Block Codes for Narrowband and Wideband Wireless Communication Over Mobile Fading Channels”, M.Eng dissertation, University of Pretoria, July 2005.

[18] C.B. Papadias and G.J. Foschini, “Capacity Approaching Space-Time Codes for Systems Employing Four Transmitter Antennas,” *IEEE Trans. Inform. Theory*, vol.49, No.3, March 2003.

[19] L. Staphorst, F. Maasdorp and L.P. Linde, "Simulation Study of a Space-Sequence Transmit Diversity Scheme for DS/SSMA Systems (Part I)," *ICT 2005 Cape Town RSA*, May 2005.

[20] L. Staphorst, F. Maasdorp and L.P. Linde, "Simulation Study of a Space-Sequence Transmit Diversity Scheme for DS/SSMA Systems (Part II)," *ICT 2005 Cape Town RSA*, May 2005.

[21] F. Maasdorp, L. Staphorst and L.P. Linde, "A Full Rate, Full Diversity Space-Time Block Code for an Arbitrary number of Transmit Antennas". Submitted to *IEEE Trans. Veh. Tech.*

[22] V. Tarokh, N. Seshadri, and A. R. Calderbank, "Space-time Block codes from orthogonal designs," *IEEE Trans. Inform. Theory*, vol. 45, no.5, pp. 1456-1467, July 1999.

[23] E. Biglieri, G. Taricco and A. Tulino, "Performance of Space-time Codes for a Large Number of Antennas," *IEEE Trans. Inform. Theory*, vol. 48, no.7, pp. 1794-1803, July 2002.

[24] C. Gao, A. M. Haimovich and D. Lao, "BER Analysis of MPSK Space-Time Block Codes," *IEEE Commun. Lett.*, vol.7, pp. 314 – 316, July 2003.

[25] V. Tarokh, N. Seshadri, and A. R. Calderbank, "Space-time block coding for wireless communications: Performance Results," *IEEE J. Select. Areas Commun.*, vol. 17, no.3, pp. 451-460, March 1999.

[26] G.J. Foschini and M.J. Gans, "On Limits of Wireless Communications in a Fading Environment When using Multiple Antennas," *Wireless Pers. Commun.*, vol. 6, pp. 311-315, 1998.

[27] I.E. Teletar, "Capacity of Multi-Antenna Gausssian Channels," *Euro. Trans. Telecommun.*, vol. 10, no. 6, pp. 585-595, Nov. 1999.

[28] R. Doostnejad, T. J. Lim and E. Sousa, "Transmitter and Receiver Designs for the MIMO Fading Broadcast Channel," Department of ECE, University of Toronto.

[29] C. E. Shannon, "A Mathematical Theory of Communication", *Bell Systems Technical Journal*, vol. 27, pp.379 – 423 and 623 – 656, 1948.

[30] J. Winters, J. Salz and R. D. Gitlin, "The impact of antenna diversity on the capacity of wireless communication systems," *IEEE Trans. Commun.*, vol. 42. no.2/3/4, pp. 1740-1751, Feb./Mar./Apr. 1994.

[31] T. Marzetta and B. Hochwald, "Capacity of a mobile multiple antenna communication link in Rayleigh flat fading," *IEEE Trans. Inform. Theory*, vol. 45, pp. 139 -158, January 1999.

[32] V. Tarokh, N. Seshadri and A. R. Calderbank, "Space-time codes for high data rate wireless communication: Performance analysis and code construction," *IEEE Trans. Inform. Theory*, vol. 44, no.2, pp. 744-765, March 1998.

[33] A. R. Hammons and H. E. Gamal, "On the theory of space-time codes for PSK modulation," *IEEE Trans. Inform. Theory*, vol. 46, pp.524-542, March 2002.

[34] S. Baro, G. Bauch and A. Hansman, "Improved codes for space-time trellis codes modulation," *IEEE Commun. Lett.*, pp. 20-22, Jan. 2000.

[35] O. Tirkkonen and A. Hottinen, "Complex space-time block codes for four Tx antennas," in *GLOBECOM Conf. Records*, vol. 2, pp. 1005-1009, San Francisco, CA, Nov.-Dec. 2000.

[36] L. A. Dalton and C. N. Georghiades, "A Four Transmit Antenna Orthogonal Space-Time Code with Full Diversity and Rate," in *Proc. 40th Annual Allerton Conf. On Commun. Control, and Computing*, Monticello, IL, October 2002.

[37] M. M. da Silva and A. Correia, "Space-Time Coding schemes for 4 or more Antennas," *Proceedings of IEEE PIMRC 2002*, Lisbon, Portugal, September 2002.

[38] B. M. Hochwald and T.L. Marzetta, "Unitary space-time modulation for multiple-antenna communication in Rayleigh flat fading", *IEEE Trans. Inform. Theory*, vol 46, pp. 543-564, March 2000.

[39] B. M. Hochwald and W. Sweldens, "Differential unitary space-time modulation," *IEEE Trans. Commun.*, vol. 48, pp. 2041-2052, December 2000.

[40] O. Tirkkonen, A. Boariu and A. Hottinen, "Minimal non-orthogonality rate 1 space-time block code for 3+ Tx," in *IEEE Int. Symposium on Spread Spectrum Techniques & Applications*, pp.429-432, New Jersey, USA, September 2000.

[41] H. Jafarkhani, "A quasi-orthogonal space-time block code," *IEEE Trans. Commun.*, vol. 49, pp. 1-4, January 2001.

[42] A. Yongacoglu and M. Siala, "Performance of diversity systems with 2 and 4 transmit antennas," in *Proceedings Int. Conf Commun. Tech. (WCC-ICCT)*, pp. 148-150, Peking, China, 2000.

[43] L. M. A Jalloul, K. Rohani, K. Kuchi and J. Chen, "Performance analysis of CDMA transmit diversity methods," in *Proc. IEEE Vehicular Tech. Conf. (VTC)*, vol. 3, pp. 1326-1330, Amsterdam, Netherlands, October 1999.

[44] S. Rouquette, S. Merigeault and K. Gosse, "Orthogonal full diversity Space-Time block coding based on transmit channel state information for 4 Tx antennas," in *Proc. IEEE Int. Conf. Commun. (ICC)*, vol. 1, pp. 558-562, New York City, NY, April-May 2002.

[45] M. O. Damen, K. Abed-Meraim and J. C. Belfiore, "Transmit diversity using rotated constellations with Hadamard transform," in *Proc. Adaptive Systems for Signal Processing, Commun. And Control Conf.*, pp. 396-401, Lake Louise, Alberta, Canada, October 2000.

[46] Y. Xin, Z. Wang and G. B. Giannakis, "Space-time diversity systems based on unitary constellation-rotating precoders," in *Proc. IEEE Int. Conf. Acoust.,Speech, Signal Processing (ICASSP)*, pp. 2429-2432, Salt Lake City, Utah, May 2001.

[47] V. M. DaSilva and E. S. Sousa, "Fading-resistant modulation using several transmitter antennas," *IEEE Trans. Commun.*,vol. 45, pp. 1236-1244, October 1997.

[48] H. El Gamal and A.R. Hammons, "On the design and performance of Algebraic Space-Time Codes for BPSK and QPSK Modulation," *IEEE Trans. Commun.*, vol. 50. no.6, pp. 907-913, June 2002.

[49] V. Tarokh and H. Jafarkhani, "A Differential Detection Scheme for Transmit Diversity," *IEEE J. Select. Areas Commun.*, vol. 18, no.7, pp. 1169-1174, July 2000.

[50] Y. Li, C.N. Georghiades and G. Huang, "Iterative Maximum-Likelihood Sequence Estimation for Space-Time Coded Systems," *IEEE Trans. Commun.*, vol. 49. no.6, pp. 948-951, June 2001.

[51] J.D. Terry and J.T. Heiskala, "Spherical Space-Time Codes (SSTC)," *IEEE Commun. Lett.*, vol.5, no.3, pp. 107-109 , March 2001.

[52] M.O. Damen, A. Tewfik and J. Belfiore, "A Construction of a Space-Time Code Based on Number Theory," *IEEE Trans. Inform. Theory*, vol. 48, no.3, pp. 753-760, March 2002.

[53] E.G. Larsson, P. Stoica and J. Li, "On Maximum-Likelihood Detection and Decoding for Space-Time Coding Systems," *IEEE Trans. Signal Processing*, vol. 50, no.4, pp. 937-944, April 2002.

[54] R. Gold, "Optimal Binary Sequences for Spread Spectrum Multiplexing," *IEEE Trans. Inform. Theory*, vol. IT-13, pp. 619–621, October 1967.

[55] M. P. Lötter and L.P. Linde, "Constant Envelope Filtering of Complex Spreading Sequences," *IEE Electronic Letters*, vol. 31, no. 17, pp. 1406 – 1407, August 1995.

[56] M. P. Lötter and L.P. Linde, "A Class of Bandlimited Complex Spreading Sequences with Analytic Properties," in *Proc. IEEE Int. Symp. on Spread Spectrum Techniques and Applications*, (Mainz, Germany), pp. 662 – 666, 22 – 25 September 1996.

[57] B. M. Popovic, "Generalised Chirp Like Polyphase Sequences with Optimum Correlation Properties," *IEEE Trans. Inform. Theory*, vol. 38, July 1992.

[58] M. Jamil, L. P. Linde, J. E. Cilliers, and D. J. van Wyk, "Comparison of Complex Spreading Sequences Based on Filtering Methods and Mean Square Correlation Characteristics," *Transactions of the SAIEE*, vol. 89, no. 3, pp. 98–112, September 1998.

[59] R. L. Frank and S. A. Zadoff, "Phase Shift Pulse Codes with Good Periodic Correlation Properties," *IRE Transactions on Information Theory*, vol. IT-7, pp. 381–382, October 1962.

[60] S. M. Korne and D. V. Sarwate, "Quadriphase Sequences for Spread Spectrum Multiple Access Communication," *IEEE Trans. Inform. Theory*, vol. IT-38, no. 3, pp. 1101 – 1113, May 1992.

[61] M. Jamil, "Comparative Study of Complex Spreading Sequences for CDMA Applications," Master's thesis, University of Pretoria, May 1999.

[62] M. P. Lötter, “A Generalised Linear Root-of-Unity Interpolation Filter,” in *Proc. IEEE COM-SIG’95s*, (University of Pretoria, Pretoria, South Africa), pp. 43 – 46, September 1995.

[63] S. Haykin and M. Moher, “Modern Wireless Communications”, Prentice-Hall, 2005.

[64] J. G. Proakis, “Contemporary Communication Systems using Matlab”, Brooks/Cole, 2000.

[65] B. Hochwald, T.L. Marzetta and C.B. Papadias, "A Transmitter Diversity Scheme for Wideband CDMA systems based on Space-Time Spreading," *IEEE J. Select. Areas Commun.*, vol. 19, no.1, pp. 48-60, January 2001.

[66] H. Huang, H. Viswanathan and G. J. Foschini, "Multiple Antennas in cellular CDMA systems: transmission, detection and spectral efficiency," *IEEE Trans. Wireless Commun.*, vol. 1, no. 3, pp. 383-392, July. 2002.

[67] J. Wang and K. Yao, "Space-Time Coded Wideband CDMA Systems," *In Proc. IEEE Veh. Tech. Conf. (VTC)*, vol.1, pp. 260 – 264, 2002.

[68] TIA/EIA IS-2000 Physical Layer Specification for CDMA Spread Spectrum Communication System, June 2000.

[69] J. Hamalainen and R. Wichman, “Closed-Loop Transmit Diversity for FDD WCDMA Systems,” Signals, *Systems and Computers 2000*, vol.1, p111-115, Nov.2000.

[70] D.J. van Wyk, P.G.W. van Rooyen and L.P. Linde, “Super-Orthogonal Space-time Turbo Transmit Diversity for CDMA”, *EURASIP Journal on Applied Signal Processing*, vol. 2005, no. 6, pp.861 – 871, January 2005.

[71] D. Gesbert, M. Shafi, D. Shiu, P.J. Smith and A. Naguib, "From Theory to Practice: An Overview of MIMO Space-Time Coded Wireless Systems", *IEEE J. Select. Areas Commun.*, vol. 21, no.3, pp. 281-302, April 2003.

[72] J.K.Cavers, “An analysis of pilot symbol assisted modulation for Rayleigh fading channels”, *IEEE Trans. Veh. Technol.*, vol. 40, pp.686 – 693, Nov. 1991.

[73] B. Raghothaman, R.T. Derryberry and G. Mandyam, “Transmit adaptive array without user-specific Pilot for 3G CDMA,” *IEEE Int. Conference on Acoustics, Speech and Signal processing (ICASSP 2000)*, vol.5, pp.3009-3012, Istanbul, Turkey, June 2000.

[74] W. C. Jakes Jr., "*Microwave Mobile Communications*", Wiley-Interscience, 1974.

[75] R.H. Clarke, "A Statistical Theory of Mobile-Radio reception", *Bell Systems Technical Journal*, vol. 47, pp 957 – 1000, 1968.

APPENDIX A

MAXIMAL - RATIO RECEIVE COMBINING

A.1 APPENDIX OVERVIEW

Until recently, diversity has been obtained by transmission from a single antenna to multiple receive antennas. This method is known as receive diversity and is achieved by a scheme known as MRRC, shown in *Figure A.1*. MRRC is presented in the remainder of *Appendix A.*

A.2 MAXIMAL - RATIO RECEIVE COMBINING

At a given time, a signal s_0 is sent from the transmitter. The channel, which undergoes Rayleigh fading may in the worst case be modelled by a complex multiplicative distortion composed of a magnitude response and a phase response. As shown in *Figure A.1*, h_0 denotes the channel between the transmit antenna and receive antenna zero and h_1 denotes the channel between the transmit antenna and receive antenna one, where

$$h_0 = \alpha_0 \exp(j\vartheta_0)$$
$$h_1 = \alpha_1 \exp(j\vartheta_1) \qquad \text{(A.1)}$$

If noise is added at the two receivers, the resulting received baseband signals are

$$r_0 = h_0 s_0 + n_0$$
$$r_1 = h_1 s_1 + n_1 \qquad \text{(A.2)}$$

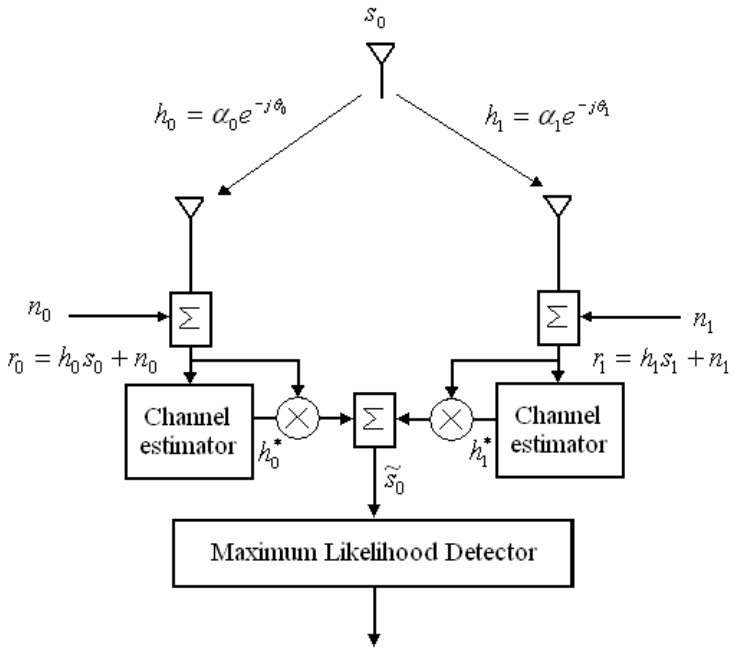

Figure A.1. Receive diversity obtained by two-branch MRRC, taken from [3].

where n_0 and n_1 represent complex Gaussian distributed noise. Because n_0 and n_1 are Gaussian distributed and given that s_0 and s_1 are equiprobable, the ML decision rule applies and the receiver chooses signal s_i, if and only if

$$d^2(r_0, h_0 s_i) + d^2(r_1, h_1 s_i) \le d^2(r_0, h_0 s_k) + d^2(r_0, h_0 s_k) \qquad \forall\, i \ne k \qquad \text{(A.3)}$$

where $d^2(x, y)$ is the squared Euclidean distance between signals x and y, calculated using *Equation (A.4)*

$$d^2(x,y) = (x-y)(x^*-y^*) \tag{A.4}$$

As shown in *Figure A.1*, the receiver's combining scheme for two-branch MRRC are given by *Equation (A.5)*:

$$\begin{aligned}\tilde{s}_0 &= h_0^* r_0 + h_1^* r_1 \\ &= h_0^*(h_0 s_0 + n_0) + h_1^*(h_1 s_0 + n_1) \\ &= (\alpha_0^2 + \alpha_1^2)s_0 + h_0^* n_0 + h_1^* n_1\end{aligned} \tag{A.5}$$

Expanding *Equation (A.3)* and using *Equations (A.4)* and *(A.5)*, *Equation (A.6)* is obtained, stating that: choose s_i if

$$(\alpha_0^2 + \alpha_1^2)|s_i|^2 - \tilde{s}_0 s_i^* - \tilde{s}_0^* s_i \le (\alpha_0^2 + \alpha_1^2)|s_k|^2 - \tilde{s}_0 s_k^* - \tilde{s}_0^* s_k \qquad \forall i \ne k \tag{A.6}$$

is met, or equivalently

$$(\alpha_0^2 + \alpha_1^2 - 1)|s_i|^2 + d^2(\tilde{s}_0, s_i) \le (\alpha_0^2 + \alpha_1^2 - 1)|s_k|^2 + d^2(\tilde{s}_0, s_k) \qquad \forall i \ne k \tag{A.7}$$

For PSK signals the energy in the constellation points are all equal, i.e.:

$$|s_i|^2 = |s_k|^2 = E_s \qquad \forall\, i,k \tag{A.8}$$

Thus, *Equation (A.7)* reduces to *Equation (A.9)* for PSK constellation signals: Choose s_i if

$$d^2(\tilde{s}_0, s_i) \le d^2(\tilde{s}_0, s_k) \qquad \forall i \ne k \tag{A.9}$$

Equation (A.9) is a joint probability function that seeks to minimize the Euclidean distance between the received signal and the constellation points. The ML detector in *Figure A.1* uses the decision rule in *Equation (A.9)* to obtain the optimal solution for $\hat{s}_0$, which is a ML estimate of s_0.

APPENDIX B

ALAMOUTI SPACE – TIME BLOCK CODING

B.1 APPENDIX OVERVIEW

In *Appendix B*, a transmit diversity scheme in baseband, originally proposed by Alamouti [3], is presented and shown in *Figure B.1*.

Appendix B is structured as follows: In *Sections B.2* to *B.4* the main functions of *Figure B.1* are decribed, i.e:

- Encoding and transmission of symbols at the transmitter,
- combing scheme at the receiver,
- decision rule for ML detection.

In *Section B.5* the error performance of the scheme is presented and compared to MRRC. Lastly, some implementation issues are highlighted and discussed in *Section B.6*.

B.2 ENCODING AND TRANSMISSION

With reference to *Figure B.1*, assume that at time *t*, two symbols s_0 and s_1, are simultaneously transmitted from antennas zero and one. At the next symbol period, $t + T$, $-s_1^*$ and s_0^* are transmitted from antennas zero and one, respectively. Thus, encoding is done in both time and space, and is known as space-time coding. The channel can be modelled as described in *Chapter 4*. Assuming that the fading is constant across two consecutive symbols, h_0 and h_1 can be written as

$$\begin{aligned} h_0(t) &= h_0(t+T) = h_0 = \alpha_0 \exp(j\vartheta_0) \\ h_1(t) &= h_1(t+T) = h_1 = \alpha_1 \exp(j\vartheta_1) \end{aligned} \qquad \text{(B.1)}$$

where *T* denotes the symbol duration.

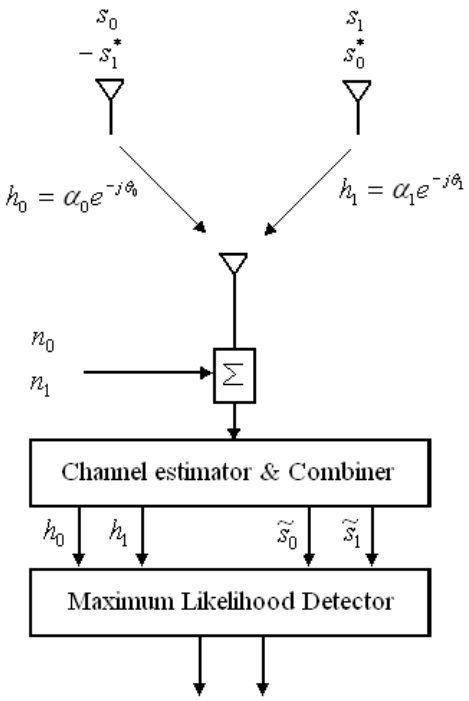

Figure B.1. Two branch transmit diversity with a single receiver, taken from [3].

It follows that the received signal at the receiver can be written as

$$r_0 = r(t) = h_0 s_0 + h_1 s_1 + \eta_0$$
$$r_1 = r(t+T) = -h_0 s_1^* + h_1 s_0^* + \eta_1 \qquad \text{(B.2)}$$

where r_0 and r_1 are the received signals at time t and $t+T$, respectively. These received signals are corrupted by receiver noise, denoted by η_0 and η_1 respectively.

B.3 COMBINING SCHEME

The combiner, as shown in *Figure B.1*, combines the following two signals, which are then passed on to the ML detector:

$$\tilde{s}_0 = h_0^* r_0 + h_1 r_1^*$$
$$\tilde{s}_1 = h_1^* r_0 - h_0 r_1^* \qquad \text{(B.3)}$$

Also note that *Equation (B.3)* differs from *Equation (A.5)*. Substituting *Equations (B.1)* and *(B.2)* into *Equation (B.3)*, *Equation (B.4)* is obtained.

$$\tilde{s}_0 = \left(\alpha_0^2 + \alpha_1^2\right) s_0 + h_0^* \eta_0 + h_1 \eta_1^*$$
$$\tilde{s}_1 = \left(\alpha_0^2 + \alpha_1^2\right) s_1 - h_0 \eta_1^* + h_1^* \eta_0 \qquad \text{(B.4)}$$

B.4 MAXIMUM LIKELIHOOD DETECTION

Using *Equation (A.8)* for $\tilde{s}_0$ and $\tilde{s}_1$, as defined in *Equation (B.4)*, the estimates for $\hat{s}_0$ and $\hat{s}_1$ can be obtained.

It should be noted that the resulting combined signal in *Equation (B.4)* is equivalent to the result in *Equation (A.5)* for MRRC. The only difference is the phase rotations on the noise

components, which do not degrade the effective SNR. Thus, the resulting diversity order of two is similar to the two branch MRRC. It was also shown by Alamouti [3] that the scheme can be extended to two transmit antennas and multiple receive antennas. Using M receive antennas, a diversity order of $2M$ can be obtained. In this dissertation only one receive antenna will be considered.

B.5 ERROR PERFORMANCE

With the performance evaluation of the scheme, the following assumptions are made:

- The total transmit power from the two antennas equals that of a single transmit antenna from the MRRC scheme.
- The amplitude of the fading from each transmit antenna to each receive antenna are mutually uncorrelated and Rayleigh distributed. However, the average signal power from each transmit antenna to each receive antenna are the same.
- Perfect CSI is assumed.

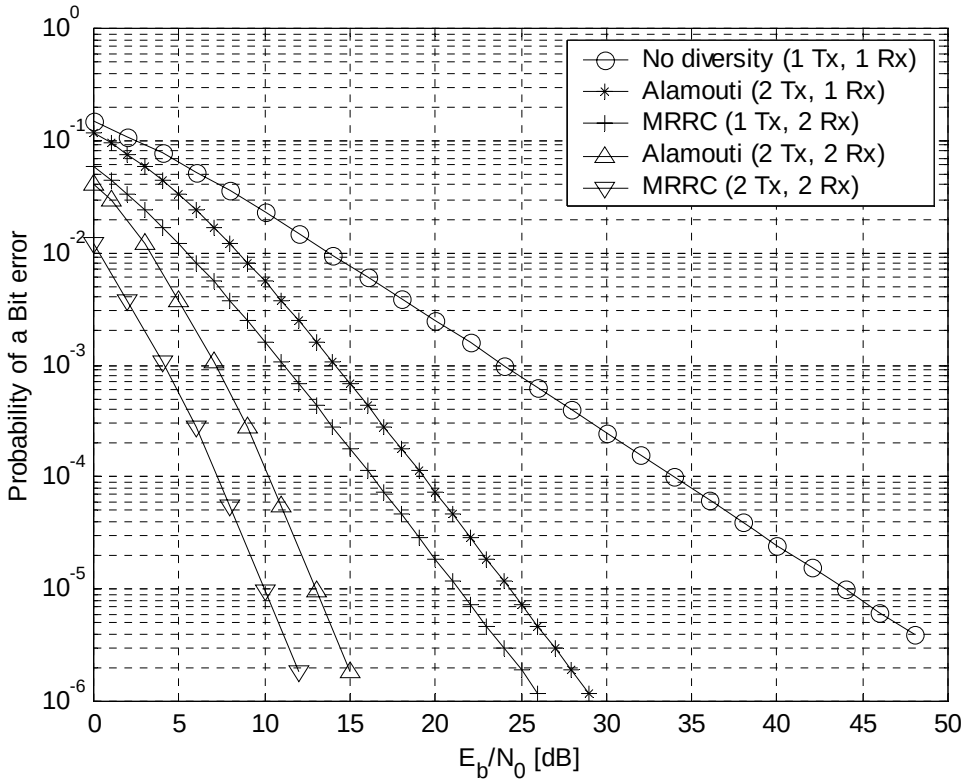

Figure B.2 BER performance of uncoded coherent BPSK for MRRC and the transmit diversity scheme in a Rayleigh fading channel [3].

These assumptions are the basis for comparing this scheme to other schemes. As seen in *Figure B.2*, the transmit diversity scheme performs similar to MRRC with the same number of antennas (see *Section B.6.1* for 3dB performance difference).

B.6 IMPLEMENTATION ISSUES

This section is concerned with the differences observed between the transmit diversity scheme and the MRRC scheme.

B.6.1 Power considerations

As seen in *Figure B.2*, the transmit diversity scheme has a 3dB penalty in SNR performance when compared to the MRRC scheme, due to the transmission of 2 symbols from two different antennas. Thus, only half the power is available to each antenna. This, however, can be a cheaper implementation, due to smaller amplifiers that need to be used.

B.6.2 Sensitivity to channel estimation errors

One method to perform channel estimation is by means of pilot insertion and extraction [72]. This is done by periodically transmitting known symbols to the receiver that are interpolated at the receiver to construct an estimate of the channel. It is interesting to note that the channel estimation error is minimized when the pilot insertion frequency is greater or equal to the channel Nyquist sampling rate. If this condition applies, the errors due to the channel estimation imperfections are minimized.

It should also be noted that twice the number of pilot symbols are added to the transmit diversity scheme, because of the extra antenna present (these pilot symbols should be orthogonal).

B.6.3 Delay effects

The delay for a 2-branch diversity scheme would be 2 symbol periods, where MRRC is only one symbol period. However, if the symbols were sent at the same time on different carriers, the symbol period would also be one.

B.6.4 Antenna Configuration

A primary requirement for diversity improvement is that the signals transmitted from different antennas should be sufficiently decorrelated (less than 70% correlation) and have almost equal gain. To satisfy this requirement, the antennas at the BS should be separated by at least 10λ, and 3λ at the MS [1, 3, 72]. This separation requirement depends on many factors such as antenna height and the scattering environment. It should also be stated that these figures apply mostly to macrocell, urban and suburban environments with relatively large base station antenna heights.

Accordingly, transmit diversity and receive diversity can both be accomplished, or only transmit diversity in the down link and receive diversity in the uplink, assuming the mobile has only a single antenna and the base station consists of multiple antennas.

B.6.5 Soft failure

Receive diversity enables a communication system to still receive a signal if one of the transmission chains fail, but with inferior quality because of the loss of diversity gain. This is called soft failure. This is also accomplished by transmit diversity. For example, suppose $h_1 = 0$ in *Equation (B.2)*, the received signal becomes:

$$r_0 = r(t) = h_0 s_0 + \eta_0$$
$$r_1 = r(t+T) = -h_0 s_1^* + \eta_1 \qquad \text{(B.6)}$$

Thus, the combiner combines the following two estimates:

$$\tilde{s}_0 = h_0^* \left(h_0 s_0 + \eta_0 \right) = \alpha_0^2 s_0 + h_0^* \eta_0$$

$$\tilde{s}_1 = -h_0 \left(-h_0^* s_1 + \eta_1 \right) = \alpha_0^2 s_1 - h_0 \eta_1^* \qquad \text{(B.7)}$$

which is similar to using no diversity at all.

B.6.6 Impact on Interference

The level of interference experienced by the transmit diversity scheme is twice as much as with the MRRC scheme. This interference can be minimized by incorporating techniques such as array processing [1, 5, 6, 7], etc.

APPENDIX C

MOBILE FADING CHANNEL THEORY AND SIMULATIONS

C.1 APPENDIX OVERVIEW

In Appendix C, a summary of multipath fading signal propagation effects contained within the simulation platform and used to generate the proposed DSSTS as well as SSTD scheme's simulation results, is presented. This Appendix is structured as follows: In *Section C.2* a general overview of small-scale multipath fading propagation is presented, followed with factors influencing small-scale fading in *Section C.3*. In *Section C.4* types of small-scale fading is presented, followed with channel models in S*ections C.5* and *C.6*. Simulation results of the Flat Fading Channel Simulator (FFCS), also see *Chapter 4*, *Section 4.1*, are presented in *Section C.7*, and lastly theoretical BERs for a AWGN channel, slow flat fading Rayleigh fading channel as well as ST coding BERs in a Rayleigh fading channel are presented in *Section C.8*.

C.2 SMALL-SCALE MUTIPATH FADING PROPAGATION

Multipath in the radio channel creates small-scale fading effects. The three most important effects are [1, 7]:

- Rapid changes in signal strength over a small distance or short time interval.
- Random frequency modulation due to varying Doppler shifts on different multipath signals.
- Time dispersion (echoes) caused by multipath propagation delays.

In built-up urban areas, the height of the mobile antennas is well below the height of surrounding structures, so that there exists no single LOS to the BS (*Figure C.1*). Fading occurs due to the movement of the MS, movement of the surrounding objects as well as the multiple paths between the BS and MS (see *Section C.3*). Even when a LOS exists between the MS and BS, multipath still occurs due to reflections from ground and surrounding structures. The incoming radio waves arrive from different directions with different propagation delays. The signal received by the mobile at any point in space may consist of a large number of plane waves having randomly distributed amplitudes, phases, and angles of arrival. These multipath components combine vectorially at the receiver antenna, causing the signal received by the mobile to distort or fade (see *Figure C.2*). Even when a mobile receiver is stationary, the received signal may fade due to movement of surrounding objects in the radio channel. If objects in the radio channel are static, and motion is considered to be only due to that of the mobile, then fading is purely a spatial phenomenon [7].

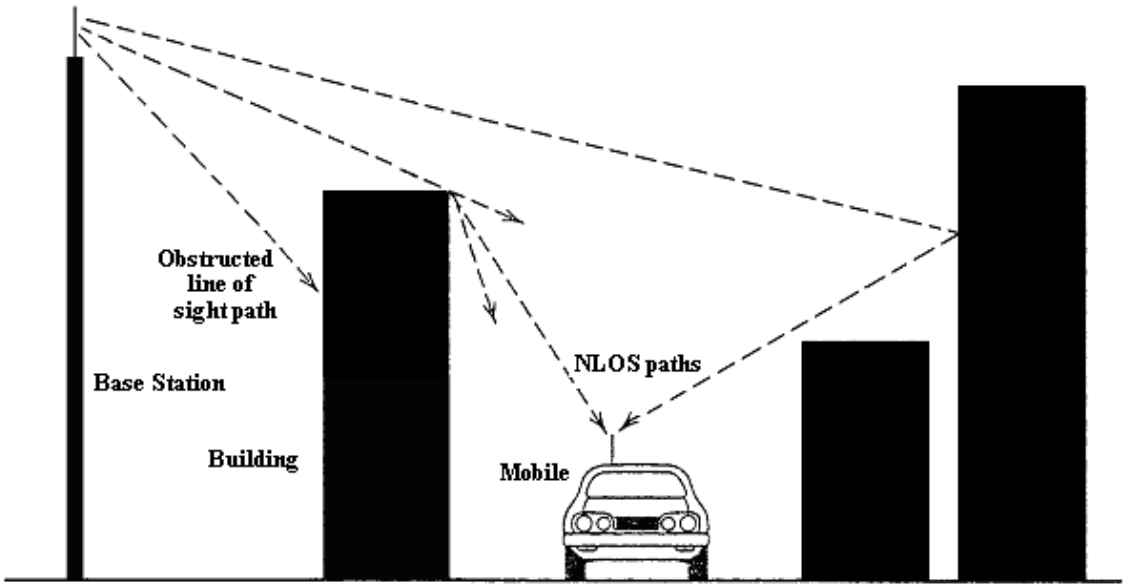

Figure C.1. Illustration of more that one NLOS propagation path towards the mobile unit.

The receiver sees the spatial variations of the resulting signal as temporal variations as it moves through the multipath field. Due to constructive and destructive effects of multipath waves summing at various points in space, a receiver moving at high speed can pass through several fades in a small period of time (See *Figures C.7* and *C.9*). Maintaining good communications can then become very difficult, although passing vehicles or people walking in the vicinity of the mobile can often disturb the field pattern, thereby diminishing the likelihood of the received signal remaining in a deep null for a long period of time. By using multiple antennas at the receiver, the likelihood that both antennas are simultaneously in a fade are less than a single receive antennas scenario, thus resulting in improved reception [9, 73]. Due to the relative motion between the mobile and the BS, each multipath wave experiences an apparent shift in frequency. The shift in received signal frequency due to motion is called the Doppler shift, and is directly proportional to the velocity and direction of motion of the mobile with respect to the direction of arrival of the received multipath wave [1, 6, 7]. See Appendix D for more information on Doppler shift and spread.

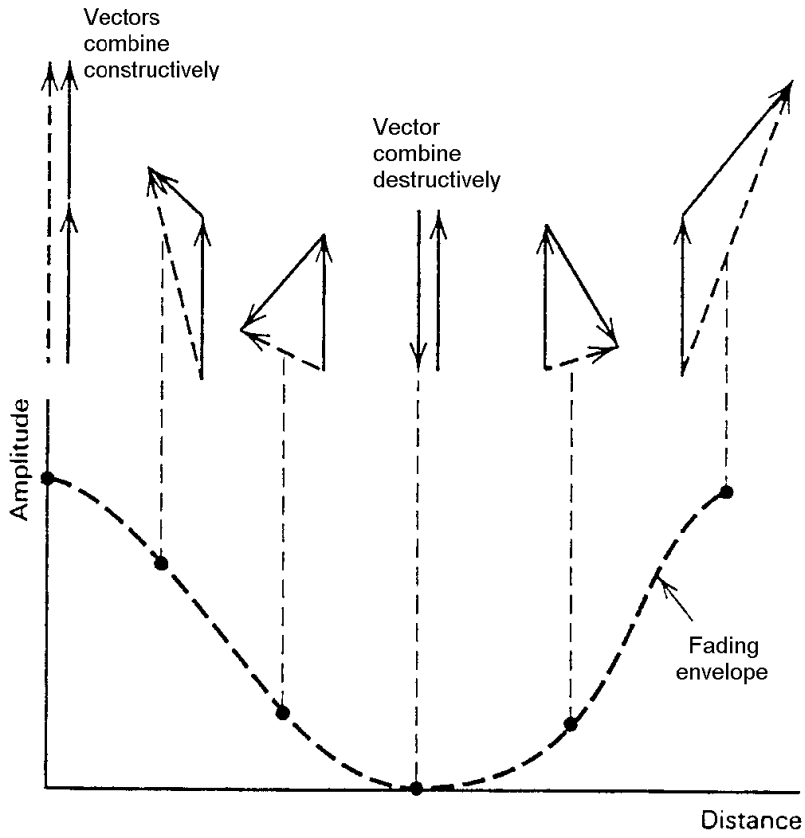

Figure C.2. Envelope fading caused by adding different phases. These phases can be represented by more than two phases adding together, taken from [7].

C.3 FACTORS INFLUENCING SMALL-SCALE MULTIPATH FADING

Many physical factors in the radio propagation channel influence small-scale fading. These include the following:

C.3.1 Multipath propagation

The presence of reflecting objects and scatterers in the channel creates a constantly changing environment that dissipates signal energy in amplitude and phase over time. These effects result in multiple versions of the transmitted signal that arrive at the receiving antenna, displaced with respect to one another in time and spatial orientation. The random phase and amplitudes of the different multipath components cause fluctuations in signal strength, thereby inducing small-scale fading. Multipath propagation often lengthens the time required for the baseband information of the signal to reach the receiver, which can cause signal smearing due to Inter Symbol Interference (ISI). For a more in depth discussion on multipath propagation, see Appendix D.

C.3.2 Speed of the mobile.

The relative motion between the BS and the mobile results in random frequency modulation due to different Doppler shifts on each of the multipath components. Doppler shift will be positive or negative depending on whether the mobile receiver is moving toward or away from the BS. For a more in depth discussion on Doppler shift, see Appendix D.

C.3.3 Speed of surrounding objects.

If objects in the radio channel are in motion, they induce a time varying Doppler shift on multipath components. If the surrounding objects move at a greater rate than the mobile, then this effect dominates the small-scale fading. Otherwise, motion of surrounding objects may be ignored, and only the speed of the mobile need be considered. The *coherence time* defines the "staticness" of the channel, and is directly impacted by the Doppler shift, and Doppler spread. Doppler spread is thus introduced by the time variations in the channel. For a more

in depth discussion on Doppler spread, see Appendix D. Widely used models for the Doppler power spectrum (Doppler spread) of mobile radio channels are the so-called Jakes model [74] and Clarke model [75]. The Doppler spectrum is defined by *Equation (C.1)* and shown in *Figure C.3.*

$$S_C(f) = \begin{cases} \frac{1}{\pi f_d} \frac{1}{\sqrt{1-(f/f_d)^2}} & (|f| \le f_d) \\ 0 & (|f| \le f_d) \end{cases} \qquad \text{(C.1)}$$

where f_d is the maximum Doppler shift. Based on the statistical characteristics of the scattered electromagnetic fields constituting the signal entering the moving receiver, the following geometrical assumptions is made for which Equation C.1 holds:

- The antenna is fixed and employs a vertically polarised omni directional antenna.
- The field incident on the receiver has M_{az} azimuthal plane waves.

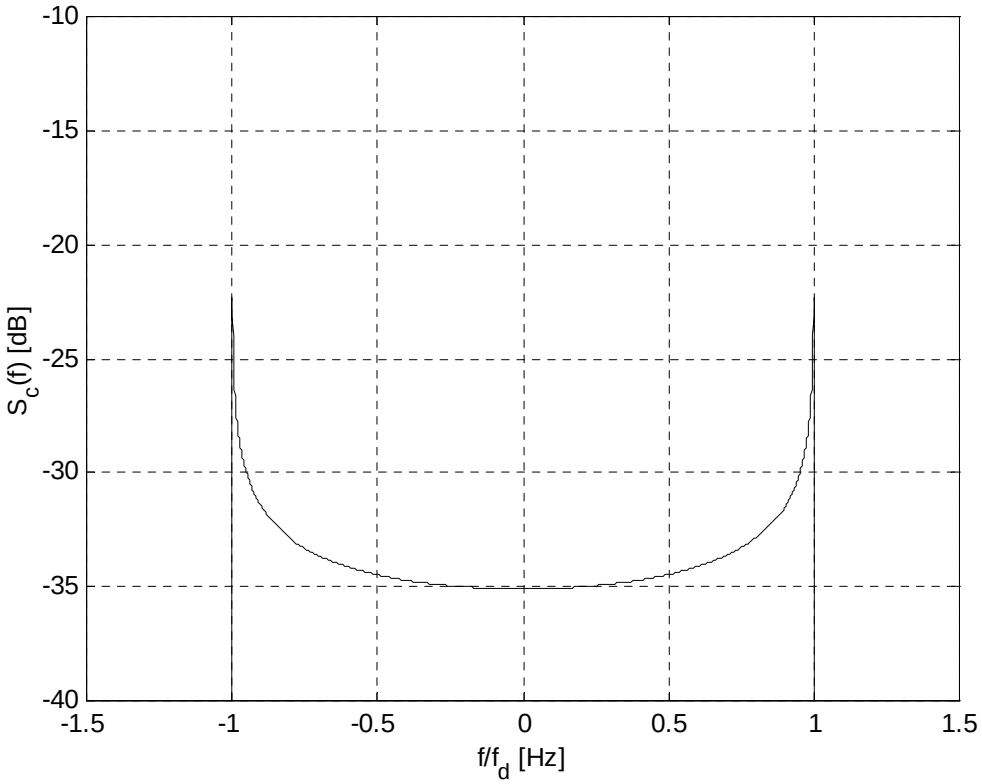

Figure C.3. Doppler power spectrum $S_c(f)$ plot for a baseband mobile radio channel.

- Each of the M_{az} azimuthal plane waves have an arbitrary carrier phase. These phases are assumed to be uniformly distributed between $-\pi$ and π.
- Each of the M_{az} azimuthal plane waves have an arbitrary angle of arrival to the receive antenna.
- The M_{az} azimuthal plane waves have equal average amplitudes, implying an absent LOS path.

C.3.4 The transmission bandwidth of the signal.

If the transmitted radio signal bandwidth is larger than the "bandwidth" of the multipath channel, the received signal will be distorted, but the received signal strength will not fade much over a local area (i.e., the small-scale signal fading will not be significant). As will be shown, the bandwidth of the channel can be quantified by the *coherence bandwidth*, which is related to the specific multipath structure of the channel. The coherence bandwidth is a measure of the maximum frequency difference for which signals are still strongly correlated in amplitude. If the transmitted signal has a narrow bandwidth compared to the channel, the amplitude of the signal will change rapidly, but the signal will not be distorted in time. Thus, the statistics of small-scale signal strength and the likelihood of signal smearing appearing over small-scale distances are very much related to the specific amplitudes and delays of the multipath channel, as well as the bandwidth of the transmitted signal.

C.4 TYPES OF SMALL-SCALE FADING

From the previous sections it is evident that the type of fading experienced by a signal propagating through a mobile radio channel depends on the nature of the transmitted signal with respect to the characteristics of the channel. Depending on the relation between the signal parameters (such as bandwidth, symbol period, etc.) and the channel parameters (such as delay spread and Doppler spread), different transmitted signals will undergo different types of fading.

The time and frequency dispersion mechanisms in a mobile radio channel lead to four possible distinct effects, which are dependant on the nature of the transmitted signal, the channel, and the relative velocity between the BS and the mobile. While multipath delay spread leads to time dispersion and frequency selective fading, Doppler spread leads to frequency dispersion and time selective fading.

C.4.1 Fading effects due to multipath time delay spread

Time dispersion due to multipath causes the transmitted signal to undergo either flat or frequency selective fading.

Flat fading

If the mobile radio channel has a constant gain and linear phase response over a bandwidth, which is greater than the bandwidth of the transmitted signal, then the received signal will undergo flat fading. Thus, the signal bandwidth is small in comparison to the coherence bandwidth. In flat fading, the multipath structure of the channel is such that the spectral characteristics of the transmitted signal are preserved at the receiver. However, the strength of the received signal changes with time, due to fluctuations in the gain of the channel caused by multipath. This is observed as a received signal with varying gain over time, with the spectrum of the transmission practically preserved. Typical flat fading channels cause deep fades, and thus may require 20 or 30 dB more transmitter power to achieve low bit error rates during times of deep fades, as compared to systems operating over non-fading channels. To summarize, a signal undergoes flat fading if

$$BW_s << BW_c \quad \text{and}$$

$$T_s >> \vartheta_\tau \qquad \text{(C.2)}$$

where T_s is symbol period, BW_s the bandwidth of the transmitted modulation, ϑ_τ the channel RMS delay spread (see Appendix D) and BW_c the channel coherence bandwidth.

Frequency Selective Fading

If the channel possesses a constant-gain and linear phase response over a bandwidth that is smaller than the bandwidth of transmitted signal, then the channel creates frequency selective fading on the received signal. Thus, the signal bandwidth is large in comparison to the coherence bandwidth. Under such conditions, the channel impulse response has a multipath delay spread which is greater than the reciprocal bandwidth of the transmitted message waveform. When this occurs, the received signal includes multiple versions of the transmitted waveform, which are attenuated (faded) and delayed in time, and hence the received signal is distorted. Viewed in the frequency domain, certain frequency components in the received signal spectrum have greater gains than others. Frequency selective fading channels are much more difficult to model than flat fading channels since each multipath signal must be modelled and the channel must be considered to be a linear filter. It is for this reason that wideband multipath measurements are made and models are developed from these measurements.

To summarize, a signal undergoes frequency selective fading if

$$BW_s > BW_c \quad \text{and}$$

$$T_s < \vartheta_\tau \qquad \text{(C.3)}$$

A common rule of thumb is that a channel is flat fading if $T_s \geq 10\ \vartheta_\tau$ [1] and a channel is frequency selective if $T_s < 10\ \vartheta_\tau$ [1].

C.4.2 Fading effects due to Doppler spread

Depending on how rapidly the transmitted baseband signal changes compared to the channel's rate of change, a channel may be classified either as a fast fading or slow fading channel.

Fast Fading

In a fast fading channel, the channel impulse response changes rapidly within the symbol duration. That is, the coherence time of the channel is smaller than the symbol period of the transmitted signal. This causes frequency dispersion (also called time selective fading) due to Doppler spreading, which leads to signal distortion. Viewed in the frequency domain, signal distortion due to fast fading increases with increasing Doppler spread relative to the bandwidth of the transmitted signal. Therefore, a signal undergoes fast fading if

$$T_s > T_c \quad \text{and}$$

$$BW_s < BW_d \tag{C.4}$$

Where BW_d is the Doppler spread bandwidth. It should be noted that when a channel is specified as a fast or slow fading channel, it does not specify whether the channel is flat fading or frequency selective in nature. Fast fading only deals with the rate of change of the channel due to motion. In the case of the flat fading channel, we can approximate the impulse response to be simply a delta distribution (no time delay). Hence, a flat, fast fading channel is a channel in which the amplitude of the delta functional varies faster than the rate of change of the transmitted baseband signal. In the case of a frequency selective, fast fading channel, the amplitudes, phases, and time delays of anyone of the multipath components vary faster than the rate of change of the transmitted signal. In practice, fast fading only occurs for very low data rates.

Slow Fading

In a slow fading channel, the channel impulse response changes at a rate much slower than the transmitted baseband signal. In this case, the channel may be assumed to be static over one or several reciprocal bandwidth intervals. In the frequency domain, this implies that the Doppler spread of the channel is much less than the bandwidth of the baseband signal. Therefore, a signal undergoes slow fading if

$$T_s << T_c \quad \text{and}$$

$$BW_s >> BW_d \tag{C.5}$$

It should be stated here that the velocity of the mobile (or velocity of objects in the channel) and the baseband signalling determines whether a signal undergoes fast fading or slow fading. It should also be emphasized that fast and slow fading deal with the relationship between the time rate of change in the channel and the transmitted signal, and not with propagation path loss models.

C.5. AWGN CHANNEL MODELS

C.5.1. Probability density function and spectral characteristics

An unavoidable limiting factor in the performance and capabilities of communication systems is AWGN. Understanding the nature of noise is therefore crucial if effective counter measures, such as channel coding, are to be designed.

Degradation of communication systems' performance in noisy channel conditions can be attributed to as variety of noise sources, e.g. interference from other communication systems, thermal noise and amplifier noise. The primary statistical characteristics of the resultant noise caused by adding the above mentioned noise sources, is that its amplitude exhibits a Gaussian distribution with a Probability Density Function (PDF) given by

$$pdf(z) = \frac{1}{\sigma_n \sqrt{2\pi}} \exp\left(-\frac{z^2}{2\sigma_n^2}\right) \tag{C.6}$$

where z is the noise amplitude, and σ_z^2 the noise variance power. The principle spectral characteristics of AWGN are that it has an essentially flat two-sided PSD for frequencies up to approximately 10^{12} Hz.

C.5.2. Obtaining Gaussian samples with required noise variance

When investigating the performance of communication systems in typical mobile communication channel conditions, two quantities, namely the SNR and the E_b/N_0 value (measured in dB), are of importance. Used more commonly in everyday speech, the SNR defines the ratio of average transmitted signal power to noise power at the receiver output. However, it is meaningless unless the noise bandwidth of the receiver is specified. Consequently the SNR is frequently normalised with respect to the noise bandwidth, resulting in the quantity E_b/N_0, which then becomes the dependent variable in the performance measurements. By stipulating the E_b/N_0 value for a specific performance measurement set up, it is possible to calculate the variance σ_n^2 of the Gaussian noise samples required to realise the correct AWGN channel conditions. Given the transmitted signal's bandwidth BW_s, the following relationship between the SNR and E_b/N_0 of uncoded binary communication systems holds:

$$SNR = \frac{\sigma_s^2}{\sigma_n^2} \quad (In\ the\ bandwidth\ BW_s) = \frac{E_b \cdot R_b}{N_0 \cdot BW_s} \tag{C.7}$$

where σ_s^2 is the variance (power) of the transmitted signal, σ_n^2 is the variance (power) of the required Gaussian noise samples, E_b is the energy in an uncoded bit, R_b is the uncoded bit rate and N_0 is the single sided PSD level of the AWGN.

Manipulation of *Equation (C.7)* can be shown to give [4]

$$psf_n = \frac{\sigma_s^2 \cdot f_{samp}}{10^{\left(\frac{1}{10}\cdot\frac{E_b}{N_0}\right)} \cdot 2R_b} \tag{C.8}$$

where f_{samp} is the sampling rate of the transmitter. Thus, the Gaussian distributed samples are scaled with a power scaling factor psf_n to produce Gaussian noise samples with variance of σ_n^2, which in turn produces the required E_b/N_0 level.

C.5.3. Probability of error for AWGN channels

The probability of a bit error of many modulation schemes in an AWGN channel is found by using the Q-function [6]. For a BPSK signal constellation the probability of a bit error is given as [1]

$$P_{e,BPSK}^{AWGN} = Q\left(\sqrt{2\Gamma}\right) \qquad \text{(C.9)}$$

where $\Gamma = E_b / N_0$ is the SNR per bit.

C.6. FLAT FADING CHANNEL MODELS

Radio channels can be modelled as a wide variety of distributions, such as an AWGN channel, a Rayleigh channel, a Rician channel, a log-normal channel etc. Due to the NLOS and LOS components, mobile radio channels are often modelled as a Rayleigh or Rician channel. Thus, only these two distributions are considered in this dissertation.

C.6.1. Rayleigh fading distribution

In mobile radio channels, the Rayleigh distribution is commonly used to describe the statistical time varying nature of the received envelope of a flat fading signal, or the envelope of an individual multipath component. It is well known that the envelope of the sum of two quadrature Gaussian noise signals obeys a Rayleigh distribution. *Figure C.4* shows a Rayleigh distributed signal envelope as a function of time. The Rayleigh distribution has a PDF given by

$$pdf(z) = \begin{cases} \dfrac{z}{\sigma_z^{\,2}} \exp\left(-\dfrac{z^2}{2\sigma_z^{\,2}}\right) & for \quad 0 \le z \le \infty \\ 0 & for \quad z < 0 \end{cases} \qquad \text{(C.10)}$$

where σ_z is the Root Mean Square (RMS) value of the received signal amplitude z before envelope detection, and σ_Z^2 is the power of the received signal before envelope detection.

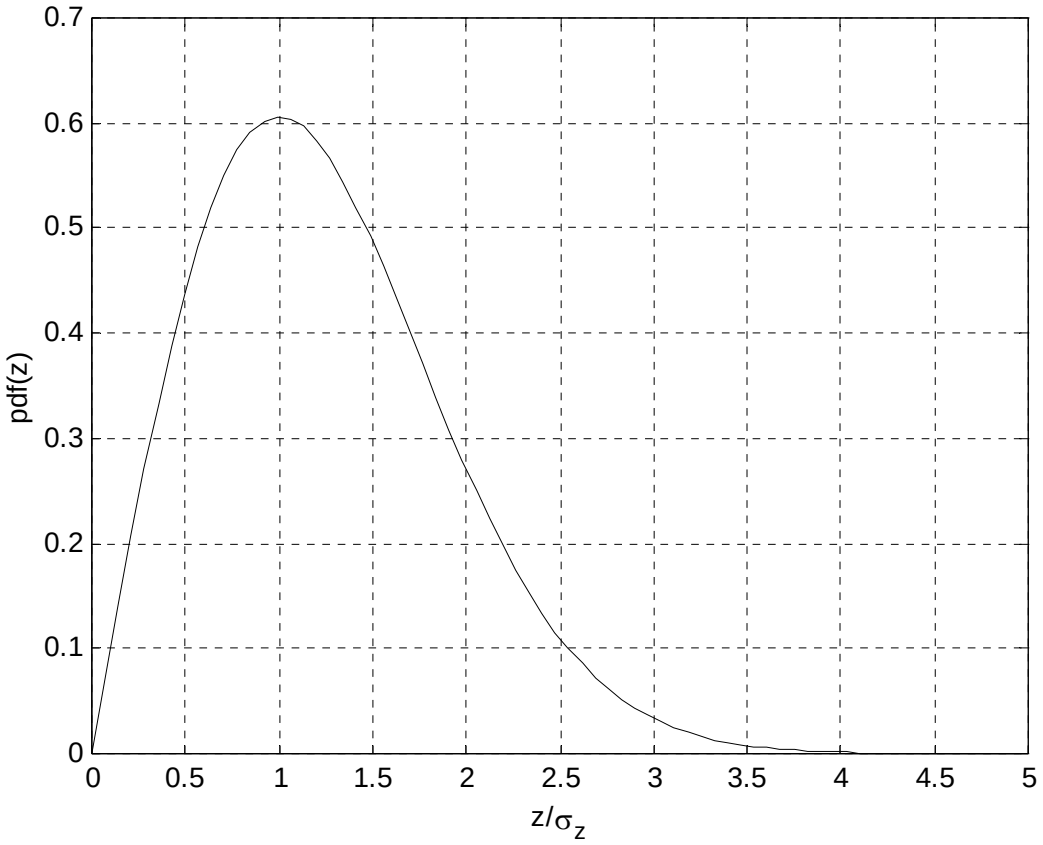

Figure C.4. PDF of a Rayleigh distribution.

C.6.2. Rayleigh fading probability of error

The probability of a bit error of coherent BPSK in a slow Rayleigh fading channel is given as [1]

$$P_{e,BPSK}^{RAY} = \frac{1}{2}\left[1-\sqrt{\frac{\Gamma}{1+\Gamma}}\right] \qquad \text{(C.11)}$$

where $\Gamma = E_b/N_0$ is the SNR per bit. The theoretical probability of error graphs for *Equations (C.9)* and *(C.11)* are presented in *Section C.8, Figure C.19* in order to show the performance difference between modulation techniques' performance in Rayleigh and AWGN channels.

C.6.3. Rician fading distribution

When there is a dominant stationary (non-fading) signal component present, i.e. a LOS propagation path, the small-scale fading envelope distribution can be modelled as Rician. In such a situation, random multipath components arriving at different angles are superimposed on a stationary dominant signal. At the output of an envelope detector, this has the effect of adding a Direct Current (DC) component to the envelope.

Just as for the case of detection of a sine wave in thermal noise, the effect of a dominant signal arriving with many weaker multipath signals gives rise to the Rician distribution. As the dominant signal becomes weaker, the composite signal resembles a noise signal with a Rayleigh fading envelope. Thus, the Rician distribution changes to a Rayleigh distribution when the LOS component fades away. The Rician distribution is given by

$$pdf(z) = \begin{cases} \dfrac{z}{\sigma_z^2}\exp\left(-\dfrac{(z^2+2K}{2\sigma_z^2}\right) I_0\left(\dfrac{\sqrt{2K}\ z}{\sigma_z^2}\right) & for \quad 0 \le z \le \infty \\ 0 & for \quad z < 0 \end{cases} \qquad \text{(C.12)}$$

The parameter $\sqrt{2K}$ denotes the peak amplitude of the dominant signal and $I_0(\bullet)$ is the modified zero-order Bessel function of the first kind. The Rician factor *K* denotes the ratio between the direct LOS signal component and the scatter component of the signal (see *Chapter 4, Section 4.1.1.*).

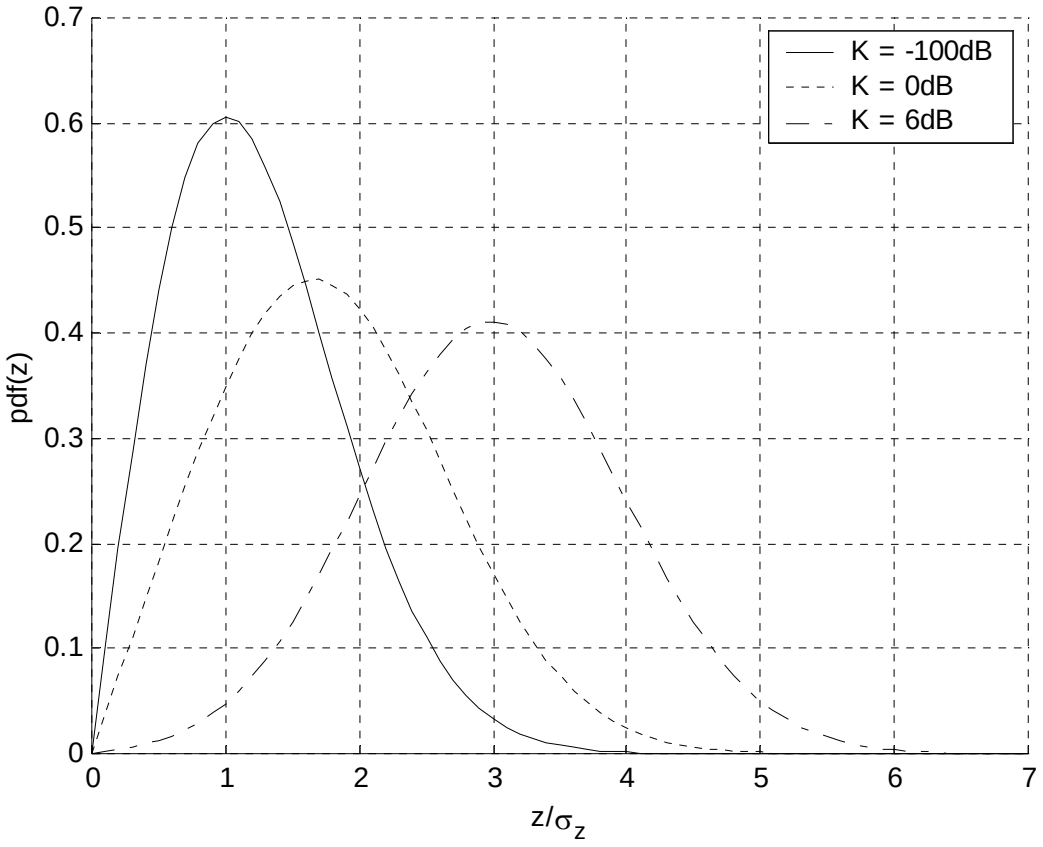

Figure C.5. Rician distribution for a LOS component (K) of -100 dB, 0 dB and 6 dB.

C.7. SIMULATION RESULTS OF THE FADING CHANNEL SIMULATOR

Simulation results for the FFCS presented in *Chapter 4*, *Section 4.1*, are presented in this section. As input to the FFCS shown in *Chapter 4*, *Section 4.1*, *Figure 4.1*, an unmodulated 1000Hz signal was used, sampled at 1MHz. It should also be stated that the received signal had constant and linear phase over the symbol duration. The following simulations were obtained for different values of the Rician constant (*K*) and speed of the mobile (different Doppler frequencies).

C.7.1. The received signal envelope

From *Figures C.6* to *C.9*, it can be seen that the received signal's envelope is fading if the channel is purely Rayleigh distributed (K = -100dB) and is much more constant with a Rician distribution (K = 6dB) as a result of the direct *LOS* component present in the Rician distribution. For a more in depth discussion on channel fade durations and fading statistics, see [1]. Comparing *Figures C.6* and *C.7*, it is evident that a low mobile speed has less fades and longer fade durations in comparison to a fast moving mobile that has significant more fades and much shorter fade durations.

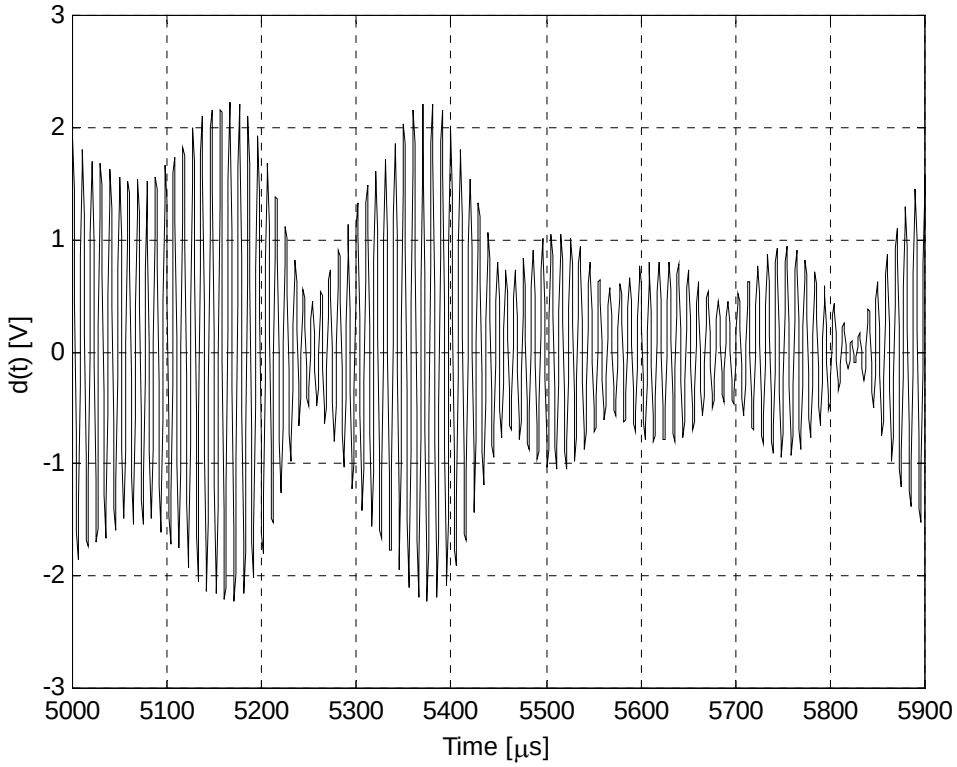

Figure C.6. Plot of a fading signal with K = -100dB and f_d = 33Hz.

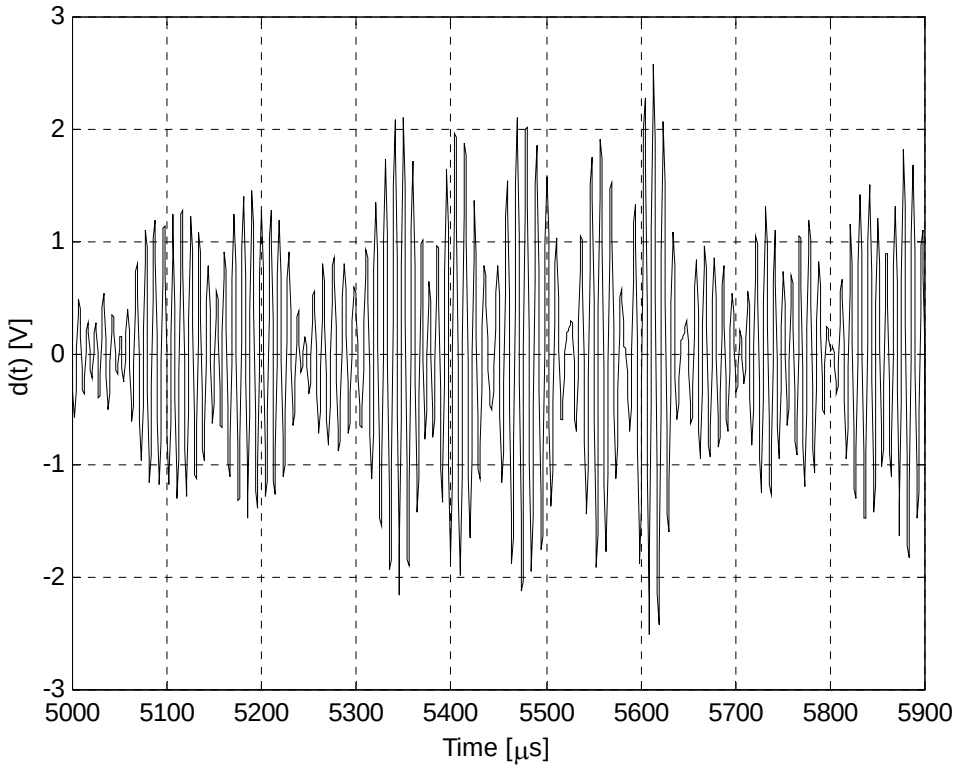

Figure C.7. Plot of a fading signal with K = -100dB and f_d = 100Hz.

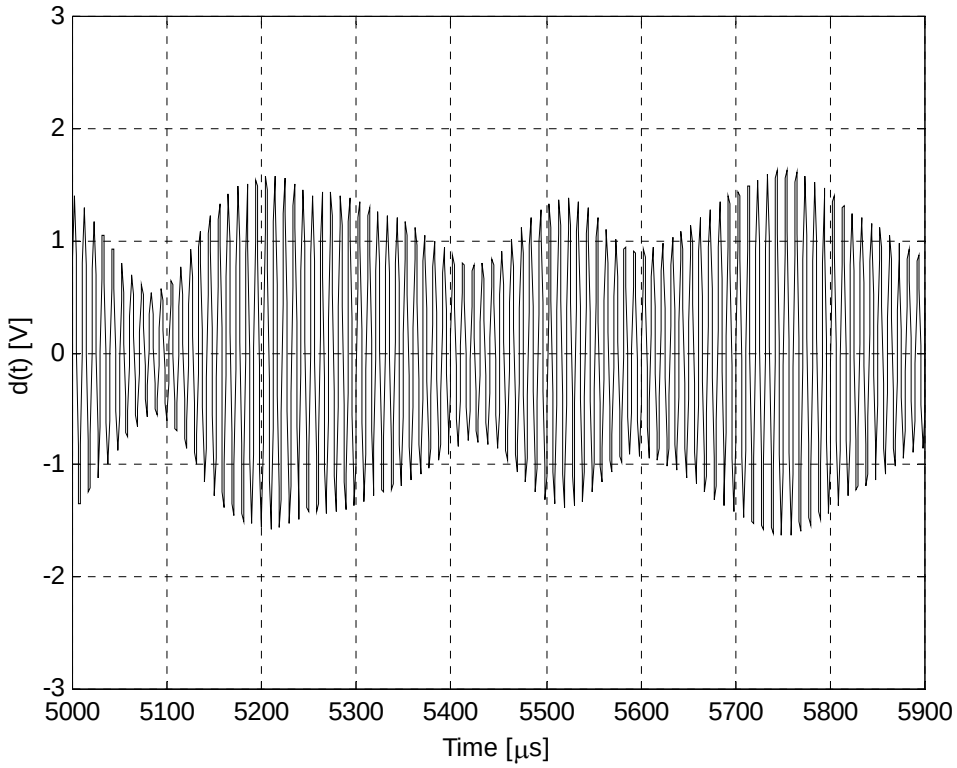

Figure C.8. Plot of a fading signal with K = 6dB and f_d = 33Hz.

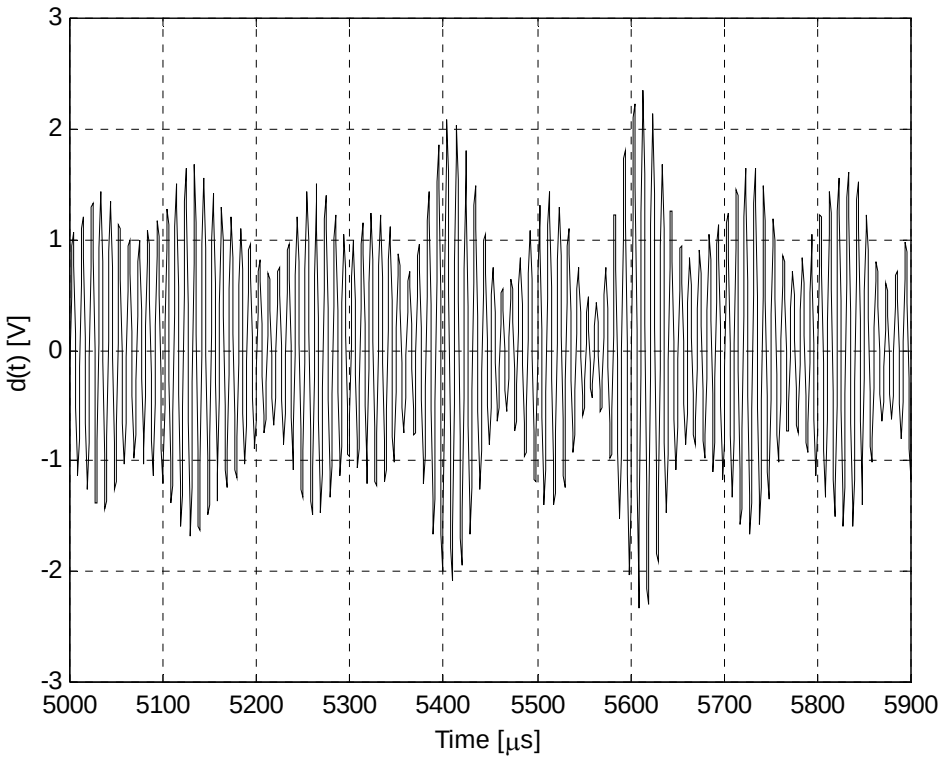

Figure C.9. Plot of a fading signal with K = 6dB and f_d = 100Hz.

C.7.2. The power spectrum of the received signal

From *Figures C.10* and *C.11* it is evident that the single frequency component in an unmodulated carrier is broadened to the Doppler power spectrum (compare with *Figure C.3* in *Section C.3*).

This Doppler spread is a function of the speed of the mobile (see Appendix D). The higher the speed of the mobile, the more frequency spread is introduced to the fading signal and visa versa. From *Figures C.12* and *C.13*, the presence of a direct *LOS* component (K) is seen as a single carrier component in the frequency spectrum at f = 1000Hz. As K becomes progressively larger, the peak power of the Doppler sidebands (i.e. frequency spread) is reduced compared to the peak power of the single carrier component. Thus, when K becomes sufficiently large, most power in the frequency spectrum lies within the single frequency component due to the input signal's frequency, showing that high *LOS* components counter the effects of Doppler spreading.

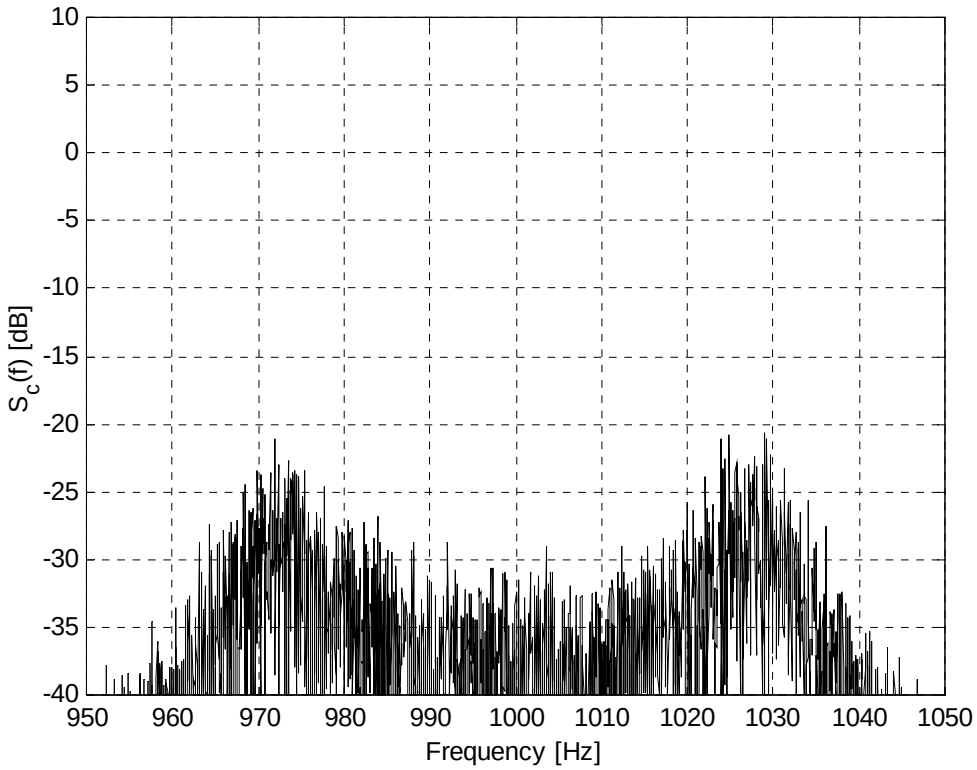

Figure C.10. The power spectrum of the fading signal shown in Figure C.6, with K = -100dB and f_d = 33Hz.

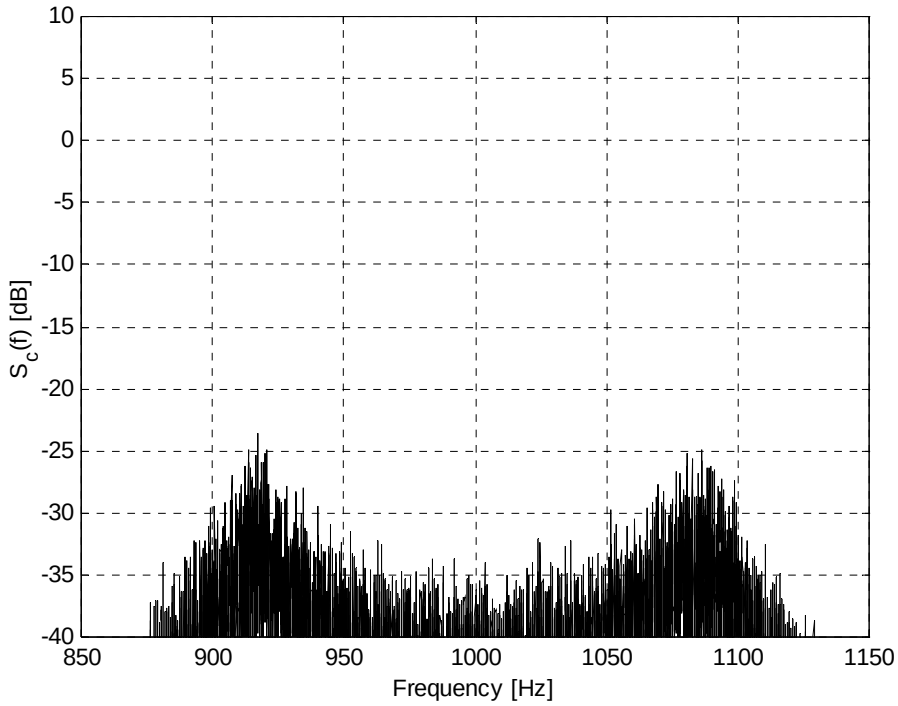

Figure C.11. The power spectrum of the fading signal shown in Figure C.7, with K = -100dB and f_d = 100Hz.

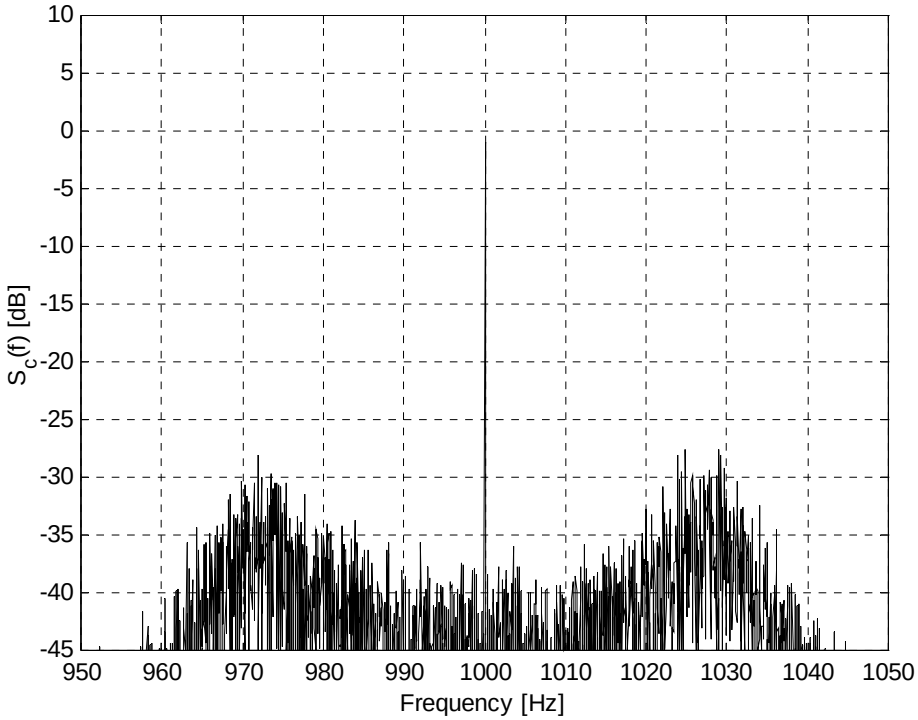

Figure C.12. The power spectrum of the fading signal shown in Figure C.8, with K = 6dB and f_d = 33Hz.

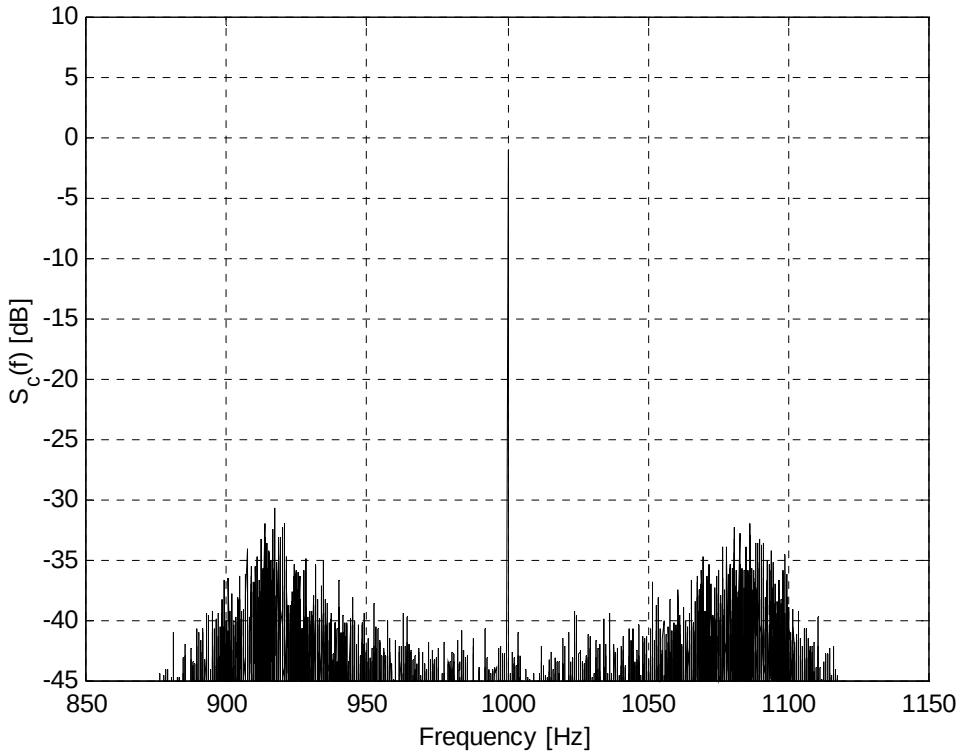

Figure C.13. The power spectrum of the fading signal shown in Figure C.9, with K = 6dB and f_d = 100Hz.

C.7.3. The PDF of the received signal

From *Figures C.14* to *C.17* it can be seen that the received signal's envelope is Rayleigh distributed when K = -100dB, and Rician distributed when K becomes larger (compare with *Figures C.4* and *C.5* in *Section C.6*). Eventually, when K = 6dB, the Rician distribution tends to be a Gauss distribution with a mean of 3 and variance of approximately 1. This is merely a result of the direct *LOS* component present in the Rician distribution. Because of identical distributions in *Figures C.14* and *C.15*, as well as *Figures C.16* and *C.17*, it can be stated that the received signal envelope is practically independent of the mobile speed (Doppler spread) in the presence of a dominant LOS signal component.

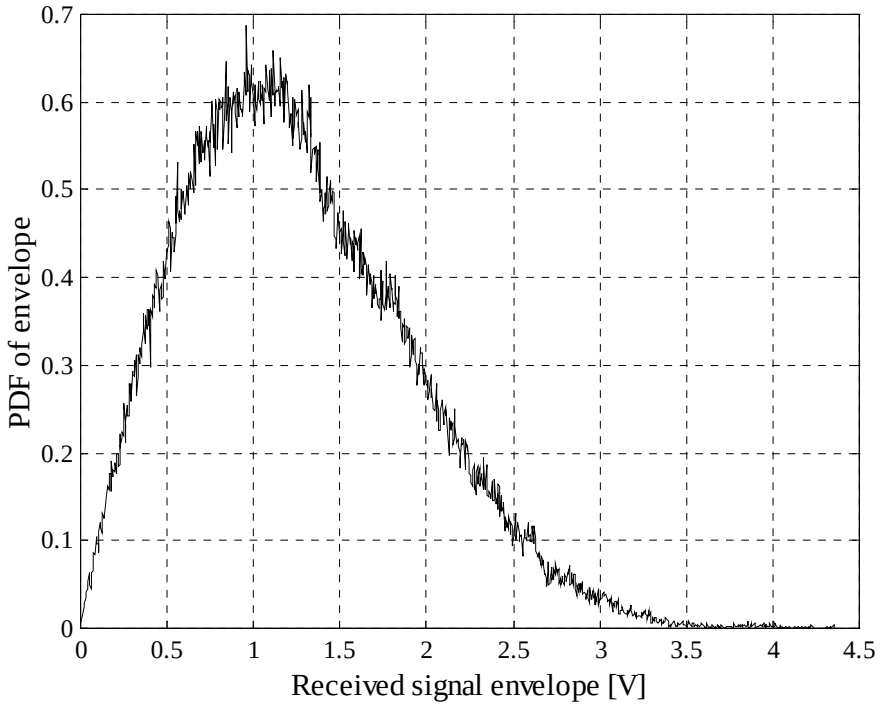

Figure C.14. The PDF of the fading signal's envelope in Figure C.6, with K = -100dB and f_d = 33Hz.

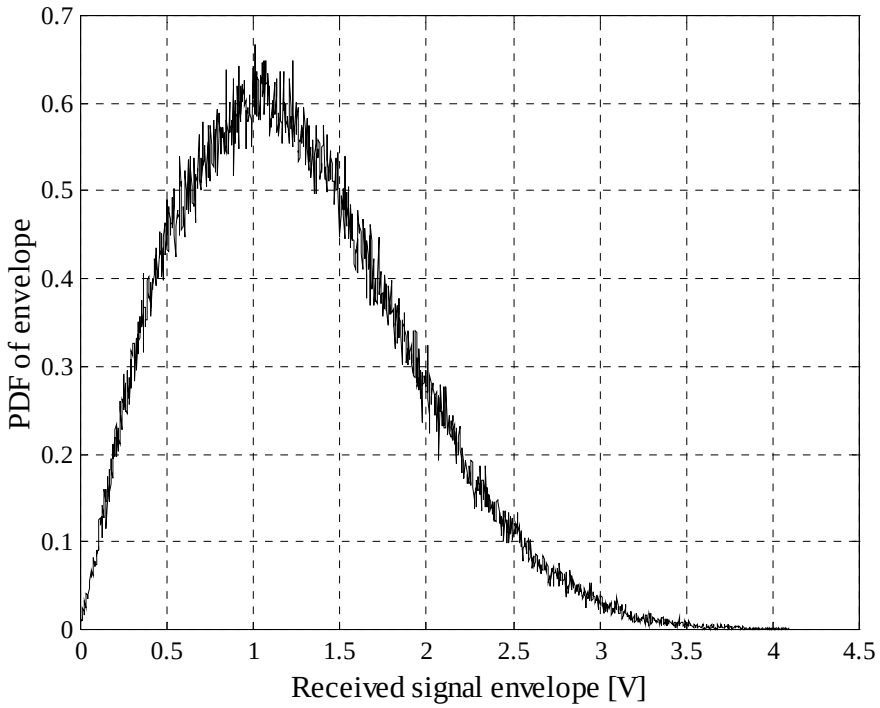

Figure C.15. The PDF of the fading signal's envelope in Figure C.7, with K = -100dB and f_d = 100Hz.

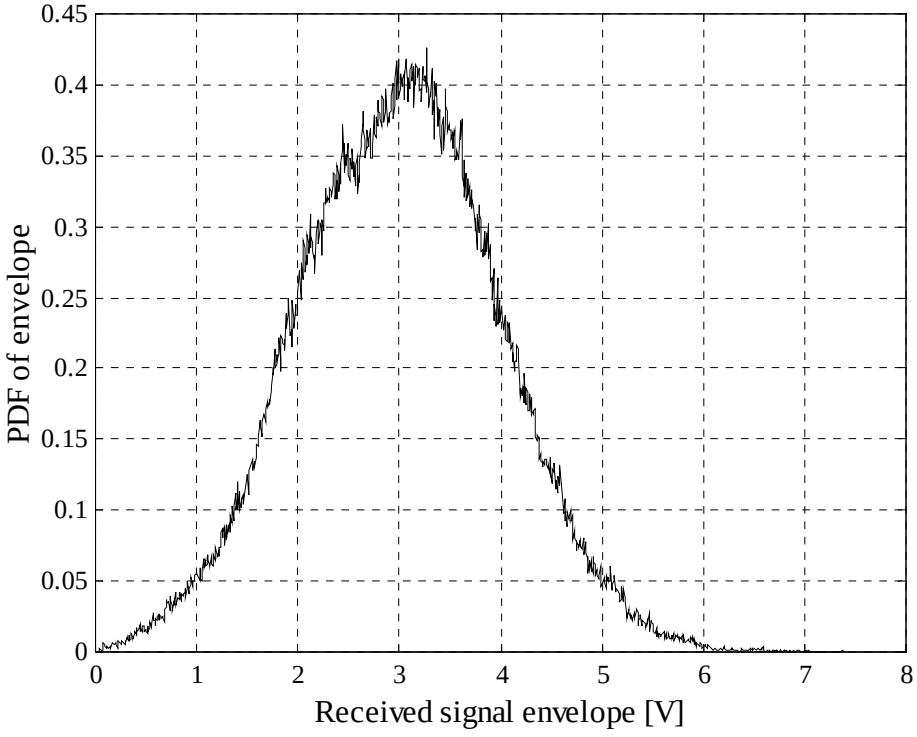

Figure C.16. The PDF of the fading signal's envelope in Figure C.8, with K = 6dB and f_d = 33Hz.

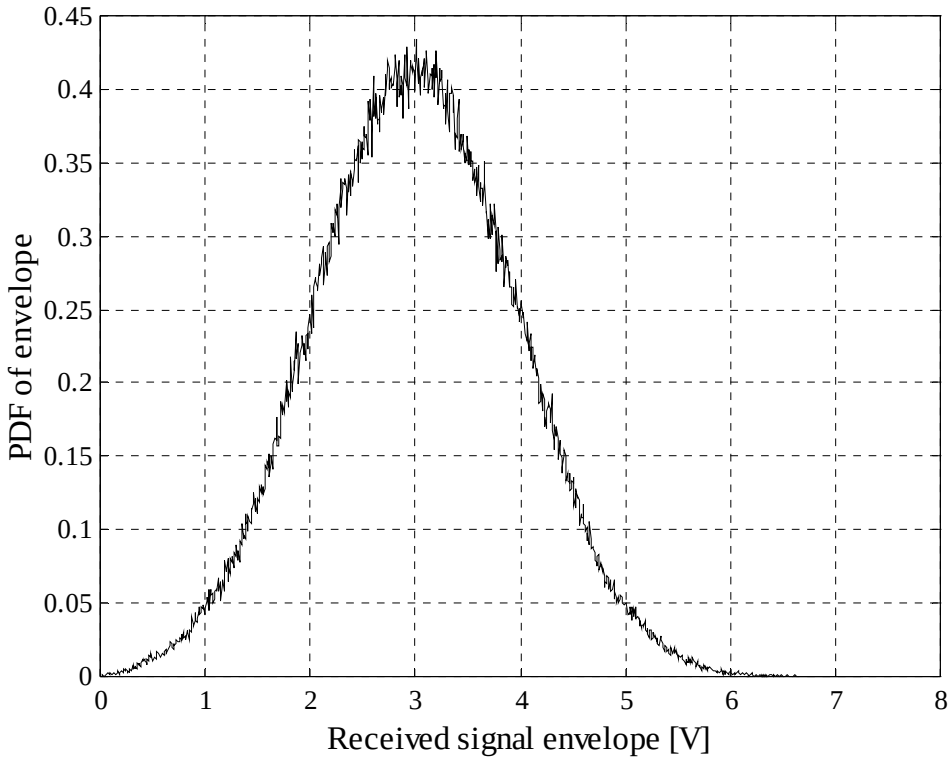

Figure C.17. The PDF of the fading signal's envelope in Figure C.9, with K = 6dB and f_d = 100Hz.

C.8. THEORETICAL BERs

In *Chapter 2*, *Equations (2.24)* and *(2.25)* were presented for ST coding error probabilities of BPSK and QPSK in a Rayleigh fading channel, respectively. These equations are plotted in *Figure C.18* for comparison purposes. The probability of error for a flat fading Rayleigh channel (see *Section C.6.2, Equation (C.11)*), is also included as a reference graph. Also note that a 3dB difference exists between the BPSK and QPSK modulation techniques. The probability of a bit error of coherent BPSK in a Rayleigh fading channel was given in *Section C.6.2, Equation (C.11),* whereas the probability of a bit error for a BPSK signal constellation in an AWGN channel is given by *Equation (C.9).* The theoretical probability of error graphs for *Equations (C.9)* and *(C.11)* are presented in *Figure C.19* and will henceforth serve as upper and lower bounds in the subsequent performance analysis of the proposed DSSTS schemes.

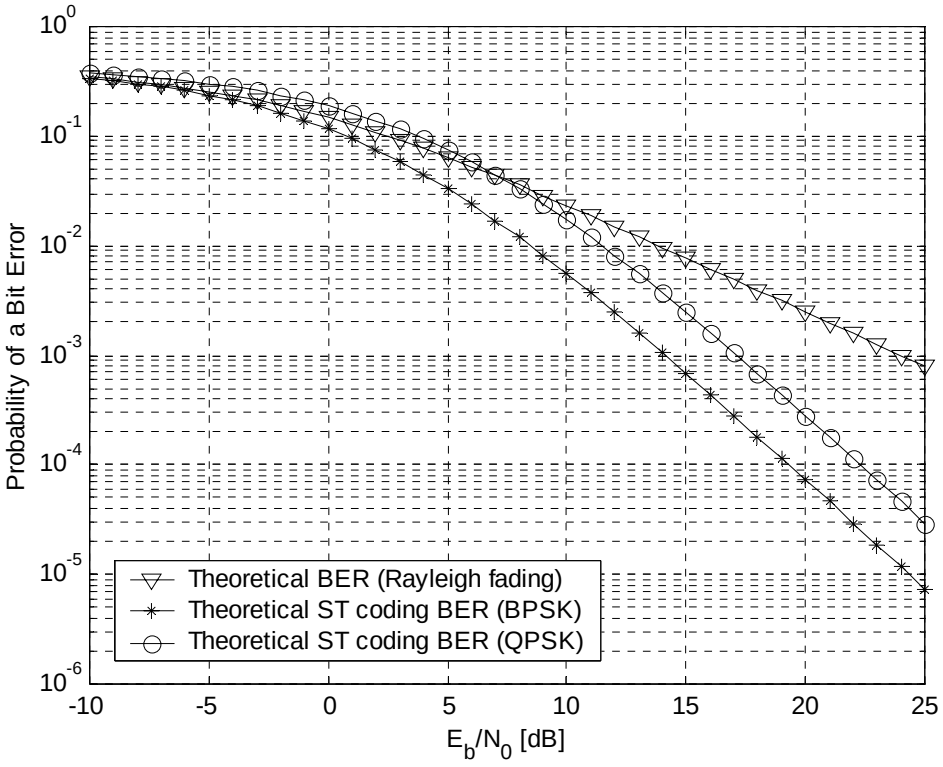

Figure C.18. Comparison of the simulation of a uncoded system, BPSK ST – and QPSK ST code's probability of error in a Rayleigh fading channel [24].

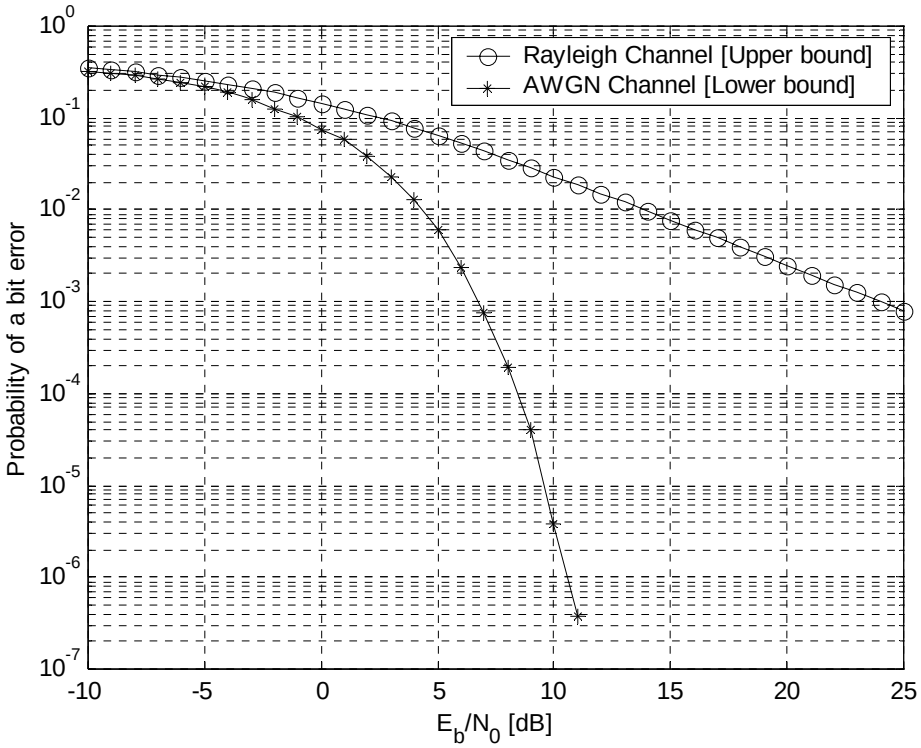

Figure C.19. Benchmark probability of error results for a BPSK system in Rayleigh as well as AWGN channel conditions.

APPENDIX D

CHANNEL EFFECTS, MATHEMATICAL ANALYSIS

D.1 APPENDIX OVERVIEW

In Appendix D an overview of different channel effects are discussed. In *Section D.2*, the Doppler effect is explained, while a statistical formulation of channel effects that occur due to multipath fading, is presented in *Section D.3* and *Section D.4*. In *Sections D.5* and *D.6* the concepts of delay spread and Doppler spread are introduced, respectively. Lastly, Clarke's fading model simulator is presented in *Section D.8* as well as the derivation of the scaling factors that were used in Chapter 4.

D.2 DOPPLER SHIFT

Signal fading is essentially a spatial phenomenon that manifests itself in the time domain as fluctuations occur in receive power as relative movement occur between the transmitter and receiver. With reference to *Figure D.1*, assume that a mobile is moving at a constant velocity v between points X and Y, receiving signals from a distant stationary source S. Assuming that X and Y are far apart, the receive angles at both point X and Y

are approximately θ. If d is the path length from X to Y, the difference in path lengths travelled by the waves from the source S to the mobile at points X and Y is $\Delta l = d\cos\theta = v\Delta t\cos\theta$ where Δt is the time required for the mobile to travel from point X to Y. Thus, the phase change in the received signal due to the difference in path length is given in *Equation (D.1)*

$$\Delta\Phi = \frac{2\pi\Delta l}{\lambda} = \frac{2\pi v\Delta t}{\lambda}\cos\theta \qquad \text{(D.1)}$$

The change in frequency, or Doppler shift f_d , due to the motion of the mobile, is given by *Equation (D.2)*

$$f_d = \frac{1}{2\pi}\frac{\Delta\Phi}{\Delta t} = \frac{v}{\lambda}\cos\theta \qquad \text{(D.2)}$$

From *Equation (D.2)* it can be seen that the Doppler shift is dependant on the speed and direction of the moving mobile. If the mobile moves towards the source S, the Doppler frequency is positive (i.e. the apparent received frequency increases), and negative as it moves away from the source (i.e. the apparent received frequency decreases).

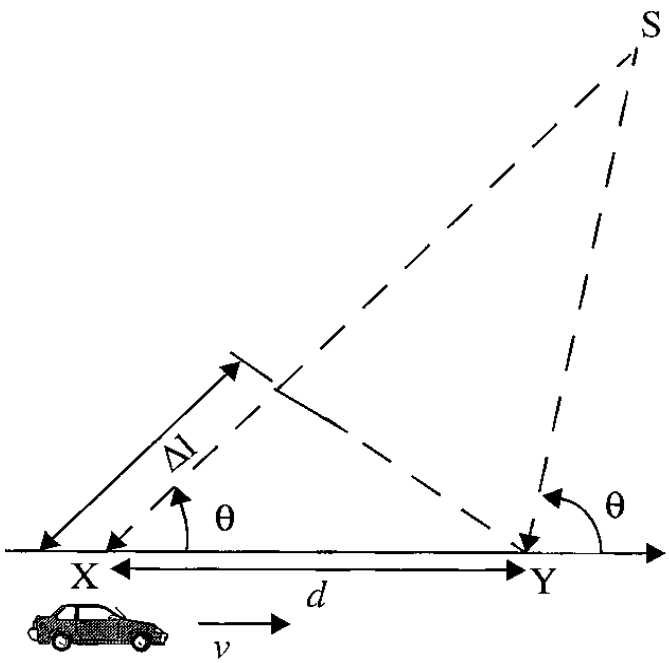

Figure D.1. Illustration of the Doppler effect, taken from Rappaport, pp.180 [1].

D.3 IMPULSE RESPONSE MODEL OF A MULTIPATH CHANNEL

If an extremely short pulse, ideally an impulse, is transmitted over a time-varying multipath channel, the received signal might appear as a train of pulses (*Figure D.2*). Note that [6] is the source for *Sections D.3* and *D.4*. Hence, two characteristics of a time-varying multipath channel that can be seen in *Figure D.2* are:

- Time spread of the signal is introduced.
- The nature of the all the multipaths varies with time in accordance to the environmental changes.

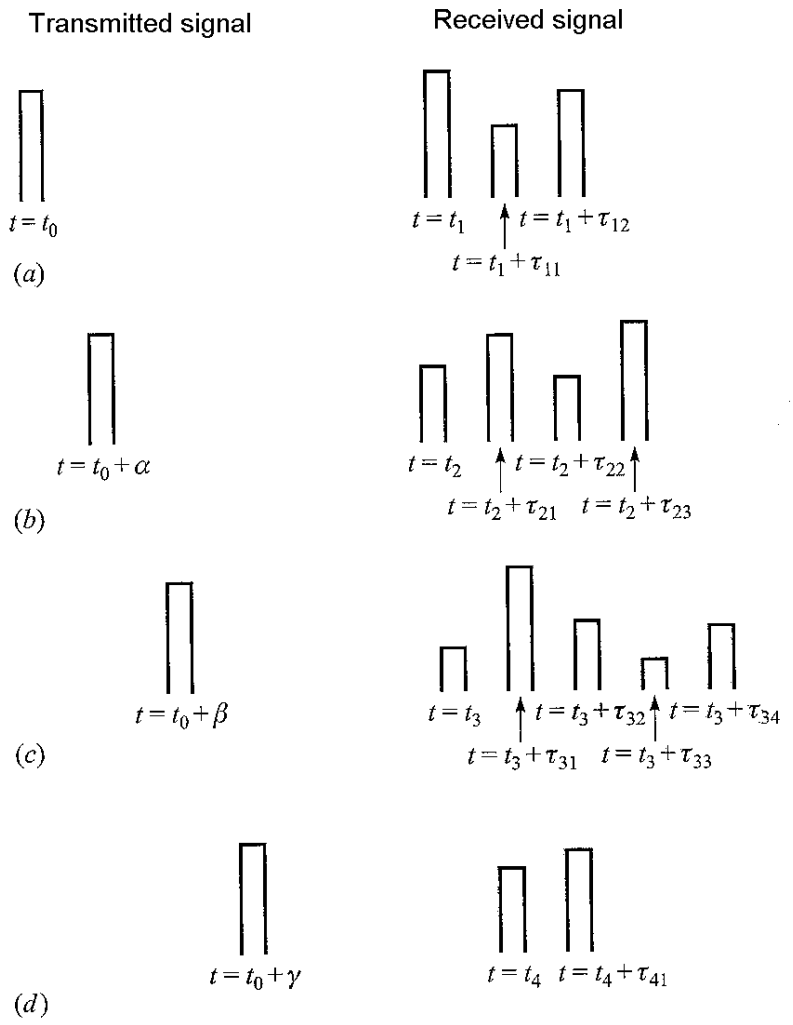

Figure D.2. Example of the response of a time variant multipath channel. Note that the same pulse in (a) to (d) is received differently in each case because of multipath, taken from Proakis, pp. 801 [6].

The time variations in the channel, as seen in *Figure D.2*, appear to be unpredictable to the user of the channel. For this reason, a time variant multipath channel is characterised statistically.

Assume a transmitted signal to be of the form

$$u(t) = \mathrm{Re}[\, u_l(t) \exp(\; j2\pi f_c t)] \tag{D.3}$$

A received band pass signal, having L multipaths that faded and introduced time spread in the signal can be represented by

$$x(t) = \sum_i^L \beta_i(t) u[t - \tau_i(t)] \tag{D.4}$$

where $\beta_i(t)$ represents the attenuation of the i^{th} path with a time delay of $\tau_i(t)$. Substitution of *Equation (D.3)* into *Equation (D.4)* yields

$$x(t) = \mathrm{Re}\left(\left\{ \sum_i^L \beta_i(t) e^{-j2\pi f_c \tau_i(t)} u_l[t - \tau_i(t)] \right\} e^{j2\pi f_c t} \right) \tag{D.5}$$

From *Equation (D.5)*, it is apparent that the equivalent low-pass received signal is

$$d_l(t) = \sum_i^L \beta_i(t) e^{-j2 f_c \tau_i(t)} u_l[t - \tau_i(t)] \tag{D.6}$$

But, $d_l(t)$ is a response of an equivalent low-pass channel to an equivalent low-pass signal $u_l(t)$. Thus, the equivalent low-pass channel is described by the time-variant impulse response in discrete form in *Equation (D.7)*

$$c(\tau; t) = \sum_i^L \beta_i(t) e^{-j2 f_c \tau_i(t)} \delta[t - \tau_i(t)] \tag{D.7}$$

In integral form, the received signal $d(t)$ is represented by

$$d(t) = \int_{-\infty}^{\infty} \beta(\tau;t)u(t-\tau)d\tau \tag{D.8}$$

where $\beta(t;\tau)$ denotes the attenuation of the signal with a delay time of τ at time instant t. By substitution of *Equation (D.3)* into *Equation (D.8)*, the received signal in integral form is

$$d(t) = \mathrm{Re}\left(\left\{ \int_{-\infty}^{\infty} \beta(\tau;t) e^{-j2\pi f_c \tau} u_l(t-\tau) d\tau \right\} e^{j2\pi f_c t} \right) \tag{D.9}$$

Because *Equation (D.9)* represents the convolution of $u_l(t)$ with an equivalent low-pass time variant impulse response, it follows that

$$c(\tau;t) = \beta(\tau;t)e^{-j2\pi f_c \tau} \tag{D.10}$$

where $c(\tau;t)$ represents the response of the channel at time t due to an impulse applied at time instant $(t - \tau)$. For example, assume an unmodulated carrier at frequency f_c. Then $u_l(t) = 1$ for all t and the received signal in the case of discrete multipath, given by *Equation (D.6)*, reduces to

$$d_l(t) = \sum_{i}^{L} \beta_i(t) e^{-j\vartheta_i(t)} \tag{D.11}$$

where $\theta_i(t) = 2\pi f_c \tau_i(t)$. Note that the subscript in *Chapter 4*, *Equation (4.12)* is dropped compared to *Equation (D.11)*, because all signals are assumed to be at baseband in *Chapters 1* to *7*. At time t, the received signal consists of the sum of a number of time-variant vectors (phasors) having amplitudes $\beta_i(t)$ and phases $\theta_i(t)$. Note that large dynamic changes in the medium are required for $\beta_i(t)$ to caused a significant change in the received signal. On the other hand, $\theta_i(t)$ will change by 2π rad whenever $\tau_i(t)$ changes by $1/f_c$. But $1/f_c$ is very small and, thus $\theta_i(t)$ can change by 2π rad with relatively small motions of the medium. As described in Appendix C, *Section C.2*, the random phases and amplitudes of

the received signal results in signal fading. The fading phenomenon is primarily a result of the time variations in the phases $\theta_i(t)$. That is, the randomly time-variant phases $\theta_i(t)$ associated with the vectors $\{\beta_i\, e^{-j\theta_i}\}$ at times result in the vectors adding destructively (see Appendix C, *Section C.2, Figure C.2*). When this occurs, the resultant received signal $d_l(t)$ is very small or practically zero. At other times, the vectors $\{\beta_i\, e^{-j\theta_i}\}$ add constructively, so that the received signal is large (see *Figure C.2*). Thus, the amplitude variations in the received signal, termed signal fading, are due to the time-variant multipath characteristics of the channel.

The delays $\tau_i(t)$, associated with the different signal paths, will also change at different rates and in an unpredictable (random) manner. This implies that the received signal $d_l(t)$ in *Equation (D.11)* can be modelled as a random process that is usually assumed to be stationary.

D.4 CHANNEL CORRELATION FUNCTIONS AND POWER SPECTRA

It is necessary to develop correlation functions and power spectral density functions that define the characteristics of a fading multipath channel. This analysis can be made in the time domain as well as the frequency domain.

D.4.1 Time domain analysis

Assuming that the channel impulse response $c(\tau;t)$ is wide sense stationary and a complex-valued random process in the t variable, the autocorrelation function of $c(\tau;t)$ can be defined as in *Equation (D.12)*

$$\Phi_c(\tau_1, \tau_2; \Delta t) = \frac{1}{2} E\left[c^*(\tau_1; t)c(\tau_2; t + \Delta t)\right] \qquad \text{(D.12)}$$

In most radio transmission media, the attenuation and phase shift of the channel associated with path delay τ_1 is uncorrelated with the attenuation and phase shift associated with path

delay τ_2, which is called uncorrelated scattering. Thus, if an assumption is made that the scattering at two different delays is uncorrelated, *Equation (D.12)* can rewritten as

$$\frac{1}{2}E\left[c^*(\tau_1;t)c(\tau_2;t+\Delta t)\right]=\Phi_c(\tau_1;\Delta t)\delta(\tau_1-\tau_2) \qquad \text{(D.13)}$$

If $\Delta t = 0$ in *Equation (D.13)*, the resulting autocorrelation function $\Phi_c(\tau;0)\equiv\Phi_c(\tau)$ is simply the average power output of the channel as a function of the time delay τ. For this reason, $\Phi_c(\tau)$ is called the multipath intensity profile or the delay power spectrum of the channel. In general, $\Phi_c(\tau;\Delta t)$ gives the average power output as a function of the time delay τ and the difference Δt in observation time.

In practice, the function $\Phi_c(\tau;\Delta t)$ is measured by transmitting very narrow pulses or, equivalently, a wideband signal and cross-correlating the received signal with a delayed version of itself. Typically, the measured function $\Phi_c(\tau)$ may appear as shown in *Figure D.3*. The range of values of τ over which $\Phi_c(\tau)$ is essentially non-zero or above a certain threshold is called the RMS delay spread of the channel and is denoted by ϑ_τ (see *Chapter 4, Figure 4.2*).

D.4.2 Frequency domain analysis

In the frequency domain the characterization of the time-variant multipath channel can be accomplished by taking the Fourier transform of *c(τ;t)*. This results in a time-variant transfer function *C(f;t)*, where *f* is the frequency variable. Thus,

$$C(f;t)=\int_{-\infty}^{\infty}c(\tau;t)e^{-j2\pi f\tau}\,d\tau \qquad \text{(D.14)}$$

If *c(τ;t)* is modelled as a complex-valued zero-mean Gaussian random process in the *t* variable, it follows that *C(f; t)* also has the same statistics. Under the assumption that the

channel is wide-sense-stationary, the autocorrelation function in the frequency domain can be defined as

$$\Phi_C(f_1, f_2; \Delta t) = \frac{1}{2} E\left[C^*(f_1; t) C(f_2; t + \Delta t)\right] \qquad \text{(D.15)}$$

Since *C(f; t)* is the Fourier transform of *c(τ;t)*, the autocorrelation function $\Phi_C(f_1, f_2; \Delta t)$ is also related to $\Phi_c(\tau; \Delta t)$ by the Fourier transform. It was shown by Proakis [6] that substitution of *Equation (D.14)* into *Equation (D.15)* resulted in

$$\Phi_C(f_1, f_2; \Delta t) \equiv \Phi_C(\Delta f; \Delta t) \qquad \text{(D.16)}$$

where $\Delta f = f_2 - f_1$. From *Equation (D.16)* it is observed that the autocorrelation function of *C(f; t)* in frequency is a function of only the frequency difference $\Delta f = f_2 - f_1$. Accordingly $\Phi_C(\Delta f; \Delta t)$ is known as the spaced-frequency, spaced-time correlation function of the channel. It can be measured in practice by transmitting a pair of sinusoids separated by Δf and cross-correlating the two separately received signals with a relative delay Δt.

D.4.3 Relationship between the frequency and time domain

Time delays in the channel

If $\Delta t = 0$ in *Equation (D.16)*, $\Phi_C(\Delta f; 0) \equiv \Phi_C(\Delta f)$ and $\Phi_c(\tau; 0) \equiv \Phi_c(\Delta \tau)$, the Fourier transform relationship is

$$\Phi_C(\Delta f) = \int_{-\infty}^{\infty} \Phi_c(\tau) e^{-j2\pi\Delta f \tau} d\tau \qquad \text{(D.17)}$$

The relationship is shown graphically in *Figure D.3*. Since $\Phi_C(\Delta f)$ is an autocorrelation function in the frequency variable, it provides a measure of the channel's frequency coherence. As a result of the Fourier transform relationship between $\Phi_C(\Delta f)$ and $\Phi_c(\tau)$,

the reciprocal of the RMS delay spread ϑ_τ is a measure of the coherence bandwidth of the channel. That is,

$$BW_c \approx \frac{1}{\vartheta_\tau} \tag{D.18}$$

where BW_c denotes the coherence bandwidth as defined in Appendix C. The coherence bandwidth is a measure of the frequency separation of two tones that will still be correlated. If the frequency separation between the two tones were larger than the coherence bandwidth, the channel affects the tones differently. Thus, if the bandwidth of an information-bearing signal is greater than the coherence bandwidth of the channel, the channel is said to be frequency selective. In this case the signal is severely distorted. If the bandwidth of the information-bearing signal is small in comparison to the coherence bandwidth of the channel, the channel is said to be non-frequency selective.

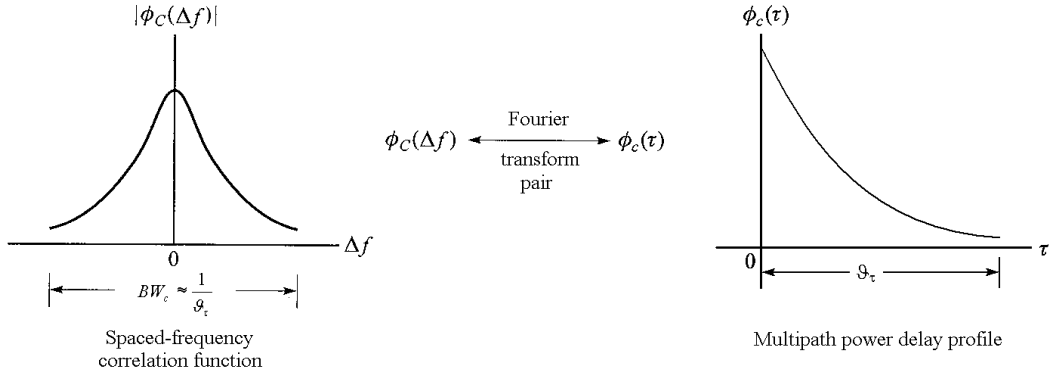

Figure D.3. Graphical relationship between $\Phi_C(\Delta f)$ and $\Phi_c(\tau)$, taken from Proakis, pp. 806 [6].

Time variations in the channel

Time variations in the channel are measured by the parameter Δt in $\Phi_C(\Delta f;\Delta t)$ and cause Doppler spreading of the signals. To relate the Doppler effects to the time variations of the channel, a function $S_c(\Delta f;f)$ is defined as the Fourier transform of $\Phi_C(\Delta f;\Delta t)$ with respect to the variable Δt. Thus,

$$S_C(\Delta f;\ f) = \int_{-\infty}^{\infty} \Phi_C(\Delta f;\Delta t) e^{-j2\pi f \Delta t} d\Delta t \qquad \text{(D.19)}$$

If Δf is set to zero, representing a single frequency tone, $S_C(0;f) \equiv S_C(f)$, and *Equation (D.19)* becomes

$$S_C(f) = \int_{-\infty}^{\infty} \Phi_C(0;\Delta t) e^{-j2\pi f \Delta t} d\Delta t \qquad \text{(D.20)}$$

$S_c(f)$ is a power spectrum that relates the signal intensity to the Doppler frequency f_d. Hence, $S_c(f)$ is called the Doppler power spectrum of the channel. If the channel is time-invariant, that is $\Phi_C(0;\Delta t) = 1$, *Equation (D.20)* reduces to the delta function, $S_c(f) = \delta(f)$. Therefore, when the channel is time-invariant, no spectral broadening is observed in the transmission of a single frequency tone.

The range of values over which $S_c(f)$ is essentially non-zero, is called the Doppler spread BW_d of the channel. Following the same argument as in the previous section, the Doppler power spectrum $S_c(f)$ is related to $\Phi_C(\Delta t)$ by the Fourier transform. Thus, the reciprocal of BW_d is a measure of the coherence time of the channel, given by

$$T_c \approx \frac{1}{BW_d} \qquad \text{(D.21)}$$

Thus, the coherence time is a time separation that will not cause any amplitude distortion in the signal. A slowly changing channel has a large coherence time, or equivalently a small Doppler spread, and visa versa. The graphical relationship between $S_c(f)$ and $\Phi_C(\Delta t)$ is shown in *Figure D.4*.

Another Fourier transform relationship exists between $\Phi_c(\tau;\Delta t)$ and $S_C(\Delta f;f)$
This relationship was derived by Proakis [6] and is denoted as

$$S(\tau;\ f_d) = \int_{-\infty}^{\infty}\int_{-\infty}^{\infty} \Phi_C(\Delta f;\Delta t) e^{-j2\pi f_d \Delta t} e^{j2\pi\tau\Delta f} d\Delta t d\Delta f \qquad \text{(D.22)}$$

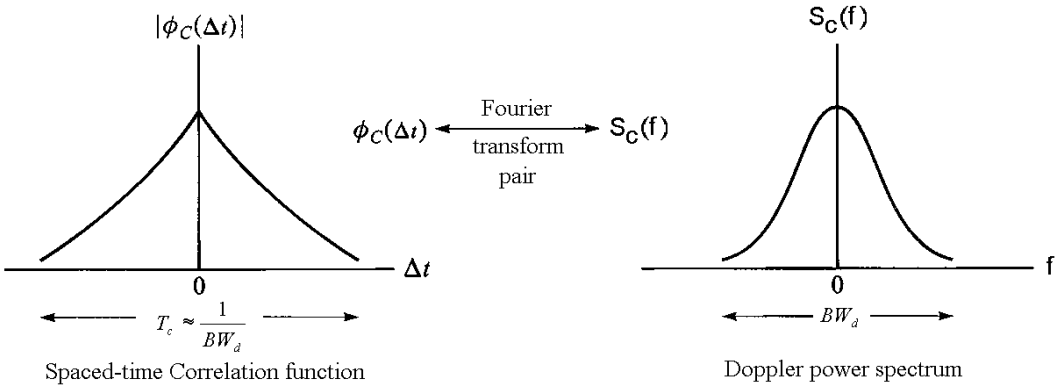

Figure D.4. Graphical relationship between $\Phi_C(\Delta t)$ and $S_C(\lambda)$, taken from Proakis, pp. 807 [6].

The function $S(\tau; f)$ is called the scattering function of the channel. The scattering function provides a statistical measure of the output power of the channel, expressed as a function of the time delay τ and the Doppler frequency f_d.

In *Section D.4*, a rough approximation was derived for the delay spread due to multipath. This was merely presented to show the graphical representation between the coherence bandwidth and delay spread, as well as the coherence time and Doppler spread. In *Sections D.5* and *D.6* more accurate approximations [1, 5, 7] are derived for the delay - and Doppler spread.

D.5 DELAY SPREAD

As stated in the previous section, if $\Delta t = 0$ in *Equation (D.13)*, $\Phi_c(\tau;0) \equiv \Phi_c(\Delta\tau)$ which is the multipath power delay profile. The multipath power delay profile may also be defined in terms of the scattering function $S(\tau; f)$, given in *Equation (D.22)*, by averaging it over all Doppler shifts f_d. That is,

$$\Phi_c(\tau) = \int_{-f_d}^{f_d} S(\tau; f)df \qquad \text{(D.23)}$$

Figure D.5 shows an example of a delay power spectrum that depicts a typical plot of the power spectral density versus the received time delays relative to shortest echo path. The

"threshold level" included in *Figure D.5* defines the power level below which the receiver fails to operate satisfactorily. Expanding on *Chapter 4*, *Section 4.2*, where only delay spread was defined, the terms excess delay, average delay and RMS delay spread are defined here. In order to do so, two statistical moments of $\Phi_c(\tau)$ are of interest, the average delay, τ_{av}, and the RMS delay spread, ϑ_τ (see *Figure D.5*). Note that the RMS delay spread defined here is the same as the delay spread defined in *Chapter 4*, *Section 4.7*. Also note that *Figure D.5* is a multipath power delay profile for an outdoor environment, where *Figure 4.2* in *Chapter* 4 is a typical indoor multipath power delay profile.

The average delay is defined as the first central moment (i.e., the mean) of $\Phi_c(\tau)$, shown by

$$\tau_{av} = \frac{\int_0^\infty \tau \Phi_c(\tau) d\tau}{\int_0^\infty \Phi_c(\tau) d\tau} \tag{D.24}$$

The RMS delay spread is defined as the root square of the second central moment of $\Phi_c(\tau)$, as shown by

$$\sigma_\tau = \left(\frac{\int_0^\infty (\tau - \tau_{av})^2 \Phi_c(\tau) d\tau}{\int_0^\infty \Phi_c(\tau) d\tau} \right)^{1/2} \tag{D.25}$$

As stated in *Section D.4* and given in *Equation (D.18)*, the reciprocal of the RMS delay spread ϑ_τ is a measure of the coherence bandwidth, BW_d, of the channel.

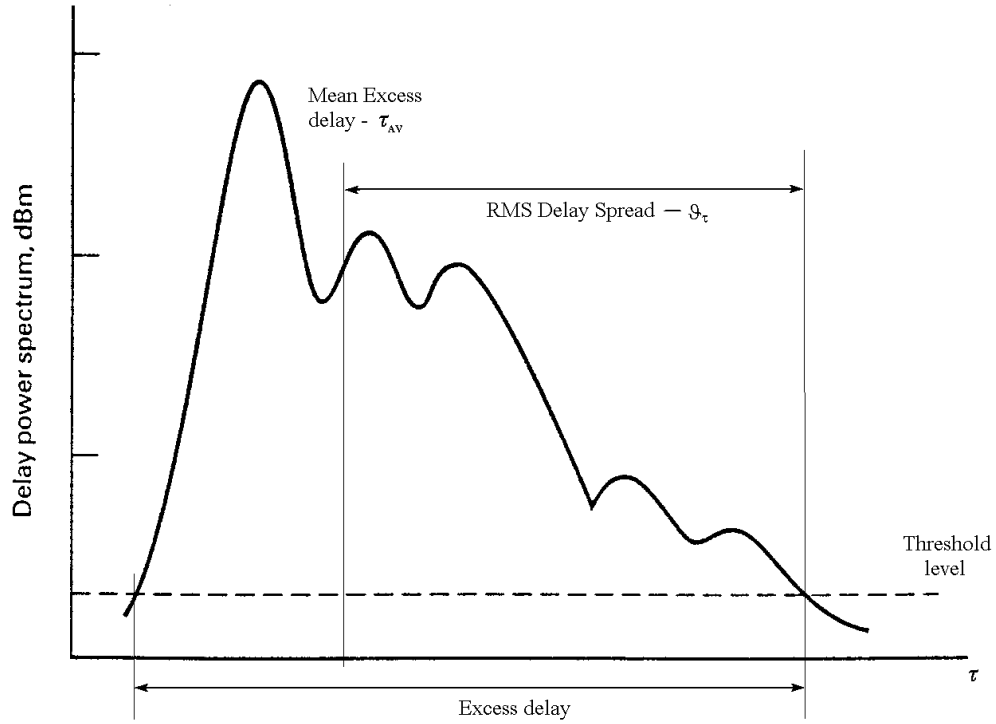

Figure D.5 The multipath power delay profile for a mobile radio channel, showing τ_{av} and ϑ_τ. Partially taken from Haykin [7].

D.5.1 Delay spread bound

Assuming that the longest propagation delay (excess delay, as shown in *Figure D.5*) between a base station and a mobile is $\tau_{max,}$ and that reflection coefficients are 100% uncorrelated, Feher [5] derived an upper bound to be

$$\tau_{\max} = \frac{1}{4\pi}\frac{1}{f}\sqrt{\frac{P_T}{P_{R\min}}} \qquad \text{(D.26)}$$

where :

P_T is the transmitted power (in dBm),

P_{Rmin} is minimum received power required at the receiver (in dBm),

f is the frequency at which the communication link operates, and

τ_{max} is the maximum excess delay time.

Delay spread field measurements

Typical RMS delay spread field measurements, obtained from Feher [5], are as follow:

- Cellular Systems, for example GSM (coverage up to 10km, RMS delay spread up to 100 μs)
- Land-mobile radio (coverage up to 70km, RMS delay spread up to 350 μs)
- Indoor PCSs, for example WLANs (coverage up to 30m, RMS delay spread up to 300 ns)

D.6 DOPPLER SPREAD

As stated earlier, the Doppler power spectrum is given by *Equation (D.20)*. The Doppler power spectrum may also be defined in terms of the scattering function $S(\tau; f)$, by averaging it over all possible propagation delays, shown in *Equation (D.27)*.

$$S_C(f) = \int_{-\infty}^{\infty} S(\tau; f) d\tau \qquad \text{(D.27)}$$

Assuming that the Doppler shift f_d may have positive and negative values with equal likelihood, the mean Doppler shift is therefore zero. The square root of the second moment of the Doppler spectrum is thus defined by

$$BW_d = \left(\frac{\int_0^{f_d} (f)^2 S_C(f) df}{\int_0^{f_d} S_C(f) df} \right)^{1/2} \qquad \text{(D.28)}$$

The parameter BW_d provides a measure of the width of the Doppler power spectrum, as shown in *Figure D.5*. Some typical values encountered in a mobile radio environment for Doppler spread, due to motion of a vehicle, ranges between 10 Hz to 200 Hz.

D.6.1 Doppler power spectrum for mobile radio channels

A widely used model for the Doppler power spectrum of mobile radio channels is the so-called Jakes's model [74]. In this model the autocorrelation, $\Phi_C(\Delta t)$ of the time-variant transfer function *C(f ; t)* from *Equation (D.15)* is given as

$$\begin{aligned}\Phi_C(\Delta t) &= \frac{1}{2}E\left[C^*(f;t)C(f;t+\Delta t)\right] \\ &= I_0\left(2\pi f_d \Delta t\right)\end{aligned} \tag{D.29}$$

where $I_0(\bullet)$ is the zero-order Bessel function of the first kind and f_d is the Doppler frequency as defined in *Equation (D.2).*

The Fourier transform of $\Phi_C(\Delta t)$, as shown in *Section D.4.3,* yields the Doppler power spectrum at baseband. That is

$$\begin{aligned}S_C(f) &= \int_{-\infty}^{\infty} \Phi_C(\Delta t) e^{-j2\pi f \Delta t} d\Delta t \\ &= \int_{-\infty}^{\infty} I_0\left(2\pi f_d \Delta t\right) e^{-j2\pi f \Delta t} d\Delta t \\ &= \begin{cases} \dfrac{1}{\pi f_d} \dfrac{1}{\sqrt{1-(f/f_d)^2}} & (|f| \le f_d) \\ 0 & (|f| \le f_d) \end{cases}\end{aligned} \tag{D.30}$$

The plot of $S_C(f)$ is shown in Appendix C, *Section C.3.3, Figure C.3.*

D.7 FADING CHANNEL SIMULATOR MODEL

In order to obtain Rayleigh and Rician statistical distributions, as described in Chapter 4, Clarke's model [75] can be used.

D.7.1 Description of the fading channel simulator

Clarke's fading simulator (*Figure D.6*) consists of two orthogonal independent Gauss noise sources with zero mean and unit variance in each branch, followed by a Doppler shaping filter. To simulate both a Rayleigh, as well as a Rician fading, a Rician factor is added to the in-phase branch (note that the fading is Rayleigh distributed when $K = -\infty$). The input signal is divided into an in-phase $S_I(t)$ branch and quadrature branch $S_Q(t)$. The quadrature branch is formed by applying the Hilbert transform to the input signal, which is only a 90-degrees phase shift from the in-phase signal frequency. The in-phase and quadrature branches are then respectively multiplied by the fading spectrum branches $n_I(t)$ and $n_Q(t)$ to produce $f_I(t)$and $f_Q(t)$. These two branches are added together and scaled by the C_{SCALE} constant to produce an output signal that has the same power as the input signal. The output signal $d(t)$ is a Rayleigh/Rician fading signal, depending on the Rician constant, which exhibits the proper Doppler spread and time correlation introduced in the channel.

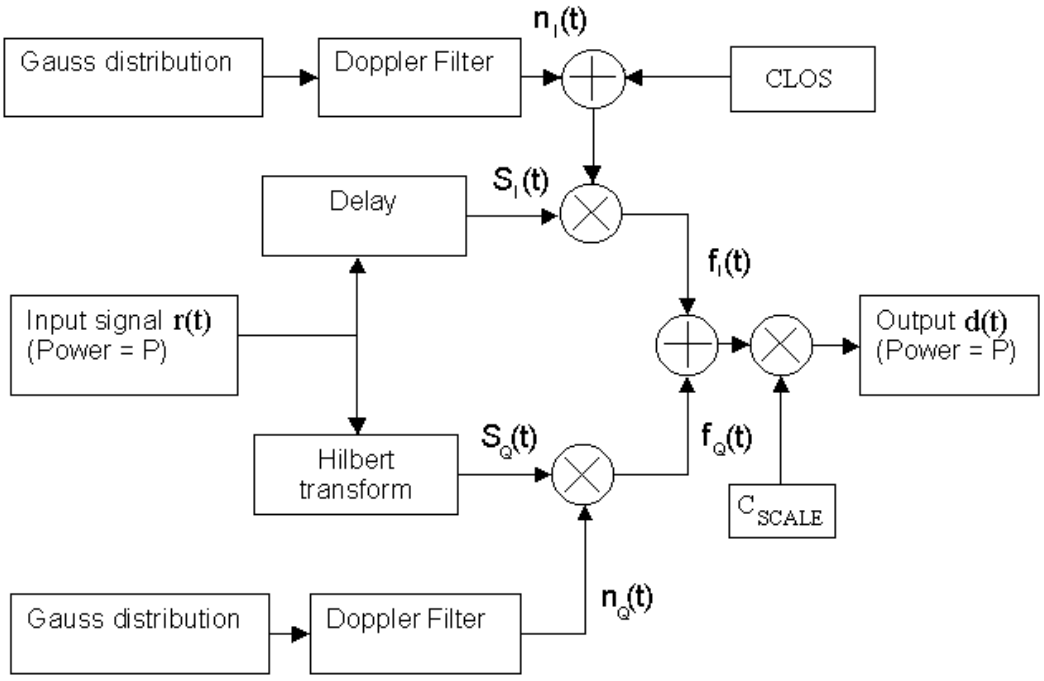

Figure D.6 Clarke's model for a fade simulator employing both Rayleigh and Rice fading.

D.7.2 Derivation of the *CLOS* and C_{SCALE} constants

From *Figure D.6* the in-phase branch is equal to

$$f_I(t) = S_I(t)\left[n_I(t) + (CLOS)\right] \tag{D.37}$$

and the quadrature branch is equal to

$$f_Q(t) = S_Q(t)\left[n_Q(t)\right] \tag{D.38}$$

The output of the fading simulator is therefore equal to

$$d(t) = C_{SCALE}\left[f_I(t) + f_Q(t)\right] \tag{D.39}$$

Substitution of *Equations (D.37)* and *(D.38)* into *Equation (D.39)* yields

$$d(t) = C_{SCALE}\left[S_I(t)n_I(t) + S_I(t)(CLOS) + S_Q(t)n_Q(t)\right] \tag{D.40}$$

Equation (D.40) can be rewritten in a form that consists of the LOS and NLOS part, that is

$$d(t) = C_{SCALE}\left[\underbrace{S_I(t)(CLOS)}_{LOS} + \underbrace{S_I(t)n_I(t) + S_Q(t)n_Q(t)}_{NLOS}\right] \tag{D.41}$$

The Rician constant K is defined as the ratio between the LOS signal component and the signal scatter components (NLOS). Thus

$$K = 10\log_{10}\left[\frac{\sigma^2{}_{LOS}}{\sigma^2{}_{NLOS}}\right] \tag{D.42}$$

If the input signal power is denoted by P, the power of the signal can be written as

$$\sigma^2{}_{u(t)} = E\left[u^2(t)\right] = P \tag{D.43}$$

The power in the in-phase and quadrature branches also equals *P*, respectively, because the Hilbert transform only produces a 90 degrees phase shift of the input signal. Thus the quadrature branch is a 90-degrees phase shift from the in-phase signal.

$$E\left[S_I{}^2(t)\right] = E\left[S_Q{}^2(t)\right] = P \tag{D.44}$$

From *Equation (D.41)*, the LOS and NLOS components of *r(t)* is

$$\begin{aligned} LOS &= S_I(t)(CLOS) \\ NLOS &= S_I(t)n_I(t) + S_Q(t)n_Q(t) \end{aligned} \tag{D.45}$$

Thus, the power of the LOS signal path is

$$\begin{aligned} \sigma^2{}_{LOS} &= E\left[LOS^2\right] = E\left[(CLOS)^2 S_I{}^2(t)\right] \\ &= (CLOS)^2 E\left[S_I{}^2(t)\right] \\ &= (CLOS)^2 P \end{aligned} \tag{D.46}$$

The power of the NLOS or scatter component of the signal is

$$\begin{aligned} \sigma^2{}_{NLOS} &= E\left[NLOS^2\right] = E\left[\left(S_I(t)n_I(t) + S_Q(t)n_Q(t)\right)^2\right] \\ &= E\left[S_I{}^2(t)n_I{}^2(t) + 2S_I(t)n_I(t)S_Q(t)n_Q(t) + S_Q{}^2(t)n_Q{}^2(t)\right] \\ &= E\left[S_I{}^2(t)n_I{}^2(t)\right] + 2E\left[S_I(t)n_I(t)S_Q(t)n_Q(t)\right] + E\left[S_Q{}^2(t)n_Q{}^2(t)\right] \\ &= E\left[S_I{}^2(t)\right]E\left[n_I{}^2(t)\right] + 2E\left[S_I(t)\right]E\left[n_I(t)\right]E\left[S_Q(t)\right]E\left[n_Q(t)\right] + E\left[S_Q{}^2(t)\right]E\left[n_Q{}^2(t)\right] \end{aligned} \tag{D.47}$$

But, $E\left[n_I{}^2(t)\right]$ and $E\left[n_Q^2(t)\right]$ is the variance of a Gauss distribution after Doppler filtering, thus

$$E\left[n_I{}^2(t)\right] = E\left[n_Q{}^2(t)\right] = 1 \tag{D.48}$$

and $E\left[n_I(t)\right]$ and $E\left[n_Q(t)\right]$ is the mean of a Gauss distribution, thus

$$E\left[n_I(t)\right] = E\left[n_Q(t)\right] = 0 \tag{D.49}$$

Using *Equation (D.48)* and *(D.49)*, *Equation (D.47)* reduces to

$$\begin{aligned}\sigma^2{}_{NLOS} &= E\left[S_I{}^2(t)\right] + E\left[S_Q{}^2(t)\right] \\ &= 2P\end{aligned} \tag{D.50}$$

Thus, from *Equation (D.46)* and *(D.50)*

$$\frac{\sigma^2{}_{LOS}}{\sigma^2{}_{NLOS}} = \frac{E\left[LOS^2\right]}{E\left[NLOS^2\right]} \tag{D.51a}$$

$$= \frac{(CLOS)^2 P}{2P} \tag{D.51b}$$

Substituting *Equation (D.51b)* into *Equation (D.42)*, the Rician factor, *CLOS*, can be written in terms of the Rician constant *K*, thus

$$CLOS = 10\log_{10}\left[\sqrt{2K}\right] \tag{D.52a}$$

in dB form and

$$CLOS = \sqrt{2K} \tag{D.52b}$$

in linear form. For unity power gain through the fading simulator, the following condition must be met:

$$P_{in} = P_{out} = P \tag{D.53}$$

Equation (D.53) states that the output power must be equal to the input power, which in this case is denoted by P (see *Figure D.6*). Thus:

$$\sigma^2{}_{u(t)} = \sigma^2{}_{d(t)}$$

$$E\left[u^2(t)\right] = E\left[d^2(t)\right]$$

But the input power is P, thus

$$P = E\left[d^2(t)\right]$$

$$= E\left[\left(C_{SCALE}\left[S_I(t)n_I(t) + S_I(t)(CLOS) + S_Q(t)n_Q(t)\right]\right)^2\right]$$

$$= E\left[(C_{SCALE})^2\left(S_I{}^2(t)(CLOS)^2 + (CLOS)S_I(t)n_I(t) + (CLOS)S_I(t)S_Q(t)n_Q(t) + \right.\right.$$

$$S_I{}^2(t)n_I{}^2(t) + (CLOS)S_I{}^2(t)n_I(t) + S_I(t)S_Q(t)n_I(t)n_Q(t) + S_Q{}^2(t)n_Q{}^2(t) +$$

$$\left.\left.(CLOS)S_I(t)S_Q(t)n_Q(t) + S_I(t)n_I(t)S_Q(t)n_Q(t)\right)\right] \qquad \text{(D.54)}$$

Using *Equations (D.48)* and *(D.49)*, *Equation (D.54)* reduces to

$$\mathrm{P} = (C_{SCALE})^2 E\left[S_I{}^2(t)(CLOS)^2 + S_I{}^2(t)n_I{}^2(t) + S_Q{}^2(t)n_Q(t)\right]$$

$$= (C_{SCALE})^2\left(E\left[S_I{}^2(t)(CLOS)^2\right] + E\left[S_I{}^2(t)n_I{}^2(t)\right] + E\left[S_Q{}^2(t)n_Q(t)\right]\right)$$

$$= (C_{SCALE})^2\left((CLOS)^2 E\left[S_I{}^2(t)\right] + E\left[S_I{}^2(t)\right]E\left[n_I{}^2(t)\right] + E\left[S_Q{}^2(t)\right]E\left[n_Q(t)\right]\right)$$

$$= (C_{SCALE})^2\left((CLOS)^2 P + P + P\right) \qquad \text{(D.55)}$$

Rewriting *Equation (D.55)* in terms of the Rician factor *CLOS* and the power P, yields

$$C_{SCALE} = \sqrt{\frac{P}{(CLOS)^2 P + 2P}}$$

$$C_{SCALE} = \sqrt{\frac{1}{CLOS^2 + 2}} \qquad \text{(D.56)}$$

and in terms of the Rician constant K:

$$C_{SCALE} = \frac{1}{\sqrt{2(1+K)}} \tag{D.57}$$